

**Effects of filler content and coupling agents on the mechanical  
properties and geometrical accuracy of selective laser sintered parts in  
glass bead-filled polyamide 12 composites**

**Thesis submitted to Cardiff University  
for the degree of Doctor of Philosophy**

**By**

**Alkir A. Mousah**

**Manufacturing Engineering Centre**

**School of Engineering**

**Cardiff University**

**United Kingdom**

**June 2011**

## **Abstract**

Improvements in existing materials and the development of new materials for use in selective laser sintering are continually being pursued in the industrial and academic domains. This research will focus on the possibilities available for improving the mechanical properties and geometric accuracy of selective laser sintered parts produced from non-commercial polyamide 12 (PA12) composites. The specific material of interest is PA 12 filled with glass beads. This thesis describes a study of the relationship between filler particles, the polymer matrix and processing parameters and their influence on the mechanical properties and geometric accuracy of the composite. The aim of the study is to better understand the effect of coupling agents on the above mentioned properties as there is a lack of information in this area.

Most of the experiments described in the thesis were performed with PA 12 filled with coated and uncoated glass beads. The production of test samples was carried out on a selective laser sintering machine (DTM Sinterstation 2000). Knowledge about different machine-material combinations has been extended by performing additional PA 12 composite experiments. The accessible information from PA 12 and glass-filled PA 12 (PA12/GF) manufacturer's data was used as a reference in comparison and assessment of the results obtained from the new machine-material combinations.

This research has shown that adding coated glass beads to PA 12 improves the tensile strength and elastic modulus but reduces the impact strength and ductility of the

resulting material. Under suitable processing conditions, the geometrical accuracy of sintered parts also improves with the addition of glass beads. The work has also shown that good interfacial bonding between the polyamide matrix and the glass beads, particularly when a coupling agent is used, is a likely cause for the observed improvements.

## **Acknowledgement**

First and foremost I would like to thank God for all of my blessings. Next, I would like to take this opportunity to express my deepest appreciation and gratitude to my supervisor Prof. Duc T Pham for his guidance, insight, patience, and time. His encouragement and advice greatly contributed to the success of this thesis. I am extremely fortunate to have been groomed under him, and in total awe of the keen insight with which he have guided me to shape this thesis into what it needed to be.

Special gratitude and thanks to Dr. Shwe Soe for his academic and technical support, understanding, for the time and knowledge he invested in starting my research project. I am also eternally grateful to Dr. Georgi Lalev for his directly helping with this research, particularly in the scanning electron microscope (SEM) to take SEM micrographs of samples.

Sincere thanks are due to MEC staff members in the Selective Laser Sintering Laboratory, especial to Technicians Justin and Paul for their invaluable technical support.

Finally, I am thankful for the unbounded support and encouragement of my Country, my Family and my Friends ... words can not thank you enough.

## **Declaration**

This work has not previously been accepted in substance for any degree and is not concurrently being submitted in candidature for any other degree.

Signed:..... (Alkir A S Mousah) Date :.....

## **Statement 1**

This thesis is being submitted in partial fulfilment of the requirements for the degree of PhD.

Signed:..... (Alkir A S Mousah) Date :.....

## **Statement 2**

This thesis is the result of my own independent work/investigation, except where otherwise stated. Other sources are acknowledged by explicit references.

Signed:..... (Alkir A S Mousah) Date :.....

## **Statement 3**

I hereby give consent for my thesis, if accepted, to be available for photocopying and for inter-library loan and for the title and summary to be made available to outside organisations.

Signed:..... (Alkir A S Mousah) Date :.....

Signed:..... (Alkir A S Mousah) Date :.....

## Contents

<b>Abstract.....</b>	<b>i</b>
<b>Acknowledgments.....</b>	<b>iii</b>
<b>Declaration.....</b>	<b>iv</b>
<b>Contents.....</b>	<b>vi</b>
<b>List of tables.....</b>	<b>x</b>
<b>List of figures.....</b>	<b>xi</b>
<b>List of symbols .....</b>	<b>xvi</b>
<b>List of abbreviations .....</b>	<b>xvii</b>
<b>Chapter 1- Introduction.....</b>	<b>1</b>
1.1 Background of common Rapid Prototyping and Manufacturing (RP&M) technologies .....	2
1.1.1 Stereolithography (SLA) .....	8
1.1.2 Fused Deposition Modelling (FDM) .....	10
1.1.3 Laminated Object Manufacturing (LOM) .....	12
1.1.4 Selective Laser Sintering (SLS) .....	14
1.2 Motivation .....	16
1.3 Aim and objectives.....	17
1.4 Research questions and hypotheses.....	17
1.5 Research approach.....	20
1.6 Thesis outline.....	20





<b>Chapter 4- Effects of processing conditions and coupling agents on mechanical properties of selective laser sintered glass beads filled- polyamide 12 composites.....</b>	<b>116</b>
4.1 Experiments.....	117
4.1.1 Materials and samples preparation.....	117
4.1.2 Equipment and methodology.....	118
4.2 Mechanical properties.....	122
4.2.1 Tensile strength.....	122
4.2.2 Young’s modulus.....	128
4.2.3 Elongation at Break.....	132
4.2.4 Flexural strength and modulus.....	134
4.2.5 Impact strength.....	138
4.2.6 Fracture toughness.....	143
4.2.6.1 Single- edge- notched three point bending fracture toughness tests.....	145
4.2.6.2 Correlation between fracture toughness and glass bead content.....	150
4.2.6.3 Effect of V- notch depth on fracture toughness.....	152
4.3 Morphological observation.....	154
4.4 Summary.....	159
<b>Chapter 5- Experimental investigations of the influence of processing parameters and material properties on curling phenomenon in selective laser sintering.....</b>	<b>161</b>

5.1	Background.....	161
5.2	Implementation of Taguchi method in the optimisation of curling in SLS.....	170
5.3	Experimental procedure.....	174
5.3.1	Description of experimental set-up.....	174
5.3.2	Design of Experiments.....	179
5.4	Curling measuring procedure.....	187
5.5	Statistical analysis of experimental data.....	188
5.5.1	Main effects.....	192
5.5.2	Analysis using signal to noise (S/N) ratio.....	196
5.5.3	Data analysis by ANOVA technique.....	200
5.6	Summary.....	207
<b>Chapter 6- Conclusions and recommended future work.....</b>		<b>208</b>
6.1	Conclusions.....	208
6.2	Suggestions for Future Work.....	211
<b>7. Appendix.....</b>		<b>213</b>
<b>8. References.....</b>		<b>223</b>

## List of tables

Table 1.1	Comparison of selected additive processing technologies.....	7
Table 1.2	Correspondence between research tasks, hypotheses, and chapters.	19
Table 3.1	Contents of glass beads blended with PA12 by weight.....	72
Table 3.2	Measured and calculated data of tapped density of composites.....	84
Table 3.3	Modification limits of composite material and LS process parameters.....	89
Table 3.4	Effects of part bed temperature in SLS process.....	97
Table 3.5	Scale factor and beam offset for PA12/GB composites.....	109
Table 3.6	Measured data of sintered density specimens.....	114
Table 4.1	Process parameters used in manufacturing of test specimens from the PA12/CP00 and PA12/CP03 composites.....	119
Table 4.2	Mechanical properties of SLS specimens (PA12; PA12/CP00 and PA12/CP03 systems).....	141
Table 4.3	Mechanical properties of SLS specimens recorded by extensometer (PA 12; PA12/CP00 and PA12/CP03 systems).....	142
Table 4.4	Test results of fracture toughness performed on PA12/GB composites.....	149
Table 5.1	The dependency of shrinkage percentage in the length of tensile bars on glass beads content.....	168
Table 5.2	The factors that may have an effect on the SLS process.....	181
Table 5.3	List of SLS experimental parameters and their factor levels.....	182
Table 5.4	The layout of the L8 orthogonal array.....	185
Table 5.5	The filled in L <sub>8</sub> for experimental runs and level combinations.....	186

Table 5.6	Values of thickness and curling for L8 orthogonal array from three set of experiments.....	191
Table 5.7	Experimental results for curling measurements (PA12/CP03 system).....	193
Table 5.8	Levels average for main effects.....	194
Table 5.9	The S/N ratio results for curling.....	198
Table 5.10	The range of each parameter.....	199
Table 5.11	ANOVA table.....	204

### List of figures

Figure 1.1	Data transfer between CAD and the RM system.....	3
Figure 1.2	Overview of additive processing technologies.....	6
Figure 1.3	A schematic drawing of the SLA.....	9
Figure 1.4	Fused Modelling System.....	11
Figure 1.5	Mechanism of a LOM machine and part building sequence of the LOM process.....	13
Figure 1.6	SLS process.....	15
Figure 1.7	Thesis organisation .....	21
Figure 2.1	Comparison between SUN and WAGNER SLS process models..	25
Figure 2.2	Interaction of the laser irradiation and polymer powder.....	28
Figure 2.3	Heat transfer mechanisms in a porous body.....	31
Figure 2.4	The Sinterstation 2000 and build chamber.....	35
Figure 2.5	Breakout station.....	36
Figure 3.1	Scanning electron micrograph of soda-lime glass beads 3000 solid sphere.....	61

Figure 3.2	Idealistic view of a silane treated surface.....	65
Figure 3.3	Coupling mechanism of a silane coupling agent.....	67
Figure 3.4	DSC curve for melting and crystallisation.....	74
Figure 3.5	DSC plot of virgin PA 12 powder.....	76
Figure 3.6	SEM micrograph showing unsintered PA 12 powder.....	78
Figure 3.7	General view of blended powder of PA 12 with glass beads.....	79
Figure 3.8	Particle size and distribution of the glass beads used by sieve analysis.....	81
Figure 3.9	The relation between filler ratio and composites tap density.....	85
Figure 3.10	Cross shaped test samples used to help in finding suitable Bed/feed temperatures.....	90
Figure 3.11	Cracks and lines on the powder surface formed due to excessive bed/feed temperatures.....	92
Figure 3.12	Growth on sintered specimens.....	94
Figure 3.13	In-build curling causes the part to shift when the roller passes over the part bed.....	95
Figure 3.14	Flowchart of beam offset and shrinkage calibration procedure....	98
Figure 3.15	Calibration standard part built and measured to calculate shrinkage scale factor and beam offset values for the composite materials.....	100
Figure 3.16	Parts for investigating the manufacturability of small-scale features in SL process.....	103
Figure 3.17	Samples for visual inspection of features definition based on bed temperature; laser power and filler content.....	105
Figure 3.18	Comparison of part surface finish and appearance between parts	

	with different glass beads content.....	107
Figure 3.19	Weight of density specimens sintered using various energy densities.....	110
Figure 3.20	The influence of energy density values on the density of sintered density specimens.....	112
Figure 4.1	Orientation of samples in the build bed of the SLS machine.....	120
Figure 4.2	Testometric materials testing machine and extensometer installed.....	123
Figure 4.3	Shape and dimensions of the tensile test specimens	123
Figure 4.4	Stress- strain curves of PA12; PA12/CP00; PA12/CP03.....	125
Figure 4.5	The variation of tensile strength of the PA12/CP00 and PA12/CP03 systems.....	127
Figure 4.6	The variation of the modulus of elasticity of PA12/GB composites with glass beads content [wt%].....	129
Figure 4.7	The variation of the elongation at break with glass bead content..	133
Figure 4.8	Shape, dimension and the arrangement of test specimen.....	136
Figure 4.9	The variation of the flexural strength and flexural modulus with glass beads content.....	137
Figure 4.10	Impact test arrangement.....	139
Figure 4.11	The variation of impact strength with glass beads weight ratios...	140
Figure 4.12	Specimen configuration for fracture toughness measurements.....	146
Figure 4.13	Load-displacement curves of: PA12; PA12/CP00; PA12/CP03...	147
Figure 4.14	Dependency of fracture toughness of polyamide 12 composites on glass bead content.....	151
Figure 4.15	Optical photomicrographs of the V- notch introduced using SLS	

	process.....	153
Figure 4.16	Dependence of $K_{IC}$ and $G_{IC}$ on notch depth.....	155
Figure 4.17	SEM micrographs. Scan surfaces.....	157
Figure 4.18	SEM scan surfaces and tensile fracture surfaces of selective laser sintered PA12/CP03 composites containing 20 [wt%] of glass bead built at different energy densities.....	158
Figure 5.1	Shape distortion in SLS.....	165
Figure 5.2	Curling up of parts during SLS process.....	166
Figure 5.3	Dependency of the shrinkage percentage on glass bead content...	169
Figure 5.4	Scheme of the major steps of implementing the Taguchi method.	172
Figure 5.5	Test bar used for curling investigation.....	177
Figure 5.6	Position of test bar with respect to the part bed and neighbouring parts.....	178
Figure 5.7	The model of the SLS process in Taguchi method.....	183
Figure 5.8	Measurement arrangement of curling.....	189
Figure 5.9	Definition for symbols: C; $t_a$ ; $h_{max}$ .....	190
Figure 5.10	Main effects graphs for average curling	195
Figure 5.11	The percentage contributions of process parameters on the amount of curling on sintered parts.....	206

### List of symbols

Symbol	Unit	Description
A	mm <sup>2</sup>	Area , cross- sectional area
BS	mm	Laser beam speed
$c_p$	J/kgK	Specific heat capacity
d	mm	Beam diameter

ED	J/mm <sup>2</sup>	Energy density
F	N	Force
G <sub>IC</sub>	J.m <sup>-2</sup>	Critical strain energy release rates
k	W/mK	Thermal conductivity
K <sub>IC</sub>	Pa.m <sup>1/2</sup>	Critical stress intensity factor
L <sub>p</sub> ; P	W	Laser power
L <sub>t</sub> , s	mm	Layer thickness
m	g	Mass
Q	J/s	Heat flow
SCSP	mm	Scan spacing
T <sub>b</sub>	°C	Part bed temperature
T <sub>g</sub>	°C	Glass transition temperature
T <sub>pc</sub>	°C	Crystallisation temperatures
T <sub>pm</sub>	°C	Melting temperature of polymer
α	m <sup>2</sup> /s	Thermal diffusivity
β	°Cmin <sup>-1</sup>	Heating rate
ρ	g/cm <sup>3</sup>	Powder density
ε	%	Strain
σ	MPa	Stress

### List of abbreviations

3DP	Three dimensional printing
ABS	Acrylonitrile butadiene styrene
ACU	Atmospheric conditioning unit
AF	Additive fabrication
ANOVA	Analysis of Variance
CAD	Computer aided design
CP00	Uncoated glass beads
CP03	Coated glass beads

DIN	Deutsche Institut fuer Normung
DOE	Design of experiments
DSC	Differential scanning calorimetry
DTM	Desktop manufacturing corporation
EOS	Electro optical system
FDM	Fused deposition modelling
GB	Glass bead
GF	Glass filled
LCVD	Laser jet chemical vapour deposition
LEFM	Linear elastic fracture mechanics
LLM	Layer Laminated Modelling
LMT	Layered manufacturing technique
LOM	Laminated object manufacturing
MSD	Mean square deviation
OA	Orthogonal array
PA 12	Polyamide 12
PC	Polycarbonate
PPSU	Polyphenylsulfone
PS	Polyester
RBO	Rough breakout station
RM	Rapid manufacturing
RMTs	Rapid manufacturing technologies
RP	Rapid prototyping
S/N	Signal-to-noise ratios
SEM	Scanning electron microscope

SFF	Solid Freeform Fabrication
SFP	Solid foil polymerisation
SLA	Stereolithography
SLS	Selective laser sintering
SMS	Selective mask sintering
STL	Stereolithography interface format
UV	Ultraviolet Light

## **Chapter 1 - Introduction**

In today's highly competitive global market, industry is looking for cost savings, improved product performance and reliability, failure prevention, longer product life and better environmental protection. Global competition is forcing companies to not only look for new ways to improve their business processes but also to focus on important factors such as product features, quality, cost and time to market to remain competitive. In response, new production techniques and advanced materials have to be established for the manufacturing of robust, complex and accurate parts.

Rapid Manufacturing Technologies (RMTs) offer opportunities to make products faster and usually at lower costs. In general, they can be a solution for the issues mentioned above, as they show advantages, such as freedom of design and tool-less fabrication, compared to conventional production methods. However, the limited range of materials that can be processed by RMTs represents one among many limitations, and despite many materials being investigated for use with RMTs, there is still a need for research into new material systems, which are likely to be composed of combinations of existing materials [1].

This thesis studies the relationship between the properties of such composite materials properties and processing parameters and their influence on the mechanical properties and geometric accuracy of parts produced using selective laser sintering (SLS). The

study began on a DTM Sinterstation 2000 machine with a composite material of polyamide 12 filled with glass beads (PA12/GB).

### **1.1. Background of common rapid prototyping and manufacturing (RP&M) technologies**

Historically, the first commercially available rapid prototyping (RP) system was introduced in the late 1980s. RP systems, as the name suggests, were originally employed for producing prototype models. RP was invented as a method to manufacture concept prototypes which may be used in processes such as design, testing and assembly. In this section, a basic overview of the different methods of (RP&M) is presented. The section proceeds with a brief discussion and comparison between these techniques.

In order to create a part by any rapid manufacturing process, it is first necessary to create a 3D drawing of the part using CAD software. The computer then divides the drawing into layers and gives the rapid manufacturing machine a description of each individual layer. The machine then creates these layers, one on top of another, to produce a whole part. Generally, the RM process relies on the discrete slicing of a CAD model, which is then built up in layers from a base material (often a powder or a resin), finally producing a full three-dimensional part without the aid of moulds, substrates or any hard tooling. Fig (1.1) shows the process of data transfer between CAD and the RM system [2], [3].

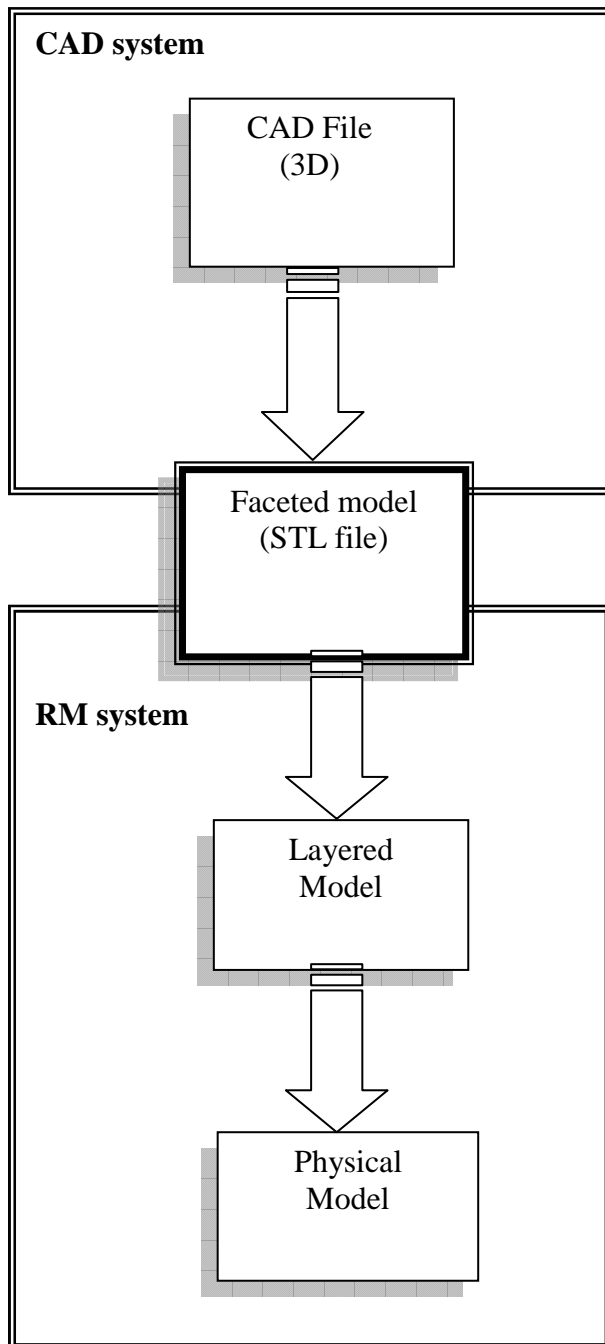


Fig (1.1) Data transfer between CAD and a RM system [3]

However, the success of this new technique marked a revolution in product development and manufacturing. Nowadays, it is evolving rapidly from prototyping towards the manufacture of functional end-user products [4], [5].

RP&M is an important technology and is also known as Layered Manufacturing Technology (LMT), Solid Freeform Fabrication (SFF), Additive Fabrication (AF), Direct CAD Manufacturing, Instant Manufacturing and E- Manufacturing. The term that is commonly used now in the literature is “Rapid Prototyping and Manufacturing (RP&M)”, which denotes the route of rapid prototyping but also explains the extension of where these techniques are trying to go in manufacturing [6].

Virtually, all RP & M technologies provide the ability to fabricate parts with unbounded geometric freedom, which is their most important advantage over subtractive methods and the main reason why they exist. For the time being, there are about thirty rapid prototyping techniques, but only few of them are widely used and dominant in the market, and these are:

- Stereolithography (SLA)
- Selective Laser Sintering (SLS)
- Fused Deposition Modelling (FDM)
- Laminated Object Manufacturing (LOM)
- Inkjet-based systems and three-dimensional printing (3DP).

Each of these technologies has its varying strengths and weaknesses depending on the manufacturing details, type of material and post-processing [4], [7].

The main advantage of RP&M processes is the ability to rapidly produce net or near-net shape parts with varying geometries using a single machine with no part-specific tooling. Among all of its features, the most important is that this technology is fast and flexible in the whole forming process as inferred by its common name, Rapid Prototyping and Manufacturing [4], [8], [9]. New manufacturing technologies offer alternative means of producing prototypes, patterns, models and low volume parts faster and at reduced costs compared to traditional manufacturing processes [10]. However, none of the processes excel in all respects; each process has restrictions imposed by costs, accuracy, materials, geometry and size.

Researchers have conducted detailed research on many important rapid prototyping techniques, which they grouped together based on the similarities of how the materials are added and bonded together. Furthermore, they have explained the basic principles and compared them by considering the cost efficiency, materials used, process time and accuracy [11], [12].

The main difference between these techniques, which are described in some detail below, is the method they use to create the layers. Furthermore, RP&M technologies use different types of materials to produce parts, including thermoplastics, wax, ceramics, metals and most commonly polymers. Fig (1.2) gives an overview of selected RP&M processes available at the moment, whereas a comparison of selected additive processing technologies is presented in Table (1.1).

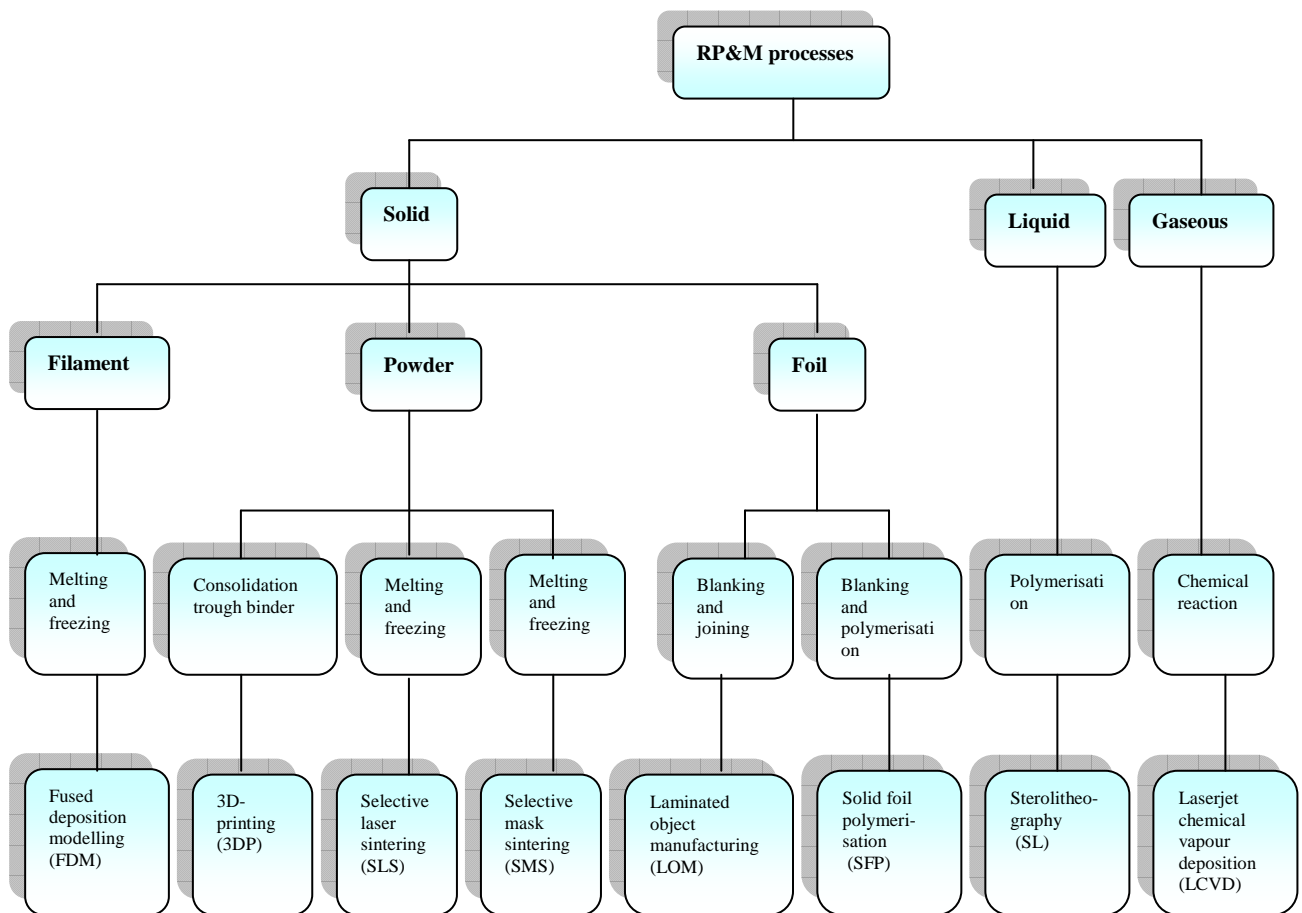


Fig (1.2) Overview of additive processing technologies [13]

Table (1.1) Comparison of selected additive processing technologies [13]

	SLA	SLS	LOM	FDM	SMS	3DP
Materials	photopolymers (acrylic and epoxy resins)	metals, sand, thermoplastics (PA12, PC, PS)	foils (paper, polymers, metals, ceramics)	thermoplastics (ABS, PC, ABS-PC-blend, PPSU)	thermoplastics (PA12)	thermoplastics, cement, cast-sand
Part size (mm)	600x600x500	700x380x550	550x800x500	600x500x600	210x297x600	508x610x406
Accuracy	<0.05 mm	0.05–0.1 mm	0.15 mm	0.1 mm	0.05–0.12 mm	0.1/600x540 dpi
Cooling-off time/ curing time	no cooling-off or curing time up to 30 min	depending on geometry and bulk	depending on geometry	no cooling-off or curing time	depending on geometry and bulk	no cooling-off or curing time
Commercially available since	1987	1991	1990	1991	2005	1998
Costs (T )	from 130	from 150	from 150	from 50	from 150	from 25
Relative sample costs <sup>a)</sup>	medium	medium–high	low–medium	low–medium	medium–high	low

a) Costs depend on the number, size and complexity of samples.

### **1.1.1. Stereolithography (SLA)**

SLA was the first RP&M technique developed and is still the most widely used process. It was developed by 3D systems of Valencia, California, USA, founded in 1986. This process is based on a photosensitive liquid resin which, when exposed to ultraviolet (UV) light, solidifies and forms a polymer. An SLA machine consists of: a build platform, resin bath, recoating blade, ultraviolet laser and a scanning device. A bath of photosensitive resin contains a vertically moving platform. The part under construction is supported by the platform which moves downward by the layer thickness for each layer. A laser beam traces out the shape of each layer and solidifies the photosensitive resin. Fig (1.3) shows the SLA process. The surrounding resin gives no mechanical stability to the built part; hence, a support structure is indispensable for the creation of overhanging layers. In a subsequent process, these structures are removed and the part is completely cured in a UV cabinet [13], [14].

Since it was the first technique, SLA is regarded as a benchmark by which other technologies are judged. In the beginning, SLA prototypes were fairly brittle and prone to curing-induced warpage and distortion, but recent improvements have largely corrected these problems. To broaden the application area of SLA, research and technology development efforts are being directed towards process optimisation. In general, SLA is inexpensive compared to other RP&M techniques; it exclusively uses a light-sensitive liquid polymer which has considerably poor mechanical properties, and so the fields of application are limited to the production of prototypes with reduced functionality [14].

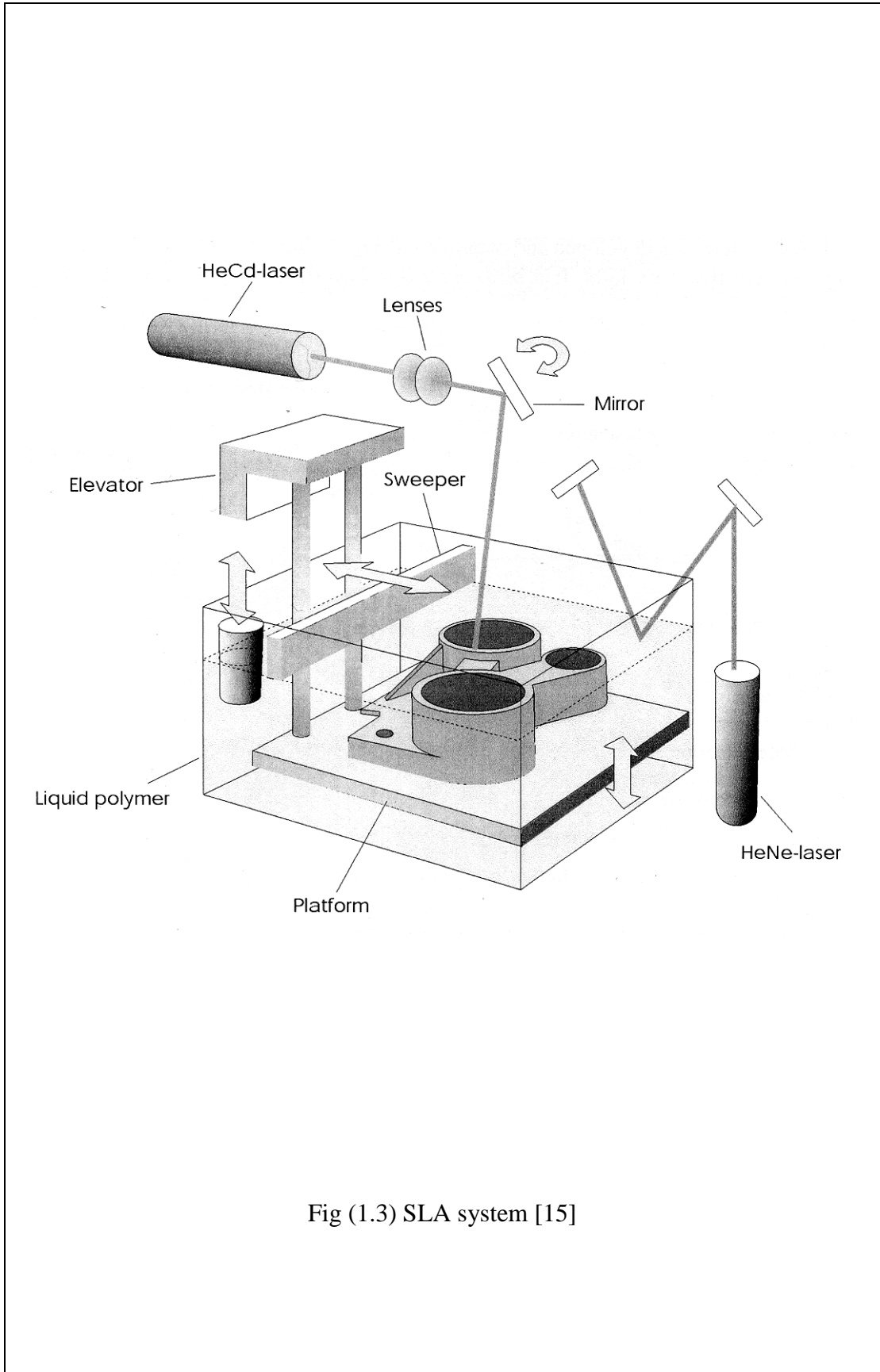


Fig (1.3) SLA system [15]

### **1.1.2. Fused deposition modelling (FDM)**

Fused deposition modelling is an additive manufacturing technology commonly used for modelling, prototyping and production applications. It was developed by Scott Crump in 1988 and was commercialised in the 1990s by Stratasys of Eden Prairie, MN, USA [16]. The system consists of a build platform, extrusion nozzle and control system, which is in its entirety contained within a chamber which is held at a temperature just below the melting point of the plastic. The overall arrangement of FDM is illustrated in Fig (1.4).

In this technique, filaments of heated thermoplastic are extruded from a tip that moves in the x-y plane. The extrusion head deposits very thin beads of material in a controlled fashion onto the build platform to form a layer. The material is heated just above its melting point so that it solidifies immediately after extrusion and cold-welds to the previous layers. The platform is kept at a lower temperature, so that the thermoplastic quickly becomes firm. After deposition of a layer, the platform lowers and the extrusion head deposits the next layer onto the previous one. Supports are built alongside the deposition where required. These are fastened to the part either with a second, weaker material or with a perforated junction [17].

The FDM process creates functional prototypes, tooling and manufactured goods from commercially available engineering thermoplastics, such as ABS, sulfones, polycarbonate, elastomers, and investment casting wax as well as medical versions of these plastics. Unlike some additive fabrication processes, FDM requires no special facilities or ventilation and involves no harmful chemicals or byproducts. FDM machines range from fast concept modellers to slower (high-precision) machines [14].

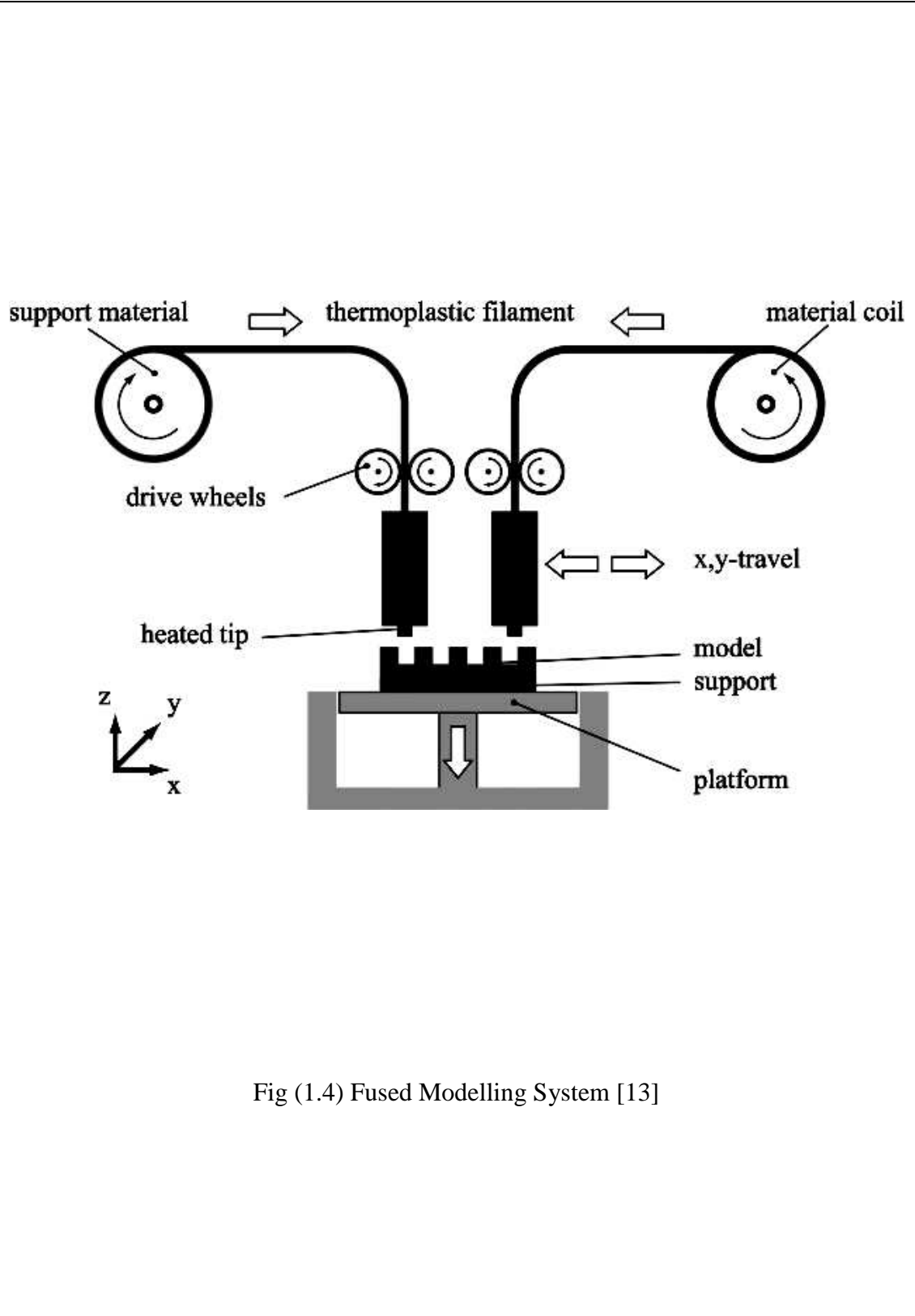


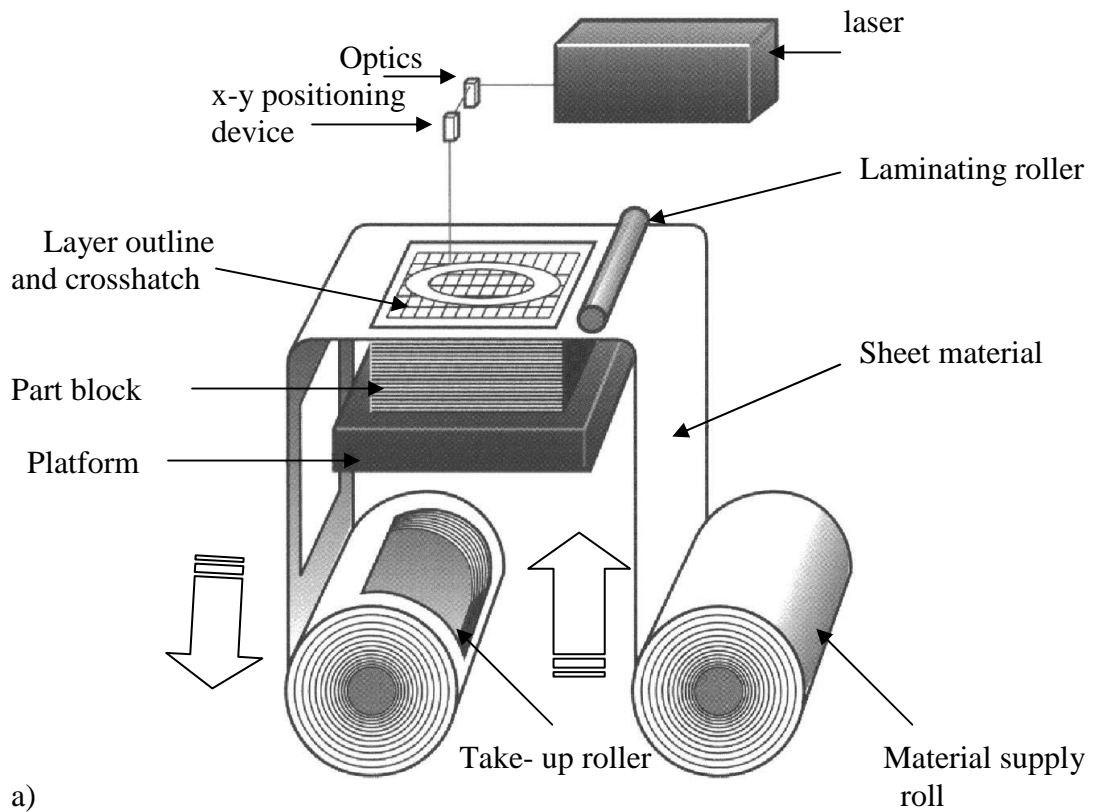
Fig (1.4) Fused Modelling System [13]

### **1.1.3. Laminated object manufacturing (LOM)**

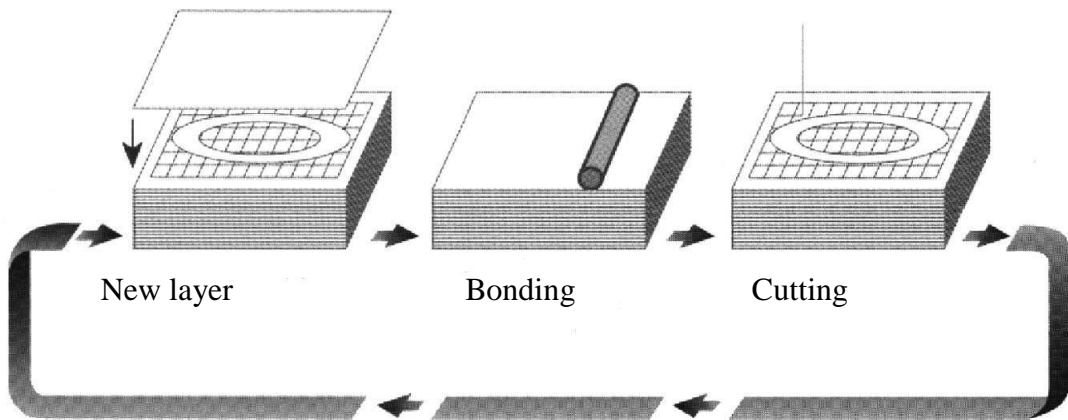
Laminated Object Manufacturing is a process based on the principle of lamination. By definition, laminated object manufacturing (also known as laminated object modelling (LOM) or layer laminated modelling (LLM)), is a hybrid prototyping method, where an additive layer laminate process generates the part from paper, ceramic, polymer or metals followed by a subtractive step which cuts the outline with a CO<sub>2</sub> laser cutter [13]. Fig (1.5-a) demonstrates the mechanism of a LOM machine.

In this technique, shapes are built with layers of paper or plastic. The binding together of the laminates is brought about by means of a thermally activated adhesive. A heated roller is used to glue the laminate to the previous layer. The outline of the part cross-section for each layer determined by the computer-aided design (CAD) file is then cut using a CO<sub>2</sub> laser beam. The laser also cuts the excess material in a cross-hatch pattern. The excess material provides support for subsequent layers. Finally, an overall rectangular outline is cut, freeing the cross-section from the paper roll. The platform moves down and the feed paper advances. The sequence repeats itself until the final layer is completed. The excess material, which is already sectioned into cross-hatched columns, is removed manually at the end of the process [18]. Fig (1.5-b) shows the part building sequence of the LOM process.

LOM is used extensively for tooling and manufacturing by producing patterns and masters for sand casting, investment casting, cavity moulds for injection and tools for thermal forming and prototype stamping (Helisys, Inc, CA USA), [18]. At the present, the commercially available machines for LOM are LOM 1015, LOM 2030 and LOM 2030E.



a)



b)

Fig (1.5) Mechanism of a LOM machine (a); and part building sequence of the LOM process (b), (source: Helisys Inc, CA, USA) [18]

#### **1.1.4. Selective laser sintering (SLS)**

Selective laser sintering (SLS) is a powder-based Rapid Prototyping & Manufacturing method developed at the University of Texas. It was initially commercially available from the DTM Corporation but was later bought out by 3D Systems in 2001. Needless to say, the SLS process, with a humble start in 1987, has grown to become synonymous with Rapid Manufacturing [19].

In SLS, a fine powder is heated with a CO<sub>2</sub> laser which causes sintering of the powder particles and as a result they are mutually bound. The process itself is a very simple, repeatable one. The building of parts, as illustrated in Fig (1.6), is a repeatable two-step process: first; a roller is positioned beside one of the feed beds. This feed bed then raises a set amount and the roller pushes the raised powder across, covering the part bed with a powder layer. Second; with the layer of powder present, the laser starts to etch out the desired shape of the part in the powder, in effect melting the powder. Once this is done, the part bed drops down a set amount and the process continues from the opposite side with the other feed bed raising and the roller distributing another layer of powder over the part bed, followed by the laser etching out the shape. The part is built up in slices with each layer of powder representing a single slice of the part. As the laser sinters the powder, each layer fuses together to give a full solid part. However, the process is self-supporting and parts can therefore be nested together. The selective nature of the laser process enables complex geometries to be achieved without compromising functionality. Finished parts are surrounded by, and often contain, unsintered powder; this loose powder is simply blasted away with an air gun and any post-processing work is then carried out [20], [21].

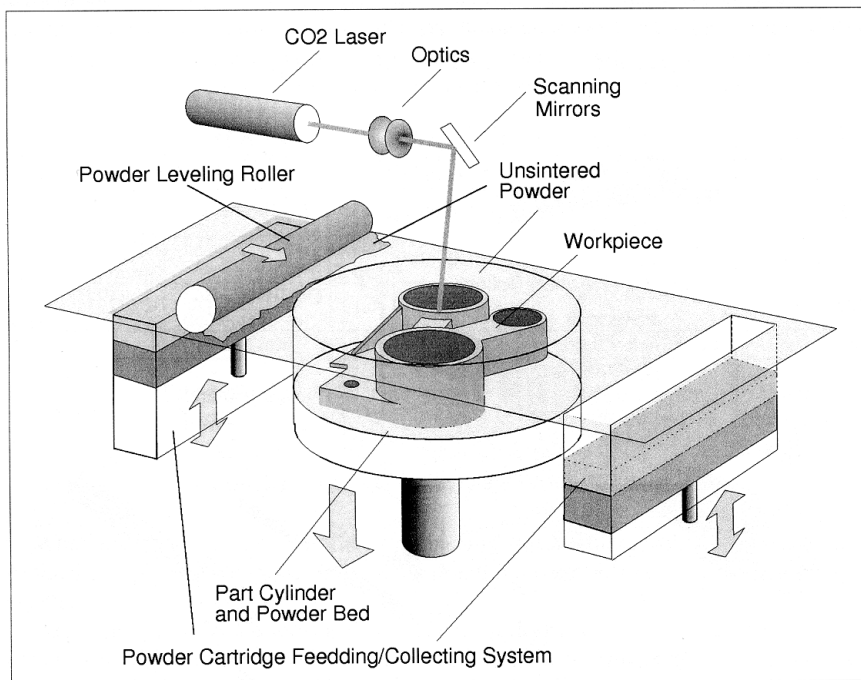


Fig (1.6) SLS process [15]

## 1.2. Motivation

Currently, Additive Manufacturing Techniques are used more and more in many industrial branches, such as aerospace, automotive and biomedical, to manufacture functional parts and end-use products rather than prototypes. Therefore, the parts are required to possess sufficient mechanical properties and quality to meet the requirements needed of their applications. In most cases, however, material properties and functional life of parts made by currently available layer manufacturing techniques seldom meet those of their counterparts produced by traditional polymer processing techniques such as injection moulding. In order to bridge this gap, research efforts have been made to develop existing materials and to find new materials, as these will play a major role in opening access to new fields of application [13], [22], [23].

In this context, traditional pure materials no longer satisfy all the requirements and there is a real need for new composite materials. The development of new polymers is a time-consuming and expensive project. By compounding, blending and reinforcing existing polymers, it is possible to obtain material properties that are not available with conventional single polymer materials, and such properties may be key factors in achieving improved properties and better quality in selective laser sintered components.

The latest trend of research includes:

- the development of new materials,
- advancements in laser technologies, software and computer integrated manufacturing support to Rapid Prototyping and Manufacturing (RP&M),
- development of new methods of layer deposition,
- improvement of the mechanical properties of components as well as their surface quality and geometric accuracy [8], [24].

### **1.3. Aim and objectives**

For Rapid Prototyping (RP) applications, the mechanical properties of the parts produced are often of low importance, as parts are intended simply for short-term visualisation purposes, as well as form, fit and function testing. As the move towards Rapid Manufacturing (RM) continues, with the production of functional end-use components, achieving improved mechanical properties and better quality in SLS components has become increasingly important.

The aim of this research was to study the mechanical properties and geometric accuracy of laser sintered non-commercial composites formed by the incorporation of glass particles into polyamide 12. The primary objectives of this research were:

1. To study the effect of filler content and surface treatment on mechanical properties.
2. To infer the effect of filler content and its surface treatment on geometric accuracy.

### **1.4. Research questions and hypotheses**

In order to produce suitable products (in terms of properties and quality), the main aspects to be considered in SLS technology are the properties of the powders used in the process and the processing parameters. The following research questions for this work were centred on the two major research activities mentioned above:

**Research question 1:** How can the general properties of polyamide 12, as a polymeric material for selective laser sintering, be improved?

**Hypothesis 1:** The properties of polyamide 12 can be improved by creating blends and composites.

**Sub-research question 1.1:** What is the role of the interfacial adhesion between the filler and the matrix in improving the mechanical properties of glass bead-filled polyamide 12 composites?

**Hypothesis 1.1:** The condition of interfacial adhesion controls the local elastic fields and the overall properties of composites.

**Research question 2:** How can the geometric accuracy of sintered component be improved?

**Hypothesis 2:** The geometric accuracy of SLS parts could be improved by controlling the properties of the material and optimising the processing parameters and conditions.

**Sub-research question 2.1:** Under what conditions is it possible to improve the geometric accuracy of selective laser sintered components from PA12?

**Hypothesis 2.1:** Geometric accuracy of selective laser sintered parts can be improved by creating blends.

Table (1.2) lists the correlation between the primary research tasks, the research questions, the corresponding hypotheses and where the research questions were addressed in this research. Answering these research questions is documented in different chapters of the thesis.

Table (1.2) Correspondence between research tasks, hypotheses, and chapters.

Thesis Chapter	Chapter 3	Chapter 4	Chapter 5
Task	Characterisation of materials and determination of process parameters.	Study of the effects of processing conditions, filler content and coupling agents on mechanical properties.	Investigations on the influence of processing parameters and material properties on the curling phenomenon in selective laser sintering.
Hypothesis		Hypothesis 1	Hypothesis 2

## **1.5. Research approach**

After conducting a literature review, which is presented in detail in chapter 2, four tasks were undertaken to help reach the goal of eventually improving the mechanical properties and geometric accuracy of parts produced using SLS, namely:

1. Compounding pure PA12 with glass beads, with different ratios and surface treatment.
2. Carrying out pre-processing studies for the characterisation of composite materials and the determination of process parameters.
3. Production of test samples using the SLS process under varying parameters and conditions.
4. Conducting experiments, measuring and determining the mechanical properties and geometric accuracy of the composite.

## **1.6. Thesis outline**

The specific goal of this research was to study the mechanical properties and geometric accuracy of selective laser sintered parts in non-commercial glass bead-filled polyamide 12 composites with filler particles of different ratios and surface treatments. This thesis is divided into six chapters. A brief overview of the topics covered in each chapter is presented in Fig (1.7). Chapter 1 serves as an introduction to the thesis. The research aim and objectives, as well as research questions are presented in this chapter. In Chapter 2, the literature review, the theoretical background and existing research activities are summarised. The working principles behind the SLS process, apparatus and materials are outlined. Chapter 3 includes details on material preparation and characterisation, such as pre-processing studies, design and fabrication of test samples, characterisation of laser sintered samples.

<p style="text-align: center;"><b>Chapter 1</b></p> <p>Introduction: The need for parts with improved mechanical properties and quality in the SLS process</p>	<p style="text-align: center;"><b>Relevance</b></p> <ul style="list-style-type: none"> <li>• PR &amp; RM techniques</li> <li>• Motivation and importance of the research</li> <li>• Aims and objectives</li> <li>• Research questions and hypotheses</li> </ul>
<p style="text-align: center;"><b>Chapter 2</b></p> <p>Literature review and previous research</p>	<ul style="list-style-type: none"> <li>• Basic information and principles</li> <li>• Fillers and additives</li> <li>• Coupling agents</li> <li>• Existing work and research gap</li> </ul>
<p style="text-align: center;"><b>Chapter 3</b></p> <p>Foundations for the study of mechanical properties and geometric accuracy</p>	<ul style="list-style-type: none"> <li>• Pre-processing studies</li> <li>• Powder and processing acquisition</li> <li>• characterisation of sintered samples</li> </ul> <p>&gt;Forms the basis for the following chapters</p>
<p style="text-align: center;"><b>Chapter 4</b></p> <p>Experimental investigation of the mechanical properties of SLS parts</p>	<ul style="list-style-type: none"> <li>• Processing parameters</li> <li>• Production of test samples</li> <li>• Determination of mechanical properties</li> </ul>
<p style="text-align: center;"><b>Chapter 5</b></p> <p>Experimental study of geometric accuracy of SLS parts</p>	<ul style="list-style-type: none"> <li>• Curling phenomenon</li> <li>• Taguchi method</li> <li>• Design of experiments</li> <li>• Statistical analyses</li> <li>• ANOVA technique</li> </ul>
<p style="text-align: center;"><b>Chapter 6</b></p> <p>Closure of the thesis</p>	<ul style="list-style-type: none"> <li>• Concludes the research work</li> <li>• Recommends future work</li> </ul>

Fig (1.7) Thesis organisation

Chapter 4 represents the backbone of this work, where the effects of processing conditions, filler content and coupling agents on mechanical properties of PA12/GB composites are detailed. Chapter 5 describes an investigation into the influence of processing parameters and material properties on the curling phenomenon which is a major cause of geometric inaccuracies. In this chapter the Taguchi method and ANOVA technique were implemented. Finally, Chapter 6 provides a brief conclusion of this thesis as well as the contributions resulting from the research work and recommendations for future work.

## **Chapter 2 - Literature review**

In this chapter, basic information for the SLS process is presented. The chapter proceeds with outlining the nature of the SLS process as well as the machines and materials involved, and it continues with a review leading into determining of a research gap in the existing literature related to SLS.

### **2.1. Basic information and principles of selective laser sintering**

Selective laser sintering is an additive manufacturing process, in which layers of preheated powder are spread and laser radiation is used to partially liquefy and fuse the powdered material. Sintered material forms parts, whilst unsintered material remains in place to support the structure. During recent years, selective laser sintering has evolved from a RP technique to a promising RM technique.

As with any machine tool, it is important to understand the capability of the selective laser sintering (SLS) process, the equipment and materials in order to produce high quality parts. The SLS systems are intended for sintering a wide range of materials with greatly different properties. This is mainly due to its suitability to process almost any material, such as polymers, metals, ceramics and many types of composites, provided it is available as a powder and that the powder particles tend to fuse or sinter when heat is applied [19].

Fundamentally, selective laser sintering represents such a complex physical process in which many single mechanisms affect each other. The SLS process needs several steps, such as energy input, energy absorption, heating of the powder bed, sintering and

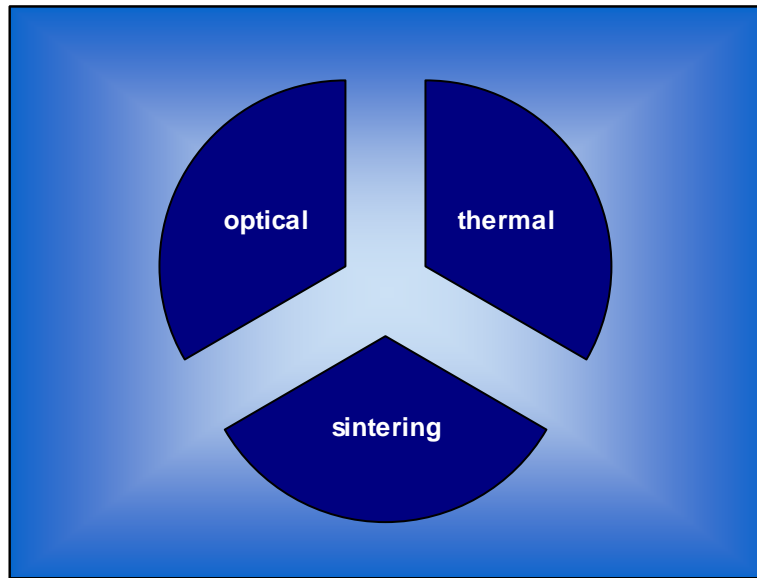
cooling of the sintered part to be complete. The investigation often requires creating submodels which enable a better understanding of partial aspects, then merging these submodels into an integrated model, representing the base for process simulation. Modelling the entire SLS process is very difficult due to the many different physical processes involved and as depicted in Fig (2.1). The integrated model of Sun is composed of three different submodels, whereas it is composed of five in the modified model of Wagner [25].

### **2.1.1. Thermal-physical issues in the SLS process**

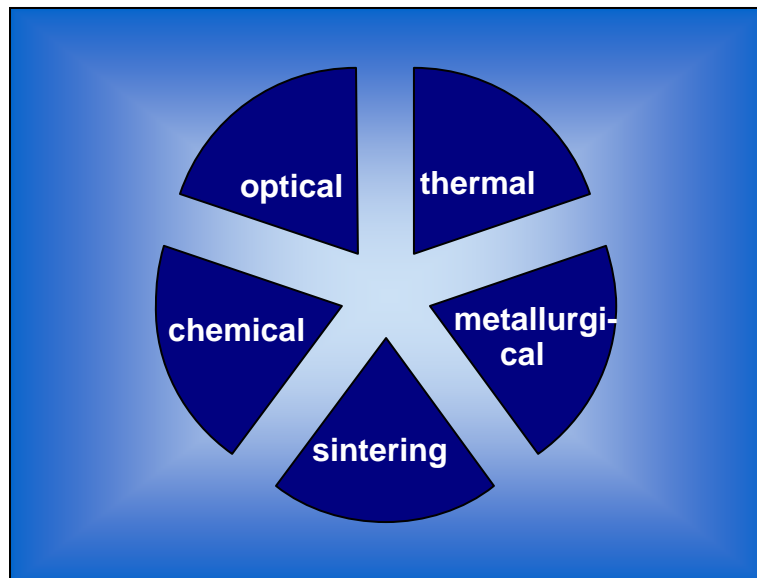
The thermal nature of SLS process influences, to great extent, the bulk powder properties as well as the properties of the sintered parts, such as the mechanical properties, geometric accuracy, surface roughness and other properties; hence, investigating and studying the thermal behaviour of the process, in particular temperature distribution within the build bed, will lead to a better understanding of the problem [26].

Although several physical phenomena are involved in the process, and coupling exists between them, the SLS process is mainly dominated by its thermal nature. It belongs to a three-dimensional unsteady heat transfer problem, which requires the application of several numerical and computational techniques to solve the unsteady state heat transfer equations. However, SLS is a complicated process, involving several physical phenomena, including:

- Heat generation and transfer, including the heating of the powder bed and the cooling of the sintered sample;
- Microstructure evolution, including porosity evolution and phase changes



(a) Three-part SLS Model (Sun)



(b) Five-part SLS Model (Wagner)

Fig (2.1) Comparison between Sun (a) and Wagner (b) SLS process models [25]

- (melting and solidification of the binder);
- Fluid problems (molten binder flowing in the solid lattice);
- Mechanical problems (lack of uniformly distributed thermal strains during the cooling stage may cause residual stresses and distortions of the produced parts).

Accordingly, knowing the temperature distribution and evolution is essential to suitably describe the SLS process. During the SLS process, the powder mixture is irradiated by a moving laser beam. This is an energy transformation process, in which the light energy of the laser beam is converted into thermal energy that causes heating of the powder bed. Understanding the interaction between the laser beam and powder bed will help not only to more easily control the process (leading to more accurate parts with enhanced mechanical properties), but also to define a set of requirements for new sintering powders (leading to easier development of more powders suitable for sintering) [27].

The laser-powder bed interaction can be initially divided into three stages: preheating; melting (with shrinkage) and resolidification. During the preheating period, the powder bed must absorb a significant amount of heat to bring the powder bed surface temperature up to the melting temperature of the low melting point powder ( $T_m$ ) [30]. The influence of the laser on the powder material includes two stages: first, powder surface reflection and absorption to the laser; second, heat conduction in the powder material. All existing models of heat transfer can be divided into three subcategories according to the physical phenomenon they take into account. These subcategories are conduction, radiation and convection [28]. A reflectivity model of powder beds developed by Sun assumes that the absorbed energy is either conducted into the powder

bed or lost through radiation and convection at the surface. Fig (2.2) schematically depicts the interaction between laser irradiation and the powder bed.

#### **2.1.1.1. Heat absorption of the powder bed during the SLS process**

In SLS, the processing medium is composed of powder particles, not a continuum. The thermal properties of the powder bed change as the powder is heated and as coalescence between particles occurs. During the scanning process in SLS, material properties change due to their dependence on temperature and degree of fusion taking place. Powder changes from the solid phase to the liquid phase and then back to the solid phase. These phase change processes are accompanied by both absorption and release of thermal energy. Therefore, the thermal properties are a function of the powder bed properties, temperature and time. The powder under the laser absorbs the energy where the temperature rises. It conducts heat exchange with the surrounding sintered powder as well as loose powder according to the thermo- mechanical law, which consists of conduction, radiation and convection [28], [29].

The laser beam is a moving heat source, whose reaction time with the powder is less than 1 ms. During the heating process, the thermal physical properties and parameters of the powder, such as specific heat and thermal conductivity change with the temperature, which is changing with time. The laser sintering process of polymer composite powder is dynamic and unsteady [29].

During selective laser sintering (SLS), the optical properties of the powder material will influence the heat transfer within the powder bed and hence its fusion behaviour. When the laser beam strikes the powder bed, part of the laser energy is reflected and

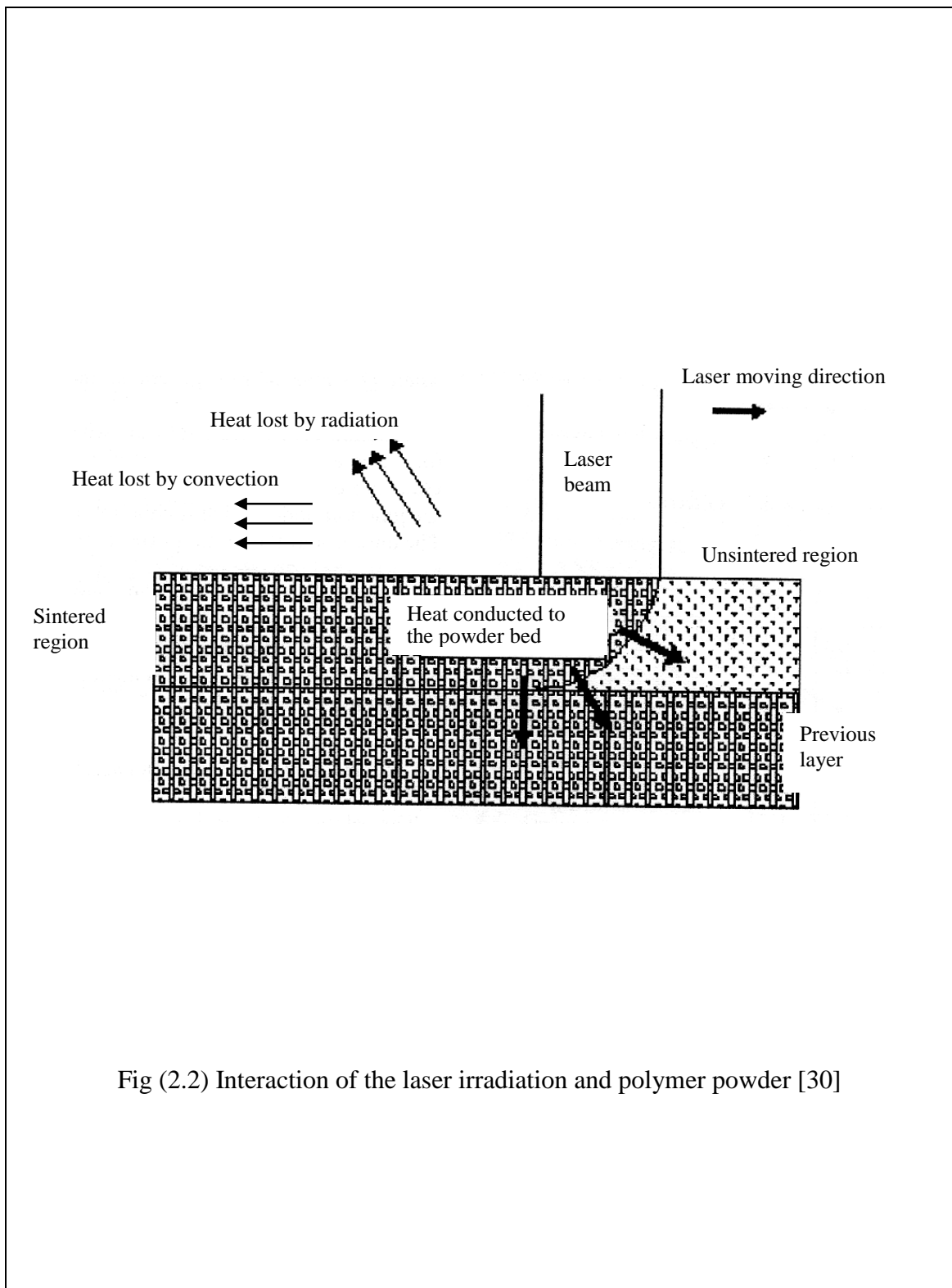


Fig (2.2) Interaction of the laser irradiation and polymer powder [30]

the rest is absorbed by it. The transmittance of the powder affects the energy distribution within the powder bed. For powders with a low transmittance, most energy will be absorbed near the surface, and the thermal gradient along the z-axis, into the powder, is large. It has been reported that the maximum absorption takes place near, but not exactly on, the powder bed surface [31].

### **2.1.1.2. Thermal diffusivity, thermal conductivity and specific heat**

The aim in this section is not to evaluate the exact thermal property values of the processing material, but to understand if those aspects can be technologically important in the definition and control of a selective laser sintering process, where it is generally believed that thermal properties play a central role during SLS of composite materials. The thermal diffusivity  $\alpha$  [ $\text{m}^2/\text{s}$ ], thermal conductivity  $k$  [ $\text{W}/\text{mK}$ ] and specific heat  $c_p$  [ $\text{J}/\text{kgK}$ ], namely the thermal properties, are the three most important physical properties of a material that are needed for heat transfer calculations. Those properties are evident when heat is added or removed from a material and are related by:

$$\alpha = \frac{k}{\rho c_p} \quad (2.1)$$

Thermal diffusivity ( $\alpha$ ) is a measure of the rate of heat propagation through a material. It is an important property in all problems involving non-steady state heat transfer, which happens during heating and cooling of a material. The thermal conductivity ( $k$ ) is described as a measure of the ability of material to transfer thermal energy by conduction. The specific heat ( $c_p$ ) is the amount of heat per unit mass required to increase the temperature by one degree Celsius, and therefore is associated with the energy consumption in the heating processes [32].

It is a well-known fact that the thermal conductivity of a powder bed can vary from point to point depending on the local temperature as well as the conditions of contact between particles and the local density [33]. Porous media are most frequently met in many engineering fields and, in particular, in rapid prototyping and manufacturing. The thermal conductivity of porous media is one of the important properties for numerical simulations. The various heat transfer mechanisms in multi-porous bodies have been identified and discussed by Yagi and Kunii and by Kunii and Smith, who have developed a simplified equivalent physical structure and a corresponding mathematical expression for the apparent conductivity in terms of porous-structure parameters and the conductivities of the solid and gas phases. The following heat transfer mechanisms, shown schematically in Fig (2.3), exist in a multi-porous body:

1. Direct solid conduction through areas of actual particle-to-particle contact
2. Direct gas conduction through areas of pore-to-pore communication
3. Series conduction through solid and gas
4. Particle-to-particle radiation across a gas layer
5. Pore-to-pore radiation by passing particles

Of these mechanisms, 1, 2, 3, and 5 may be considered to be in parallel, and 4 to be in parallel with the gas part of 3. Once these heat transfer mechanisms have been identified and their relationships noted, it is possible to formulate a simplified physical model of a multi-porous body and its resulting heat transfer properties [34].

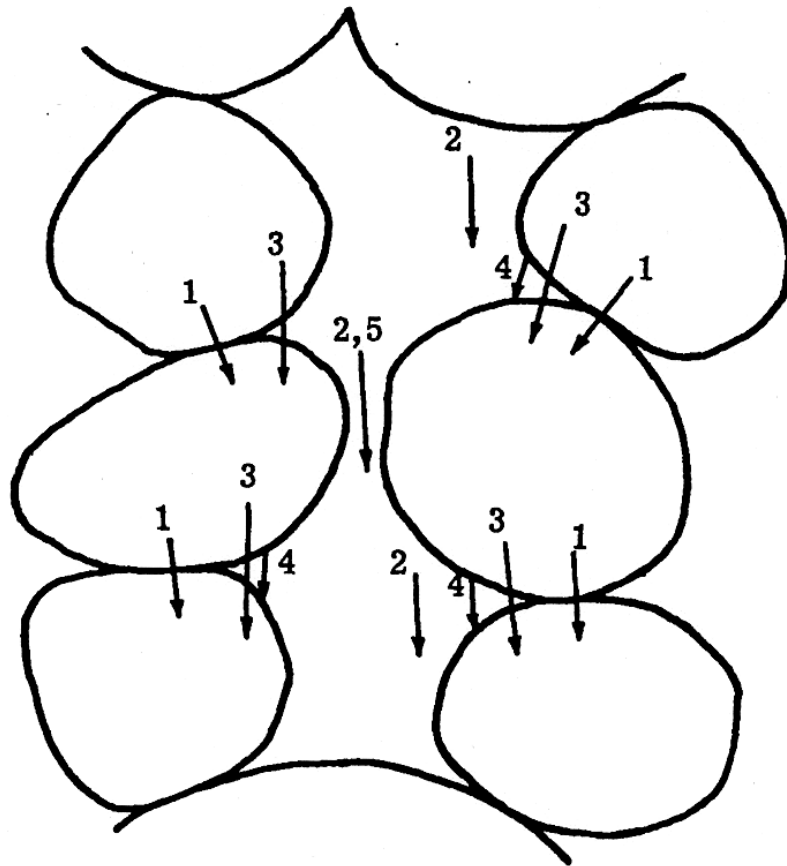


Fig (2.3) Heat transfer mechanisms in a porous body [34]

1,2,3 ... Conduction  
4,5 ... Radiation

The prediction of the thermal conductivity of heterogeneous or composite materials comprises a significant portion of the heat transfer literature, and a significant number of effective thermal conductivity models have been proposed. Thermal property evaluation is very important in the prediction of the melting process of the powder bed, where there are three components in the powder bed: low melting point powder, high melting point powder and gas (or gases) [35], [36].

### **2.1.2. Processing parameters and operating cycle of the SLS process**

The most important factors of the laser sintering process can be classified into material, machine, part, laser, environment and exposure. Therefore, these factors have to be taken into account for the system and materials. Beyond this, process-specific factors and the selection of the material components e.g. mean density or optical characteristics have to be considered and possibly adopted. The most important process-controlled variables are:

- Laser energy
- Layer thickness
- Scan velocity
- Beam offset
- Exposure strategies

The laser energy is one of the most important process variables, since by increasing the laser energy higher temperatures in the powder can be achieved. Thus, the proportion of the liquid phase, the density and the mechanical strength of the laser sintered part increases. The beam offset and the scan velocity have a crucial influence on the build speed, the strength of the part and, beyond that, it also determines together with the

particle size of the applied powder the surface roughness of the horizontal surfaces [37].

The operating cycle of the SLS process is almost the same in all SLS machines. A full build cycle of the SLS process consists mainly of three stages:

(1) Warm up stage: The chamber is inerted with nitrogen gas, the process chamber and feed material are warmed up and a number of layers are spread without being sintered. Depending on the material being used, this stage takes between one and two hours.

(2) Build stage: The part is built. The time to build a single layer using the SLS process is influenced by two time elements: the time taken to spread a layer of powder and the time taken for the laser to scan and sinter the appropriate area. The first element remains constant through a build cycle, while the second factor is a function of the size of the area to be scanned.

(3) Cool down stage: The chamber is returned to ambient temperature in a controlled way. This stage takes between one and three hours [38].

### **2.1.3. Selective laser sintering machines**

In this section, some general information about the machine that was used for the research is presented. Along with that information, the purpose of the machine and what it lends to the research is explained. At the heart of this research work is the SLS machine that processed the material from which the parts were made and produced the numerous test parts to be measured. The first prototype selective laser sintering (SLS) machine was created at the University of Texas at Austin, Texas, USA in 1986. In 1987, the DTM Corporation was founded and produced the SLS Model 125 [38]. Nowadays, SLS machines are produced by two major manufacturers; EOS GmbH

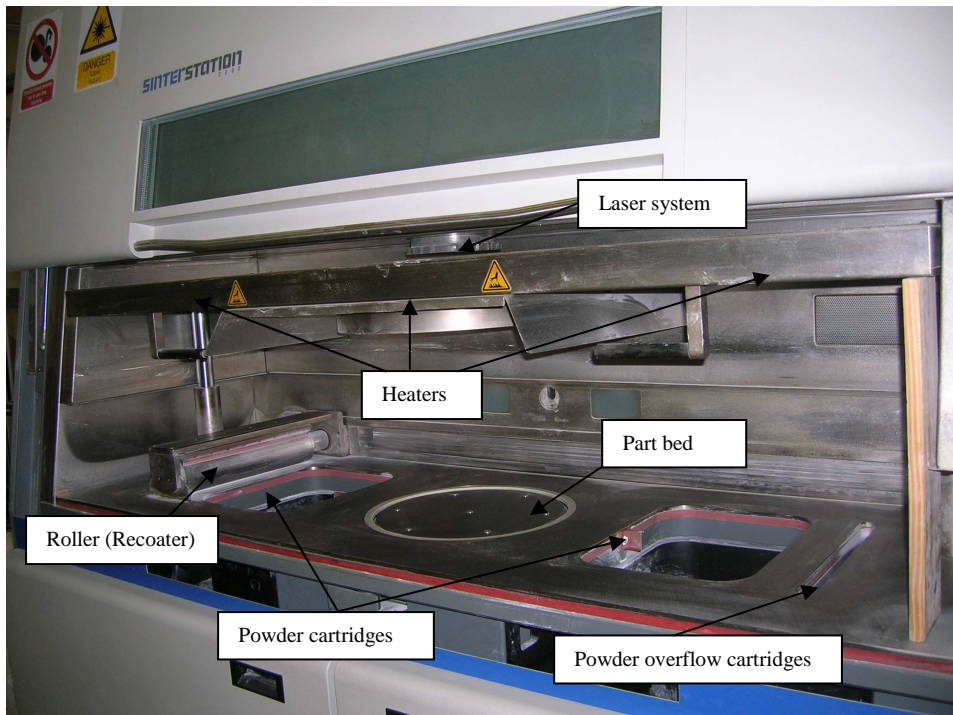
based near Munich, Germany and DTM (now owned by 3D Systems Inc. of California). Commercial SLS machines (DTM and EOS) are all equipped with CO<sub>2</sub> lasers with maximum power ratings between 50 and 200W. Besides the HQ 2500, the EOSINT P 700, a production version from DTM, known as the Sinterstation 2000, was installed in the Department of Manufacturing Engineering Centre at Cardiff University in 1997. This machine was used in the current work, both for study and research.

In general, a typical SLS machine includes a laser source, optics, a powder laying unit (recoater), powder bins and a platform all within a build chamber (Fig. 2.4). The main units of Sinterstation 2000 are [38]:

- 1- Powder engine/process chamber/laser scanner in which the SLS build process is carried out
2. Atmospheric conditioning unit (ACU) containing the cooling, air conditioning and gas insertion systems required by the process chamber
3. Controls cabinet containing the computer, programmable logic controllers, power systems, modem and Ethernet connections
4. Rough breakout (RBO) station for breaking out the sintered parts from the cake of unsintered powder at the end of the run, Fig (2.5)



a)



b)

Fig (2.4) The Sinterstation 2000 (a); build chamber (b)



Fig (2.5) Breakout station

#### **2.1.4. Materials available for the SLS process**

There are various grades of materials used in SLS, each with their own characteristics, but each is used in the same way within the SLS machine. In order to produce suitable products the main aspects to be considered, first and foremost in SLS technology, are the properties of the powders used in the process and processing parameters.

Polymers were the first material to be processed by SLS, and this is because there are several properties of polymers that make them easier to process by SLS than other materials. Polymers have a relatively high viscosity in the liquid state, relatively low surface energy, low reactivity with most gases and low thermal conductivity. However, the effect of the properties of the polymer materials, such as molecular weight, molten viscosity, crystallisation rate and the particle size of the powder, on the mechanical properties and the quality of selective laser sintered parts is one among many important factors which should be highly considered when characterising polymers in selective laser sintering [39], [40]. Hence, the requirements for maximum suitability of a polymer for laser sintering should be:

- 1- A very high difference between melting point and solidification point.
- 2- A very high enthalpy of fusion.

The explanation is that, since in pure polymer powders the solidification point is determined by basic physical data, an increase of the melting point by forming a new crystal modification implies a great advantage. The larger the difference, the smaller the shrinkage on solidification, leading to more precise achievement of the desired dimensions of the shaped article. A very high enthalpy prevents powder particles located in the neighbourhood of the particles affected by the laser beam from beginning to melt as a result of unavoidable conduction of heat, which results in sintering outside

the desired area. The suitability of polymer powders is a function of their physical characteristics as well as their chemical nature [41]. Materials currently available for SLS include:

### **Polycarbonate (PC)**

Powders of polycarbonate are able to produce parts with very good dimensional accuracy, feature resolution and surface finish, but they are only partially consolidated. As a result, the parts produced from PC are only useful for applications that do not require part strength and durability [42].

### **Nylon**

Nylon (polyamide PA) is an aliphatic polyamide with a low monomer content in melt-equilibrium, low moisture absorption and low density compared with other polymers. It is not sensitive to stress cracking and has excellent impact strength at dry or low temperatures, which makes this material desirable for rapid prototyping purposes. It is the most commonly used material in SLS, producing parts with good long-term stability, strength and durability required for functional testing and end-use. It can be sintered to fully dense parts with mechanical properties that approximate those of injection moulded parts [43].

### **Glass-filled nylon**

Glass-filled nylon powder is characterised by excellent stiffness in combination with good elongation at break. Still better parts are obtained by using glass bead-filled nylon powder for use in deep drawing dies and within the engine area of cars. Glass bead-filled nylon provides greater rigidity and is perfect when prototyping rigid parts

intended for production in advanced engineered thermoplastics. Adding the filler (glass beads and not fibre) to nylon predominantly increases the stiffness, but not the strength of the part [44].

**Alumide™:**

Alumide is a metallic grey aluminium-filled polyamide 12 powder, which is characterised by its high stiffness, excellent dimensional accuracy, metallic appearance and good post-processing possibilities. The surfaces of Alumide parts can be refined very easily by grinding, polishing or coating. The machining of Alumide laser-sintered parts is simplified through the cut breaking effect of the aluminium filling. A typical application for Alumide is the manufacture of stiff parts for applications in automotive manufacture, for tool inserts for injecting and moulding small production runs, for illustrative models, for education and jig manufacture, among other aspects [45], [46].

**Windform™:**

This is a light grey composite polyamide-based material with added aluminium and glass, with improved heat deflection temperature and superior stiffness, excellent surface finish, wear resistance and first-rate detail reproduction. It offers an attractive, gleaming metallic look, appreciable in many applications, such as in wind tunnels, in design and functional applications. Moreover, it absorbs slightly less liquid and is particularly suitable for applications which require a superior surface finish [47].

## 2.2. Fillers

Although the use of fillers in the plastics industry has been popular for several decades, there is still a very large interest in all fields for the development of composite materials with enhanced properties. Especially, high tech products accelerate the research of advanced composites, which demand extensive knowledge of all the factors that determine the final properties of polymeric composite materials.

Modification of organic polymers through the incorporation of fillers yields, with few exceptions, multiphase systems containing the filler embedded in a continuous polymeric matrix. The resulting mixtures are characterised by the unique microstructures or macrostructures that are responsible for their properties. The primary reasons for using fillers are:

- property modification or enhancement
- overall cost reduction
- improvement and control of processing characteristics
- reduced shrinkage
- improved crack resistance
- control of viscosity

Particle-filled polymer composites have become attractive owing to their low cost and widespread applications in the household, automobile and electrical industries. In general, the mechanical properties of particulate-filled polymer composites depend strongly on the size, shape and distribution of filler particles in the matrix polymer, and good adhesion at the interface surface [48], [49].

### **2.3 Coupling agents**

Improving the interfacial adhesion between the inorganic particles and the polymer matrix by modifying the filler surface is essential to achieved toughening of polymer-matrix composites. The adhesion between polymeric materials and particulate fillers is usually weak due to poor compatibility of the polymer with the mineral surface. In order to increase the adhesion between these two unlike surfaces, it is logical to use a third material containing special functional groups which can adhere to both surfaces. To improve compatibility, adhesion promoters are commonly required [50] [51], [52]. The main role of coupling agents is to promote adhesion which will result in developments in mechanical properties. The coupling agent functions as a molecular bridge at the interface of dissimilar polymer binders and fillers, resulting in the formation of covalent bonds across the interface, which subsequently improves the properties of the composite system [52]. The most widely used coupling agents are the silane coupling agents.

### **2.4. Interfacial adhesion**

Adhesion is a complex phenomenon related to physical effects and chemical reactions at the interface. Interfacial bonding conditions are one of the most important factors that control the local elastic fields and the overall properties of composites. Imperfect interfacial bonding may be due to damage in a very thin interfacial layer known as the interphase or interface. The term “imperfect interface” is used to characterise a situation in which the displacements are discontinuous at the interface between the inclusion and the matrix. However, adhesion can be defined as a connection between two materials which can transfer forces. This adhesion can sometimes be achieved or improved by the use of an adhesive or coupling agent [53], [54], [55].

Basically, the properties of heterogeneous polymers composites are determined by four factors, namely: component properties, composition, structure and interfacial interactions. Interfacial adhesion is extremely important in all composites used in load-bearing applications. Improper adhesion leads to the de-bonding of the components and the development of voids which may merge into large cracks and lead to the premature failure of the part.

The importance of interfacial adhesion is shown by the fact that a large number of surface modification techniques are used in practice for all kinds of composites. According to some authors, interfacial adhesion is the decisive factor in determining the properties of composites. Appropriate adjustments of interphase properties and adhesion strength are the most important conditions for achieving acceptable properties. The debate also continues on the most proper adhesion strength in composites. Very strong adhesion is claimed to lead to stiff and brittle composites, while in the case of weak adhesion, the components de-bond under the effect of external load with the consequences mentioned above. Medium or appropriate strength is claimed to be the most advantageous; however, a quantitative value is never assigned to this claim [56].

In this context, an enhancement of mechanical properties can only be achieved by the addition of a rigid filler if sufficient interfacial coupling exists for stress transfer between the matrix and the particles. The interfacial adhesion can sometimes be improved by the use of coupling agents. Great numbers of fillers are already provided during fabrication with a coupling agent developed for the adhesion with a particular matrix polymer.

### **2.4.1. Wettability**

When two dissimilar materials are brought into intimate contact, a new interface is formed at the expense of the two free surfaces in air. The nature of the interaction at the interface determines the strength of the bond, which forms between the matrix and the filler. The extent of these interactions is greatly determined by the wettability of one phase by the other. The first criterion for good adhesion is intimate contact, which is good wetting of the surface. However, wetting is a necessary, but not sufficient, condition for good adhesion [57].

### **2.4.2. Mechanisms of adhesion**

Adhesion is a phenomenon by which two materials form a contact region that is able to sustain or transmit stress. There are a variety of mechanisms or factors that contribute to the adhesion between two materials. These include interfacial Van der Waals forces that lead to adsorption; interdiffusion of molecules across the interface; interfacial chemical bonding and/or hydrogen bonding; mechanical interlocking and electrostatic interactions [50].

However, mechanisms of adhesion are only operational if and only if effective wetting is present between the phases. Adhesion generally occurs when the filler and the matrix are held together by interfacial molecular contact in such a way that a unit is formed. Following the outline of the review articles on the science of adhesion, four main mechanisms of adhesion can be distinguished [51], [53]:

- 1) Mechanical
- 2) Chemical
- 3) Diffusion

#### 4) Electronic

Basically, mechanical interlocking action occurs when the matrix bonds both mechanically and chemically, onto the surface of the filler which contains pores, holes, crevices and voids and solidifies during the solidification stage. In this manner, it acts as a mechanical anchor. The penetration of the polymer melt or the coupling agent into the irregularities of the filler surface can establish mechanical interlocking, where the surface roughness greatly affects the interfacial area between the matrix and the filler. However, the fact that good adhesion is also observed between smooth surfaces shows that this theory is not generally applicable [53], [54].

The adsorption theory of adhesion is the most generally accepted theory in the field of composite materials. This theory proposes that the materials will adhere because of the forces acting between the atoms in the two surfaces. Two types of forces may be present. The strongest or primary interfacial bonds are of a chemical nature (ionic, covalent or metallic bonds). The formation of covalent chemical bonds across the interface takes place between the matrix and filler surfaces. This type of bonding is the strongest and most durable. The secondary, weaker bonds, also referred to as physical interactions, cover the ever-present Van der Waals forces, dipole-dipole interactions and hydrogen bonds which are the strongest of the secondary bonds and may play an important role in the case of a polyamide 12 matrix [58].

The diffusion theory of adhesion explains adhesion of high polymers to themselves and to each other by mutual diffusion of polymer molecules across the interface. This theory could only be applicable to the coupling agent/matrix interface if the coupling agent is a macromolecule or becomes one during the coating or extrusion process by

auto-condensation. Moreover, this theory requires the two components to be mutually soluble and to have sufficient mobility [58].

The electronic theory suggests that adhesion can be obtained by electrostatic forces arising from contact or junction potentials between two components with different electronic band structures. This theory seems to be less useful for explaining the interfacial adhesion in particle-reinforced composites because at least one of the two components should have metallic properties.

## **2.5. Previous work on the relationship between part properties, fillers and process parameters in SLS**

Processing parameters and composite material properties were the two issues which were initially explored to study the influence of filler content and its surface treatment on the mechanical properties and geometric accuracy of laser sintered polyamide 12 with glass beads. Previous attempts to improve the mechanical or physical properties of polymeric laser sintered parts have involved reinforcing them with micron-sized inorganic fillers, such as glass beads, silicon carbide, hydroxyapatite, aluminium powder, or even nano-sized fillers such as clay, nanosilica and nano- $\text{Al}_2\text{O}_3$  [4], [24]. However, the mechanical properties of the produced part were not solely controlled by the base material itself; they were also influenced by the production process. Likewise, to produce a high quality selective laser sintered part (in terms of dimensional and geometrical accuracies), the process parameters need to be tuned up and optimised according to powder properties and the requirements of application [59], [60], [61].

The issue of achieving geometrically accurate and mechanically robust parts by the SLS process has been studied by a number of researchers in an attempt to enhance their mechanical properties and quality and to enable their use in wider RP&M applications. In conjunction with the development of the research presented in this thesis, the following research areas were reviewed.

Several attempts have been made to study the effects of process parameters and filler content on the mechanical properties of selective laser sintered parts. This work is concerned with the mechanical properties and geometrical accuracy of parts sintered from non-commercial glass bead-filled polyamide 12 composites (PA12/GB).

### **2.5.1. Mechanical properties of selective laser sintered parts**

The influence of fabrication parameters on the material properties of SLS parts has been investigated by Gibson and Shi [62]. In achieving this, they have carried out experiments measuring the tensile strength and density of sintered samples produced from fine nylon in different orientations with different fabrication parameters. They showed that mechanical properties vary when different powders are used if similar process parameters are selected. The porosity decreases and mechanical properties increase when laser power increases and the scanning speed and scan spacing decrease. They concluded that, besides powder material properties, fabrication parameters, orientation and building position also influence the mechanical properties, where some of these can be improved with post-processing as a compensation for some limitations of the SLS process.

Wong et al. [63] studied the SLS of blended powder from PA12 and organically modified rectorite (OREC). The effects of OREC on the sintering parameters and mechanical properties of the sintered samples were investigated. Compared with pure PA12, the results showed that the laser power needed for sintering greatly decreased and the mechanical properties of the sintered samples were considerably improved with the addition of OREC (0-5 wt%). Moreover, they concluded from the XRD and SEM results that rectorite was intercalated by PA12 and PA12/ORCE nanocomposites were formed.

Experimental investigations into the production of particulate silicon carbide (SiC) polyamide matrix composites using the selective laser sintering process have been conducted by Gill et al. [64]. SiC grit was blended with Duraform polyamide to produce a powder blend at a composition of 50 by weight of grit to polyamide. A full factorial experimental approach was applied to examine the effects and interactions of key fabrication parameters, with regard to the tensile strength and porosity of the composite SLS produced samples. Their investigation revealed that the optimum energy density for producing samples of maximum strength was independent of the initial powder blend composition. In another paper by the same authors [65], dealing with the same composite, they showed that the tensile strength of the samples was dependent not only on individual parameter settings but also on the interaction and combination of fabrication parameters. Furthermore, they reported that the effects of parameter changes are related to the initial powder blend composition and energy density, with lower polyamide content resulting in greater sensitivity to process parameters.

For SLS applications, Mozzoli et al. [66] developed and characterised a new aluminium-filled polyamide powder from a rheological point of view. They reported that the new material allowed SLS manufacturing of models with considerably high dimensional accuracy, strength and resistance to mechanical stresses. Moreover, the aluminium-filled polyamide material promised a smoother surface, better finishing properties, excellent accuracy and high stiffness in the direct manufacturing of metallic-looking plastic parts.

A study of mechanical anisotropy due to build orientation and the end-of-vector effects in the laser sintering process was presented by Ajoku et al. [67]. In their investigation, they used tensile, flexural and compression testing methods to assess the changes in the mechanical properties of laser sintered nylon 12 samples. The results from the tests showed that the build orientation of the samples had an effect on the mechanical properties obtained. They reported that differences in the tensile strength, modulus and flexural strength of samples built in the x, y and z axes were observed. They concluded that the orientation of a part in the laser sintering machine is the primary variable which affects its mechanical properties and the end-of-vector effect is a secondary factor which is more prominent in parts with small x dimensions.

Another paper investigating the mechanical properties of parts produced via SLS has been published by Caulfield et al. [59]. They investigated the influence of process parameters (such as energy density, distance between scan lines and the speed of the laser beam) on the physical and mechanical properties of polyamide 12 parts. They performed tensile tests with a video extensometer to determine the mechanical properties according to the standard ASTM D638 and compared all the results for 0 and

90 degrees of orientation of the parts. They took some SEM pictures to visualise the fracture surfaces. The results of the tests showed that, as they related to the energy density level, the material properties of samples generated at lower energy densities were porous, weak and anisotropic, but became more isotropic, solid and stronger as the energy density level increased. They generally showed that the mechanical properties of parts are highly dependent on process parameters and part orientations.

Salmoria et al. [68] investigated the processing of blends of polyamide 12 (PA12) and high-density polyethylene (HDPE) by selective laser sintering using a CO<sub>2</sub> laser. They studied the effect of components on elastic/plastic behaviour and evaluated the mixture composition, processing conditions and their influence on the dynamic- mechanical properties of the fabricated samples. The study demonstrated that the average value of the elastic modulus of PA12 samples was higher than that of the HDPE samples. Moreover, it showed that the low values of ultimate strength were an indication of low chemical affinity between matrix and filler. On the other hand, the creep and fatigue behaviour also changed as a function of the component quantities and the viscous-dissipative behaviour of HDPE phase was observed, providing significant plastic deformation and toughness.

Majewski et al. [69] have studied the effect of the degree of particle melt on mechanical properties in selective laser sintered nylon 12 parts. They investigated the use of a novel method of interpreting a DSC curve to indicate the level of melting within semi-crystalline selective laser sintered parts, or the degree of particle melt (DPM). They confirmed that changes in build parameters in the SLS process can cause variations in the DPM. Furthermore, the results shown that, as the DPM increases, the tensile

strength and elongation at break also increase, whilst there is no significant effect on the Young's modulus. They concluded that their findings will enhance the ability to optimise and predict the properties of the SLS process; furthermore, they showed that the measurement of DPM has potential for use as a tool to enable the analysis of new materials and machines by indicating how the material has melted.

Majewski et al. [23] proposed a method of off-line casting, where the tensile strength of parts produced (from Duraform GF, which consists of a mixture of 50% nylon 12 and 50% glass filler) using this method were compared with the properties achieved in selective laser sintered parts produced with the same materials. For materials tested, the results demonstrated that the casting method provided an acceptable correlation with the properties of the selective laser sintered parts, and the use of a manual casting method can provide a relatively good indication of some tensile properties and help with assessing the properties of selective laser sintering material without the requirement to produce a full build.

Experimental investigations have been made by Jain et al. [70] to understand effect of delay time on part strength in selective laser sintering. Tensile samples of polyamide (PA 2200) material as per the ASTM standard were fabricated on an SLS machine while keeping the delay time range constant for all the samples. An optimum delay time range was found experimentally. They successfully developed an algorithm and implemented it to predict part orientation for improved part strength by considering delay time. They concluded that comparatively higher strength can be achieved by orienting the part so that the maximum area on all layers falls within the optimum delay time range.

The relationship between strength and the various process parameters, namely layer thickness, refresh rate, part bed temperature and hatch pattern have been investigated by Jain et al. [21]. Experiments were conducted based on the Taguchi method using an L16 modified orthogonal array. Tensile samples of polyamide (PA2200) material as per the standard ASTM D638 were fabricated on an SLS machine with constant energy density and tested on a universal testing machine for tensile strength. The experiments revealed that there was small range in part bed temperature within which parts with desirable quality could be produced. They concluded that the results of their work will help to understand the consequences of varying these parameters in an SLS process on the quality of parts, production costs and processing time.

An experimental investigation was carried out by Jain et al. [71] to study the feasibility of processing blended powder of polyamide (PA) and organically modified nanoclay using selective laser sintering. The effect of nanoclay on the sintering parameters and mechanical properties of the sintered samples were studied. The relationship between the mechanical properties and a few important process parameters, namely beam speed, laser power and scan spacing, was studied using Taguchi's L9 orthogonal array. The authors found that the addition of clay did not improve the mechanical properties of the laser sintered polyamide; rather, it resulted in decreased mechanical properties. These results suggest that it is feasible to process PA2200/clay blended powder using an SLS process; however, for improving mechanical properties using such materials in an SLS process, further investigations need to be made to find suitable conditions in view of the partial melting of polyamide particles and the very short period of time involved in processing.

Yang et al. [72] have developed a dissolution-precipitation process to produce polyamide12/potassium titanium whisker (PTW) composites for applications in SLS. They reported a new method for preparing polyamide 12 (PA12)/PTW composite (PPC) powders for applications in SLS that uses a dissolution-precipitation process. The sintering characteristics and mechanical properties of the PA12 powder, the glass-filled PA12 (GF-PA) and PPCs were compared. Based on their results, they reported that the sintering characteristics of PPCs were as good as those of PA12 and the mechanical properties were greatly improved by PTW. The tensile strength, bending strength and bending modulus of the composites containing PTW were much higher than those of PA12 and GF-PA. PTW was much better than glass as a filler material for PA12 in SLS. They concluded that fillers significantly contribute to improving the tensile strength, bending strength and bending modulus of PA12 composites with little effect on the impact properties.

Goodridge et al. [24] have presented initial research into the reinforcement of laser sintered polyamides with carbon nanofibres (CNF). They investigated the effects of CNF addition on the processing parameters and mechanical properties of laser sintered parts and demonstrated that CNF can increase the strength of a base polyamide 12 laser sintering polymer prepared using a melt-mixing technique. After the characterisation of the polymer nanocomposite parts and dynamic mechanical testing, they reached the conclusion that the nanofibres were well-dispersed within the polymer matrix and increased the storage modulus compared to the base material. Improvements to the production of the nanocomposite starting powder were required to use these materials effectively with laser sintering.

### **2.5.2. Geometric accuracy of selective laser sintered parts**

Raghunath and Pandey [73] studied the effect of process parameters on the process and material shrinkage. They investigated the relationship between shrinkage and various process parameters, namely laser power, beam speed, hatch spacing, part bed temperature and scan length in SLS. Cuboids from polyamide with suitable dimensions were fabricated rather than fabricating long parts along the X, Y and z directions in order to study shrinkage, as it was expected that the shrinkage along the X, Y and z directions is not independent. They found that scan length influences shrinkage in the x direction. They derived empirical relationships for percentage shrinkage in terms of scan length using the Taguchi method. However, they used scaling factors based on the maximum dimensions, not on the individual scan lengths while compensating using the model developed by them. The obtained results were validated and they were found to be in good agreement with other experiments. They also showed that the shrinkage model led to the development of more accurate parts.

The main goal in the study carried out by Senthilkumaran et al. [74] was to understand the nature of shrinkage occurring in the SLS process to improve the accuracy of parts produced from polyamide 12. They focused on the shrinkage behaviour by subjecting the shrinkage calibration samples to varying conditions. They investigated the variations in error patterns due to different strategies in building the calibration part and reported that certain compensations other than shrinkage were needed to get an accurate estimate of the shrinkage. They also found that beam offset, inertia of the scanning mirror and positioning errors in hatch generations affected the shrinkage pattern. Moreover, the results showed that the exposure strategies and part orientation influenced the accuracy of the part to be produced. They concluded that investigations

on the shrinkage behaviour of plastic parts are likely to make the process of compensation efficient and hence aid in improving the accuracy of the process.

Finite element analysis was used by Dalgarno et al. [75] in an attempt to model the development of the curling phenomenon in the SLS of polycarbonate. They reported on the use of finite element techniques to model curling. The model has been validated through a comparison of the finite element results of experimental builds, and extended to allow the influence of bases on the development of curling to be examined. The result from their analysis of the effect of bases on curling showed a qualitative agreement between the analysis and the experiments. They concluded that the characteristic shape of components exhibiting curling is thought to arise from the interaction of strain developed in the layer of the part during the build process and the force of gravity.

Jamal et al. [76] have presented an analysis of curling development in the SLS of polycarbonate. They reported on the use of finite element techniques to model curling development in polymer materials, and particularly on the influence of viscoelasticity on how curling develops. Their aim was to develop improved finite element models in order to provide greater understanding of curling development using a coupled thermal analysis. The development of time-dependent material models was reported. The results of the implementation of these models were presented together with a comparison of the results with experimental data. The analysis gave a qualitative insight into the development of curling and the effect of viscoelasticity on this phenomenon.

In their study of the curling phenomenon in selective laser sintering of polycarbonate, Berzins et al. [77] identified that the curling extends with different radii, particularly closer to the edge regions of the part. Furthermore, they observed that curling occurs with the sintering of the first layer and develops as further layers are added. The results showed that densification, shrinkage and thermal stresses were the main factors affecting curling.

## **2.6. Research gap addressed**

None of the abovementioned studies considered the mechanical properties of laser sintered plastic parts by investigating the relationship between surface pre-treated filler and, in particular, the effect of coupling agents on the mechanical properties of selective laser sintered glass bead-filled polyamide 12 composites. Currently, to the best of our knowledge, no such studies have been reported for PA 12/GB composites processed using the SLS technique. In the present work, a first attempt has been made to address this by experimentally analysing the influence of coupling agents on the mechanical properties of sintered components in polyamide 12 composites.

The same applies to warpage and curling phenomena. In most studies which have reported on investigating curling, the finite element, based on thermal stress and heat transfer analyses, was used to predict the development of curling on SLS polymer materials, in particular polycarbonate. Furthermore, a review of the literature has shown that the majority of research has been focused on shrinkage compensation, as well as modelling the impact of thermal stresses and heat transfer on geometrical accuracy. These investigations have mainly been based on properties of pure materials (rather than composites) and processing parameters. Not much research work has been done to

examine the effect of material composition on curling which occurs in selective laser sintered polyamide 12 parts.

In carrying out this work, tangible tools (such as the SLS process, testing equipment and machines) as well as intangible ones (such as the design of experiments and ANOVA) have been used to complete the research. These tools and the decisions behind choosing them are a matter of discussion in different parts of this work.

In chapter 1, a summary of the most important rapid prototyping and manufacturing techniques was given; however, selecting available RP&M process for a specific application is a challenging task, which requires knowledge not only of the currently available RP&M processes, but also an understanding of their capabilities, advantages and drawbacks. In this thesis, the RP&M technology field is the broad table that contains the area of concern. Within this large area of diverse processes, which vary mainly in their respective deposition methods and materials, selective laser sintering is the first step in narrowing the focus.

The availability of SLS machines (Sinterstation 2000, HQ2500, and EOSINT P 700), materials (PA12, PA12/GF) and well qualified personnel at the Manufacturing Engineering Centre (MEC) at Cardiff University was the first and foremost reason which drove the selection of selective laser sintering technology for the work described here.

## **2.7. Summary**

This chapter has surveyed previous work related to the improvement of mechanical properties and geometrical accuracy of selective laser sintered parts in order to establish the foundations necessary to carry out this research.

The literature review reported in this chapter has led to the identification of a research gap, which has been the guiding principle and central goal of this research project. In addition to this, the methods, tools, materials and some related factors which can affect the mechanical properties and geometric accuracy have been described.

In subsequent chapters, the possibilities for improving the mechanical properties and geometrical accuracy of selective laser sintered parts will be presented.

## **Chapter 3 - Selective laser sintering of glass bead-filled polyamide**

### **12 composites**

For any manufacturing process, the accuracy and mechanical properties of the components produced by the process will increase as the process and its parameters become understood. The SLS process is no different in this respect. In order to master well the SLS technology for sintering glass bead-filled polyamide 12 composites and to optimise the process through the processing and material parameters, each new material combination requires extensive testing.

Despite many materials which have been successfully used with the SLS process, there is still a need to investigate new materials from the point of view of improved properties and qualities. However, this can be expensive and time-consuming. The development of analytical and numerical tools to simulate the SLS process can be helpful to address the time and cost issue [27].

When developing a new material system for use with selective laser sintering technology, optimisation of the process must be undertaken. It is also important to understand the effects and interactions that fabrication parameters have on the material properties of the final parts. A series of experiments aimed at achieving this goal, focusing on the mechanical properties and geometric accuracy of SLS-processed composite samples, are described in this work.

This chapter provides the background needed for subsequent chapters on the investigation of mechanical properties and geometric accuracy of glass bead/polyamide 12 composites. It introduces the topic of determination of material and process parameters, describes the pre-processing studies required and methods used, reviews the factors influencing the process, and comments on the latest advances in the SLS of polymer composites. The main focus is on polyamide 12 filled with hard inorganic glass particles. To investigate the feasibility of producing sound parts from these composites using the SLS process, an experimental study had to be carried out.

### **3.1. Materials details and characterisation**

When developing a new material system for use with the SLS process, certain pre-processing studies are required in order to check the feasibility of the material to be used on the SLS machine. Before producing test samples of glass bead/ polyamide12 (PA12/GB) blends, a systematic study was carried out. The relevant material properties of PA12 and PA12/GB powders were determined using well-known characterisation techniques, such as differential scanning calorimetry (DSC), scanning electron microscopy (SEM) and powder packing analysis.

Samples of unsintered and sintered PA12/GB composites were examined by Scanning Electron Microscopy (SEM; ZEISS XB 1540 workstation) and Differential Scanning Calorimetry (DSC 1 STAR<sup>e</sup> System/ METTLER TOLEDO AG) to assess any morphological, physical or chemical changes that had taken place during processing.

### 3.1.1. Glass beads

Glass beads (GB) are one of many types of filler used to prepare polyamide composites. Glass beads have been widely used as fillers in thermoplastics for various industrial applications because they can enhance load-bearing capability in the elastic deformation range. This has motivated many researchers to investigate the effects of glass beads on the mechanical properties and geometric accuracy of many filled engineering polymers. As shown in Fig (3.1), the glass beads or microspheres are classified into solid and hollow spheres with densities varying from 2.5 [g/cm<sup>3</sup>] to 0.1 [g/cm<sup>3</sup>]. Spheres clearly have no aspect ratio to provide reinforcement properties, but their geometry affords important advantages in processing. They have the smallest surface area of any shapes and therefore they have the smallest influence on viscosity and melt flow. The unique shape of glass spheres also decreases high stress concentrations associated with regularly shaped and sharp-edged particulate fillers that result in severely reduced mechanical properties.

Depending on the specifications of the glass beads, the treatment (surface treated or untreated) to which the beads are subjected before being mixed with the polymer material and the bead/polymer quantity ratio, the presence of the glass beads can facilitate processing of the composite material and can, in various respects, enhance some mechanical properties and accuracy of the parts formed from the composite. Additionally, due to the isotropic character of the composite, the mechanical properties are more reproducible and more suitable for a mathematical description [54], [78].

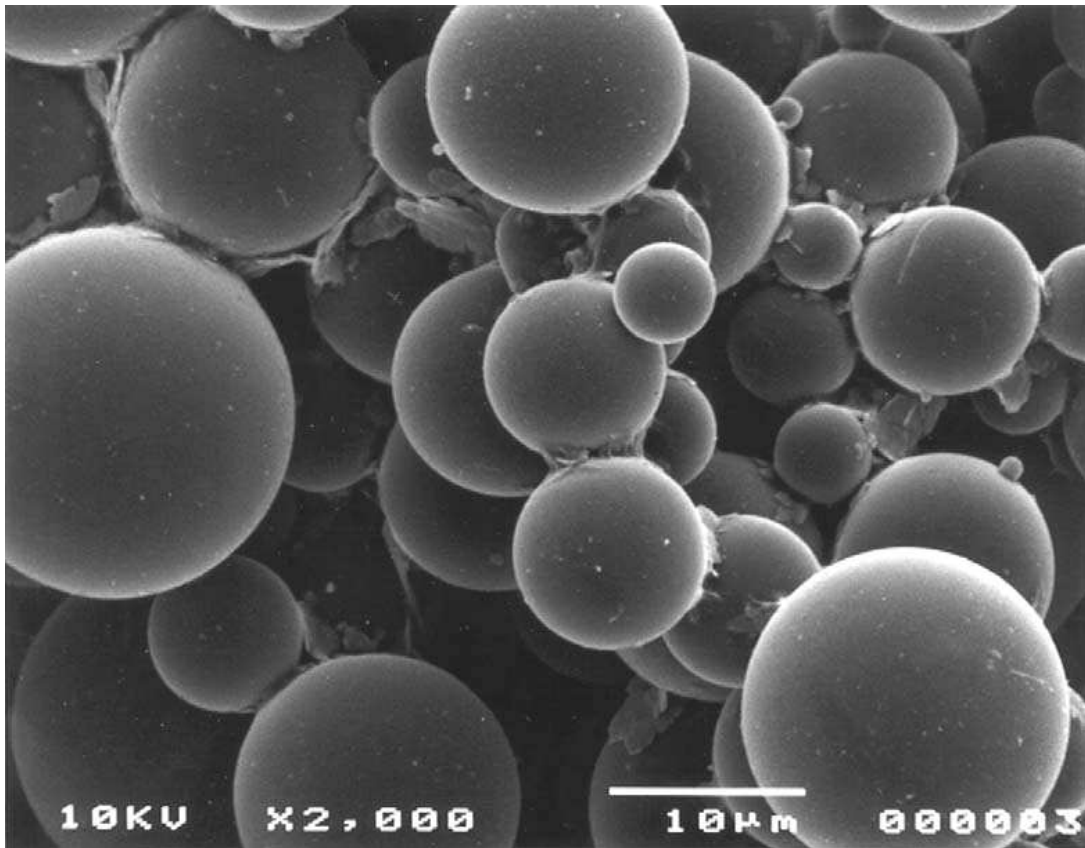


Fig (3.1) Scanning electron micrograph of soda-lime glass beads (3000 solid spheres)  
[79]

However, the effects of glass beads on the mechanical behaviour of the composites are highly dependent on the quality and the level of adhesion between the glass beads and the polymer matrix. Fillers are mainly added into the polymer matrix for one or more of the following reasons:

- reduced cost
- increased modulus (stiffness)
- reduced shrinkage
- improved crack resistance
- controlled viscosity

In this work, both surface-modified glass beads (3000CP03) and surface untreated (3000CP00) with a diameter of 35 [ $\mu\text{m}$ ] supplied by Potters Industrial Inc/Omya UK Ltd. were used. The treated glass beads were already provided with a coating during their production. This coating contained a silane coupling agent.

### **3.1.2. Silane coupling agents**

Generally, the inorganic glass bead particles exhibit low interaction with the organic PA12 matrix, which leads to poor adhesion of the filler to the matrix. Therefore, improving the interfacial adhesion between the inorganic particles and the polymer matrix by modifying the filler surface is essential in polymer composites [49]. The adhesion between polymeric materials and particulate fillers is usually weak due to poor compatibility of the polymer with the mineral surface. In order to increase the adhesion between these two unlike surfaces, it is logical to use a third material containing special functional groups which can adhere to both surfaces. To improve compatibility, adhesion promoters are commonly required [30], [31].

To make glass beads miscible with PA12 matrix, converting the hydrophilic silicate surface to an organophilic surface is needed. This can be done by replacing the charge-balancing interlayer cations (typically sodium), present on the glass bead surface, with alkyl ammonium cations. Alkyl ammonium cations in organosilicates lower the surface energy of the inorganic host and improve the wetting characteristics (organophilicity) of the polymer matrix, and results in a larger interlayer spacing. Additionally, the alkyl ammonium cations can provide functional groups that can react with the polymer matrix, or in some cases initiate the polymerisation of monomers to improve the strength of the interface between the inorganic component and the polymer matrix [71].

The main role of coupling agents is to promote adhesion which will result in developments in mechanical properties such as tensile and flexural strength, fracture toughness and tensile modulus. The coupling agent functions as a molecular bridge at the interface of dissimilar polymer binders and fillers, resulting in the formation of covalent bonds across the interface, which subsequently improves the properties of the composite system [32].

Silane coupling agents are widely used silicon-based chemicals that contain two types of reactivity, inorganic and organic, in the same molecule. A typical general structure is  $Y - R - Si - (X)_3$ , where Y denotes a functional group that links with organic materials, while X is a functional group that undergoes hydrolysis and links with inorganic materials. Silane coupling agents are effective for improved adhesion at the interface between the organic and inorganic materials and have been frequently utilised to enhance the strength and to improve the performance of glass bead-reinforced plastics [80], [81]. Fig (3.2) shows an idealistic view of a silane-treated surface.

Among all kinds of coupling agents used to modify the surface of glass beads, organofunctional silanes have been chosen because of their commercial availability and the good results they offer. Silane coupling agents present three main advantages:

1. They are commercially available at a large scale.
2. At one end, they have alkoxy silane groups capable of reacting with OH-rich surfaces.
3. At the other end, they have a large number of functional groups which can be tailored as a function of the matrix to be used [50].

In addition, many investigations have shown that the silane coupling agent did not significantly change the morphology of the sintered samples; however, it slightly improved the strength of sample due to better adhesion at the filler/polymer interface [82].

The silane coupling agents have little effect on the packing fractions of the glass microsphere-filled composites. This is not surprising as the surface treatments did not significantly change the size and shape of the filler. Nevertheless, the silane treatment had little effect on the reflectance of the glass microspheres. This phenomenon can be attributed to the fact that the silane layer is very thin and it does not significantly change the surface morphology of the glass microspheres. Silane treatment of glass microspheres had little effect on the reflectance of both the filler and the composite powder as a whole [83].

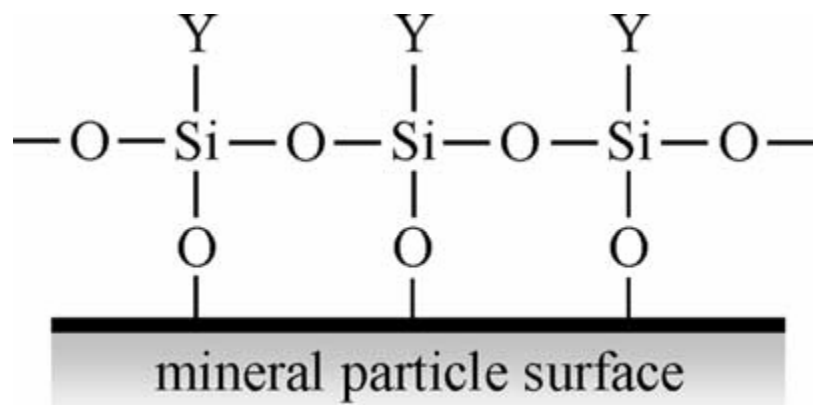


Fig (3.2) Idealistic view of a silane-treated surface [83].

### *Mode of action*

A silane coupling agent acts at the interface as a link between an inorganic substrate (such as glass, metal or mineral) and an organic material (such as an organic polymer, coating or adhesive) to bond, or couple, the two dissimilar materials together. In the cross-linking process, the first step is generally the grafting of the silane to the polymer backbone; second step is linking the polymer chains together via condensation of silanols. Fig (3.3) reveals a simplified picture of the coupling mechanism [83].

### *Methods of applying silane*

Since different materials are used for different applications, methods of applying silanes to fillers should be chosen appropriately for each case. In the integral blend method, silane is added to the mixture of filler and polymer followed by mixing. The simplest and most effective laboratory treatment of particulate fillers is to mix the filler with a dilute solution of silane in an organic solvent. In another method, silane is submerged in water by stirring and after hydrolysing silane, glass beads are added to the solution. This method is very effective for coarse fillers. However, a monomolecular layer of silane on the filler results in optimal adhesion to the matrix [52]. The optimum amount of silane can be calculated as follows (Eq. 3.1):

$$\text{silane}(g) = \frac{\text{filler weight}(g) \times \text{filler specific area}(m^2 / g)}{\text{wetting specific area of silane}(m^2 / g)} \quad \dots (3.1)$$

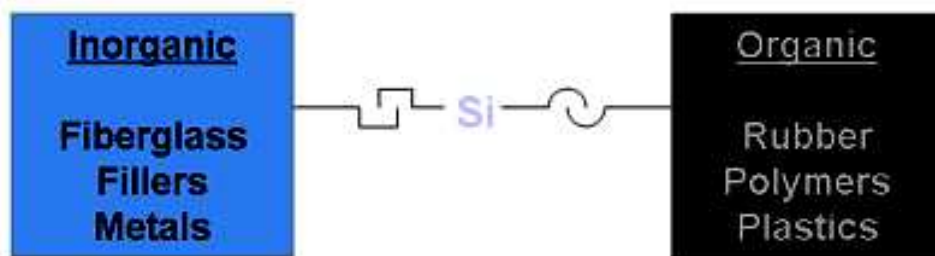


Fig (3.3) Coupling mechanism of a silane coupling agent [83]

### *Operating temperature*

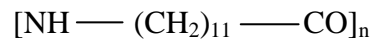
Silane coupling agents can withstand temperatures of about 200 [°C] and laser powers of 50 [W]. These agents do not degrade, particularly in a nitrogen atmosphere, with a short time of exposure to energy, which is the case in the processing chamber of selective laser sintering machines. The physical and chemical data of the silane coupling agent (according to the manufacturer) were:

- Boiling point > 68 [°C] (DIN 51356)
- Flame point  $\approx$  93 [°C] (DIN 51758)

### **3.1.3. Nylon 12**

Nylons are an important thermoplastic silky material. They were first prepared by Wallace Hume Carothers in the 1930s at Dupont, and first used commercially between 1938 and 1940. They are made of repeating units linked by peptide bonds (or amide bonds) and are frequently referred to as polyamides (PA). Polyamides are crystalline polymers with a number of advantages, such as higher modulus, strength, impact properties, good processing properties and low cost. Parts fabricated from nylon have excellent mechanical properties, very smooth surfaces and high accuracy. Nylon usually used for the production of housings and thermally stressed parts. However, its drawbacks (such as dimensional instability, shrinkage and notch sensitivity) are also outstanding. Therefore, the modification and toughening of polyamide have received close attention in recent years. Several methods for toughening PA have been proposed, among which the usual methods making use of inorganic rigid particles such as glass beads, mica, etc. [62], [57], [84].

Today, the production of prototypes (RP) and functional parts (RM) by SLS is basically limited to nylon, the most researched polymer (polyamide PA), which has become synonymous with SLS plastics. The base material used in this study was nylon 12 (polyamide 12, PA12) with an average particle size of 60 [ $\mu\text{m}$ ], commercially known as fine polyamide powder (PA2200), which was used in the SLS process (supplied by EOS GmbH Germany). The chemical structure of nylon 12 is given below:



According to the properties required for selective laser sintering materials, nylon is well suited for selective laser sintering, due to its relatively low melting temperature and low heat conductivity, which facilitate a local limitation of the sintering process. This material shows a large distance between its melting and crystallisation temperatures, low melt viscosity and high surface tension. The almost spherical particle shape and narrow particle size distribution of commercially-distributed powders maintain good flowability and a high packing density of the powder [85].

At present, four nylon materials are commercially available for the SLS process, namely standard nylon, fine nylon, fine nylon medical grade and nylon composite. The production of nylon parts is generally cost effective when a small number of parts is required. The material with best mechanical properties for producing functional parts with the SLS process is a nylon composite. SLS glass-filled nylon can be processed to near density and has a high modulus and good heat and chemical resistance [86].

### **3.2. Powder mixing and blend preparation**

Mixing of powders is a common operation in the SLS process. In the production of laser sintered parts, the distribution of particle sizes in the polymer powder is highly important for producing parts of good quality. In the case of polymer blends, the particle size distribution becomes even more important to assure that good mixing occurs before the polymer melts. In the present work, a mechanical mixer was used for blend preparation. The dispersion of glass beads in the powdered PA 12 was achieved by the blending process using a portable drum mixer type BS 125 (speed of mixing drum: 26- 30 [rpm/min]) for 30 minutes to produce the composites.

Mixtures of PA12/GB powders were produced by physically blending pure PA 12 and glass bead powders in different weight percentages. In producing the blends, PA 12 was the matrix material and the glass bead powders were added and dispersed into the PA 12 powder to achieve composite blends having 10, 20, 30 and 40 wt% glass bead contents. Accordingly, eight powder blends (plus pure PA 12 powder) were prepared, namely four blends of PA 12 with untreated glass beads (PA12/3000CP00) and another four blends with surface-treated glass beads (PA12/3000CP03) in weight percentage. Table (3.1) shows the mix ratios of the glass beads and PA 12.

The prepared powder blends were then processed on a commercial SLS system (DTM Sinterstation 2000) to produce the test samples. Except for changing the process parameters on the operating software of the SLS system, no modifications were made to the SLS system for processing the PA12/GB composites. All of the experiments described in this work were performed with PA 12 and PA 12 filled with glass beads. This combination has been chosen as a model composite since it shows a number of

experimental advantages. Glass beads are easily dispersed in polyamide 12 by a portable drum mixer. The spherical form of these fillers gives rise to distinct functions and properties compared with other directional fillers. These include [74]:

1. high packing fractions, little effect on viscosity, and high attainable levels
2. better flow characteristics than high aspect ratio fillers
3. more uniform stress distribution around the spherical inclusions and better dimension stability
4. no orientation effects and enhanced isotropy
5. reduced uniform and predictable shrinkage and less warpage

### **3.3. Powder and processing acquisition**

#### **3.3.1. Differential scanning calorimetry analysis**

Differential scanning calorimetry (DSC) is a thermal analysis technique that is used to investigate thermally-induced phase transitions. Semi-crystalline polymers exhibit a first order solid/liquid phase transition; differential scanning calorimetry can be used to determine the melting temperature range, the enthalpy or latent heat of melting, the re-crystallisation temperature range and the enthalpy of fusion for semi-crystalline polymers. The temperature at which the phase transition occurs and the breadth of the transition are both heating rate-dependent; the higher the heating rate, the higher the transition temperature and the wider the temperature range of the transition [10].

DSC measures the heat flow into or out of a material when it is heated, cooled or kept at a constant temperature. The signal from the DSC measurement is heat-flow and it can be calculated by multiplying the sample mass by the sample specific heat capacity and the heating rate. The equation is written as:

Table (3.1) Contents of glass beads (coated and uncoated) blended with PA 12 by weight

<b>Glass beads [wt%]</b>	<b>PA12 [wt%]</b>	<b>Ratio [wt%]</b>
0	100	0:100
10	90	10:90
20	80	20:80
30	70	30:70
40	60	40:60

$$Q = m \cdot c_p \cdot \beta \quad \dots (3.2)$$

Where  $Q$  is heat flow  
 $m$  is sample mass  
 $c_p$  is sample specific heat capacity  
 $\beta$  is heating rate.

Therefore, an increase in the sample mass or the heating rate will, in turn, increase the heat flow signal.

In this work, DSC analysis of PA12/3000CP00 and PA12/3000CP03 blends was carried out on the DSC1 STAR<sup>®</sup> System/METTLER TOLEDO AG. Samples weighing 11-18 [mg] were heated from 20 to 200 [°C] at a heating rate of 10 [°Cmin<sup>-1</sup>]. The heating and cooling were carried out under the same conditions. Heating and cooling curves are presented in Figs (3.4a; b) for the abovementioned systems.

It is well-known that a polymer powder with a slow re-crystallisation rate, with non-overlapping or slightly overlapping endothermic and exothermic peaks during the heating and respective cooling phases of the DSC analysis, might result in nearly fully dense parts with minimal distortion, while highly overlapping peaks will yield bad results. As depicted in Figs (3.4-a; 3.4-b), both systems have almost similar melting and re-crystallisation peaks **compared** to normal PA12 powder Fig (3.5). A larger temperature difference ( $dT$ ) range between those peaks allows for a larger process window in term of fluctuations of temperature in time and space within the processing chamber and build part. The window of sinterability, that is, the difference between the melting temperature and the crystallisation temperature of a material, is crucial in the SLS process because sintering is completed in a very short period of time and the difference in the two temperatures should be large enough [71], [87].

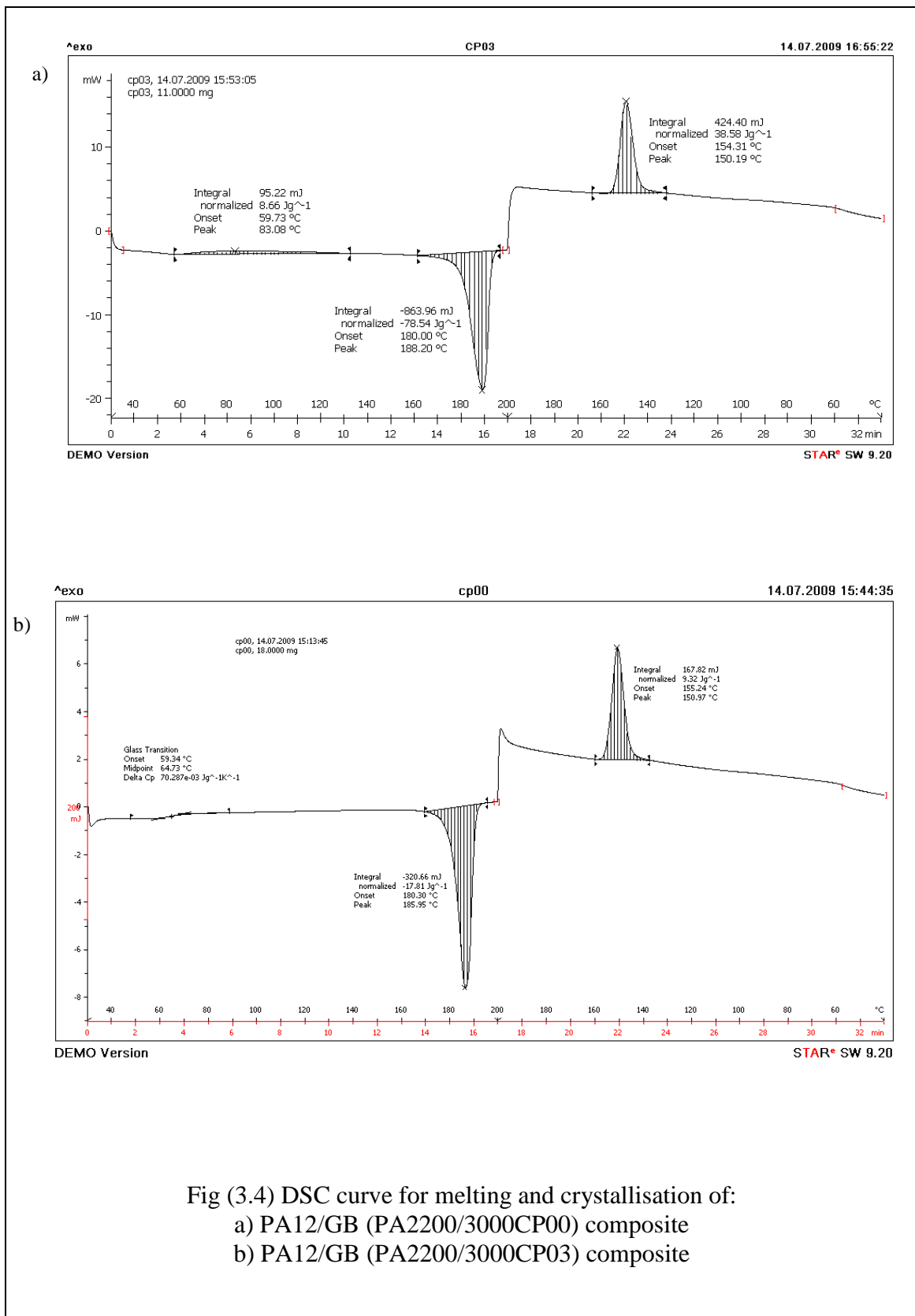


Fig (3.4) DSC curve for melting and crystallisation of:  
 a) PA12/GB (PA2200/3000CP00) composite  
 b) PA12/GB (PA2200/3000CP03) composite

It was found from the DSC analysis that the difference in the melting and crystallisation temperatures for PA12/GB was within the prescribed limit and was almost same as that found for PA12. From the DSC results, it was concluded that the PA12/GB blends could be sintered using the SLS process. The melting temperature of the polymer, around 170 [°C], was taken from this graph and used with, glaze point (the temperature at which the powder glistens as it starts to melts) to aid in the determination of the required pre-heat and build temperatures for the powder bed.

DSC analysis showed that the melting temperatures of PA12 and PA12 with 40% glass bead content, that is, PA12/CP00 and PA12/CP03 blends, respectively, were almost the same. However, the heat of fusion (the area under the melting peak) was comparatively higher for the PA12 blend with 40% glass beads. This might be the possible reason for the slightly higher part bed temperature required for sintering in the case of PA12/GB blends, despite the almost identical melting temperatures. It has also been observed in the DSC analysis presented in Fig (3.4a; b) that the crystallisation temperature for PA12/GB was slightly increased with a narrowed crystalline peak. This shows that the glass beads increased the crystallisation rate of the composites. The majority of the energy for fusing the matrix (PA12) was provided by the heaters located directly over the powder bed. The powder temperature in the part build area should be slightly lower than the melting point of the PA 12 (10-16 [°C] below the PA 12 melting temperature,  $T_m$ ).

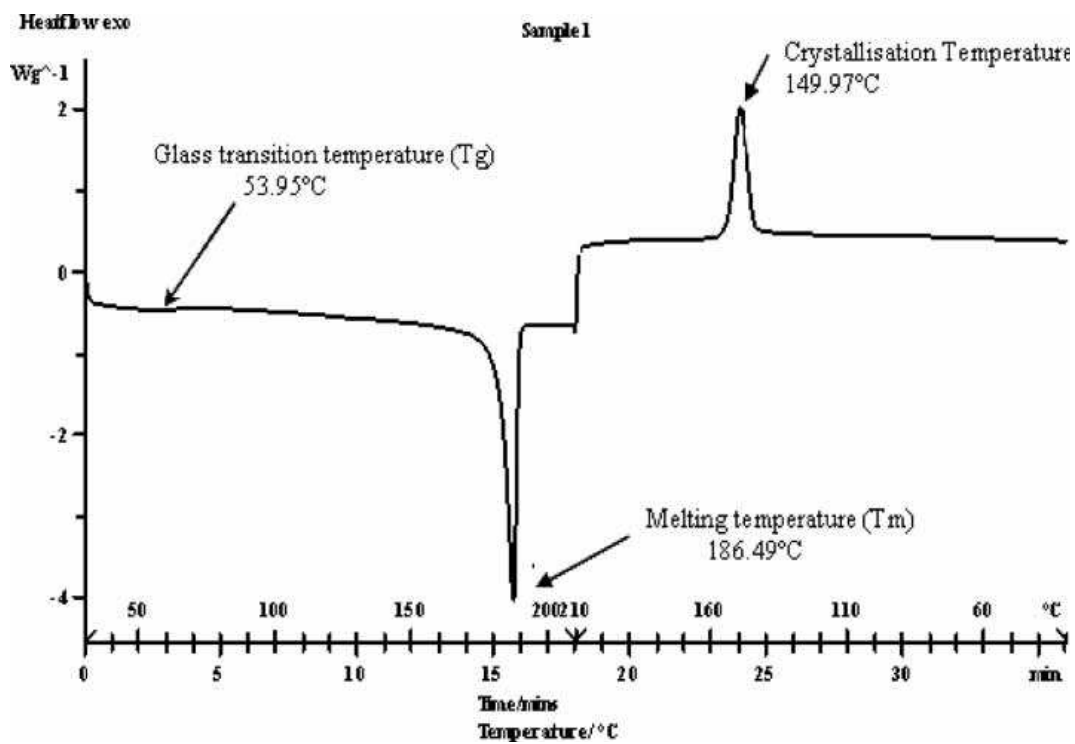


Fig (3.5) DSC plot of a virgin PA 12 powder [89]

### 3.3.2. Particle size; shape and distribution

Controlling the particle size distribution of powders is vital in order to deliver a final component with the required properties. Particle size also affects the SLS process as fine powders tend to exhibit poor flowability, partly because of their packing behaviour (the particles interlock). The primary effect of particle size and shape on part accuracy is on the trueness of features. Smaller particles with a high degree of sphericity produce parts with sharper edges and corners and improved detail resolution.

Fig (3.6) shows a general view of PA 12 powder. It has particles in the size range of 20-80 [ $\mu\text{m}$ ] with near spherical shape and smooth surface. Figs (3.7) present the micrographs taken for powder blend containing 30 [wt%] glass bead. GB particles in all four powder blends were observed in increasing amounts with increased percentage of GB content in the PA 12. It is worthwhile to note that regardless of the composition, Optical Microscope observation of GB particles in all samples indicated that mixtures with good dispersion and distribution of GB were obtained.

The PA 12/GB composites, PA12/CP00 and PA12/CP03, had average particle diameters of approximately 32-63 [ $\mu\text{m}$ ]. The shape of both the PA 12 and glass beads particles was to a large extent spherical. A uniform mixture of the glass bead particles with polyamide was clearly observed in all blends. The impact of filler content was more subtle but, in general, parts built with a glass bead content of 10 [wt%] had improved definition compared to parts build with filler contents of 40 [wt%] composites.



Fig (3.6) SEM micrograph showing unsintered PA12 powder (Source FHSG-St. Gallen)

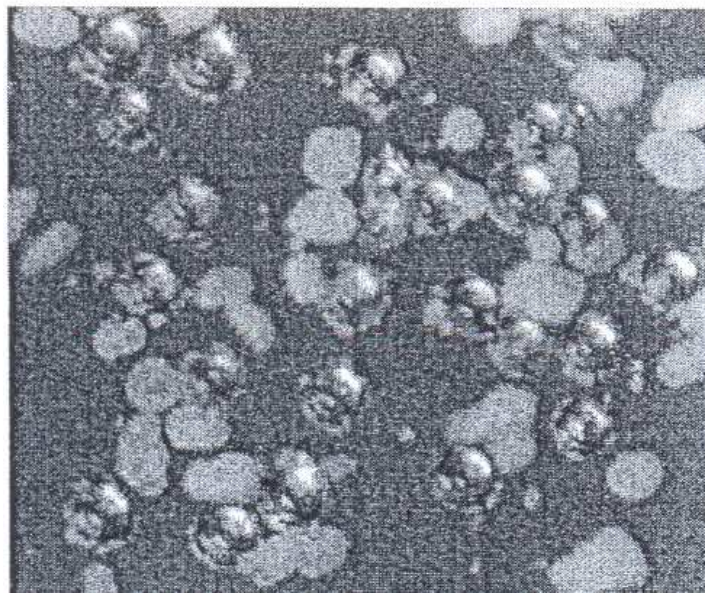


Fig (3.7) General view of blended powder of PA12 with 30 [wt%] glass beads content

For SLS technology, it has been reported that the process resolution is proportional to the inverse of the particle diameter cubed. This means that the resolution increases substantially as particle size is reduced. Parts made with smaller particles have improved definition as characterised by the sharpness of edges and corners; this is particularly true for materials which undergo limited densification and melting in the SLS process. For such materials, particle shape is not greatly altered in the SLS process [90].

Further, it is generally believed that the effects of the filler particle size and distribution on the mechanical properties of composites are very important, in addition to the filler surface treatment. Fig (3.8) shows the distribution of the glass beads obtained by sieve analysis (Analysette 3 Pro, Fritsch, Germany). It can be seen that the majority of glass beads were in the 32-63 [ $\mu\text{m}$ ] range which is the preferred range for SLS processing [78].

### **3.3.3. Tapped bulk density of glass bead-filled polyamide 12 composites**

For precise property control of sintered products, it is important to know the powder characteristics, especially the packing density of the powder. In the selective laser sintering process, one important characteristic is tapped bulk density, that is, the maximum packing density of a powder or blend of powders achieved under the influence of well-defined, externally applied forces. It mainly depends on a number of factors including particle size distribution, true density, particle shape and cohesiveness due to surface forces, including moisture. Therefore, the tap density of a material can be used to predict both its flow properties and its compressibility.

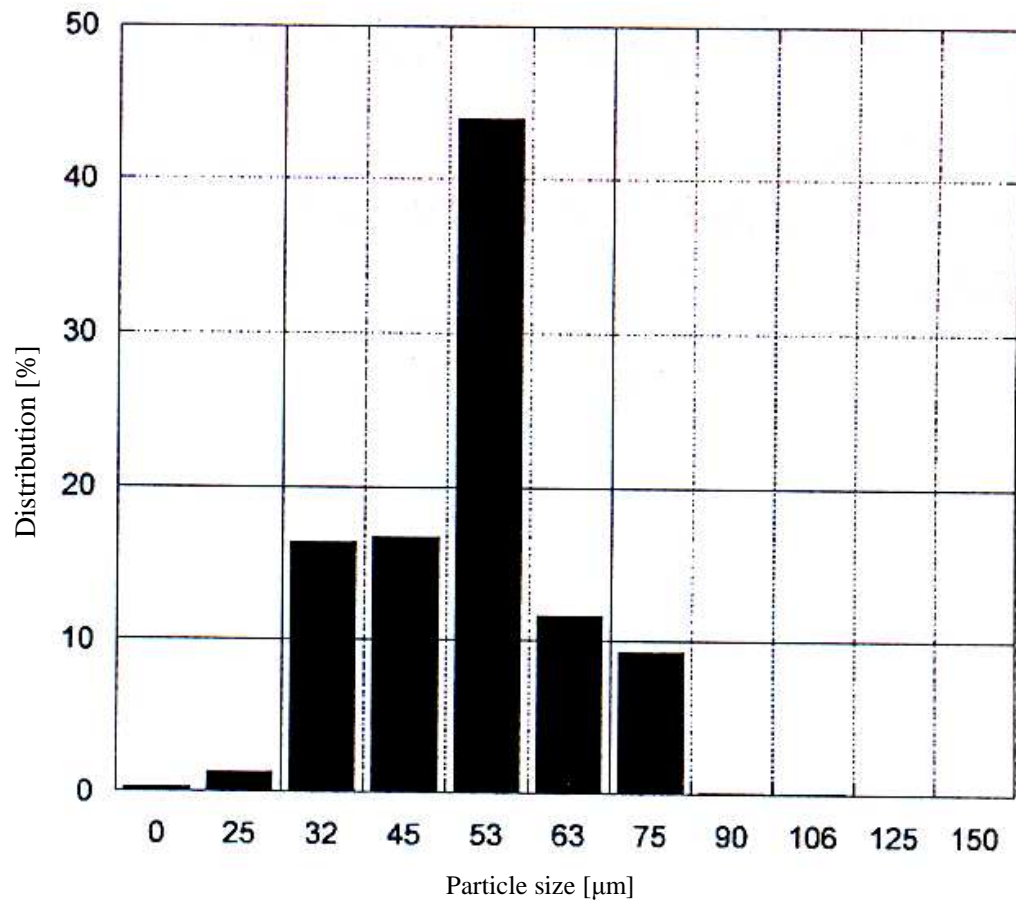


Fig (3.8) Particle size and distribution of the glass beads used (Potters A glass spheres) by sieve analysis [78]

The tap densities of the composite powders were measured to quantify the packing characteristics of the powders. In powder processing methods, the initial packing density of the particles being consolidated is of significant importance; the higher the initial packing density, the smaller the change in volume and the amount of energy required to reach the desired relative density.

The density of a composite material can have dramatic effects on the global performance of the component during use. The addition of a high-density filler will subsequently increase the overall composite density. The composite samples used in this work consisted of a PA 12 matrix loaded with varying amounts of solid glass bead filler. The solid glass spheres were obtained from Potters Industries Inc., under their registered trade name Spheriglass. The bulk density of PA12/GB composites was measured using a simple method in which a measuring cylinder of a certain mass (157 [g]) was filled with water and weighed. After determining the mass of water using a sensitive scale, the measuring cylinder was emptied then was filled again with a composite powder and weighed. Raising and dropping the cylinder 20 times from a height of about 25 [mm] onto a hard surface will normally give a consistent value of the tapped density. This will align with the lightest condition of powder that is spread by roller movement on the part bed in the selective laser sintering machine. After each measurement, the sample was poured out of the cylinder and the cylinder was filled again. The volume and weight were recorded and the tapped density was calculated. Table (3.2) presents the measurement data of the tapped density of the composites.

One of several stages of composite analysis, however, was the determination of the effect of the weight content of the filler to the density of the composite. Fig (3.9) shows

the relation between filler ratio and composite tap density and, as expected, the density of the composites increased with increasing weight ratio of the glass beads.

### **3.4. Processing system**

Processing of the composite powders was carried out on a DTM Sinterstation 2000 Laser Sintering machine, as described in chapter 2. In this commercial system, the powder bed is pre-heated to a temperature just below the melting point of the composite material. The laser is then used to tip the powder over this point and sinter the composite material into a solid mass. The powder in the feed chambers is also heated to a temperature below that of the powder bed so that when it is spread over the build area, minimal provision of thermal energy is required [91].

The default operating parameters in commercial SLS systems, recommended by the manufacturer for a specific powder, do not satisfy the demand of all applications. Therefore, a trial-and-error method is often adopted to obtain suitable operating parameters to satisfy the demands of a specific application. Several operating parameters are critical for the SLS manufacturing process. Careful controls and extensive empirical testing are usually required for a new material. In order to achieve this, a number of parameters can be changed and varied on this machine to meet the requirements and conditions of the processed composite material. The relevant machine parameters to this work are defined as follows [91], [92] and [93]:

- Bed temperature [ $^{\circ}$ C]: Temperature of the powder in the build chamber (as recorded by an infrared optical pyrometer).

Table (3.2) Measured and calculated data of the tapped density of the composites

<b>materials</b>	<b>Ratios [%]</b>	<b>m<sub>Gross</sub> [g]</b>	<b>m<sub>Net</sub> [g]</b>	<b>ρ[g/cm<sup>3</sup>]</b>
Water	-	378.0	221	1.000
PA 12	-	268.9	111.4	0.504
PA 12/CP03	90:10	279.1	121.6	0.550
	80: 20	287.3	129.8	0.587
	70:30	298.9	141.4	0.640
	60:40	308.9	151.4	0.685
PA3200/GF	(EOS)	310.7	153.2	0.693

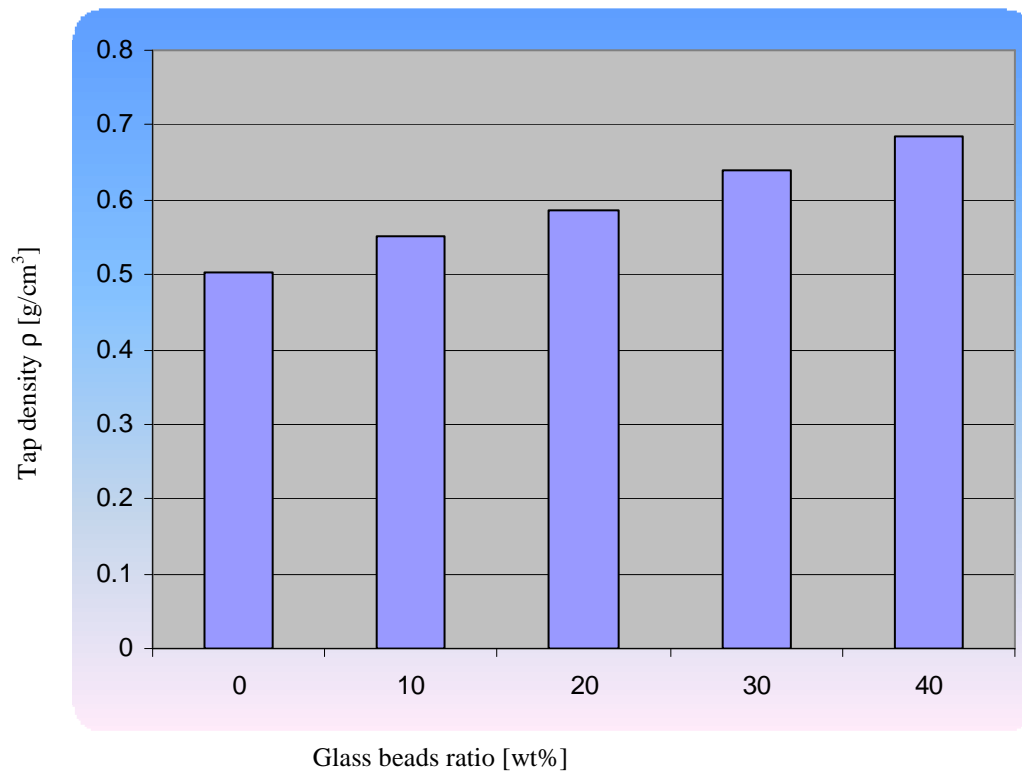


Fig (3.9) The relation between filler ratio and composite tap density

- Feed temperature [ $^{\circ}\text{C}$ ]: Temperature at which the powder is stored in the feed chambers before being spread across the build area (as recorded by an infrared optical sensor).
- (Fill) Laser power [W]: Applied power of the laser as it scans the area of each layer.
- Roller speed [mm/s]: Velocity at which the roller travels as it spreads the powder over the build area.
- Rotate scan order: when selected, it sets the laser beam to alternate between the parts every other layer, rather than just at the first part nested in the build bed.

### **3.4.1. Laser sintering trials**

It is a well-known fact that for every new material, all parameters of the SLS machine need to be tuned. Therefore, the material needs to be characterised before building the SLS parts. Certain common characters of the material powder are also needed for the successful and good SLS processing. In order to establish suitable parameters for processing glass bead-filled polyamide 12 composites, a range of processing conditions were attempted as outlined in this section.

Basically, laser scan speed is one among many important parameters in laser sintering. The operating system of Sinterstation 2000 does not allow for varying scan speed, and thus this was kept constant at 914 [mm/s]. Other parameters, including a laser scan spacing of 0.15 [mm], a roller speed of 127.0 [mm/s], a layer thickness of 0.1 [mm] and laser beam diameter of 0.4 [mm] were also kept constant.

### **3.4.1.1. Preheating process and part bed temperature**

In the selective laser sintering process, the powder is fused and processed into a part by applying heat energy. Preheating of the powder on the surface of the powder bed is an important process which guarantees that parts can be successfully fabricated and which influences the accuracy of parts fabricated using SLS technology. The uniformity of temperature on the powder bed influences the accuracy and performance of parts. It is necessary to understand the influences of the parameters of preheating set on the uniformity of the temperature on the surface of the powder bed. The initial step in the process was to determine the best operating parameters for the composite powder: laser power, feed temperature and part bed temperature. These critical parameters were kept constant for all of the future builds to provide consistent heat input to the powder. However, these parameters can vary from machine to machine [94], [95].

Before sintering the samples, approximate bed and feed temperatures should be determined by observing the flow of powder across the build area as it is spread by the roller. This was carried out initially at five degree intervals between 80 and 95 [°C] for feed temperature and at two degree intervals between 170 and 178 [°C] for bed temperature, and then at one degree intervals as the temperatures became closer to the optimum. The most appropriate combinations of bed temperature, feed temperature and laser power that could produce good parts in terms of mechanical properties and geometrical accuracy, as determined by uniform powder flow and a smooth powder bed coupled with an unhardened powder cake, were then used to produce test samples and conforming parts.

During this investigation, several key SLS operating parameters had to be tuned to produce parts of sufficient quality and improved mechanical properties. The glass bead-filled polyamide 12 composites were given a 2-4 [hr] warm-up period, similar to that recommended for commercial polyamide 12 materials. Twelve millimetre layers were then rolled over the build area prior to sintering, adding further heat to the system. During this first stage, the process chamber was gradually preheated and the part bed temperature was increased.

Five cross-shaped parts (Fig 3.10), four at the four quadrants and one at the centre of the build cylinder, were fabricated on the SLS machine. The process was started at a temperature of 170 [°C] and a laser power of 6 [W], where the initial layers were carefully observed for curling. If curling occurred, the part bed temperature was increased by 1-2 [°C] and the whole process was repeated until the suitable part bed temperature was found. In the case of glass bead-filled polyamide 12 powders, the part bed temperature was found to be slightly higher as compared to that for the pure polyamide powder. Table (3.3) shows the modification limits of the composite materials and the SLS process parameters and summarises the observations and results while finding suitable part bed and feed temperatures for various powder mixtures.

The temperature in the areas of the two powder cartridges was held at a low enough temperature between room temperature and the temperature in the part build area so the powder remained free-flowing and could be spread by the roller during SLS processing.

Table (3.3) Modification limits of composite materials, SLS process parameters and the effects of part bed temperature

Bed temp. [°C]	Feed temp. [°C]	Laser power [W]	Rotate scan order	Material [wt%]				
170–180	80–95	6–18	1 (On)	0 -40				
<b>Observations</b>				0:100	10:90	20:80	30:70	40:60
				<b>Powder bed temperature (Feed temp.) [°C]</b>				
Parts warp seriously and shift when the powder spreading recoater passes over				170 (80)	170 (80)	170 (80)	170 (80)	170 (80)
Parts warp and shift				172 (85)	172 (85)	172 (85)	172 (85)	172 (85)
A slight warp, no shift				174 (90)	174	174 (90)	174 (90)	174 (90)
Satisfactory parts with smooth surface				176 (90)	176 (90)	176 (90)	177 (90)	177 (90)
Powder surrounding parts agglomerates slightly during sintering, and it is difficult to remove unsintered powder				178 (95)	178 (95)	180 (95)	180 (95)	180 (95)

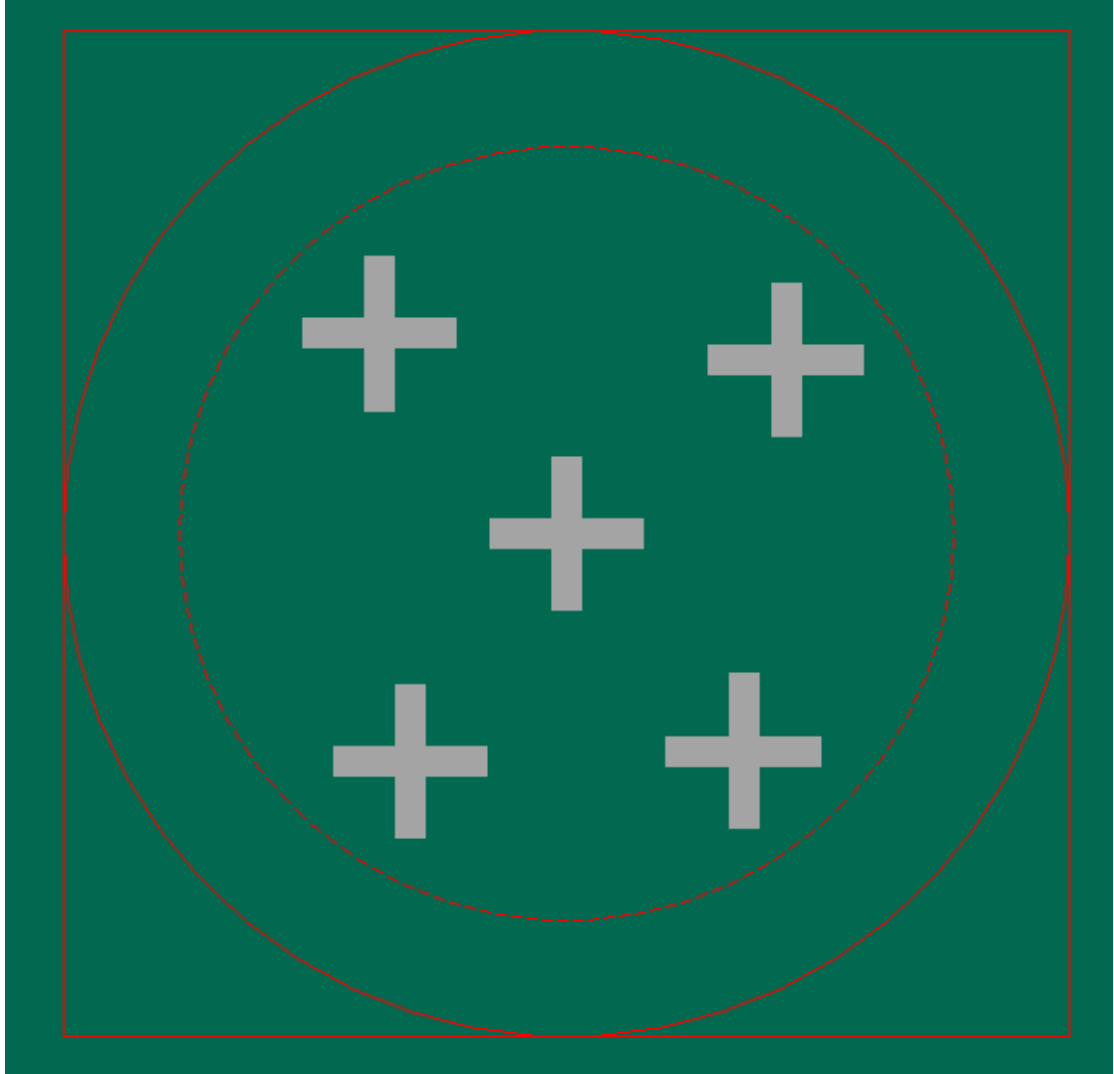


Fig (3.10) Cross-shaped test samples used to find suitable bed and feed temperatures

If the powder temperature was set too high in the powder cartridge areas, the powder clumped together and did not spread evenly during SLS processing. Moreover, the surface of the part or powder bed cracked open on the surface and was streaked with lines as the roller moved across it due to an excessive heating rate or temperature from the heaters and due to partial melting of the powder which resulted in short feed or no feed, Fig (3.11). The measures to be taken in this case were a gradual reduction to the heater setting and waiting for the system to add a few layers. The temperature was repeatedly reduced until the cracking disappeared. However, to produce geometrically accurate and mechanically robust parts by SLS, a balance must be struck between maximising the temperature to increase part density and minimising the temperature to maintain geometric accuracy.

In order to minimise thermal distortion and facilitate fusion to the previous layer, the entire bed is heated to a temperature just below the melting point of the material which is done prior to the commencement of sintering. The laser is modulated in such a way that only the grains which are directly exposed to the beam are affected, and heating is done to a level such that the surface tension of the particles is overcome and they fuse together [96].

Too high bed temperature (above 178 [°C]) caused growth of the part as the surrounding powder bonded to the desired boundaries of the part. Growth is caused by heat transfer from the consolidated part to the surrounding support powder. Growth (Fig. 3.12) occurs as powder sinters on the part, blurring features and altering part dimensions. It is particularly apparent with small features or small holes.



Fig (3.11) Cracks and lines on the powder surface formed due to excessive bed/feed temperatures

The sintered parts become difficult or even impossible to break out due to a caking phenomenon in which the powder particles stick together and a large amount of the powder forms as a lump. Reduction of the part heater set point parameter and laser power parameter was necessary to eliminate growth and prevent powder from caking.

On the other hand, too low a bed temperature (below 170 [°C]) caused the lasered composite to shrink significantly from the surrounding bed, which resulted in movement of the part on the subsequent pass of the roller. Moreover, the phenomenon of curling was observed in this case when the part bed temperature was too low. Curling is a phenomenon in which the sintered layers become non-planar due to a high thermal gradient between the sintered and unsintered powder material. In-build curling occurs when the edges or corners of the part rise above the powder bed surface, mainly due to uneven temperature distribution in the part bed when the part temperature dips too low after the feed powder is added (chapter 5). As shown in Fig (3.13), in-build curling can cause the part to shift when the roller passes over the part bed.

The investigation of pre-heating and part bed temperature showed that, when the powder bed temperature was kept close to the powder melting temperature, relatively low heat input from the laser beam was sufficient to sinter the powder. Therefore, the sintering process must be performed at a part bed temperature as close as possible to the melting temperature of the composite material. This shows that the selection of a suitable part bed temperature is very important to facilitate successful sintering as well as to ensure the reuse of the unsintered powder material. A suitable part bed temperature was found by conducting a typical cross test [71], [97].

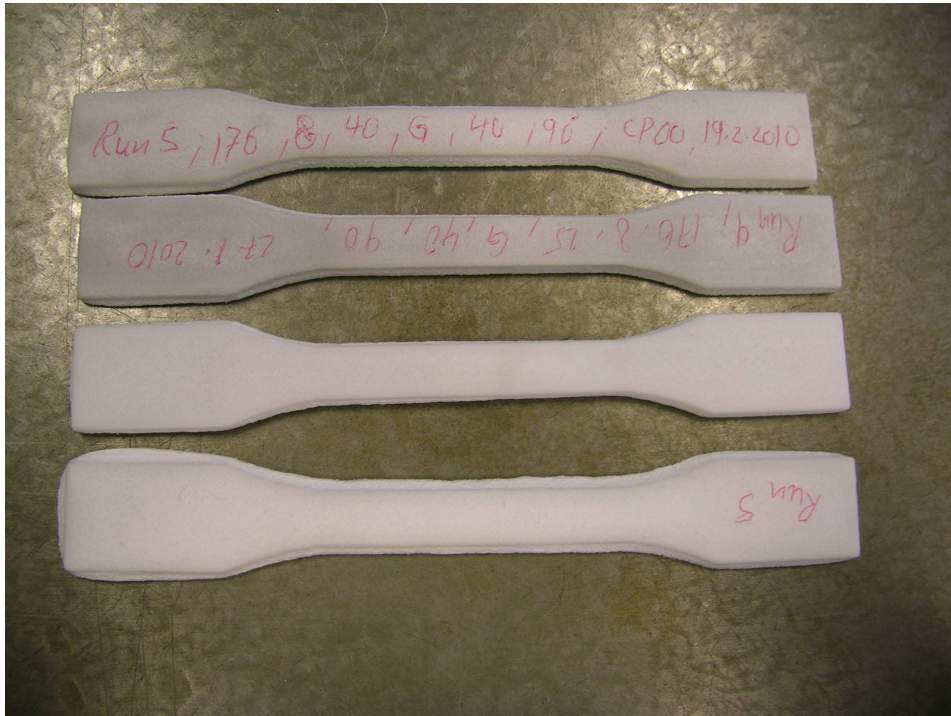


Fig (3.12) Growth on sintered samples

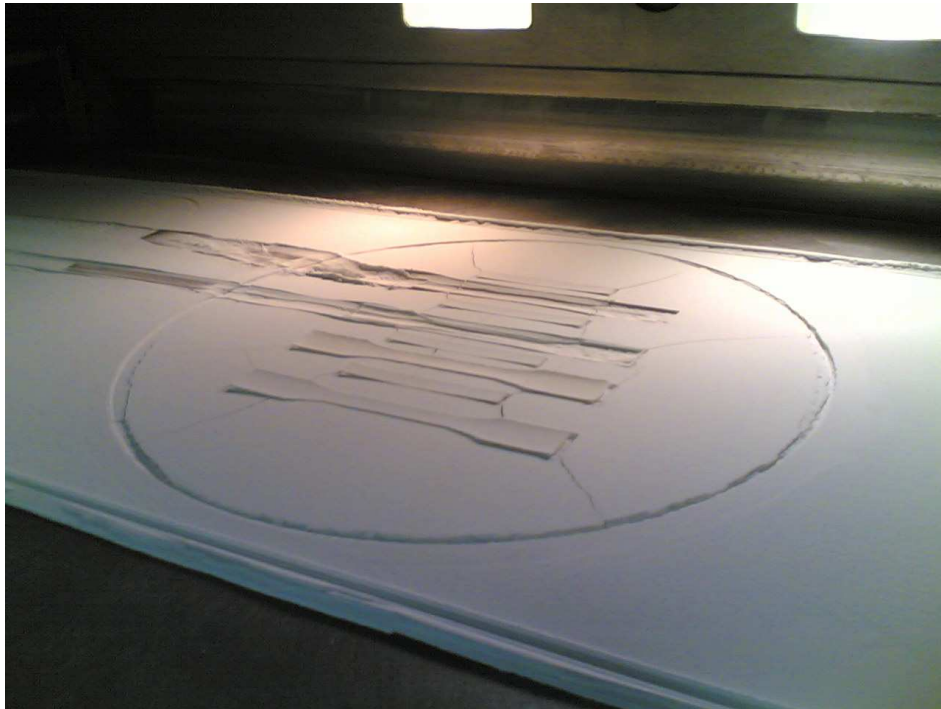


Fig (3.13) In-built curling causes the part to shift when the roller passes over the part bed

### **3.4.1.2. Shrinkage scale factors and laser beam offset values**

Beam offset calibration and shrinkage compensation are two of the most important parameters that affect the part building accuracy of the SLS process. Beam offset includes the diameter of the laser spot, the heat-affected area and the deflection angle during the laser scan. It differs from one sintering to another [98].

It is not difficult to conclude that accuracy is material- and also machine-dependent. During the whole fabrication process, the samples shrink along the X, Y and Z directions. In order to compensate for this shrinkage, the input part geometry is modified applying scaling factors in the X, Y and Z directions correspondingly. Shrinkage depends very much on part geometry and its orientation during laser sintering. The inside and outside surfaces are offset to compensate for the size of the sintering spot of the laser beam (beam offset) [99]. The right selection of the scaling factors and beam offset determines the extent to which the systematic factors due to input data can be compensated; Table (3.4) presents the experimentally obtained scale factor and beam offset for PA12/GB composites, where Fig (3.14) illustrates the calibration procedure of beam offset and shrinkage compensation.

Selective laser sintered part accuracy is influenced by a number of machine and material characteristics. Crystalline or semi-crystalline materials exhibit high shrinkage associated with both the material phase change and the high degree of consolidation obtained during processing, but the amount of growth is usually limited by relatively low laser powers which are required to completely melt the material [81].

Table (3.4) Scale factor and beam offset for PA12/GB composites

Shrinkage scale factor [mm]		X, Y offset & Z compensation [mm]	
		fill	outline
X	1.01809	0.194	0.000
Y	1.02304	0.160	0.000
Z	1.02000	0.127	-

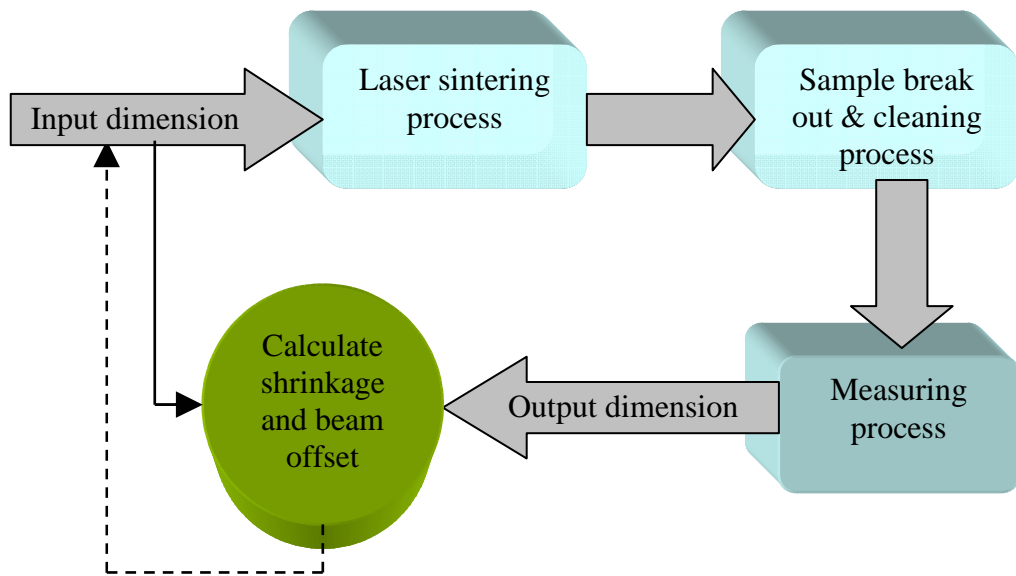


Fig (3.14) Flow chart of beam offset and shrinkage calibration procedure

Nonetheless, some of the most significant sources of error are associated with laser beam positioning on the part bed surface and uncertainty in the calibration factors used to compensate for material shrinkage and growth as well as the finite width of the laser beam. Another source of error is the minimum resolution of the process, which is dependent on the particle size and the shape of the material. However, it is well-known that there are dimensional changes associated with material shrinkage and growth during the fabrication of SLS parts.

Software is available to compensate for these effects, given the proper scale and offset values. The scale and offset procedure includes the building and measurement of purpose-built parts, (Fig 3.15) that contain nominal dimensions. However, while software is used to compensate for the dimensional changes associated with material shrink and growth, the best accuracy is usually obtained when these compensations are small. From a practical standpoint, the effects of growth and finite beam diameter on part accuracy are indistinguishable since they both cause a constant increase in part dimensions [90].

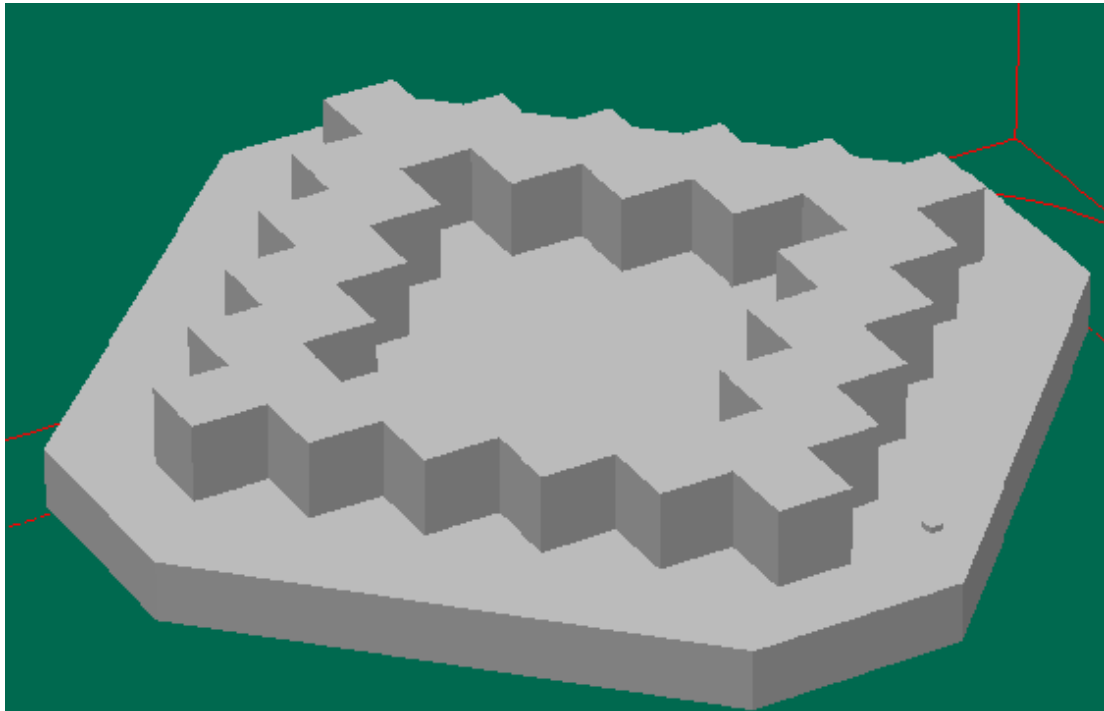


Fig (3.15) Calibration standard part built and measured to calculate shrinkage scale factor and beam offset values for the composite materials.

### **3.5. Characterisation of laser sintered samples**

Process parameters are the pre-defined values that control the sintering of the powders during the SLS process. The mechanical properties and geometrical output of the laser sintered parts are all influenced by the quantity of energy delivered to the powders. Selective laser sintering part accuracy has been reported in a number of studies. In nearly all of these studies, accuracy has been reported as the deviation of measured dimensions from the desired dimensions. However, other components of accuracy are also important to users of these technologies. In particular, trueness of features as characterised by the sharpness of corners and edges and detail resolution is quite important as is the ease of part fit and assembly.

#### **3.5.1. Geometric definition**

Process parameters are the defined variables that influence and control the SLS process. A number of parameters (some user-defined and others defined by geometry or material consideration) affect the quality of parts fabricated. The response of the SLS process is usually described by the geometry and mechanical properties of the object produced. Geometric problems such as curling, shrinkage, growth and poor edge definition and the physical properties such as density, strength and degradation are all influenced by the quantity and timing of energy delivered to the part surface.

Processing PA12/GB composites with laser powers below 8 [W] was not sufficient to provide enough structural integrity for the parts to be handled. They did not sinter the particles sufficiently to a degree that would allow removal from the machine. At the optimum bed temperature, in terms of ease of removal from the powder cake, spreading of powder, etc., a laser power between 8 and 10 [W] was found to be suitable. Laser

power above 18 [W] caused the lased material to degrade significantly. However, even for parts built in the 16-18 [W] range, poor definition was seen around the outline of the parts due to the conduction of heat into the surrounding supporting powder, Fig. (3.16).

To investigate the geometric and dimensional accuracy, purpose-designed parts were manufactured. Two pairs, male and female, of sintered parts were fabricated from PA12/GB composites using various bed temperatures, laser powers and filler content. As shown in Fig (3.16-a) one pair of the parts contains a series of small ribs, slots and hols, while the other pair (Fig 3.16-b) possesses slots, bosses, ribs, circular and rectangular shapes. After the parts were fabricated, each part was measured using digital calliper. Furthermore, the suitability for the facility of assembly, the geometric accuracy after assembly and the manufacturability of sub-millscale features were checked.

The assembly process of pairs fabricated using 8 [W] was carried out easily without any post-working; the parts were fitted in with each other firmly. Milliscale features on pairs produced applying a laser power of 10 [W] were fairly fitted in with each other, while the sub-milliscale features were not present or difficult to assemble. The dimensional accuracy first decreased with increasing laser power and reached the lowest level at a laser power of 18 [W].

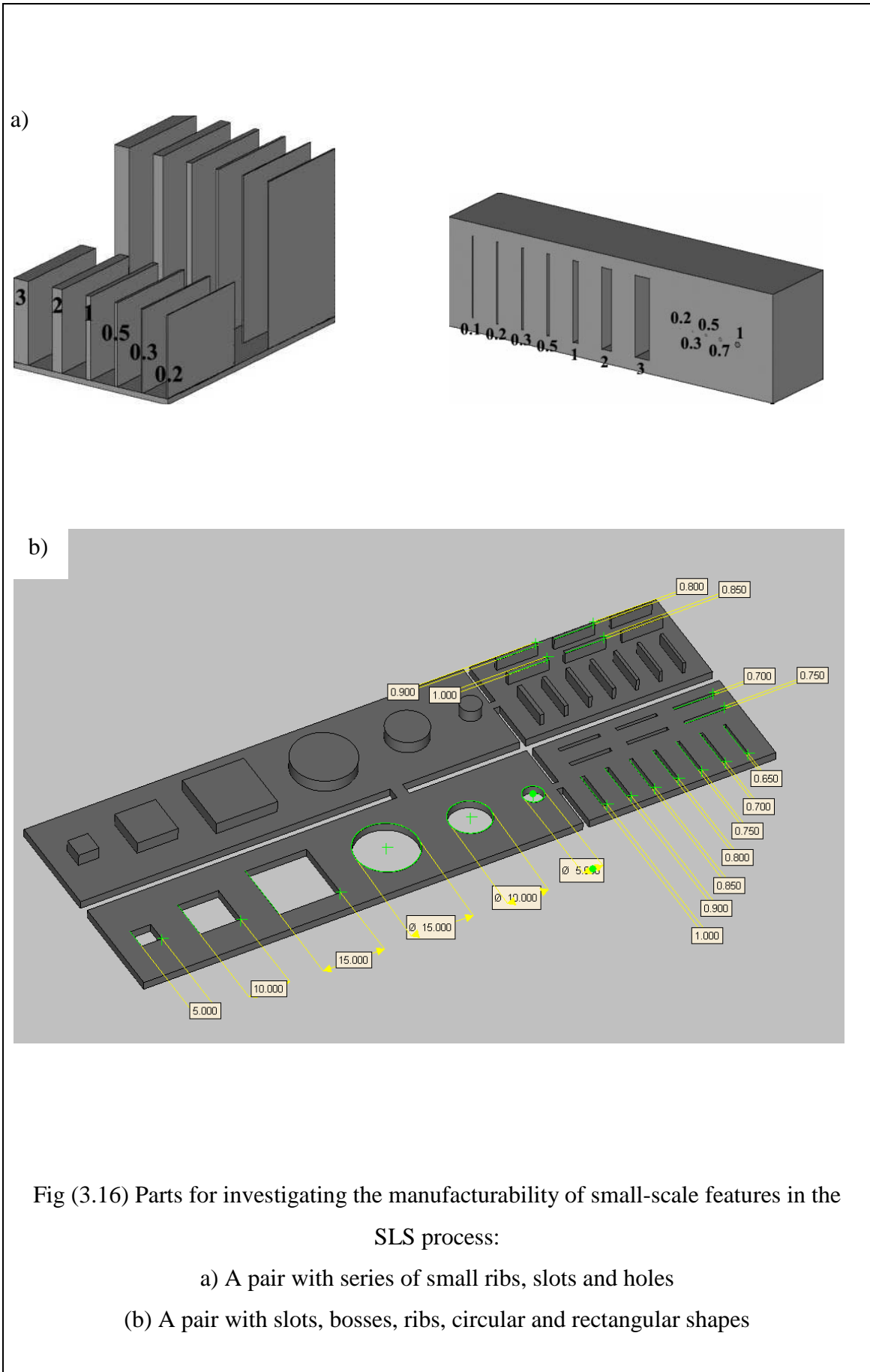


Fig (3.16) Parts for investigating the manufacturability of small-scale features in the

SLS process:

a) A pair with series of small ribs, slots and holes

(b) A pair with slots, bosses, ribs, circular and rectangular shapes

### 3.5.2. Visual observation and evaluation

A visual observation was made to describe the surface geometrical accuracy with comparison to the CAD files. After the samples were broken out from the powder cake, cleaned up and sandblasted, they were visually inspected and photographically recorded. A subjective evaluation was used to determine the quality of parts produced under varying conditions (bed and feed temperatures were kept constant, laser power was varied) on a run-by-run basis. The evaluation was used to judge the effect of processing parameters on glass bead-filled polyamide 12 composites in terms of surface finish and features definition. The evaluation was performed as a qualitative assessment.

As the first look, the parts fabricated applying laser powers of 8 and 10 [W] were complete and almost identical to the CAD model. This means that these laser powers and the corresponding processing parameters (bed temperature of 176 [°C], feed temperature of 95 [°C]) were generally suitable in producing accurate parts. The other samples fabricated using relatively higher laser powers (12-18 [W]) had many missed details and blurred features, as shown in Fig (3.17). Further, an effect of glass bead content and shape on part accuracy (the trueness of features) was observed. A lower content of glass beads (0-10 [wt%]) produced parts with sharper edges and corners and improved detail resolution compared to similar parts with a relatively higher content (40 [wt%]). In addition, visual evaluation of parts from the builds indicated that the surface finish was excellent for the builds from composites containing 0-20 [wt%] glass beads, and was acceptable for the builds with 30-40 [wt%] glass beads. However, the glass beads had a small average particle size (35 [µm]) compared to the commercial PA12 laser sintering powders (50-60 [µm]), which had a nominal effect

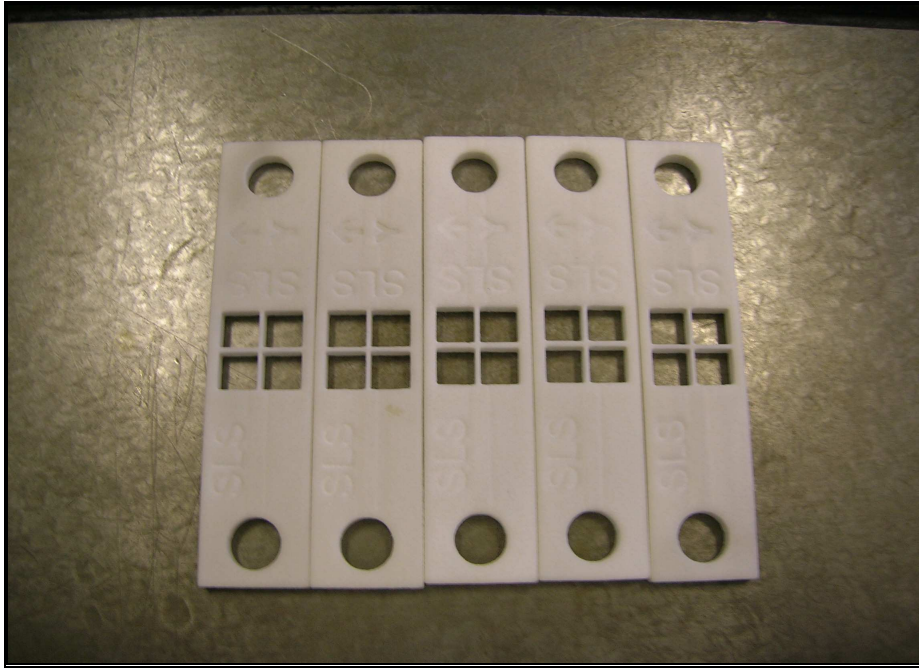


Fig (3.17) Samples for visual inspection of features definition based on bed temperature, laser power and filler content

on the surface finish of the produced parts, observed by the naked eye. Fig (3.18) shows parts with good and acceptable surface finish.

### **3.5.3. Density measurements of sintered density samples**

It is well-known that the density of selective laser sintered components has an important influence on the mechanical properties. Regions in the material which are not fully consolidated have a lower mass/volume ratio leading to lower absolute strength at stiffness values. Also, stress concentrations are more likely to occur in these regions, leading to crack initiation and failure [100].

A nearly full relative density is one of the most important properties required for functional parts. The aim of SLS is to attain high density parts, which need suitable SLS process parameters. Many parameters affect the quality of sintered parts, including sintering material properties, powder properties, the specifications of the SLS machine and process parameters, such as laser power, scan speed, scan spacing and layer thickness. But once the SLS machine is certain and the sintering powder has been selected, the main factors affecting part density are the process parameters. It must be pointed out that the sintered part from powder is porous and its density represents its quality. Though part quality should be evaluated by a combination of mechanical properties, sintered part density is the most important factor. In comparison of a half-density part to a full-density part, the former is inferior to the latter in terms of mechanical properties and surface quality. Therefore, density prediction of SLS parts provides suitable guidelines in the selection of appropriate process parameters. As mentioned above, sintered part quality can be evaluated by its

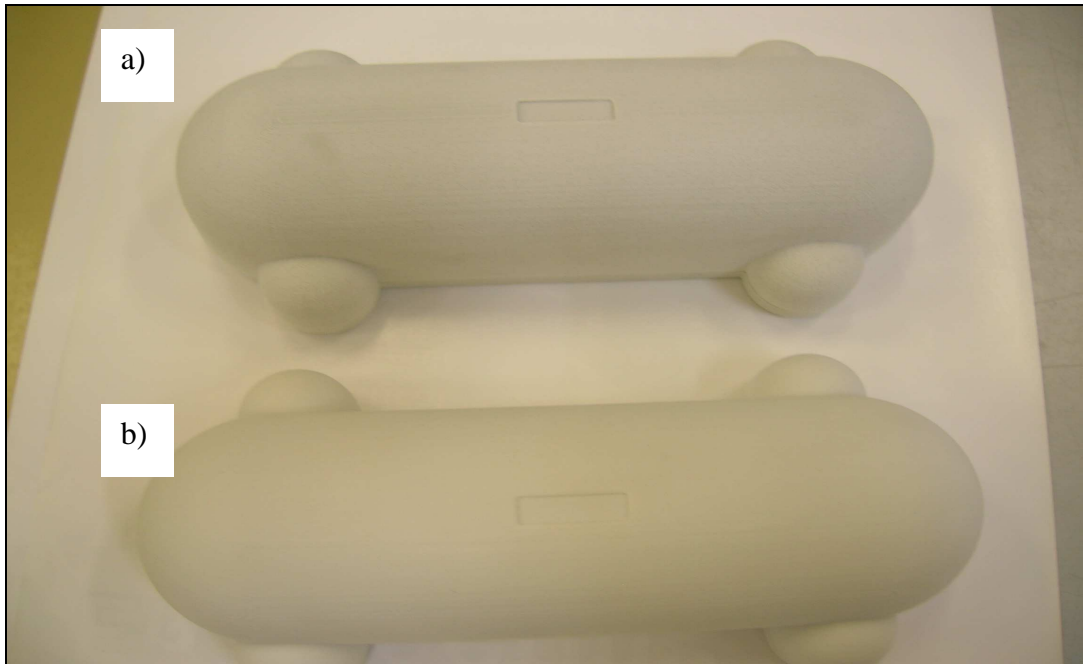


Fig (3.18) Comparison of part surface finish and appearance between parts with different glass bead contents. a) Part contains 40 [wt%]; b) part contains 10 [wt%]

density and SLS process parameters, include laser power, scan speed, scan spacing and layer thickness [101].

The density of the PA12/GB composites was found by building density samples under the same conditions as the other testing samples. The density samples were small square prisms with the intended dimensions 20 x 20 x 5 [mm<sup>3</sup>]. Once the density samples were built, their dimensions were determined manually by measuring with a digital calliper and they were weighed as shown in Table (3.5). Subsequently, the apparent density was found by dividing mass by volume. The average density of the sintered samples was 0.92 [g/cm<sup>3</sup>] obtained from six measurements. Fig (3.19) illustrates the dependency of the weight of the density sample on energy density.

The addition of glass beads with different fractions to the PA 12 matrix affected the density of the PA 12, which could be varied systematically in accordance with other processing parameters. The density ( $\rho$ ) usually increases during sintering and the density of the produced part is usually higher than the powder density, but it is generally believed that the porosity of the powder material can not be completely eliminated. Furthermore, it is often occurs that powder temperature within the area of the part cylinder of the SLS machine is not uniform because of the nature of the powder bed heating temperature system. As a result, this affects the density of the sintered parts being produced, which in turn also affects the mechanical properties and the accuracy of the parts.

Table (3.5) Measured data of sintered density samples

<b>Energy density</b> <b>[J/mm<sup>2</sup>]</b>	<b>l</b> <b>[mm]</b>	<b>w</b> <b>[mm]</b>	<b>h</b> <b>[mm]</b>	<b>m</b> <b>[g]</b>	<b>V</b> <b>[mm<sup>3</sup>]</b>	<b>ρ</b> <b>[g/cm<sup>3</sup>]</b>
0.058	20.64	20.64	5.74	2.2	2445.3	0.90
0.073	20.46	20.46	5.56	2.2	2327.5	0.94
0.087	20.24	20.24	5.40	2.1	2212.1	0.95
0.100	20.04	20.04	5.17	2.0	2076.3	0.96
0.117	20.40	20.40	5.48	2.0	2280.5	0.88
0.131	20.43	20.43	5.75	2.1	2400.0	0.87

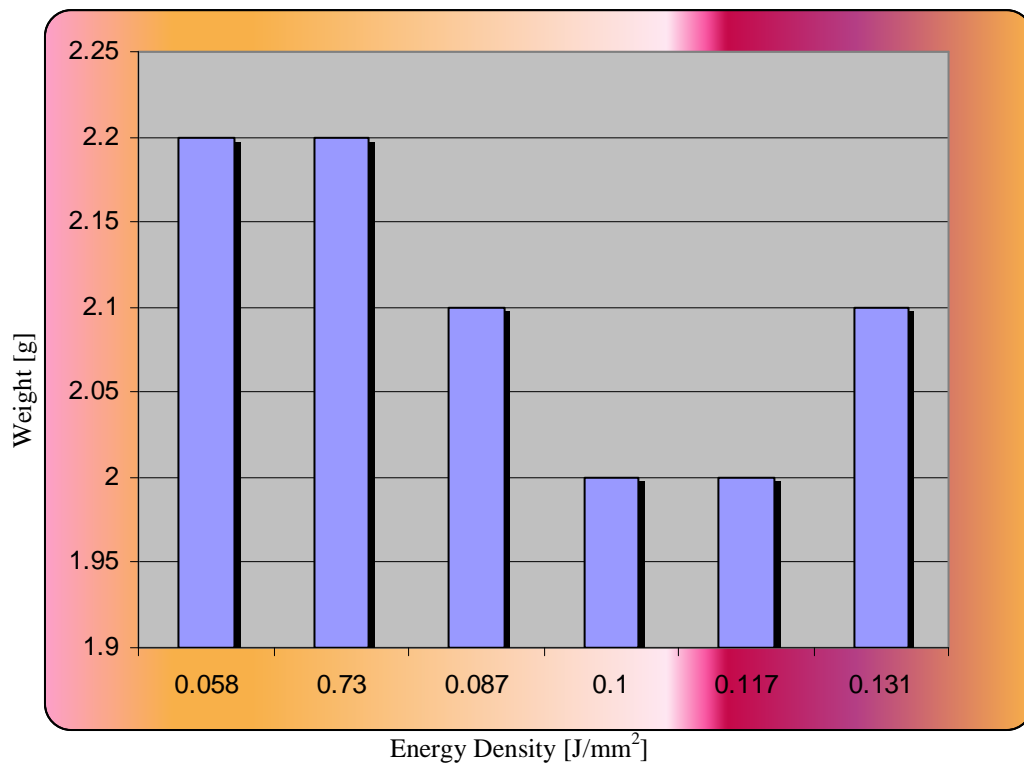


Fig (3.19) Weight of density samples sintered using various energy densities

As it illustrated in Fig (3.20), the density increased with increasing energy density. This can be explained by the fact that higher energy densities cause a better fusion of the powder particles, resulting in a more solid part being formed. Applying too high a laser power not only causes heat to be conducted into the powder bed, melting the surrounding powder particles in addition to those actually targeted by the laser, but it also leads somewhat to degradation of the material composite. However, it was found that the relationship between energy density and part density was not linear. This may possibly be due to the inconsistent variation of heat conditions in the part bed and sample position/location [91].

Part density has been found to increase with bed temperature, so the aim was to keep the part bed temperature as high as possible. The experimentally obtained results show that at a powder bed temperature of 176 [°C], a nearly full density, 0.92 [g/m<sup>3</sup>], can be obtained at an energy density of 0.058 [J/mm<sup>2</sup>], while it decreased by powder bed temperature below 172 [°C], at same energy density. This means that the powder bed temperature, beside other factors, affects the density of the sintered samples. From the result of these experiments, it can be concluded that powder bed temperature affects the density of sintered parts. The lower the powder bed temperature, the lower the sintered part density. However, even with the abovementioned measures, it is very difficult to produce parts with exactly the same densities.

### **3.6. Design and fabrication of test samples**

A switch to test samples production can first be conducted when preliminary experiments are complete and the various procedures have been established. Based on the above discussed pre-sintering studies, the test samples were produced as described

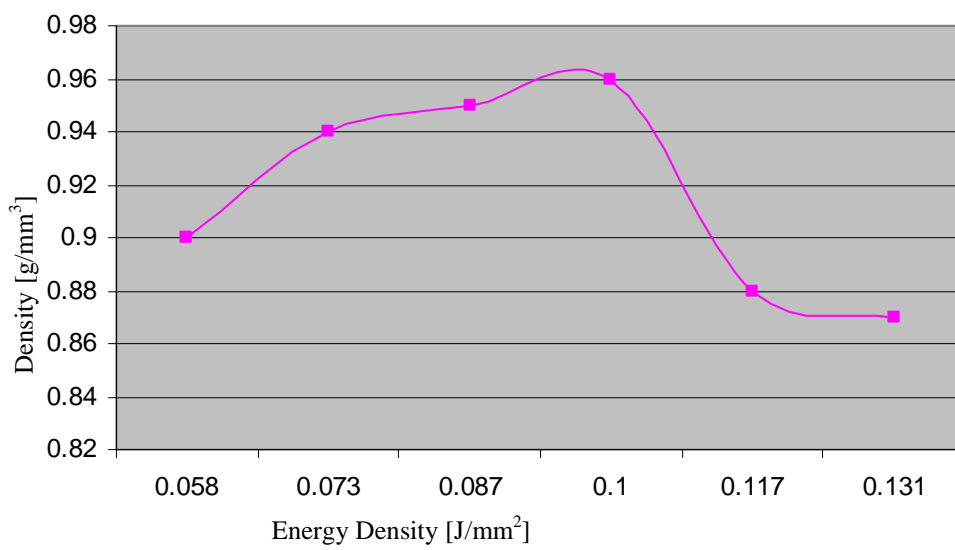


Fig (3.20) Influence of energy density values on the density of sintered density samples

in chapter 4. The test samples were designed according to different British standards for the examination of mechanical properties and an investigation on geometrical accuracy. The CAD model of the test samples was generated using standard CAD software (Magic software, version 7.5) and exported in the STL file format for uploading into the SLS system. Prior to experimenting with PA12/GB composites, pure PA12 was first subjected to laser sintering at different laser powers and bed temperatures. The aim was to establish a set of suitable processing parameters for subsequent processing of the PA12/GB composites. Experiments were carried out to obtain the optimal parameters of SLS and the composition of the composite for successful fabrication.

Using the parameters determined previously, test samples of polymer blends comprising GB and PA 12 were then fabricated on the SLS machine to be used in comparison with pure PA 12. By varying the process parameters (laser power and part bed temperature) and filler ratio, nine groups of samples comprising different blends of PA 12 and GB were fabricated. The nine groups were pure PA 12 and physically blended PA12/GB composites (uncoated and surface coated) consisting of 10, 20, 30 and 40 [wt%] GB. The range of laser power and the part bed temperature settings for fabricating the various samples are tabulated in Table (3.6). Testing of samples for mechanical properties was carried out on a Testometric Materials Testing Machine AX (M350– 5kN) and a Pendulum Impact Test Machine Type (W&T AVERY Ltd.).

Table (3.6) Process parameters used in manufacturing test samples from the PA12/CP00 and PA12/CP03 composites

<b>PA12/GB [wt/wt%]</b>	<b>100/0</b>	<b>90/10</b>	<b>80/20</b>	<b>70/30</b>	<b>60/40</b>
<b>PA12/CP00; PA12/CP03</b>					
Laser power [W]	8				
	10				
Energy density [J/mm <sup>2</sup> ]	0.058				
	0.073				
Scan Speed [mm/s]	914				
Powder bed temperature [°C]	176				
Feed Temperature [°C]	95				
Layer thickness [mm]	0.10				
Roller speed [mm/s]	127.0				
Rotate scan order [-]	1				

### 3.7. Summary

This chapter has provided a description of the composite materials and process parameter data, obtained from preliminary experiments, needed for the subsequent chapters on the investigation of the mechanical properties and geometric accuracy of glass bead/polyamide 12 composites. Material properties play an important role in determining fabrication parameters and affect the mechanical properties and geometric accuracy of SLS components. The glass transition temperature  $T_g$  and melting temperature  $T_m$  are two important factors for determining part bed temperature and laser power.

In this chapter, different powder bed temperatures, laser power settings and powder constitutions were applied to determine the most suitable processing temperature for the PA12/GB composites. A higher bed temperature and energy density generally result in better fusion of the polymer matrix particles. They enable the production of a more compact structure and near fully solid, dense parts with a smooth surface. However, when these parameters become excessively high, numerous phenomena, such as curling, caking, growth and polymer degradation problems are accordingly observed.

A DTM system Sinterstation 2000 machine was used for conducting experiments on PA 12 and PA12/GB composites with different weight contents of glass beads (10-40%) with and without surface treatment. The optimal parameters for selective laser sintering of these composites were experimentally determined. Optical Microscopy and Scanning Electron Microscopy (SEM) were used for characterising the powder material and the resulting sintered parts.

## **Chapter 4- Effects of processing conditions and coupling agents on mechanical properties of selective laser sintered glass bead-filled polyamide 12 composites**

For any given application, certain mechanical properties will be of more importance than others. It is therefore essential to identify and rank the most relevant properties and formulate or purchase the least expensive composite material that satisfies the requirements. The mechanical properties of interest for most applications are modulus (tensile or flexural), yield strength, impact strength and fracture toughness [102].

Due to their unique attributes including ease of production, light weight and often ductile nature, polymer systems are widely used in the industry. However, polymers generally have lower mechanical properties (modulus and strength) as compared to metals and ceramics. In order to improve the mechanical properties of polymers, the forming of polymer matrix composites by the inclusion of fillers is one among many ways for achieving this goal [80].

Polyamide-based composites have proven to have great potential for rapid manufacturing in fabricating functional parts; however, the mechanical properties (strength, in particular) of classic sintered polyamide 12 are only approximately 80% of that of an injection moulded polyamide specimen. In selective laser sintering, the mechanical properties of the part are largely influenced by many factors such as powders, processing parameters, fabrication position and orientation. For these reasons, significant research efforts have been directed toward finding SLS materials with

improved mechanical properties. To this end, it has been well established in the literature that material properties are directly related to process parameters in the Selective Laser Sintering process and hence can be varied by changing process parameters [62], [72], [104].

## **4.1. Experiments**

### **4.1.1. Materials and sample preparation**

#### *Materials and Processing*

The polyamide 12 (Nylon 12; PA12; PA2200) used in this work as a matrix material was a commercial fine polyamide PA2200 for EOSINT P supplied by EOS GmbH. The density according to DIN 53466 was 0.435-0.445 [g.cm<sup>-3</sup>]. Two types of A-glass beads (Spherglass 3000: CP00 with no surface pre-treatment and CP03 surface pre-treated with a silane coupling agent) with mean diameter of 35 [μm] were selected as the filler. The glass beads, small solid spherical particles with a density of 2.5 [g/cm<sup>3</sup>], were supplied by Potters Industrial Inc/Omya UK Ltd.

#### *Sample preparation*

In the sample preparation process, the polyamide 12 was compounded with glass beads with 10, 20, 30 and 40 [wt%] ratios, using a rotating drum mixer type BS 125 for 30 minutes to produce the composites. Selective laser sintering (SLS) was performed using a DTM Sinterstation 2000 System to manufacture specimens from glass bead-filled polyamide 12 composites with a fill laser power (P) of 8 or 10 [W], a laser beam speed (BS) of 914 [mm/s], a scan spacing (SCSP) of 0.15 [mm], layer thickness (L<sub>r</sub>) of 0.1 [mm], beam diameter (d) of 0.4 [mm] and powder bed temperature (T<sub>b</sub>) of 176 [°C].

The energy density (ED), regarded as the relative applied laser energy per unit area, can be calculated as follows [59],

$$ED = \frac{P}{BS \times SCSP} \quad \dots (4.1)$$

therefore, the corresponding laser energy densities ranged from 0.058 to 0.073 [J/mm<sup>2</sup>]. In addition, some samples were prepared for the purpose of comparison from the pure polyamide 12 powder. Table (4.1) summarises the process parameters used in manufacturing the test samples from the PA12/CP00 and PA12/CP03 composites.

#### **4.1.2. Equipment and methodology**

Mechanical testing plays an important role in evaluating the fundamental properties of engineering materials as well as in developing new materials and in controlling the quality of materials for use in design and construction. If a material is to be used as a part of an engineering structure that will be subjected to a load, it is important to know that the material is strong enough and rigid enough to withstand the loads that it will experience in service. As a result, engineers have developed a number of experimental techniques for mechanical testing of engineering materials subjected to tension, compression, bending or torsion loading.

In the testing step, the tensile, flexural, Izod impact SEN samples with BS EN ISO 527 and 178-180/1A standards, respectively, were produced using an SLS machine (DTM Sinterstation 2000). The direction of the samples in the build chamber was on the X-axis parallel to the front of the machine and in the X-Y plane of the build chamber, Fig (4.1).

Table (4.1) Process parameters used in manufacturing test specimens from the PA12/CP00 and PA12/CP03 composites

PA12/GB [wt/wt%]	90/10	80/20	70/30	60/40
Laser power [W]	10			
Energy density [J/mm <sup>2</sup> ]	0.073			
Scan Speed [mm/s]	914			
Powder bed temperature [°C]	176			

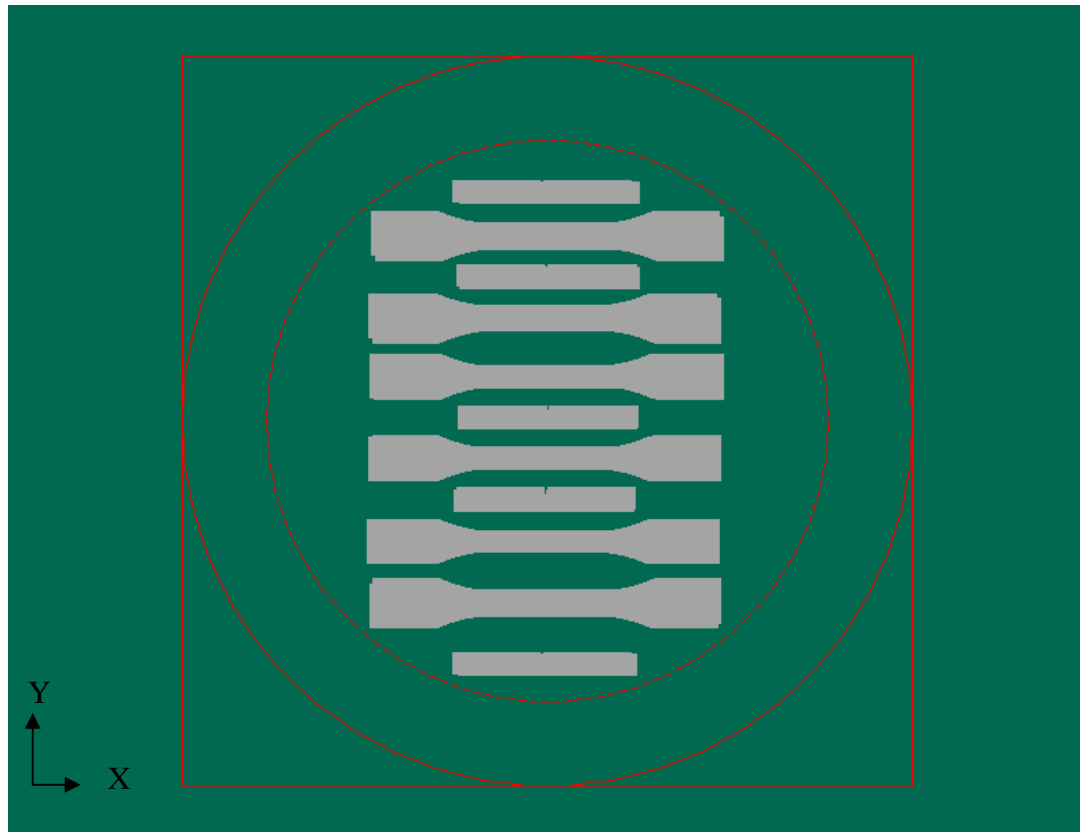


Fig (4.1) Orientation of samples in the build bed of the SLS machine

The fabrication of specimens was carried out for both systems under the same conditions. While the weight ratio varied, the bed temperature was kept fixed.

After production, the samples were removed from the part cake and cleaned manually. Sandblasting and pressurised air were used to remove powder remnants. The dimensions of the specimens were obtained using digital micrometers and callipers. Each dimension was taken three times and an average of these values was associated with each part.

The tensile, flexural and fracture toughness tests were carried out using a Testometric materials testing machine AX (M350 – 5 kN). To measure the elastic tensile modulus, an extensometer was installed with a cross-head speed of 1mm/min. The test results (tensile and flexural properties) were the mean values of six specimens.

The impact test was carried out at room temperature using a pendulum impact test machine type W&T AVERY Ltd. The tensile strength, elastic modulus, elongation at break, impact strength and flexural strength were recorded and obtained.

To observe the morphological structure of scan surfaces and the fracture cross-section of tensile bars, a Scanning Electron Microscope (ZEISS XB 1540 workstation) was used. Samples were taken from the fracture zone of the dumb-bell bars and were coated with gold before observation.

## **4.2. Mechanical properties**

Several figures of merit are used to characterise the mechanical properties of materials. Young's modulus is a measure of stiffness, the amount of stress needed to create a small recoverable (elastic) deformation. Yield strength is the stress needed to create an irrecoverable (plastic) deformation. Flow stress is the stress needed to steadily stretch the material beyond the yield point. Toughness expresses the amount of energy needed to fracture a specimen of the material, which is highly dependent not only on the material's properties, but on strain rate, temperature, sample geometry and pre-existing flaws [104].

### **4.2.1. Tensile strength**

The tensile strength of a material is defined as the maximum stress that the material can sustain under uniaxial tensile loading. For particulate composites, this relies on the effectiveness of stress transfer between the matrix and the filler. Factors like particle size, particle/matrix interfacial strength and particle content significantly affect the composite strength [105]. The tensile properties of glass bead-filled polyamide 12 composites were determined according to BS EN ISO 527 standards. The testing machine, the shape and the most important dimensions of the tensile specimen are summarised in Figs (4.2) and (4.3).

#### *Tensile curves*

The stress-strain curve is a graphical representation of the relationship between stress and strain. The nature of the curve varies from material to material. Stress-strain curves can not only be used to identify some mechanical properties such as

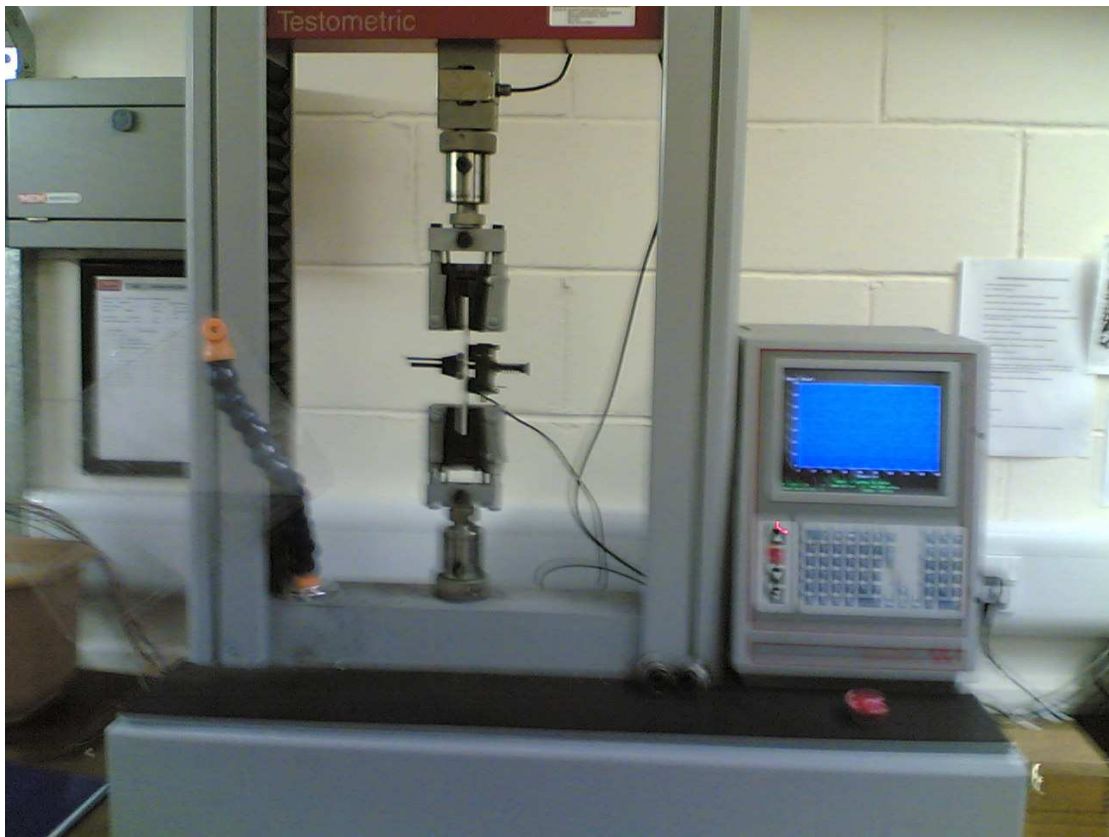
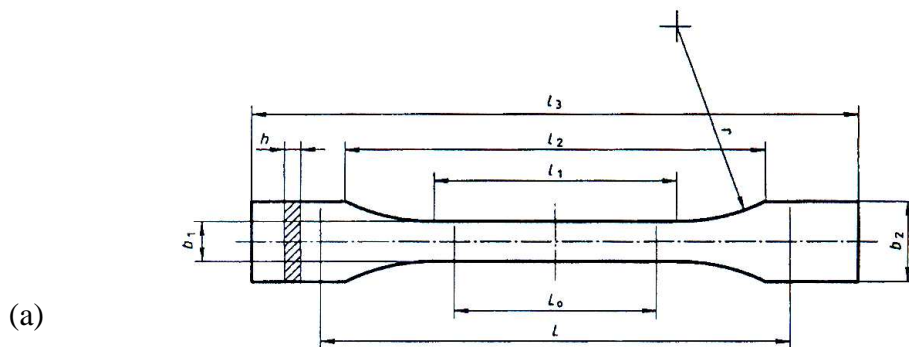


Fig (4.2) Testometric materials testing machine and extensometer installed



(b)

	Specimen type	1A
$l_3$	Overall length	$\geq 150$
$l_1$	Length of narrow parallel-sided portions	$80 \pm 2$
$r$	radius	20 ... 25
$l_2$	Distance between broad parallel-sided portions	104 ... 113
$b_2$	Width at ends	$20 \pm 0.2$
$b_1$	Width of narrow portions	$10 \pm 0.2$
$h$	Preferred thickness	$4.0 \pm 0.2$
$L_0$	Gage length	$50 \pm 0.5$
$L$	Initial distance between grips	$115 \pm 1$

Fig (4.3) Shape and dimensions of the tensile test samples

Young's modulus, yield strength, fracture strength and elongation at break, but they also allow for making statements and predications about a material's behaviour.

Fig. (4.4) demonstrates the tensile stress-strain curves of the PA12/CP00 and PA12/CP03 systems under uniaxial tension at room temperature. Generally, it can be seen from these figures that the maximum tensile stress ( $\sigma$ ) and tensile strain ( $\epsilon$ ) tended to decrease with increasing weight ratio. However, the samples of glass bead- filled polyamide had a different maximum stress compared to that of the unfilled polyamide 12, where the elongation at break of the neat PA12 was **significantly higher** than that of the composites. Each curve shows a maximum stress, which is assumed to be the yield strength of the material. After 30 [wt%] beads, the stress decreased noticeably with strain for both systems. The stress-strain curves of the PA12/CP03 system remained slightly above these of PA12/CP00.

#### *Stress calculation*

The tensile specimens had a nominal thickness of 4 [mm], width of 10 [mm] and other dimensions were determined with reference to BS EN ISO 527-2 Type 1A, (Fig 4.3). The as-sintered specimens were tested under ambient conditions and at a crosshead speed of 1 [mm/min]. The average tensile strength was obtained from six tests.

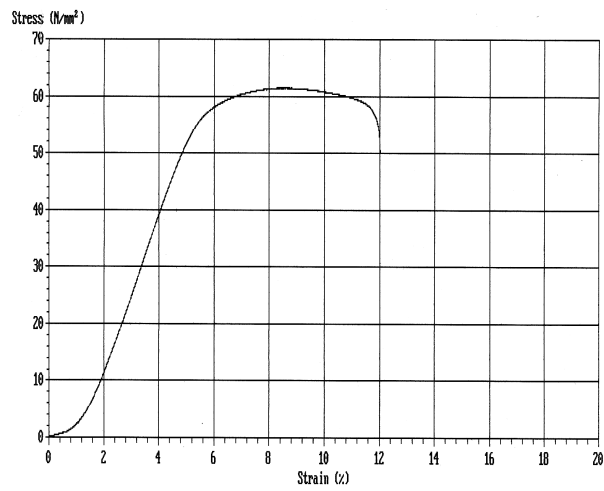
The tensile stress is calculated according to equation (4.2) [BS EN ISO 527]:

$$\sigma = \frac{F}{A} \quad \dots (4.2)$$

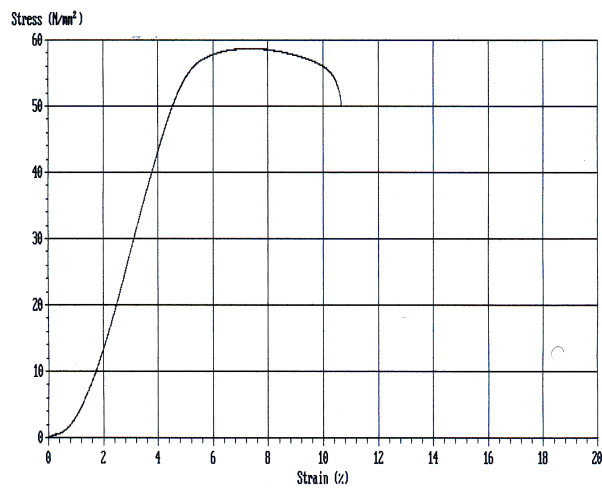
where :  $\sigma$  is the tensile stress value in question [MPa]

F is measured force concerned [N]

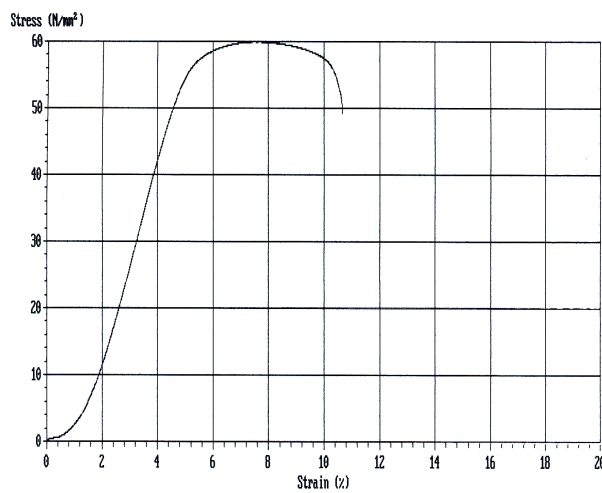
A is the initial cross- sectional area of the specimen [mm<sup>2</sup>]



(a)



(b)



(c)

Fig (4.4) Stress-strain curves: (a) Polyamide12; (b) PA12/CP00 (90:10 [wt%]), (c) PA12/CP03 (90:10 [wt%]); laser power: 10 [W]

Fig. (4.5) displays the variation of tensile strength of the polyamide composites with glass beads by weight percentages for both systems. It is clear that the tensile strength increased to some extent with increased glass bead weight percentage, namely, from 48 [MPa] at 10 [wt%] to 55 [MPa] at 20 [wt%], where the influence was quite remarkable. Above 20 [wt%], the addition of increasing amounts of glass beads led to a decrease in the tensile strength. The composite strength decreased with increasing glass bead content and was lower than that of the polymer matrix, but better interfacial adhesion gave higher composite strength. In accordance with this, the strength of the composites containing treated glass beads (CP03) was slightly greater than that of the composites filled with the uncoated glass beads (CP00). This means that the interfacial adhesion between the glass beads and polyamide plays an important role in the improvement of the strength of filled polyamide. However, the strength of glass bead-filled polyamide composites is determined not only by the energy density, particle size and particle/matrix interfacial adhesion, but also by the particle contents.

The reduction in strength with the addition of beads may be attributed to the reduction of aggregate bonding strength of the matrix composite due to less polyamide and increasing structural microporosity. The tensile strength increased at first and then became slightly constant in the interface-treated composites, and decreased in the composites filled with untreated glass beads. In addition, it can be seen that the figs (4.5a, b) are not quite similar and the curves follow different pattern; however the calculated values of tensile strength using Eq. (4.2) tend to be slightly different to those recorded by extensometer as it is presented in Table (4.3).

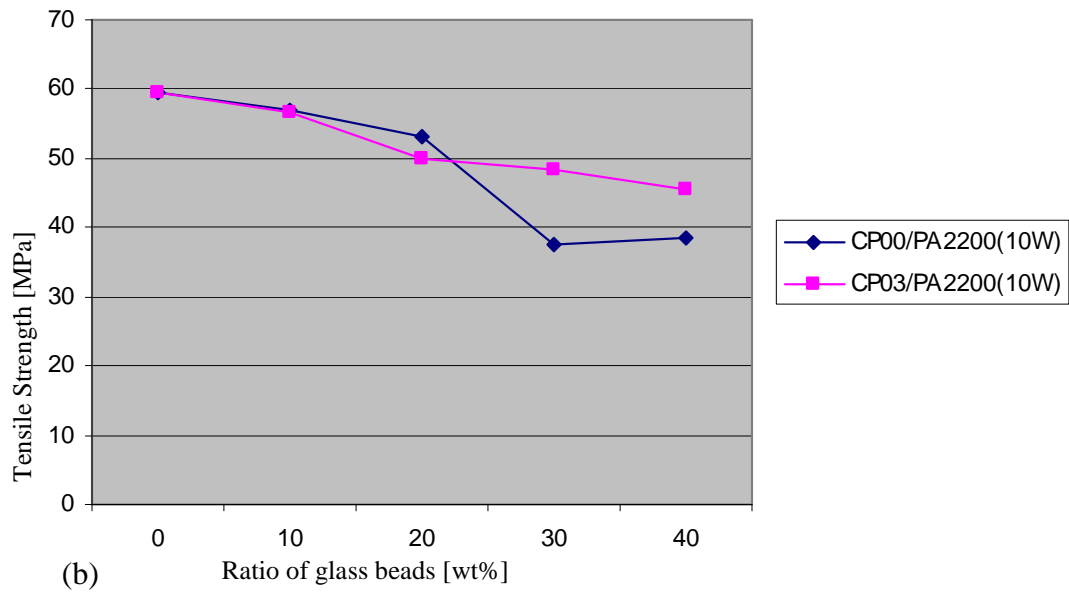
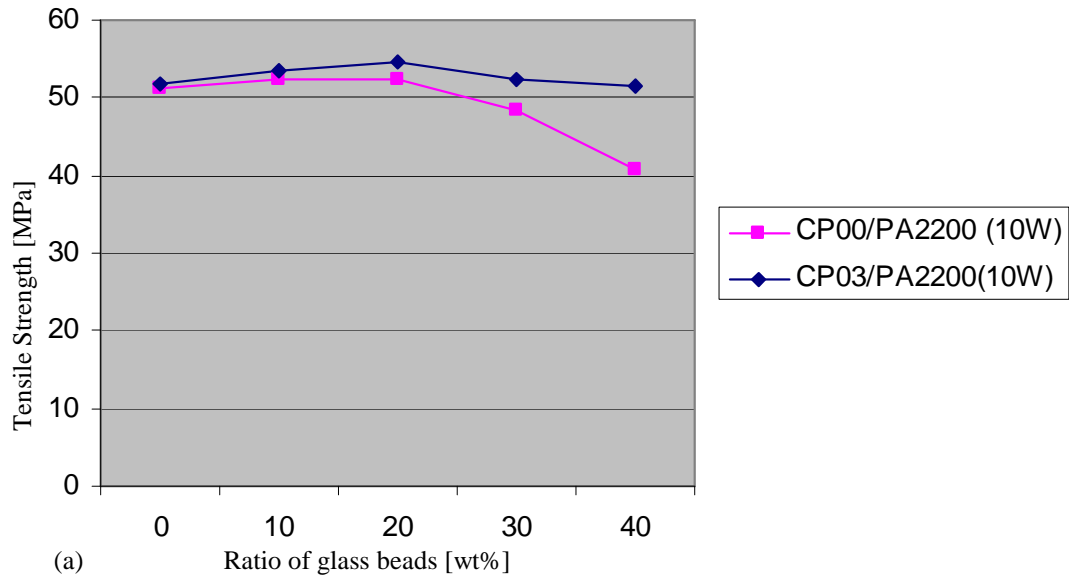


Fig (4.5) The variation in tensile strength of the PA2200/CP00 and PA2200/CP03 systems. (a) by calculation; (b) by extensometer

### 4.2.2. Young's modulus

Young's modulus, in general, is the stiffness of a material at the elastic stage of the tensile test. It is defined as the ratio of the uniaxial stress over the uniaxial strain in the range of stress in which Hooke's law holds. Young's modulus is markedly improved by adding rigid particles to a polymer matrix since the rigidity of inorganic fillers is generally higher than that of the polymers. The composite modulus consistently increases with increasing particle content.

The strain can be calculated using equation (5.2), [BS EN ISO 527]:

$$\varepsilon = \frac{\Delta L_0}{L_0} \quad \dots (4.3)$$

where:  $\varepsilon$  is strain [%] ;  $\Delta L_0$  is the elongation [mm] ;  $L_0$  is measurement length of the specimen.

The modulus of elasticity in tensile stress is calculated according to the equation (4.4):

$$E = \frac{\sigma_2 - \sigma_1}{\varepsilon_2 - \varepsilon_1} \quad \dots (4.4)$$

where:  $\sigma_1$  and  $\sigma_2$  are tensile stress;  $\varepsilon_1 = 0.0025$  and  $\varepsilon_2 = 0.0005$  are strains

Fig. (4.6) shows the variation of the modulus of elasticity with the glass bead weight ratio. It can be observed that increasing the weight percentage of glass beads led to an increase in the Young's modulus of the test specimens produced for both systems. The calculation results show that an increase in glass beads from 10 to 40 [wt%] led to an increase in the modulus of elasticity from approximately 1700 to 6500 [MPa].

Generally, the increase in the modulus of elasticity is explained by the percolation theory, which states that a matrix zone around each particle is affected by stress concentration. Therefore, if the distance between particles is small enough, these zones join together and form a percolation network, which increases the modulus.

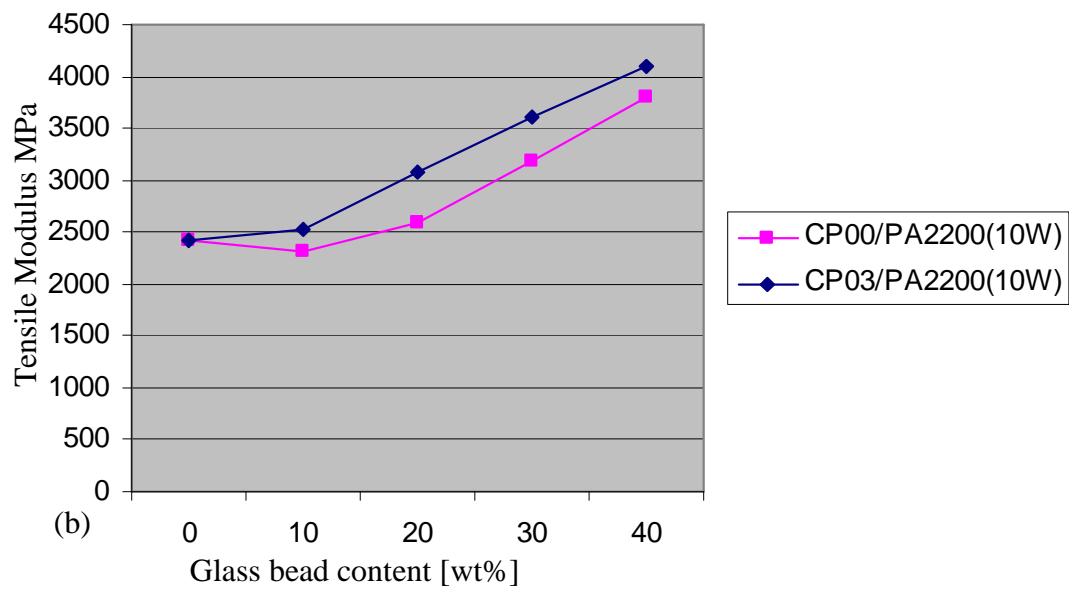
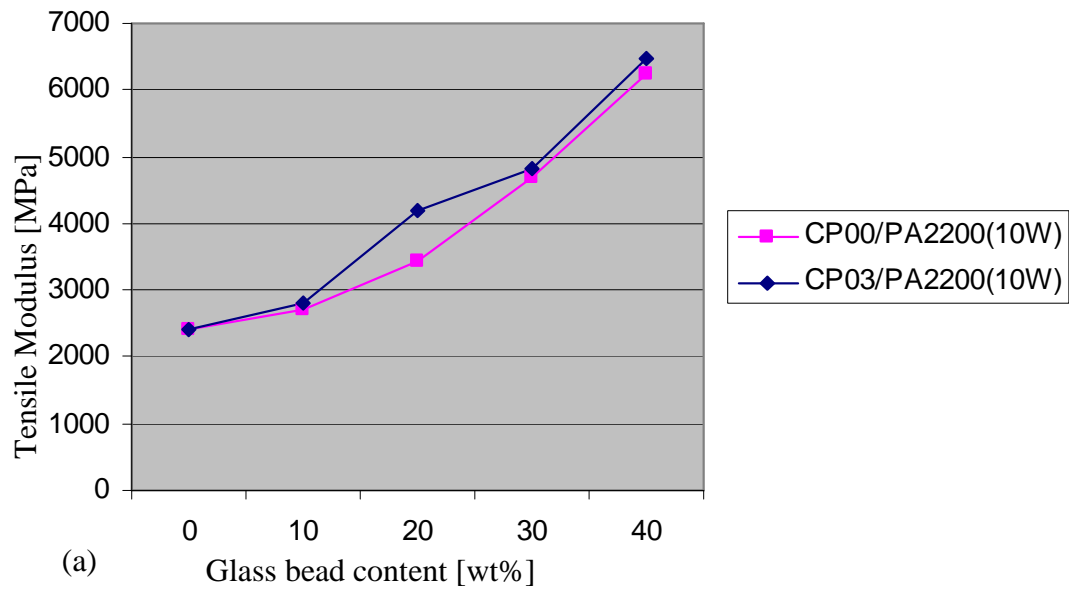


Fig (4.6) The variation of the modulus of elasticity of PA12/ glass bead composites with glass beads content [wt%]: (a) by calculation; (b) by extensometer.

On the other hand it is well-known that for rigid particulate-filled polymer composites (in addition to the difference in modulus between the particles and polymer), some physical cross-linking points might be generated. Furthermore, the movement of the molecular chains of the matrix polymer could experience a blockage, to some extent, due to the addition of the glass beads, leading to an improvement in the stiffness of the composite. However, the Young's modulus of the materials increases correspondingly with an increase in the particle content regardless of interface treatment, because it is determined from the initial elastic deformation without damage [55], [106].

However, since one of the project goals was to either maintain or increase the modulus, or stiffness, the particles must carry part of the load at small deformations. If the particles are completely loose from the matrix, then they effectively act as voids within the material, and the modulus will be diminished by an amount proportional to the particle weight ratio. If they do bind tightly at small strains, then they will carry part of the load, and since they are stiffer than the matrix, the overall modulus will increase. Moreover, the better the dispersion of the particles in the matrix and interfacial bonding between the matrix and the glass beads, the better the stiffness of the composite. For these reasons, the adhesion between the particles and the matrix must be of intermediate strength in order to accomplish the goal of simultaneous stiffening and toughening [104].

The values of modulus for the PA12/CP03 system were slightly higher than those for the PA12/CP00 system having the same filler content. When the weight ratio was  $> 20\%$ , the difference in modulus between the two systems was more evident. This indicates that the enhancement of interfacial adhesion between the matrix and the glass

beads is helpful in improving the stiffness of the filled PA12 composites. Furthermore, it can be seen that the Figs (4.6a; b) are similar yet slightly different. The curves follow the same pattern; however the calculated data of Young's modulus using Eq. (4.4) tend to be higher than those recorded by the extensometer as shown in Table (4.3). However, when comparing calculated values (using the stress obtained by crosshead movement) for tensile strength and Young's modulus, to those recorded using the extensometer, differences have been observed. These differences can be explained by the following factors. Firstly, measuring imprecision and the practice of sliding a ruler along a graph in order to determine the above mentioned properties leave plenty of room for inaccuracies. Secondly, the calculations of the stress **are** based on the force the crosshead applies and the preset dimensions for the cross-sectional area. If the actual dimensions do not accurately represent the area of the sample, it will result in stress values that are higher or lower to those of the extensometer. Thirdly, if the specimen slips at all, while in the grips of the testing machine, it can alter the collected data. The same holds true if the sample extends in the transition region rather than just in the gauge region. The extensometer is used to prevent these two issues. Lastly, a plastic stress curve versus strain curve most often contains a linear elastic region, as well as a non-linear plastic region. Very little strain occurs within the linear region. Because modulus is measured within this region, an extensometer with a high resolution is necessary. The mechanical transverse extensometer used typically has limited travel and must be removed from the specimen during a test. The inaccuracy of recorded data for elastic modulus is most likely due to the fact that it is difficult to determine strictly the exact point at which the extensometer should be removed from the specimen.

### 4.2.3. Elongation at break

Elongation at break is an important parameter of the tensile fracture toughness of a material. Fig (4.7) presents the variation of the elongation at break value with the ratio of glass beads. The results show that the elongation at break decreased drastically with increased glass bead ratio. The measured elongation at break with 10 [wt%] glass beads was 3.17% and decreased to 0.13% at glass bead content of 40 [wt%]. This is generally explained by immobilisation of the macromolecular chains by the filler which increases the brittleness of the polymer. On the other hand, the increase in deformability of the PA12/CP03 system due to the presence of a coupling agent indicates that silane coupling agents probably provide a plasticising (or lubrication) effect because of the formation of physisorbed layers in the interphase [33], [107].

The calculation of percentage elongation at break in relation to the original gauge length can be carried out using the following equation:

$$E_p = \frac{l - l_0}{l_0} \times 100 \quad \dots (4.5)$$

where

- $E_p$  is the percentage elongation at break
- $l$  is the distance between reference marks, at break [mm]
- $l_0$  is the original length [mm]

Evaluation of elongation at break showed that small differences at a lower filler content are the consequence of a small impact of filler on the polyamide matrix due to the small interfacial area. In this case, the elongation at break values were primarily influenced by the decrease in specimen cross-section during elongation or strain hardening. At higher filler contents, the effect of the filler on the polyamide matrix

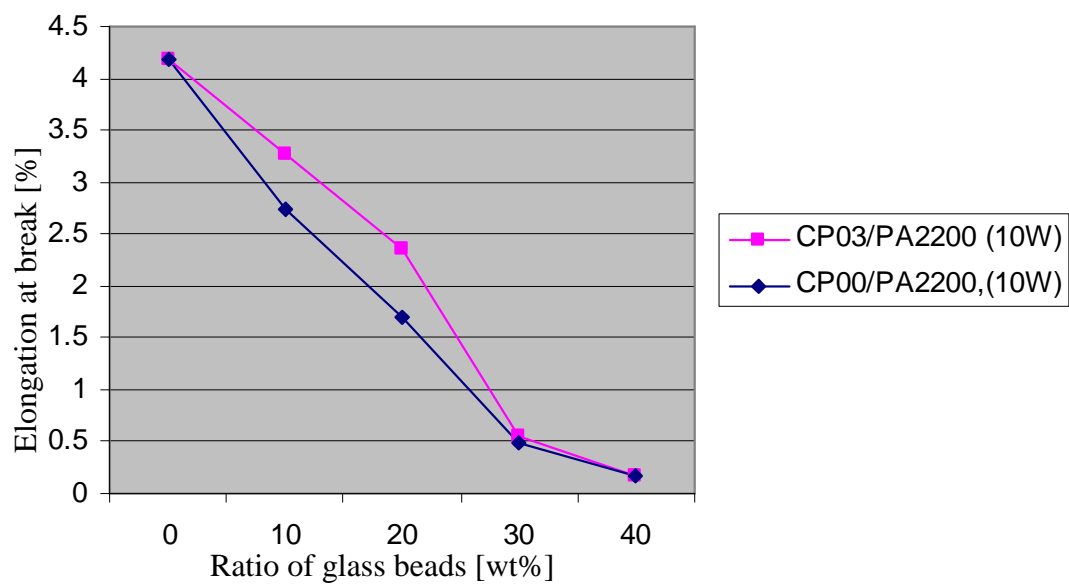


Fig (4.7) The variation of the elongation at break with glass bead content.

was much more extensive due to the enlargement of the interfacial area and the formation of increased interfacial interactions between the filler and the matrix.

However, as it can be seen from Fig (4.7) that the values of elongation at break of composites increased with silane coupling agent treatment compared to the untreated cases at a constant glass bead content due to the plasticiser effect of silane coupling agents.

#### **4.2.4. Flexural strength and modulus**

In many applications for particulate-filled plastics, especially particulate-filled thermoplastics such as polyamides, the product must not only be strong, but also stiff or rigid to perform as designed. The flexural strength of a material is defined as its ability to resist deformation under load. The flexural modulus is the ratio of stress to strain in flexural deformation, or the tendency for a material to bend. Adding glass beads increases the stiffness or flexural modulus of a polyamide composite. Generally, the more glass beads used, the greater the increase in flexural modulus.

Flexural strength and the modulus of elasticity were obtained through a three-point bending test. Most commonly, the sample was placed on a support span and the load was applied to the centre by the loading nose, producing three-point bending at a specified rate. The parameters for this test are the support span, the speed of loading and the maximum deflection for the test. These parameters are based on the test specimen thickness and are defined by ISO 178. Fig. (4.8) summarises the shape, dimension and arrangement of the test samples.

## Stress calculations

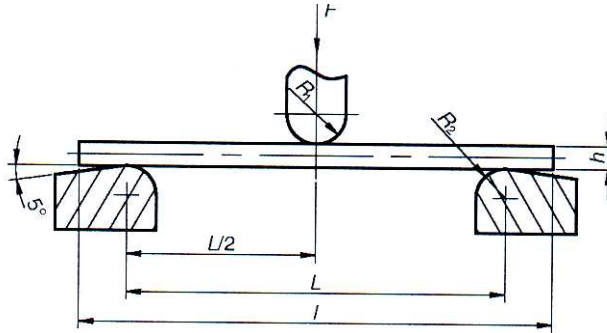
For a rectangular sample under a load in a three-point bending setup:

$$\sigma_f = \frac{3FL}{2bh^2} \quad \dots (4.5)$$

where:  $\sigma_f$  flexural stress [MPa]  
F the load (force) at the fracture point [N]  
L the length of the support span [mm] ,  $L = 16 h = 16 \times 4 = 64$  [mm]  
b width [mm]  
h thickness [mm]

The flexural properties are presented in Table (4.2). Table (4.2) reveals that the glass bead-filled polyamide exhibited a lower flexural strength and higher modulus than that of the uncoated system.

Fig. (4.9) demonstrates the variation of the flexural strength and flexural modulus with glass bead content. The results from the experiments show that flexural strength increased gradually, whilst the flexural modulus values increased steadily as glass bead loading increased from 10 to 40 [wt%]. However the flexural strength and flexural modulus values of the PA12/CP03 system with coated glass beads were slightly higher than those of the PA12/CP00 system, where is generally believed that the coupling agent would soften the PA12 matrix around the glass beads, which have a smooth spherical surface and should not initiate fine cracks in the matrix around them.



Loading and supports		Dimension
Loading radius		$R_1 = 5 \pm 0.1$ [mm]
Support radii		$R_2 = 2 \pm 0.2$ [mm] – for test specimens of thickness $\leq 3$ [mm]
		$R_2 = 2 \pm 0.2$ [mm] – for test specimens of thickness $\geq 3$ [mm]
Test specimen		
Length		$l = 80 \pm 2$ [mm]
Width		$b = 10 \pm 0.2$ [mm]
Thickness		$h = 4 \pm 2$ [mm]

Fig (4.8) Shape, dimension and arrangement of test samples

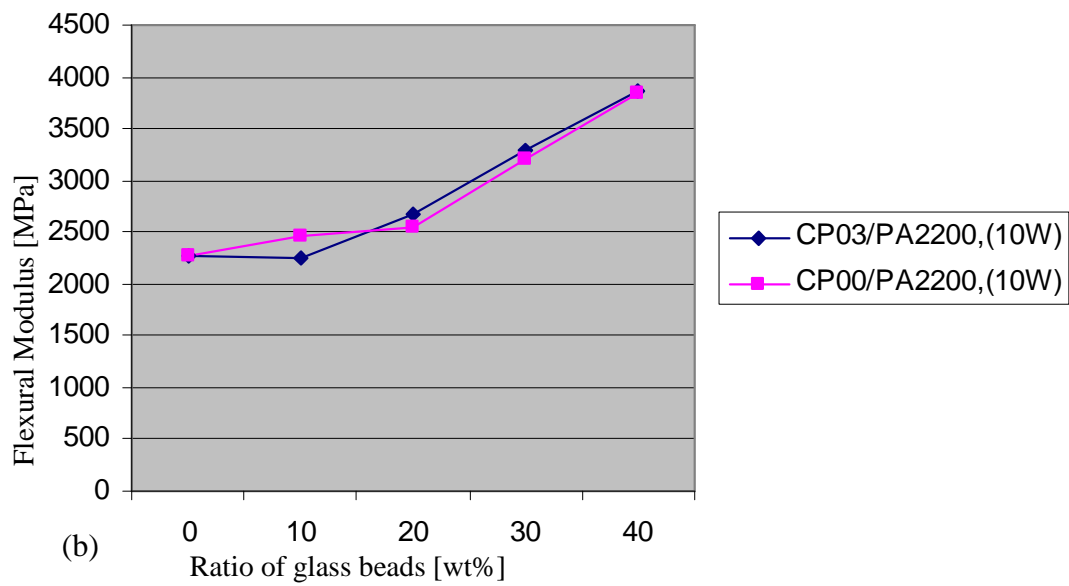
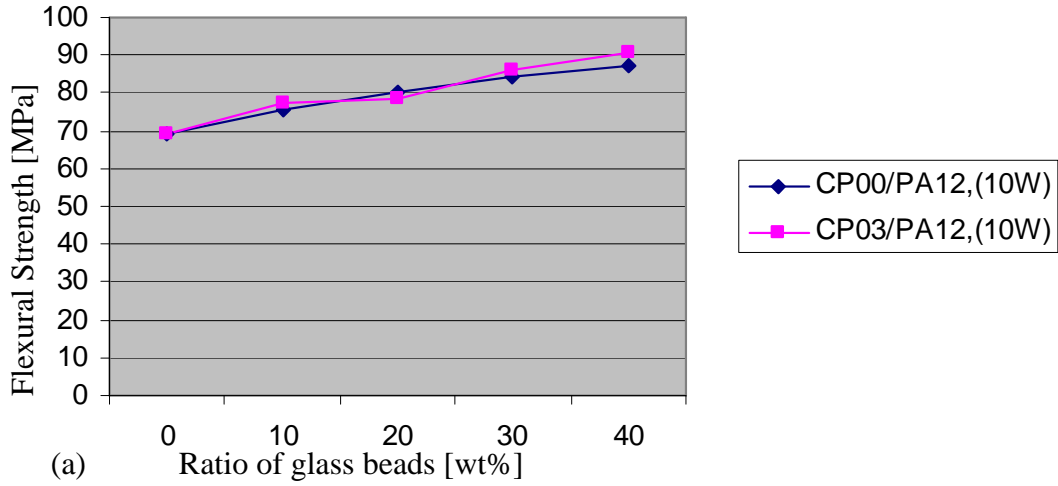


Fig (4.9) The variation of the flexural strength (a); and flexural modulus (b) with glass bead content

#### 4.2.5. Impact strength

The impact strength of notched samples was measured at ambient temperature by the notched Izod test. Izod impact tests were carried out on 80x10x4 [mm] rectangular bars with a single-edge 45° V-shaped notch (tip radius 0.25 [mm], depth 1.5 [mm]). The test was performed at room temperature using a pendulum impact test machine type W&T AVERY Ltd., with a pendulum speed at impact of 2.44 [m/s], Fig (4.10).

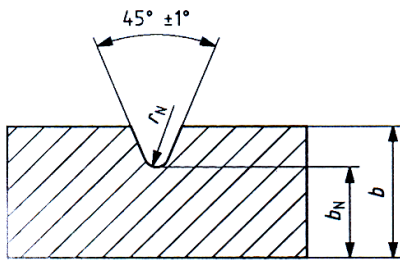
The Izod fracture test was carried out to characterise the impact strength of glass bead-filled polyamide 12 composites. The samples used were the notched rectangular bar described above. The average values were calculated from six samples and the measured results for impact strength are listed in Tables (4.2) and (4.3).

The impact strength of different PA12/GB composites with different filler content is shown in Fig. (4.11). It is clear from this figure that the impact strength increased to some extent with increased glass bead weight percentage. As the weight ratio of glass beads increased, the impact strength of the polyamide was reduced. With loading up to 20 [%wt], the significant drop in impact strength was readily apparent. This degradation in impact properties can be attributed to the immobilisation of the macromolecular chains by the glass beads, which limits their ability to deform freely and makes the composite less ductile.

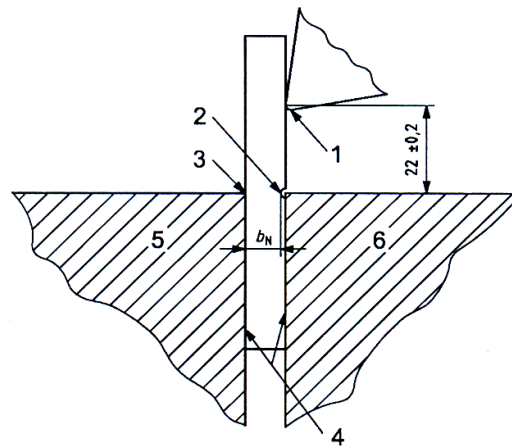
From the impact experiment, it was found that the impact strengths of composites filled with uncoated glass beads decreased monotonically from 13.97 to 9.84 [kJ m<sup>-2</sup>] with increasing particle weight ratio, probably due to the poor interfacial adhesion between polyamide and glass beads.



(a) Avery Izod pendulum impact machine



(b)



(c)

Method designation	Specimen	Notch type	Notch base radius, $r_N$	Remaining with, $b_N$ , at notch base
ISO 180/A	Length $l = 80 \pm 2$ [mm] Width $b = 10.0 \pm 0.2$ [mm] Thickness $h = 4.0 \pm 0.2$ [mm]	A	$0.25 \pm 0.05$	$8.0 \pm 0.2$

Fig (4.10) Impact test arrangement: (a) testing machine; (b) Notch type; (c) Sample geometry and loading arrangements.

1 striking edge; 2 notch; 3 vice jaw; 4 face of jaws in contact with the sample; 5 fixed vice jaw; 6 movable vice jaw;  $b_N$  remaining width at notch base

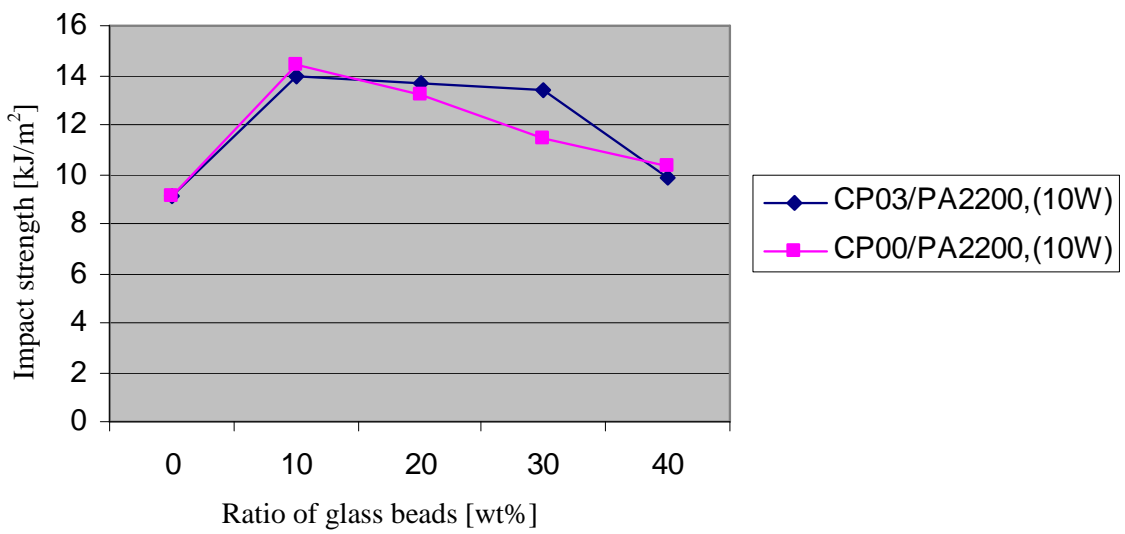


Fig (4.11) The variation of impact strength with glass bead weight ratios

Table (4.2) Mechanical properties of SLS samples (PA12; PA12/CP00 system; PA12/CP03 system) by calculation

PA12/ CP00 ratios [%]		100/0	90/10	80/20	70/30	60/40	Max percent variation
Laser power [W]	10 [W]						
Properties; Material: PA12/CP00							
Tensile strength [MPa]	average	52.89	52.39	52.40	48.40	40.85	22.76
	SD*	0.81	0.70	0.53	1.40	1.13	
Tensile modulus [MPa]	average	1721.9	2716.55	3399.60	4675.32	6250.16	72.45
	SD	214.09	383.57	493.75	275.77	232.56	
Ultimate elongation [%]	average	4.18	3.27	2.36	0.55	0.17	95.93
	SD	0.53	0.64	0.42	0.11	0.08	
Flexural strength [MPa]	average	69.97	75.43	80.41	84.38	87.20	19.75
	SD	3.07	1.01	1.90	1.95	3.14	
Flexural modulus [MPa]	average	2262.91	2252.98	2675.18	3280.86	3870.03	41.78
	SD	361.15	222.16	115.58	150.47	366.19	
Impact strength [kJ/m <sup>2</sup> ]	average	9.14	13.97	13.65	13.41	9.84	34.57
	SD	0.58	0.65	1.06	1.43	0.65	
PA12/ CP03 ratios [%]		0/100	10/90	20/80	30/70	40/60	Max percent variation
Laser power [W]	10 [W]						
Properties; Material: PA12/CP03							
Tensile strength [MPa]	average	52.89	53.59	54.61	52.23	51.54	5.62
	SD	0.81	0.99	0.74	0.47	2.36	
Tensile modulus [MPa]	average	1721.9	2800.95	4190.34	4820.07	6470.73	73.39
	SD	214.09	571.72	477.71	498.21	375.54	
Ultimate elongation [%]	average	4.18	2.74	1.70	0.48	0.18	95.69
	SD	0.53	0.48	0.39	0.08	0.03	
Flexural strength [MPa]	average	69.97	77.07	78.61	86.14	90.70	22.85
	SD	3.07	1.59	3.43	1.10	0.89	
Flexural modulus [MPa]	average	2262.91	2460.51	2549.98	3208.68	3849.12	41.21
	SD	361.15	99.75	226.96	203.27	273.62	
Impact strength [kJ/m <sup>2</sup> ]	average	9.14	14.40	13.18	11.46	10.29	36.53
	SD	0.58	1.18	2.16	1.09	0.74	

(\*) SD ... Standard deviation

Table (4.3) Mechanical properties of SLS samples recorded by an extensometer (PA12; PA12/CP00 system and PA12/CP03 system)

No.	LP	Stress at Peak [MPa]	Stress at Upper Yield [MPa]	Young's Modulus [MPa]	Stress at Break [MPa]
Material: PA 12					
1	10W	59.720	55.480	2050.3	42.897
2		58.812	54.875	1974.4	39.885
3		60.400	57.147	2302.4	45.995
Material: PA12/CP00; 90:10					
4	10W	57.128	54.833	2666.8	42.222
5		56.655	55.430	2377.2	53.480
6		57.583	56.267	2521.2	48.591
Material: PA12/CP00; 80:20					
7	10W	53.257	52.815	3081.5	48.230
8		52.515	51.97	3091.7	49.042
9		53.290	53.073	3086.6	49.722
Material: PA12/CP00; 70:30					
10	10W	39.257	39.208	3187.9	35.308
11		38.655	38.120	3110.0	36.692
12		34.390	32.890	3255.0	32.495
Material : PA12/CP00 ; 60:40					
13	10W	39.683	39.537	3925.7	38.99
14		38.320	38.287	4160.8	37.987
15		37.270	37.245	4210.5	36.698
Material: PA12/CP03; 90:10					
16	10W	57.612	55.720	2504.5	44.755
17		56.355	53.160	2233.8	48.042
18		55.628	54.000	2233.8	42.498
Material: PA12/CP03; 20:80					
19	10W	48.153	48.787	2582.8	48.140
20		49.995	49.715	2811.2	47.905
21		51.260	51.105	2395.7	48.623
Material: PA12/CP03; 70:30					
22	10W	49.002	48.955	3366.5	46.820
23		48.592	48.025	4178.4	47.517
24		47.933	47.873	3279.8	47.125
Material: PA12/CP03; 60:40					
25	10W	48.147	48.140	3625.0	48.110
26		41.055	41.055	3992.8	41.010
27		47.740	47.545	3627.2	47.158

The impact strength of PA12/CP03 composites filled with treated glass bead particles decreased from 14.40 and 10.29 [kJm<sup>-2</sup>]. However, with treated glass beads, the impact strengths were somewhat higher than those of untreated composites. This indicates that the impact strength of the PA12 composites can be improved by coated glass beads. As discussed above, the silane coating agent on the glass bead surface improves the interfacial adhesion between the glass bead and the PA12 matrix. The improved interfacial adhesion is favourable for transmitting the impact force and absorbing the fracture energy. On the other hand, reducing the size of glass beads is helpful for improving the toughness of composites [108],[109].

#### **4.2.6. Fracture toughness**

Fracture toughness is a property which describes the ability of a material containing a crack to resist fracture, and is one of the most important properties of any material for virtually all design applications. Fracture toughness is an indication of the amount of stress required to propagate a pre-existing flaw. It is a very important material property since the occurrence of flaws is not completely avoidable in processing, fabrication, or service of a material/component. Flaws may appear as cracks, voids, metallurgical inclusions, delamination, weld defects, design discontinuities, or some combination thereof [110].

The aim of this section was to experimentally investigate the fracture toughness of the glass bead-filled polyamide12 composites under quasi-static load. In the case of the simpler mechanical properties such as Young's modulus or yield strength, the testing techniques are simple and require little thought or interpretation. However, toughness is a more difficult property to characterise.

Basically, the fracture mechanics concept to material design considers the effects of cracks and defects on strength. To determine fracture toughness, which is a material property, there are two approaches: the stress intensity approach and the energy approach. The first approach yields a fracture toughness ( $K_c$ ) which relates the crack size to fracture strength. The energy approach provides a critical energy release rate ( $G_c$ ) which is the work dissipation required to spread a crack of a unit area.

Linear elastic fracture mechanics (LEFM) is one of the most frequently used methods to characterise polymer fracture. The fracture toughness in LEFM may be represented in terms of the stress-intensity factor ( $K$ ) or the strain-energy release rate ( $G$ ). However, fracture toughness characterisation using LEFM becomes difficult when ductile polymers, especially polymer blends with high fracture toughness to yield strength ratios are involved. The formation of a large plastic zone prior to crack initiation violates the limit of small scale yielding, which ensures the validity of LEFM [111].

The expression for  $K_c$  and its relation to  $G_c$  were originally derived for homogenous, isotropic materials. However, these equations can be applied to particle-filled composites provided that the heterogeneities are very small compared to specimen dimensions and notch length. Under these conditions,  $G_c$  and  $K_c$  are connected by:

$$G_c = \frac{K_c^2}{E_c} \quad \dots (4.6)$$

where  $E_c$  is the effective composite modulus.

#### 4.2.6.1. Single-edge-notched three-point bending fracture toughness tests

Toughness tests were also performed on the composites at a slower rate than impact conditions by drawing out the notched rectangular bar samples. For this purpose, five sets from which five replicate samples of each were produced and tested at room temperature on a Testometric materials testing machine AX at a cross-head speed of 1 [mm/min] using a span of 64 [mm]. Single-edge-notched (SEN) type specimens were prepared for the determination of the critical stress intensity factor ( $K_{IC}$ ) in the three-point bending (3PB) test.

The fracture toughness specimens were produced using an SLS machine under the same conditions applied to other testing specimens. The length (L), thickness (B) and width (W) of the specimens were 80, 10 and 4 [mm], respectively, Fig (4.12). The single-edge V-shaped notches of 45°, with a tip radius of 0.25 [mm] and different depths, were introduced using the SLS machine. The resulting load-displacement curves of glass bead-filled polyamide composites are given in Fig (4.13).

The load-displacement curves allowed for making statements about the behaviour of the composites. Looking at the effect of glass bead content on the load-displacement curves of the specimen, as presented in Fig. (4.13), it is clear that as the filler content increased, the load and the displacement decreased.

*Calculation of fracture toughness:*

The  $K_{IC}$  values were determined using the relationship [112]:

$$K_{IC} = \frac{3PS\sqrt{a}}{2BW^2} f\left(\frac{a}{W}\right)$$

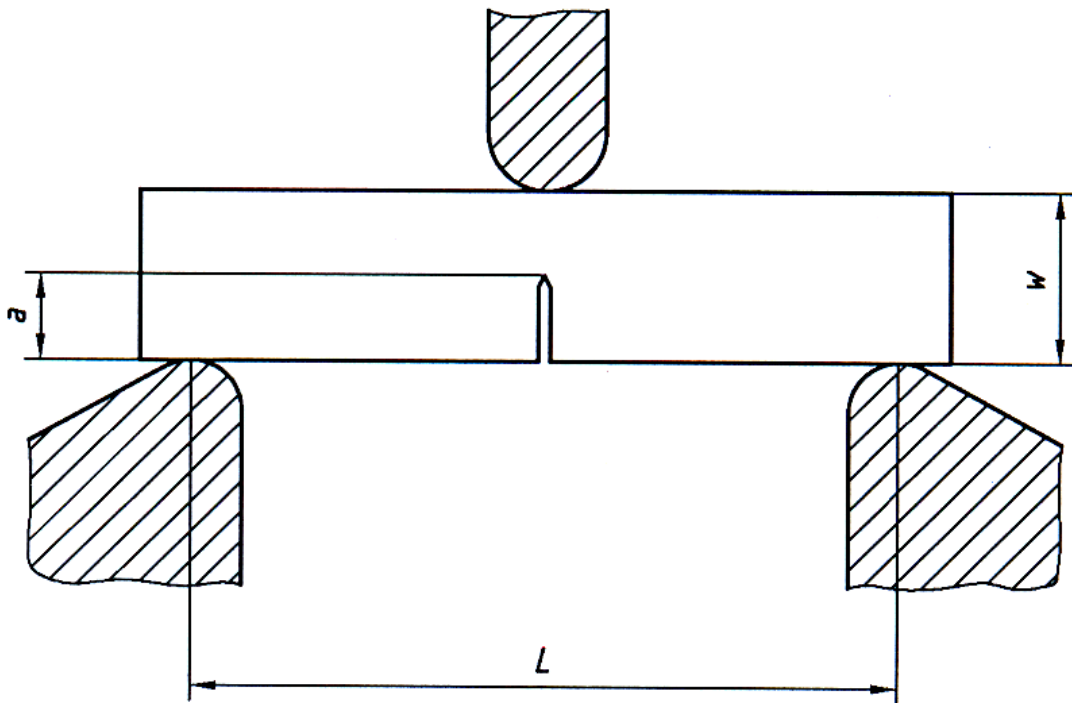
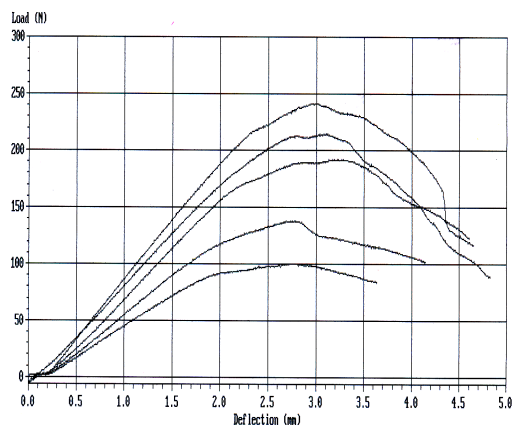
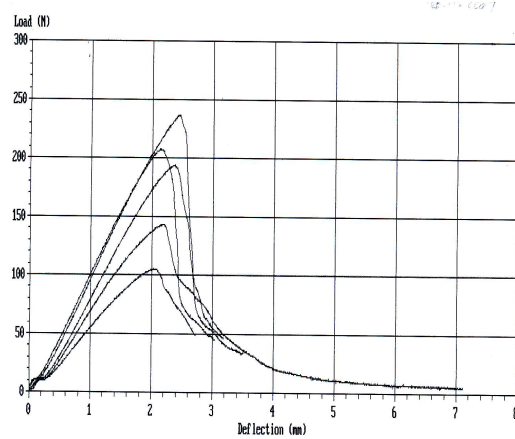


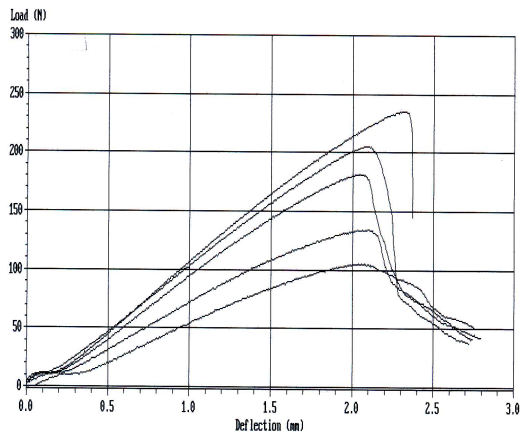
Fig (4.12) Specimen configuration and dimensions for fracture toughness measurements



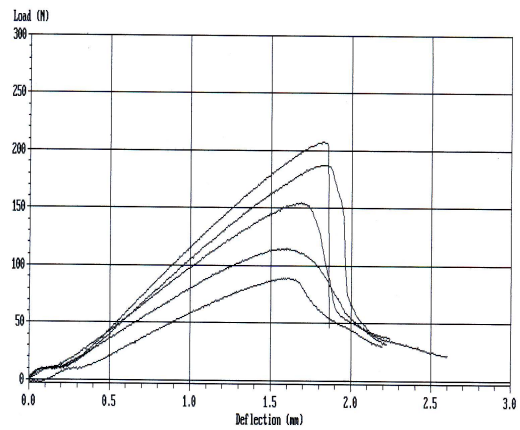
(a)



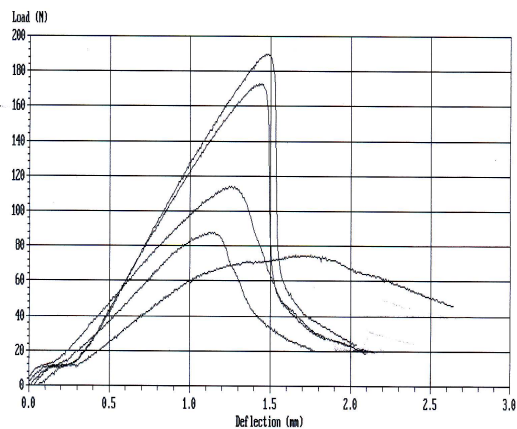
(b)



(c)



(d)



(e)

Fig (4.13) Load-displacement curves of: (a) PA12; (b) CP00/PA12; 10:90 [wt%]; (c) CP03/PA12; 20:80 [wt%]; (d) CP03/PA12; 30:70 [wt%]; (e) CP03/PA12; 40:60 [wt%]

$$f\left(\frac{a}{W}\right) = 1.93 - 3.07\left(\frac{a}{f}\right) + 4.53\left(\frac{a}{f}\right)^2 - 25.11\left(\frac{a}{f}\right)^3 + 25.8\left(\frac{a}{f}\right)^4 \quad \dots (4.7)$$

where  $f\left(\frac{a}{W}\right)$  is a shape factor,  $P$  is the load at failure,  $S$  is the length of the span and  $a$  is the notch depth.

Critical strain energy release rates ( $G_{IC}$ ) were calculated from the stress intensity values using the following relationship:

$$G_{IC} = \frac{K_{IC}^2}{E}(1 - \nu^2) \quad \dots (4.8)$$

where  $E$  is the modulus of elasticity obtained from the tensile tests and  $\nu$  is the Poisson's ratio of the polymer, taken to be 0.35 [113].

Shown below is an example for the calculation of  $K_{IC}$  and  $G_{IC}$  for the CP03/PA12 composite, weight ratio 40:60 and laser power of 10 [W] :

Span:  $S = 0.064$  [m]; Thickness:  $B = 0.004$  [m]; Width:  $W = 0.010$  [m]; Young's modulus:  $E_{avg} = 3364500000$  [N/m<sup>2</sup>].

Crack depth:  $CD = 0.001$  m; load:  $F = 189$  [N]:

1 - Shape factor:  $f\left(\frac{a}{W}\right) = 1.74578$

2-  $K_{IC} = 2504162.80$  [Pa.m<sup>1/2</sup>]  $\approx 2.50$  [MPa m<sup>1/2</sup>]

3-  $G_{IC} = 1863.82$  [J.m<sup>-2</sup>]  $\approx 1.86$  [kJ/m<sup>2</sup>]

The results of critical stress intensity factor ( $K_{IC}$ ) and critical energy release rate ( $G_{IC}$ ) are summarised in Table (4.3).

Table (4.4) Test results of fracture toughness performed on Polyamide 12/ glass bead composites.

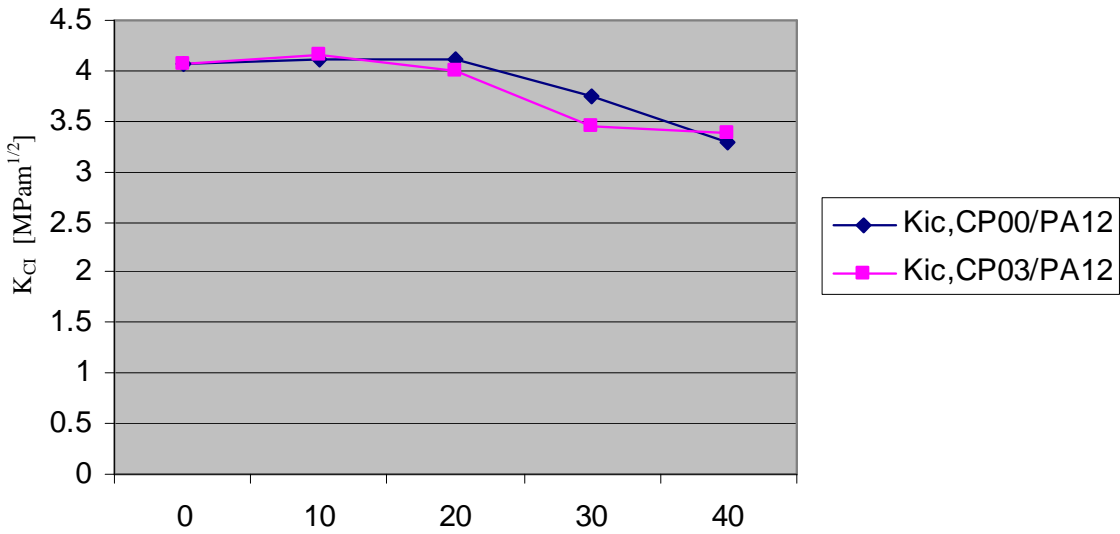
<b>Material: PA12</b>			
Crack Depth [m]	Laser Power [W]	$K_{IC}$ [MPa m <sup>1/2</sup> ]	$G_{IC}$ [kJ/m <sup>2</sup> ]
0.001	10	3.17	4.46
0.002		3.97	6.97
0.003		4.63	9.51
0.004		4.32	8.26
0.005		4.24	7.96
<b>Composite material: PA12/CP00; 90:10</b>			
0.001	10	3.14	3.62
0.002		3.93	5.70
0.003		4.54	7.59
0.004		4.42	7.19
0.005		4.58	7.74
<b>Composite material: PA12/CP00; 80:20</b>			
0.001	10	3.11	3.14
0.002		3.84	4.78
0.003		4.68	7.12
0.004		4.51	6.60
0.005		4.41	6.31
<b>Composite material: PA12/CP00; 70:30</b>			
0.001	10	2.82	2.73
0.002		3.71	4.72
0.003		4.15	5.91
0.004		3.98	5.42
0.005		4.07	5.69
<b>Composite material: PA12/CP00; 60:40</b>			
0.001	10	2.49	1.61
0.002		3.23	2.69
0.003		3.72	3.58
0.004		3.63	3.42
0.005		3.39	2.99
<b>Composite material: PA12/CP03; 90:10</b>			
0.001	10	3.08	3.80
0.002		3.80	5.78
0.003		4.78	9.14
0.004		4.19	7.04
0.005		4.88	9.51
<b>Composite material: PA12/CP03; 80:20</b>			
0.001	10	3.11	3.73
0.002		3.82	5.63
0.003		4.37	7.36
0.004		4.23	6.89
0.005		4.41	7.50
<b>Composite material: PA12/CP03; 70:30</b>			
0.001	10	2.74	2.11
0.002		3.49	3.42
0.003		3.74	3.93
0.004		3.59	3.59
0.005		3.73	3.92
<b>Composite material: CP3/PA12; 40:60</b>			
0.001	10	2.50	1.86
0.002		3.21	3.06
0.003		3.86	4.43
0.004		3.57	3.78
0.005		3.69	4.05

#### 4.2.6.2. Correlation between fracture toughness and glass bead content

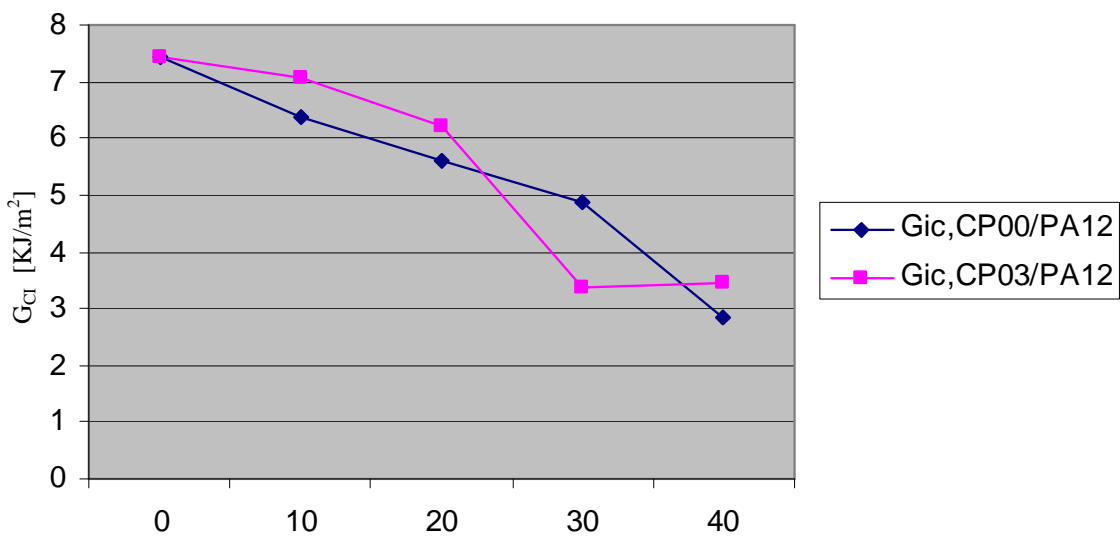
The dependency of plain strain fracture toughness, i.e. the critical stress intensity factor ( $K_{IC}$ ), of glass bead-filled polyamide 12 is given in Fig (4.14). The most distinctive feature in this figure is that the fracture toughness of two composite systems did not show any significant increase with increasing glass bead content. In fact, it decreased with the increase in glass bead content. It was seen, upon increasing the glass bead content that the  $K_{IC}$  decreased. In other words, the addition of glass beads led to composites with brittle behaviour.

The critical strain energy release rates ( $G_{IC}$ ) calculated from the ( $K_{IC}$ ) and modulus data can be found in Fig (4.14-b). The general trend of this figure is the same as that of Fig (4.14-a): fracture toughness decreased with increasing glass bead content. Nonetheless, in all systems, as glass bead content increased, the decrease in fracture toughness per unit increase of glass bead content became greater more rapidly in Fig (4.14-b) than in Fig (4.14-a). This difference between  $K_{IC}$  and  $G_{IC}$  values can be easily understood by considering how they are related:  $G_{IC}$  depends on  $K_{IC}$  and modulus under the linear elastic fracture assumption.

From the abovementioned figures, it can also be observed that the influence of surface treatment, i.e. coupling agents, on fracture toughness is insignificant, therefore a little bit of energy can be damped via de-bonding. Besides, a crack can propagate through an interface easily because of a weak interface. This is why fracture toughness decreased with increasing glass bead content; however the interfacial-treated composites were superior in tensile strength.



(a) Content of Glass Beads [wt%]



(b) Content of Glass Bead [wt%]

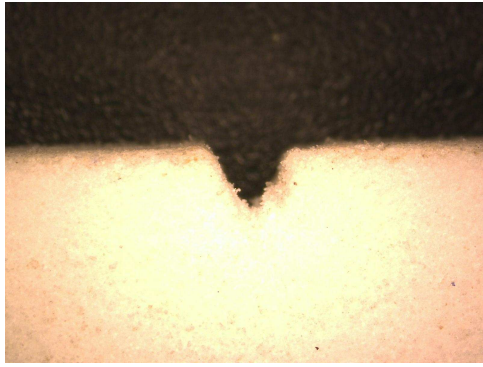
Fig (4.14) Dependency of fracture toughness of polyamide 12 composites on glass bead content.

(a) critical stress intensity factor ( $K_{IC}$ ) ; (b) critical strain energy release rate ( $G_{IC}$ ) .

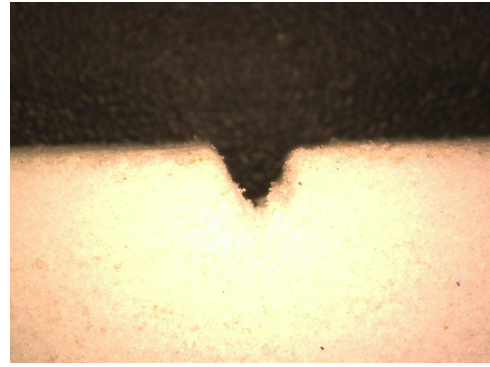
#### **4.2.6.3. Effect of V-notch depth on fracture toughness**

In fracture toughness testing it is common, for reasons of simplicity and reproducibility, to use notches to approximate sharp cracks. Hence, because of the lower stress concentration ahead of a notch, as compared to a truly sharp crack, a greater force is required to cause a notch tip crack to extend. This deviation increases with increasing notch width and results in the commonly reported dependence of fracture toughness ( $K_{IC}$ ) on notch root radius. This can be explained as a consequence of the interaction of a distorted stress field with material flaws in front of a notch. In conventional impact testing, the required notches are usually mechanically introduced into the test samples in accordance with the relevant ISO Standard. However, with RP/RM processes, it is entirely possible to include the notch into the CAD file and manufacture this design detail as the part is being built [112], [114].

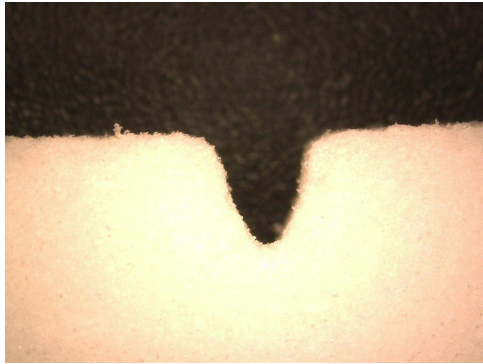
Owing to the effects of the manufacturing method, specimens with sintered-in notches do not give results comparable to those obtained from specimens with machined notches. It has been shown that to measure true fracture toughness, sharp notches with the size of microstructural features are required. Fracture toughness values determined with sharp-notched specimens are compared with the results of experiments with conventional sawn-in notches. It has been shown that sharp notches deliver considerably lower, more accurate and reproducible values of  $K_{IC}$ , for materials with fine microstructures. In this sense, in order to minimise the staircase effect of the build process on the notch profile, all the specimens under investigation were built in the flat orientation, as shown in Fig (4.2). Fig (4.15) shows optical photomicrographs of SLS-introduced notches.



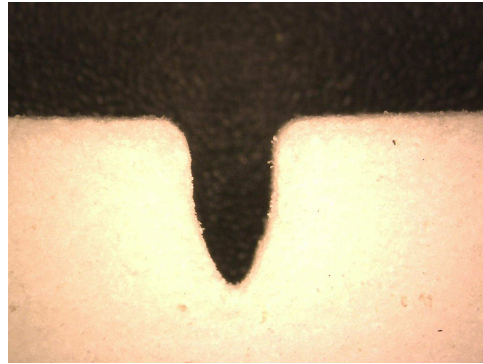
(a)



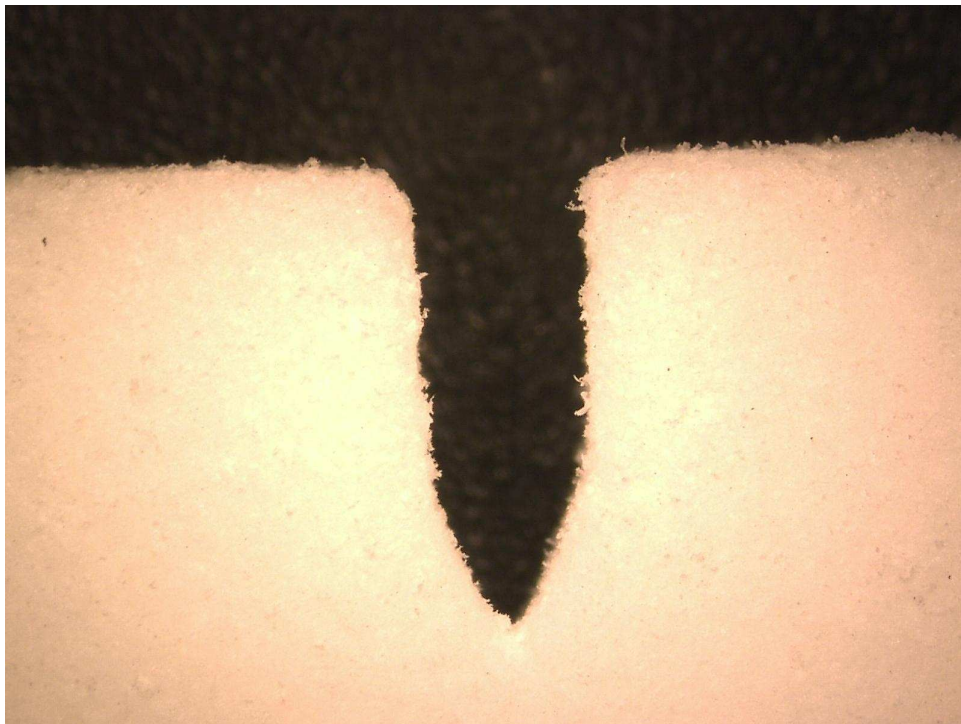
(b)



(c)



(d)



(e)

Fig (4.15) Optical photomicrographs of the V-notch introduced using the SLS process  
(a) notch depth 1 [mm]; (b) 2 [mm] ; (c) 3 [mm]; (d) 4 [mm]; (e) 5 [mm]

V-notches are one of the simplest and most frequent geometries that appear in testing samples and in notched structural components. Generally, notches concentrate stress for purely elastic responses and they generate enhanced plastic strain rates at the notch root when local yielding occurs. Therefore, experiments were performed to explore the effect of non-standard SEN-3PB type samples with increased notch depths. Fig (4.16) shows the dependence of  $K_{IC}$  and  $G_{IC}$  on notch depth. Most of the composites, including unfilled PA12, absorbed less energy as the notch depth increased, i.e. as the stress or strain-rate concentration increased. The blends with a higher weight ratio of glass beads, however, maintained essentially the same  $K_{IC}$  and  $G_{IC}$  independent of notch depth in the range investigated.

In fact, the data on the fracture toughness of selective laser sintered glass bead-filled polyamide 12 are roughly comparable with those for standard injection moulded samples from nylon, rubber-modified polymethyl methacrylate (PMMA-RT) and polyvinylchloride (PVC), [BS ISO 17281:2002].

### **4.3. Morphological observation**

The morphological study in this work included the intrinsic microstructures of the blends of the sintered and fractured surfaces after tensile tests. A scanning electron microscope (ZEISS XB 1540 workstation) operating at an acceleration voltage of 30 [kV] was used to analyse the micrographs of scan surfaces and fracture cross-sections of tensile bars. Prior to observation, the surfaces were coated with a thin layer of gold to make them conductive and to avoid the concentration of electron emission on the surface during examination. The SEM micrographs of the glass bead-filled polyamide 12 composites sintered at two different energy densities (ED) and different glass bead

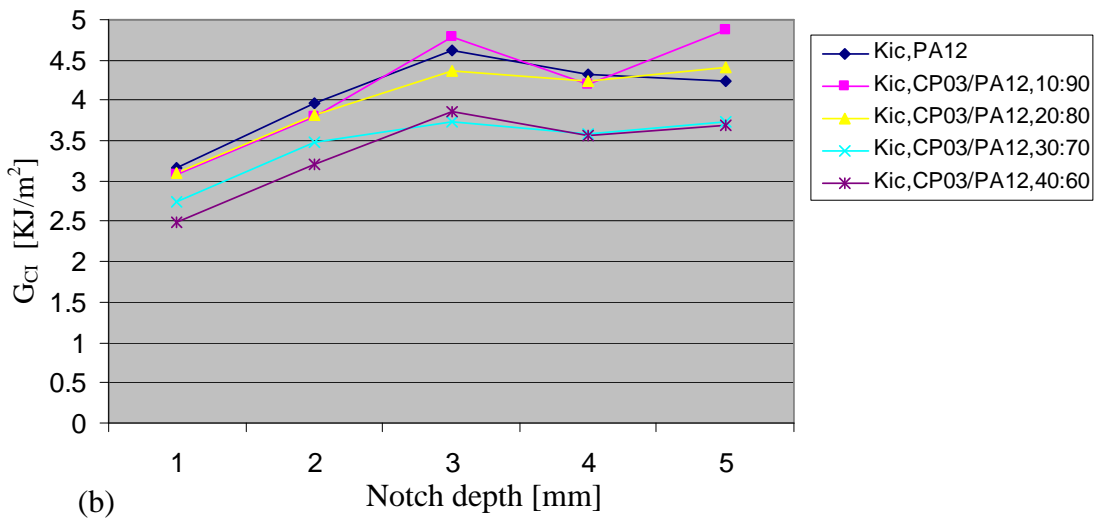
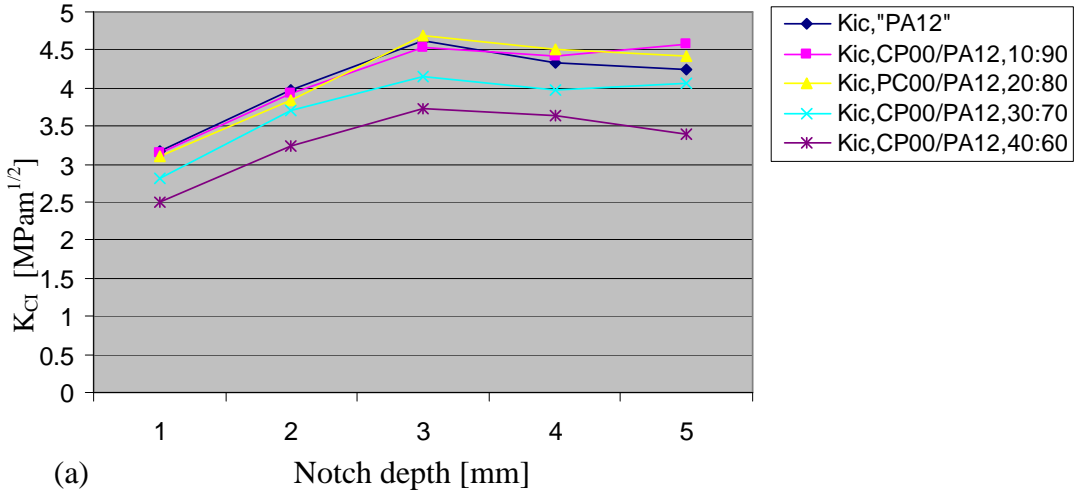


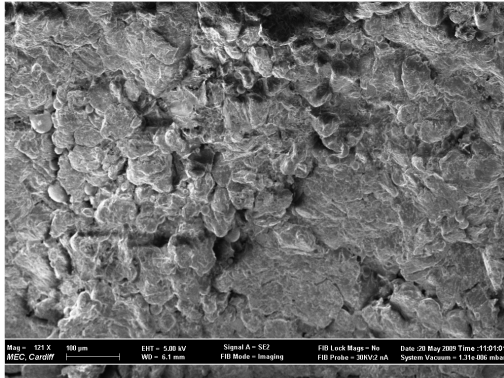
Fig (4.16) Dependence of  $K_{IC}$  and  $G_{IC}$  on notch depth (the standard notch depth is 2 mm). (a) PA12/CP00 system; (b) PA12/ CP03 system

contents with different surface treatments are shown in Figs (4.17) and (4.18). For the PA12/CP00 system, it can be noted from Fig (4.17-a) that the particles on the scan surface formed at an ED of 0.058 [J/mm<sup>2</sup>] were only slightly fused together at points of contact and a number of voids could also be seen compared to those formed at an ED of 0.073 [J/mm<sup>2</sup>], Fig (4.17-b), where the particles were strongly fused together. This indicates that the flow of the composite was facilitated by relatively higher energy density. Fig (4.17-c;d) shows the morphology of a tensile fracture cross-section of the PA12/CP00 system with a glass bead weight ratio equal to 20%. One can see that the connection between the glass beads and PA12 was not perfect, that many glass beads had been pulled out and that PA12 was stretched during breakage, resulting in a rough spongy surface. However, the tensile fracture surface of the un-treated glass beads in the composite after de-bonding was very smooth. This indicates that the interfacial adhesion was poor and therefore its tensile strength as lower than that of the PA12/CP03 system (see Fig 4.5).

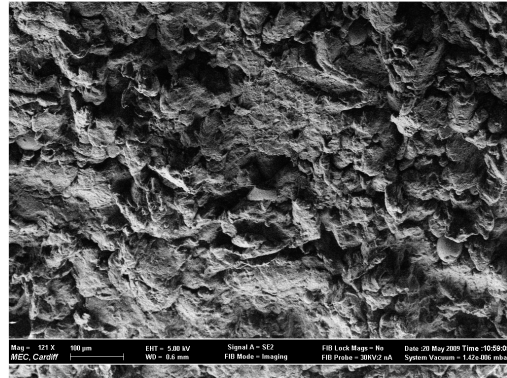
Fig (4.18a;b) is an SEM micrograph taken of the scan surfaces and the tensile fracture cross-sections of the PA12/CP03 system with a glass bead weight ratio of 20% at energy densities of 0.058 [J/mm<sup>2</sup>] and 0.073 [J/mm<sup>2</sup>]. In general, it can be observed that there is not a significant influence of the coupling agent on the scan surface.

The treated glass beads, Fig. (4.18-c;d), were uniformly distributed in the PA12 matrix, and their surface became very rough. Hence, the bonding between the glass bead and the matrix was strengthened. These results indicate that the silane agent coated on the surface of glass bead enhanced the interaction between the glass beads and PA12, and improved both the adhesion and morphological structure of the PA-

Scan surfaces pictures



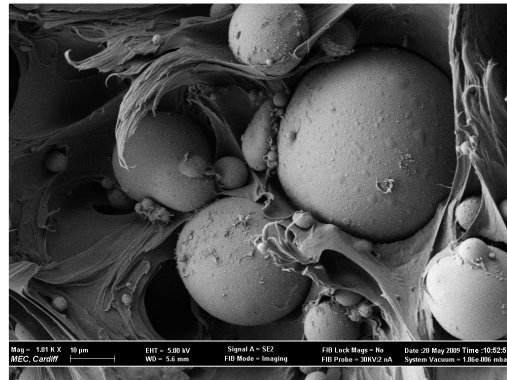
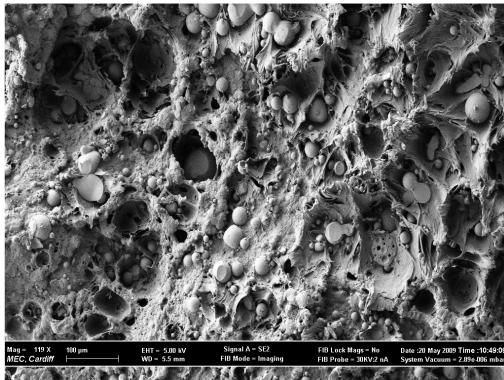
(a) LB=8 [W]; ED = 0.058 [J/mm<sup>2</sup>]



(b) LB = 10 [W]; ED = 0.073 [J/mm<sup>2</sup>]

Tensile fracture surfaces

(c) LB=8 [W]; ED = 0.058 [J/mm<sup>2</sup>]



(d) LB = 10 [W]; ED = 0.073 [J/mm<sup>2</sup>]

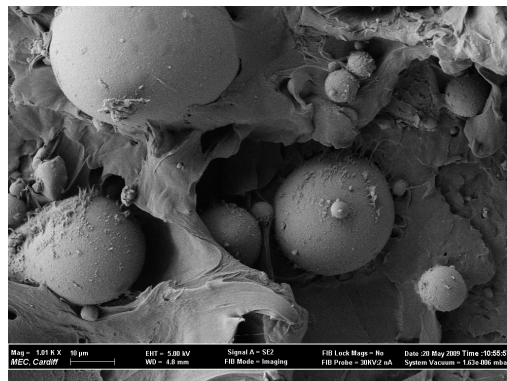
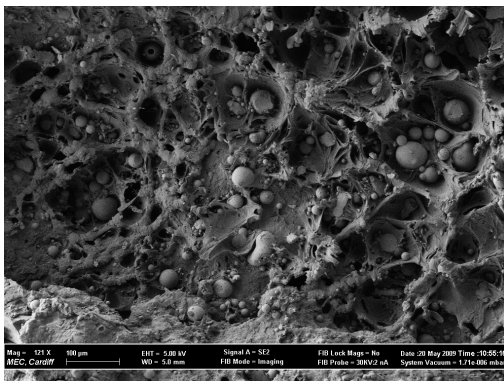
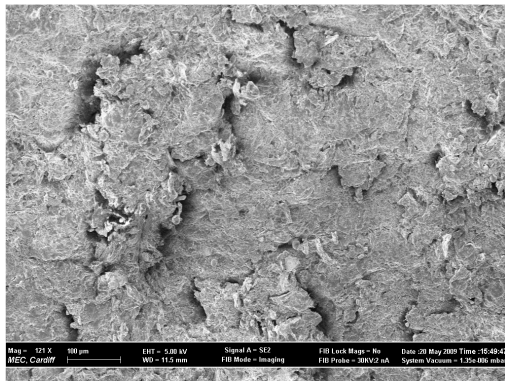
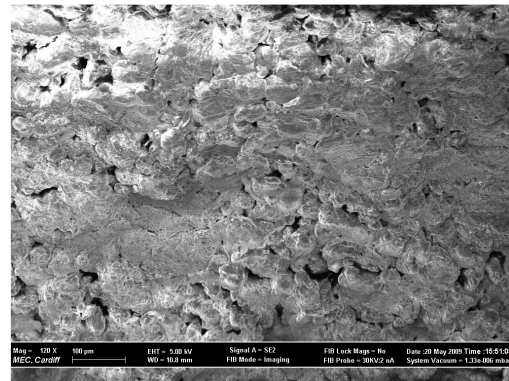


Fig (4.17) SEM micrographs of scan surfaces: (a); (b) and tensile fracture surfaces: (c); (d) of selective laser sintered PA12/CP00 composites containing 20 [wt%] glass beads built at two different energy densities

Scan surfaces pictures



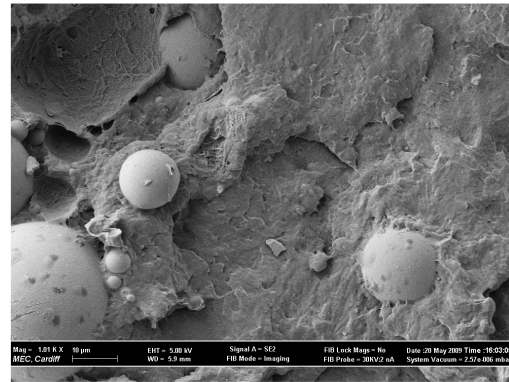
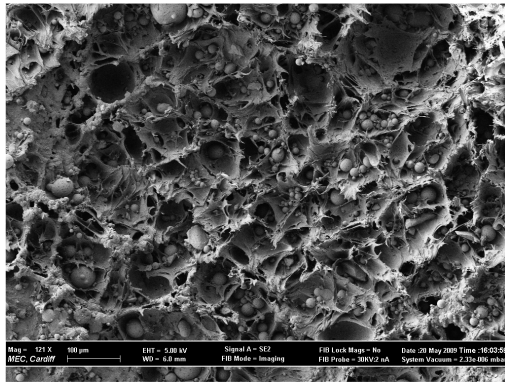
(a) LB=8 [W]; ED = 0.058 [J/mm<sup>2</sup>]



(b) LB = 10 [W]; ED = 0.073 [J/mm<sup>2</sup>]

Tensile fracture surfaces

(c) LB=8 [W]; ED = 0.058 [J/mm<sup>2</sup>]



(d) LB = 10 [W]; ED = 0.073 [J/mm<sup>2</sup>]

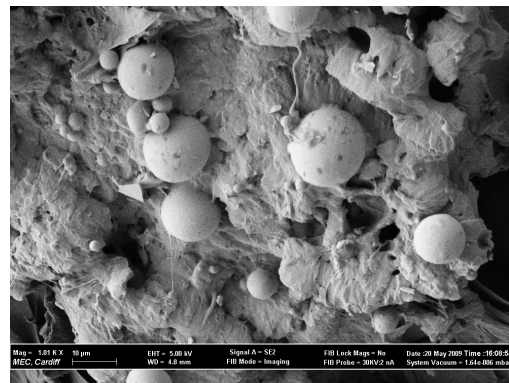
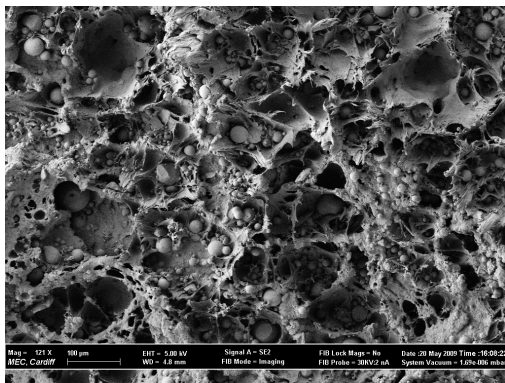


Fig (4.18) SEM micrographs of scan surfaces: (a); (b) and tensile fracture surfaces: (c); (d) of selective laser sintered PA12/CP03 composites containing 20 [wt%] glass beads built at two different energy densities

matrix composites. Therefore, the tensile strength was higher than that of the former, (see Fig 4.5).

#### **4.4. Summary**

The results presented in this chapter have shown that, over the range tested, an increasing proportion of glass beads will cause a corresponding increase in stiffness. The notable increase in strength and modulus, achievable with a relatively small decrease in tensile strength, is promising when considering the requirement to tailor the stiffness of SLS parts and components. However, the fairly large decrease in elongation at break may prevent the use of very high ratios of glass beads. Different from elongation at break, the flexural strength and modulus increase steadily with increasing glass bead content.

From the impact experiment, it was found that the impact strengths of glass bead-filled polyamide composites decreases monotonically, in general, regardless of the surface treatment applied on the glass beads, where the glass beads are thought to make the composite less ductile.

In terms of fracture toughness, both composite systems do not show any significant increase with increasing glass bead content. In fact, it decreases with an increase in glass bead content.

The results have shown that it is possible to vary the properties of selective laser sintered parts by adding controlled proportions of glass beads to standard PA12 powder besides surface treatment and process parameters.

Generally, high impact strength coupled with a large tensile modulus suggests a tough composite material; high impact strength and small tensile modulus indicate a ductile, flexible material; low impact and large tensile modulus typify a brittle composite material. However, the interface-treated composites are superior in tensile strength, and inferior in fracture toughness to the interface-untreated composites. The SEM micrographs showed that the silane coupling agent improves both the adhesion and the morphological structure of PA12 composites.

## **Chapter 5- Experimental investigation of the influence of processing parameters and material properties on the curling phenomenon in selective laser sintering**

### **5.1. Background**

It is a well-known approach that, to be able to infer the science behind the observed phenomenon, researchers have to plan and conduct several experiments to obtain enough relevant data. This can be done by the trial-and-error approach, design of experiments and the Taguchi method. Experiments, however, are necessary for the development of new materials, for the introduction of new technologies, for optimisation of processing parameters and for improvements to known techniques.

Indeed, with more manufacturers using the SLS process for rapid manufacturing, it is vital that designers understand the properties of the materials that are being used. In this direction, much work has been focused on determining the most appropriate parameters for the SLS process. Selective laser sintering (SLS) is one of the most popular rapid manufacturing techniques. It has the capability to produce a part in hours without any tooling, which is a powerful advantage for many industries. However, the parts produced tend to shrink and warp from its designed form and dimensions, forcing the user to run several trials of a part to reach its ideal dimension or settle for a slightly inaccurate part. Improvement of geometric accuracy by optimising processing parameters in selective laser sintering has been and remains a major concern.

Basically, part accuracy is one of the main challenges in layered manufacturing techniques. Compared to conventional manufacturing processes, the parts produced

using SLS or any other additive manufacturing process are generally poor and inferior in terms of accuracy, where shrinkage and warping represent the most common sources of inaccuracy in SLS process. In selective laser sintering there are four major elements that may affect part accuracy, namely the CAD model approximation, distortion caused during building, the stair-step effect on curved surfaces and surface roughness resulting from the process. Distortions such as curling, glazing and bonus- Z are common problems in the SLS machines. These problems can be reduced as a result of improvement in the properties of SLS materials [51], [105].

Distortions are changes of geometry during or after the building process. In this sense, geometric distortion in selective laser sintering greatly affects the accuracy of the shaped parts by SLS. One of the main sources of size and shape variations of selective laser sintered parts is shrinkage during processing. Shrinkage is strongly influenced by the processing parameters (such as laser parameters, build chamber temperature, cooling rate) and the geometry of the part. The total shrinkage in the SLS process is a result of material shrinkage, process shrinkage and thermal shrinkage.

It is well-established that materials chosen to be used for SLS have a large difference between the melting and crystallisation temperature. If this temperature range is too narrow, warping can occur in the SLS part after it has been sintered. If the range is large enough, warping will not be as serious or will not occur at all. When the material has been sintered, the melted powder will stay in the liquid phase as it cools down. While in the liquid phase, the material does not accumulate stress, so the cooling process should be slow and gradual. If the part cools down too quickly, then stress points can accumulate on the part which causes it to warp once it has hardened.

Therefore, polymer materials which have a large difference between the melting and crystallisation temperatures are desired [64]. During crystallisation, the molecules arrange themselves and occupy less volume, thus leading to material shrinkage. During processing, the powder particles fuse together to produce dense parts, leading to a decrease in porosity and volume. During heating, the part expands due to the coefficient of thermal expansion and then shrinks during cooling.

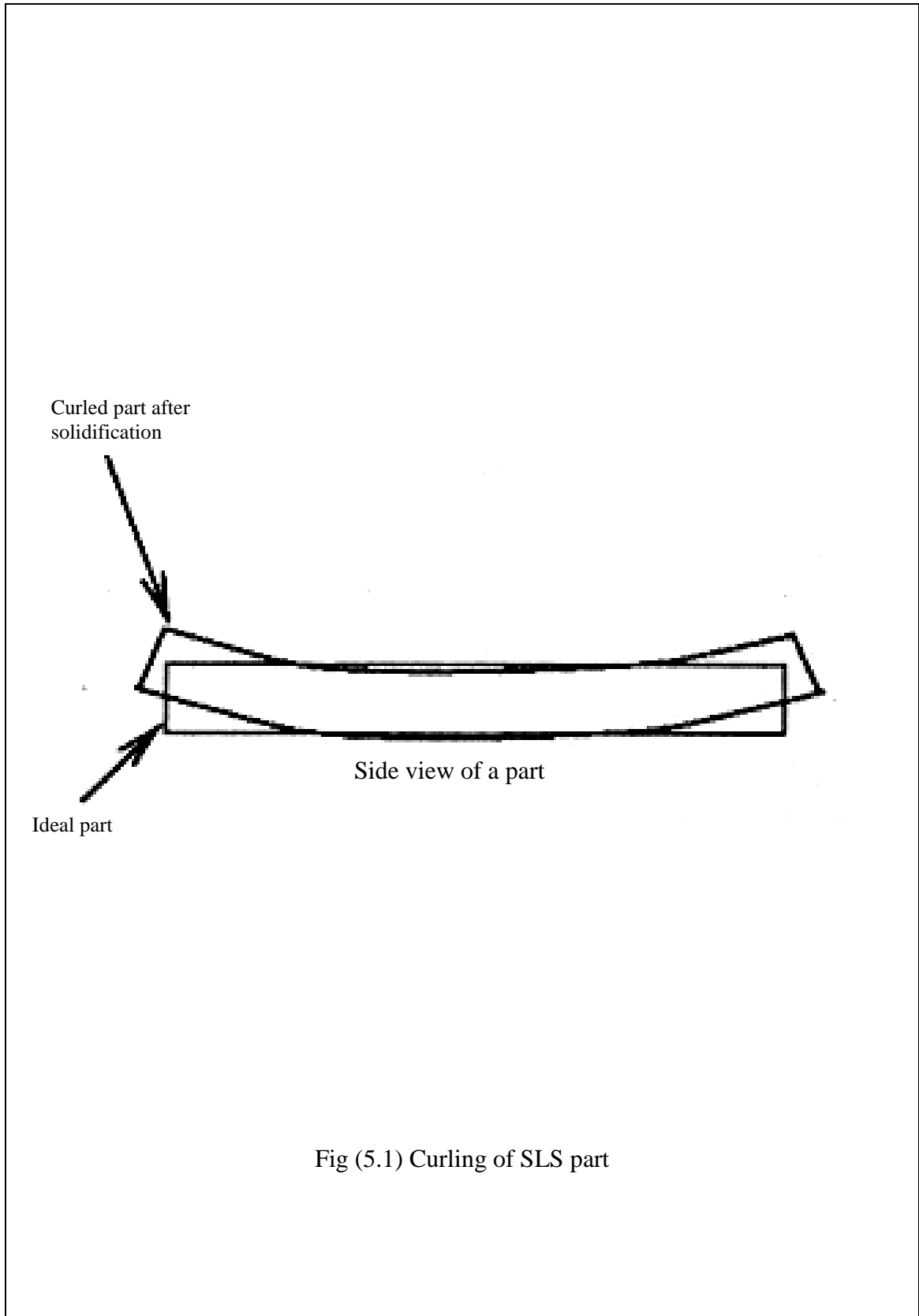
The result of shrinkage and warping is the curling phenomenon, which is identified when the downward-facing surface of a part, intended to be flat, exhibits a curved profile close to the free edges (in which the surface profile of a specimen that was designed to be flat becomes concave in shape after sintering). In general, curling is caused by uneven shrinkage between the top and bottom of the part. Fig (5.1) shows shape distortion in the SLS process.

However, adequate thermal control is necessary to prevent accuracy problems associated with curling. Curling can occur at the part bed surface or in-build, or as the part is cooled from the build temperature to room temperature or post-build. In-build curling is caused by thermal stresses and layerwise shrinkage stresses. These stresses can be minimised by maintaining the part bed at a temperature near the melting temperature of the material. At this temperature, the thermal gradients between the part and surrounding powder are minimised [93].

In the build stage, in-build curling occurs when the edges or corners of the part rise above the powder bed surface. This is mainly due to uneven temperature distribution in the part bed. In-build curling develops when the part temperature dips too low after the

feed powder is added. However, strong curling up of the part can cause the part to shift when the roller passes, Fig (5.2). On the other hand, an excessive cooling rate and thermal gradients produce unbalanced stresses in the sintered part, causing the final part to become curved. If the part is not allowed to cool in a controlled environment for a long time, the part will tend to warp due to faster cooling in the outside environment. In addition, during faster cooling, the part develops significant stresses causing post-build warpage.

Additionally, curling has also been reported to vary according to the location of the part in the part bed. Surfaces of the part bed and cylinder wall are typically cooler than the sintered part and its surrounding powder. Therefore, parts placed close to these surfaces were seen to experience more curling than other positions in the part bed due to the heterogeneous cooling taking place within the part. However, in order to decrease the differential shrinkage, minimise the thermal distortion and facilitate fusion of powder particles, the SLS machine manufacturer (DTM) recommends, as a corrective measure, that the entire machine bed be heated to a temperature below the melting point of the material before the laser scans. To this end, in order to improve the accuracy of the sintered parts, the shrinkage behaviour of parts during manufacture needs to be better understood. Considerable research has been performed on developing methods to investigate this issue.



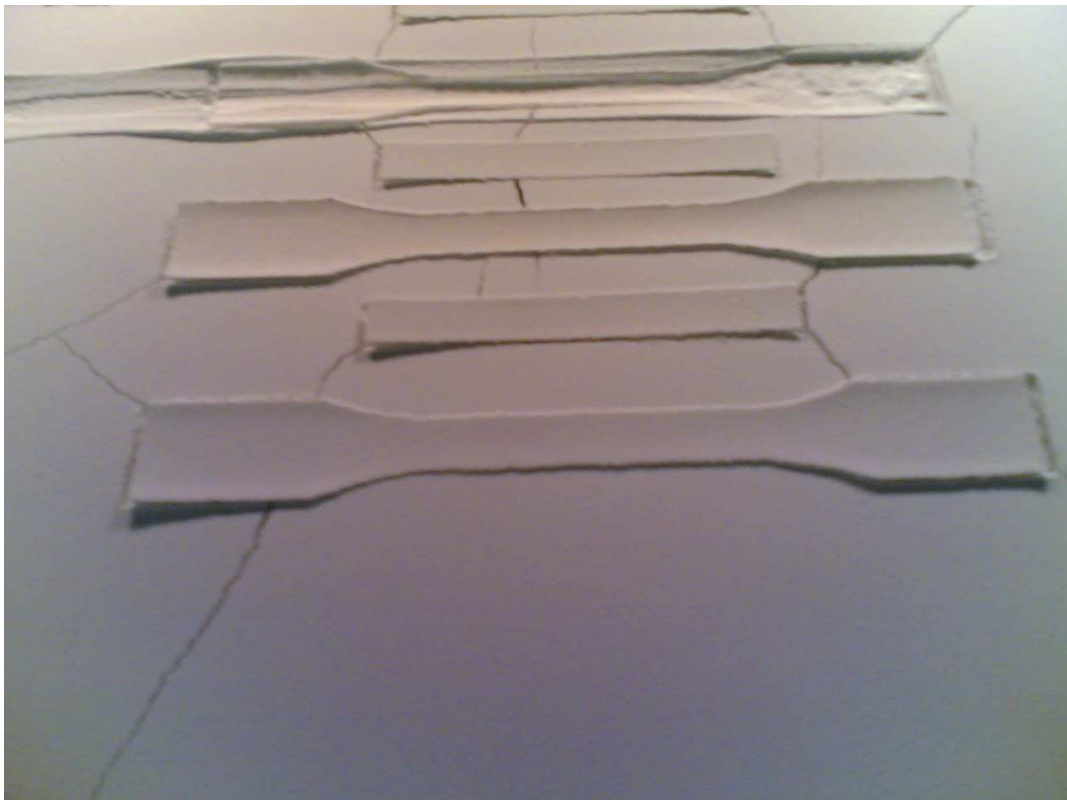


Fig (5.2) Curling up of parts during the SLS process

The present investigation is concerned with improvements to the geometrical accuracy in producing plastic parts by the SLS process. Previous studies in this direction have concentrated primarily on the effects of heat transfer and thermal stress analysis on part curling. There has been no detailed study on the effect of other important process parameters such as laser power, powder composition, powder base thickness, layer cooling time, etc., on the curling phenomenon. In this chapter, the effect of these parameters is investigated.

It is evident from the review of the literature in chapter 2 that the understanding which has developed on variations in curling due to material properties and process parameters is useful for finding an optimum set of process parameters to produce accurate parts. This experimental study was an attempt to enrich the existing knowledge about the influence of processing parameters and material properties on shape distortions in SLS of polyamide 12 composites.

For a given composite material, it is possible to moderate shrinkage and growth by adding a reinforcement or filler to the system. It is also possible to achieve near-zero shrinkage with multiphase coated particle morphologies [93]. Table (5.1) and Fig(5.3) show the relationship between percentage shrinkage and filler content. It can be seen that the shrinkage amount decreases significantly with the increase of glass beads ratio.

Table (5.1) Dependency of percentage shrinkage in the length of tensile bars on glass beads content

Materials	PA12	PA12/CP03 composites [wt%]			
	0:100	90/10	80/20	70/30	60/40
	Measured length L [mm]				
	154.09	154.40	154.94	155.36	155.49
	154.40	154.69	155.11	155.51	155.72
	154.36	154.74	155.11	155.54	155.85
	154.12	154.65	155.03	155.40	155.58
	154.14	154.65	154.97	155.46	155.52
	154.10	154.52	154.95	155.43	155.44
	Percentage shrinkage [%]				
	0.59	0.39	0.04	-0.23	-0.32
	0.38	0.20	-0.07	-0.33	-0.46
	0.41	0.17	-0.07	-0.35	-0.55
	0.57	0.22	-0.02	-0.26	-0.37
	0.55	0.22	0.02	-0.30	-0.33
	0.58	0.31	0.03	-0.28	-0.28
Average	0.51	0.25	-0.01	-0.29	-0.38

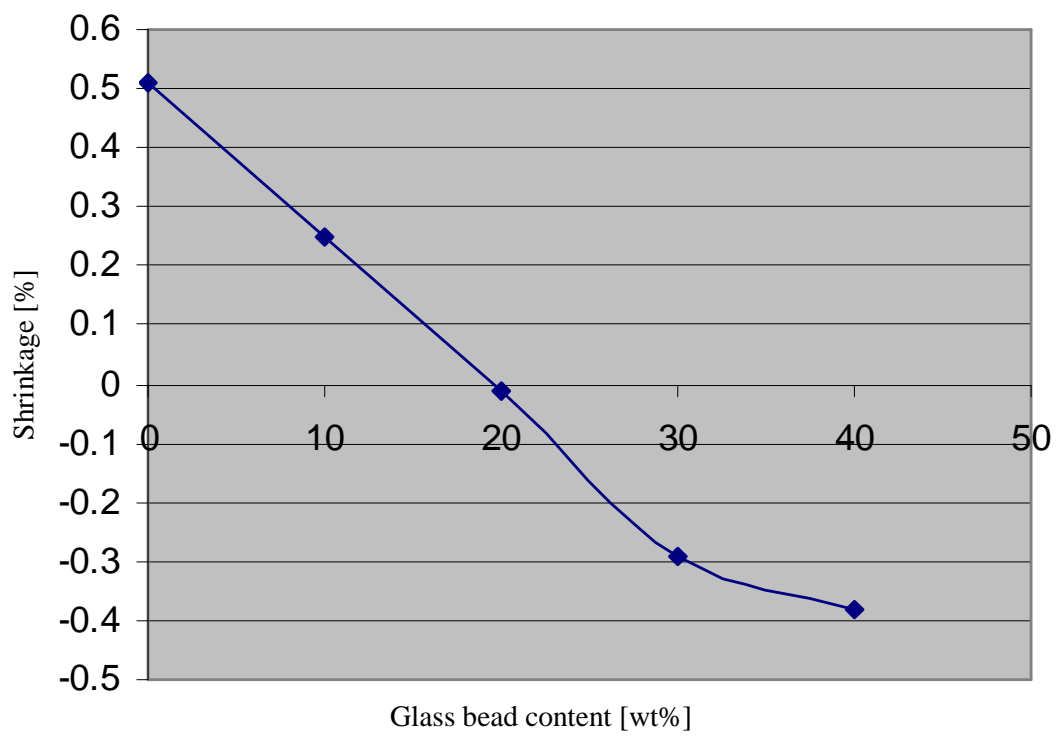


Fig (5.3) Dependency of percentage shrinkage on glass bead content

## **5.2. Implementation of Taguchi method in the optimisation of curling in**

### **SLS**

Optimising parameter design problems is routinely performed in the manufacturing industry, particularly in setting final optimal process parameters. Previously, trial-and-error processes were used, depending on experience and intuition, to determine optimal process parameter settings. However, the trial-and-error process is costly and time consuming, and thus it is not suitable for complex manufacturing processes [115], [116]. Subsequently, the Taguchi parameter design method was applied in the current study to determine the optimal process parameter settings.

Since curling has a direct impact on the accuracy and the qualities of the produced part, the design of experiments (DOE) method was proposed in this study to identify an optimal process parameter setting that can reduce or even eliminate curling on sintered parts [117]. The Taguchi method involves reducing the variation in a process through robust design of experiments. The overall objective of the method is to produce a high quality product at a low cost to the manufacturer.

The experimental design proposed by Taguchi involves using orthogonal arrays to organise the parameters affecting the process and the levels at which they should be varied. Instead of having to test all possible combinations as in factorial design, the Taguchi method tests pairs of combinations. This allows for the collection of the necessary data to determine which factors most affect product quality with a minimum amount of experimentation, thus saving time and resources. The Taguchi method is best used when there is an intermediate number of variables (3 to 50), few interactions between variables, and when only a few variables contribute significantly [118].

The major steps of implementing the Taguchi method are: (1) to identify the factors/interactions, (2) to identify the levels of each factor, (3) to select an appropriate orthogonal array (OA), (4) to assign the factors/interactions to columns of the OA, (5) to conduct the experiments, (6) to analyse the data and determine the optimal levels and (7) to conduct the confirmation experiment. Fig (5.4) illustrates the scheme of the major steps of implementing the Taguchi method. Taguchi method is a technique for designing and performing experiments to investigate processes where the output depends on many factors (variables, inputs) without having to tediously and uneconomically run the process using all possible combinations of values [119], [120].

In Taguchi methodology, the desired design is finalised by selecting the best performance under given conditions. Basically, the Taguchi method uses two important tools, namely orthogonal arrays (OA) and signal-to-noise (S/N) ratios. OA is the matrix of numbers arranged in columns and rows. It has a balancing property in which every factor setting occurs in the same number of times for every setting of all other factors in the experiment. Orthogonal arrays allow for studying many design parameters simultaneously and can be used to estimate the effects of each factor independent of the other factors. Therefore, information about the design parameters can be obtained with minimum time and resources. The signal-to-noise ratio is simply a quality indicator by which the effect of changing a particular design parameter on the performance of the process or product can be evaluated.

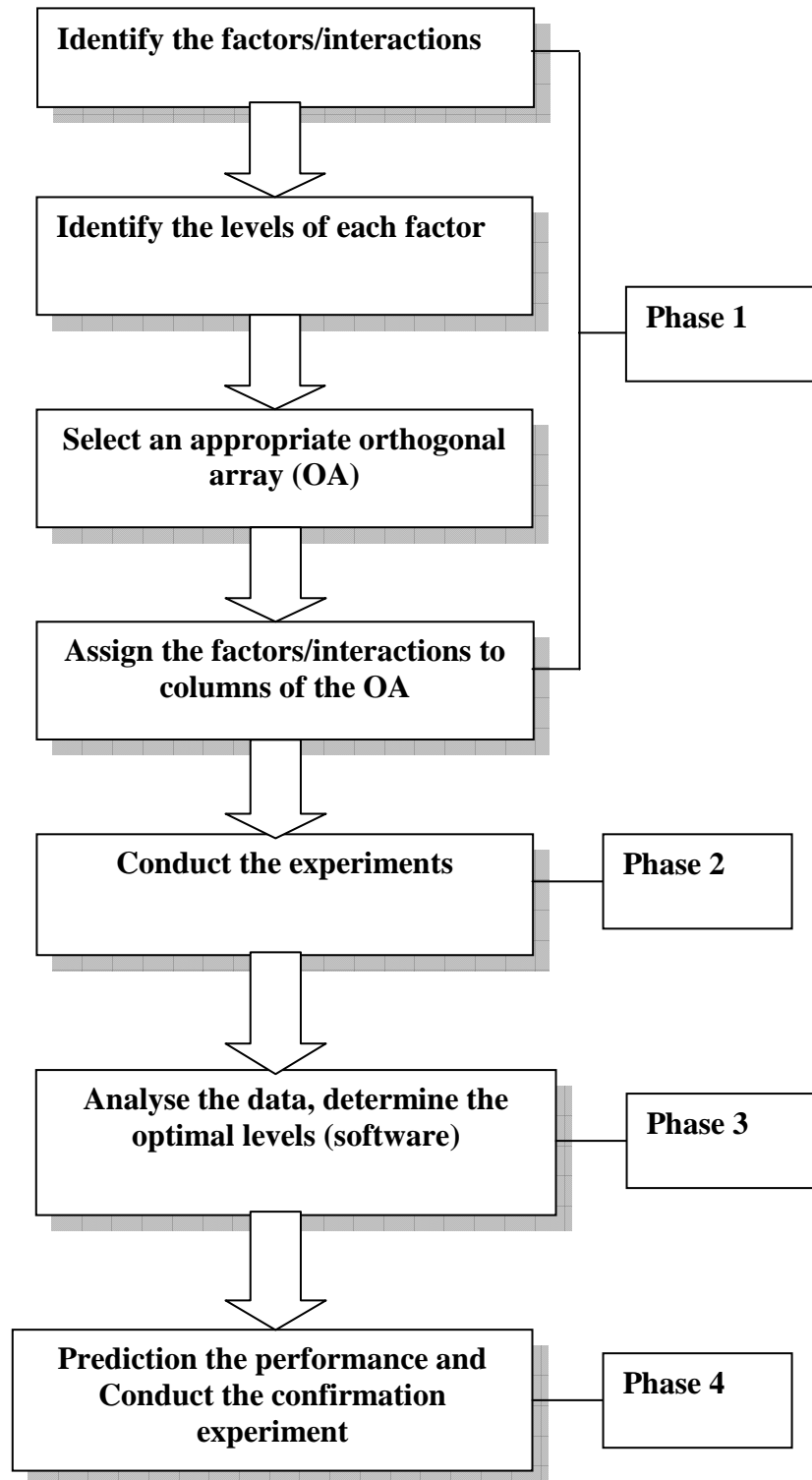


Fig (5.4) Scheme of the major steps of implementing the Taguchi method [120]

The Taguchi method employs a signal-to-noise (S/N) ratio to quantify the present variation. These S/N ratios are meant to be used as measures of the effect of noise factors on performance characteristics. S/N ratios take into account both the amount of variability in the response data and the closeness of the average response to the target. Generally, there are several S/N ratios available depending on the type of characteristics, such as smaller is better, nominal is best and larger is better [120], [121].

### *Advantages and disadvantages*

An advantage of the Taguchi method is that it emphasises a mean performance characteristic value close to the target value rather than a value within certain specification limits, thus improving the product quality. Additionally, the Taguchi method for experimental design is straightforward and easy to apply to many engineering situations, making it a powerful yet simple tool. It can be used to quickly narrow down the scope of a research project or to identify problems in a manufacturing process from data already in existence. Also, the Taguchi method allows for the analysis of many different parameters without a prohibitively high amount of experimentation. In this way, it allows for the identification of key parameters that have the most effect on the performance characteristic value so that further experimentation on these parameters can be performed and the parameters that have little effect can be ignored [118].

The main disadvantage of the Taguchi method is that the results obtained are only relative and do not exactly indicate what parameter has the highest effect on the performance characteristic value. Taguchi parameter design method however, can only

find the best specified process parameter level combination, which includes discrete setting values of the process parameters. Also, since orthogonal arrays do not test all variable combinations, this method should not be used when all relationships between all variables are needed. The Taguchi method has been criticised in the literature for difficulty in accounting for interactions between parameters. Furthermore, since Taguchi methods deal with designing quality into products and processes rather than correcting for poor quality, they are applied most effectively at early stages of process development. After design variables are specified, the use of experimental design may be less cost effective [115], [118].

### **5.3. Experimental procedure**

#### **5.3.1. Description of experimental set-up**

The SLS process involves a large number of process parameters that are carefully controlled by the operator. Most of the process parameters are decided by the knowledge and experience of the machine builder and machine operator.

The experimental study presented in this chapter aims, based on the Taguchi method, to investigate the curling behaviour of polyamide/glass bead composites sintered using a DTM 2000 laser sintering machine with changes in material compositions, part bed temperature, powder base thickness, laser power and layer cooling time. Experiments based on the DOE method were utilised to determine an optimal parameter setting for achieving a minimum or zero amount of curling on specimens fabricated using the selective laser sintering (SLS) process.

### *Selection of process parameters and fabrication*

Notably, there are many factors that should be considered in the fabrication of sintered parts. Some of them are straightforwardly related to the fabrication process itself, while others are more difficult to control, related to properties of the material and machine condition. Scan speed, layer thickness, scan spacing, laser power, powder particle size, powder size distribution, scanning strategy and part bed temperature represent important parameters which affect the SLS process. The effect of several combinations of these parameters on the accuracy of SLS parts have been investigated by numerous researchers. In this present experimental study of curling five controlled parameters, with two levels for each factor, including part bed temperature, laser energy, powder base thickness, layer cooling time (which is taken into account by varying the number of specimens contained in the build) and filler ratio were adopted.

Although the variation of scan speed and layer thickness could affect sintered parts in terms of the quality and the production speed, the effect of these two parameters was not considered in this study. They were kept constant as default settings recommended by the manufacturer of the Sinterstation 2000 machine. Additionally, the installed SLS software in this machine does not allow changes on the two above mentioned parameters to be applied.

In fact, many specimens were made and measurements were conducted before using the Taguchi method to find a parameter range in which effective processing takes place with reasonable stability and consistency of the SLS machine.

### *Details of the material*

The specimens used in this study were produced using PA12/CP03 composites. Polyamide 12 (PA12, PA2200) is a semi-crystalline polymer which represents a modification of nylon 12 developed for use in SLS machines. However, in the SLS process, it is common to use composite materials. Glass beads 3000 (CP00: coated and CP03: uncoated) were blended in different ratios with refreshed polyamide 12 (mixing ratio of 50% fresh powder and 50% used) to produce the composites.

### *Geometry of the test specimens*

Since curling was to be studied, a test bar was designed as shown in Fig (5.5). In this section, the geometry of the specimen and the SLS machine parameters used in its fabrication are introduced. The specimen was a polyamide/glass bead test bar 250 [mm] in length and 10x4 [mm<sup>2</sup>] in cross-sectional area.

As previously mentioned, the SLS process consisted of three stages, namely warm-up, build and cool-down. In the warm-up stage, layers of powder were deposited onto the part piston. The overall thickness of the powder spread in that stage was approximately 25.54 [mm] (default). This was then followed by the build stage, where the temperature of the powder in the feed cartridges was maintained at 95 [°C]. Layers of powder were spread by the roller, with the part heater raising the temperature of the top surface of the added layer to a set point temperature prior to sintering taking place. The test bar was produced, in the centre of the part bed, in an arrangement illustrated in Fig (5.6). The SLS machine parameters selected in fabrication, i.e. laser power (P), beam speed (BS) and scan spacing (SCSP) were 8 or 10 [W], 914 [mm/s] and 0.25 [mm], respectively.

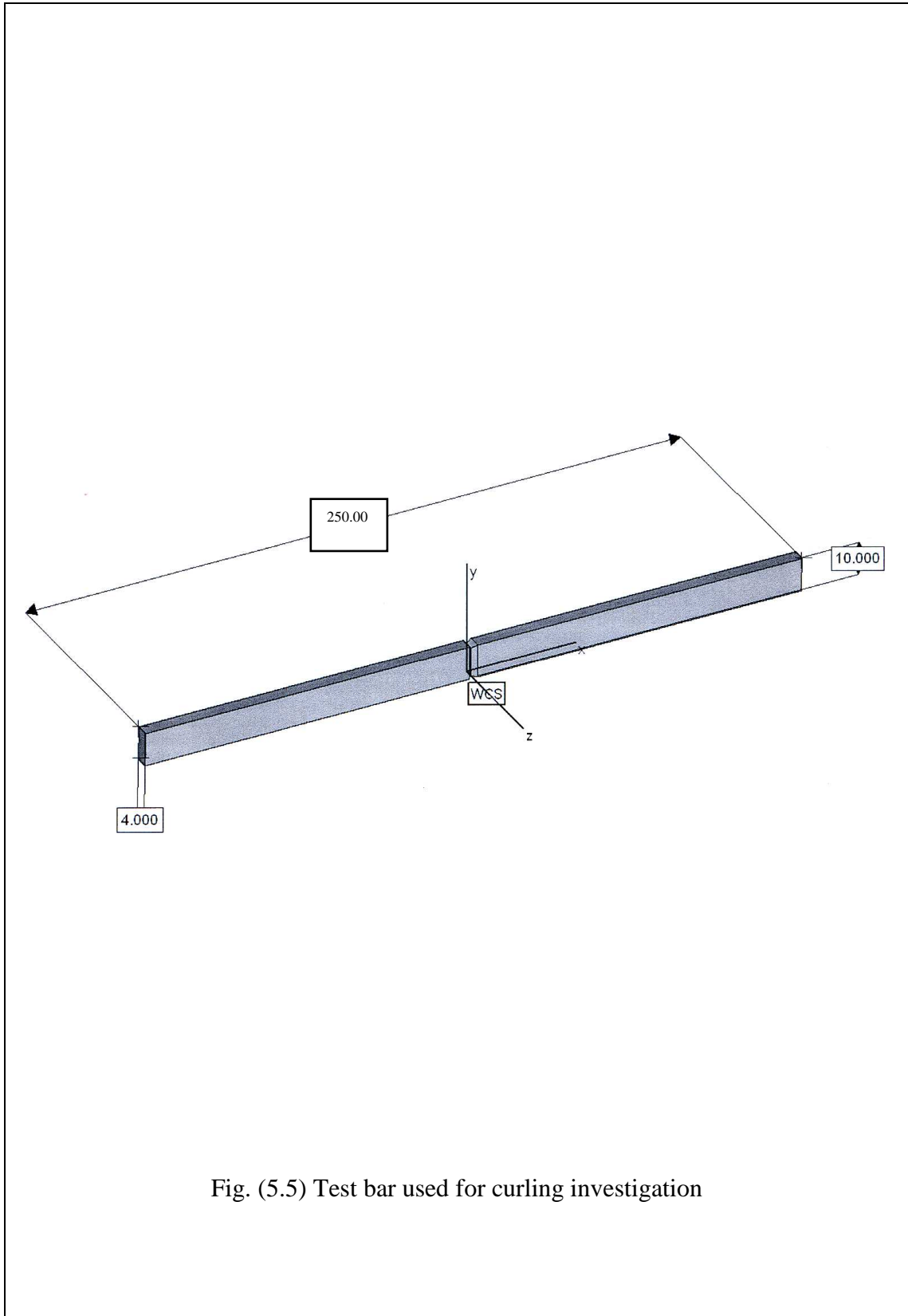


Fig. (5.5) Test bar used for curling investigation

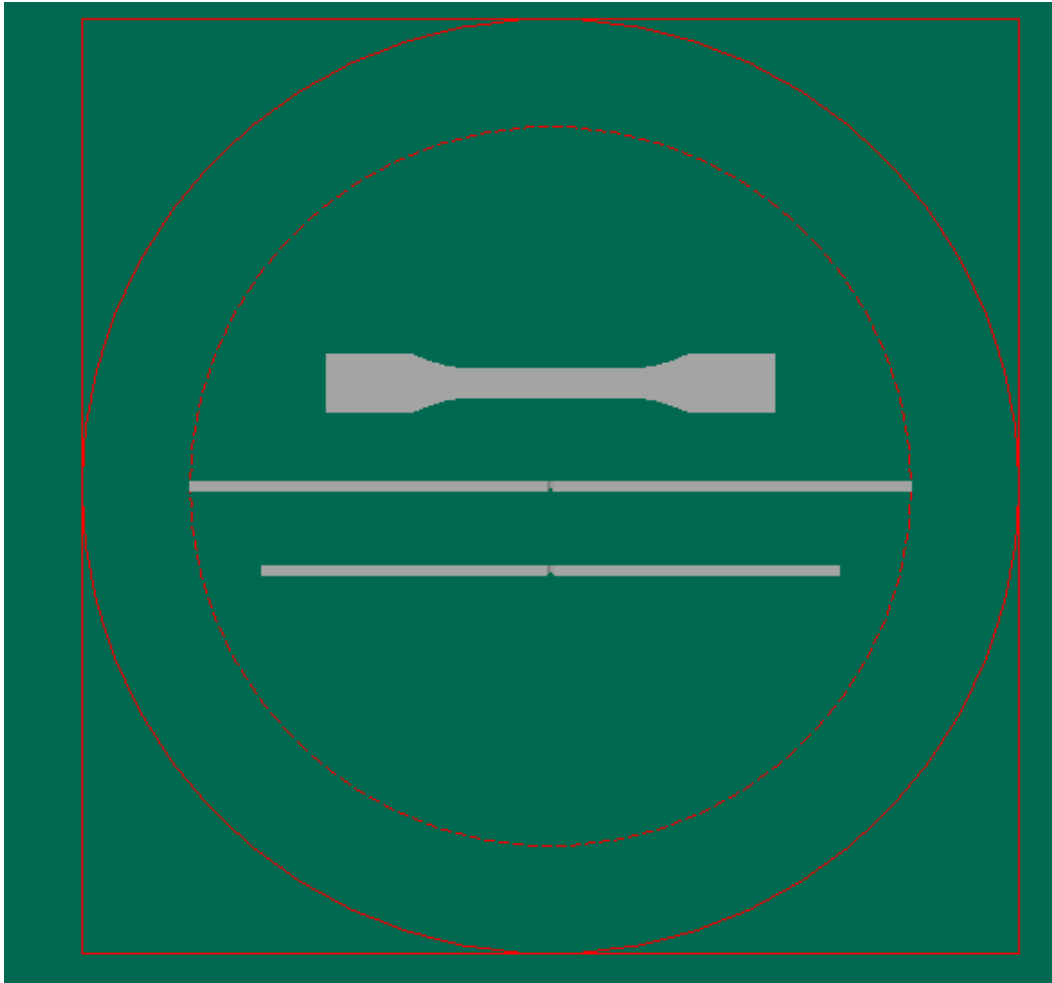


Fig (5.6) Position of the test bar with respect to the part bed and neighbouring parts

### **5.3.2. Design of experiments**

A design of experiment is a methodology of experimentation by which the total information from a system can be obtained by doing minimum number of experiments. Although the technique is well-known and has been widely used in manufacturing processes, few of these studies have been reported in the case of SLS.

The main objective of the present investigation was to apply the Taguchi method to establish the optimal set of control parameters for the minimising of curling on selective laser sintered parts from polyamide composites. The Taguchi method was employed in this work to determine the optimal combination of design parameters, including part bed temperature, laser power, powder base thickness, layer cooling time and filler ratio.

#### *Selection of control factors and noise factors*

Before designing the experiments, an exhaustive evaluation of the factors that could influence the optimisation of the quality characteristic was carried out. Previous studies indicated that part bed temperature, laser power, layer cooling time and part location/position/orientation have an influence on curling in the selective laser sintering process (SLS). In this study, as controllable factors, part bed temperature (A), laser power (B), powder base thickness (C), layer cooling time (D) and filler ratio (E) were selected. Based on experimental trials and experience with the SLS process, five main parameters were chosen. These parameters are considered as control variables. However, besides these parameters, which are controlled, there are also uncontrolled factors that have an effect on the SLS process. The controllable and uncontrollable factors generate signals and noise. Signals are the factors that work in favour of

sintering process performance and noise is the factors that work against sintering process performance. The goal of the experiments was to increase the signal within the chosen factors and to reduce the noise from uncontrollable factors [122]. Tables (5.2) and (5.3) list the variable factor levels and noise factors, respectively. The model of the SLS process is shown in Fig (5.7).

In order to achieve the abovementioned goal, the following guidelines were taken into consideration for the DOE:

- The design and analysis of the experiment must be as simple as possible.
- The inputs of the SLS process are defined on the basis of theoretical and practical knowledge.
- It is important to distinguish between the practical and statistical significance of the results
- The physical and engineering knowledge about the problem, because a statistical evaluation is not enough if the results are not evaluated properly [123], [124].

#### *Selection of the orthogonal array*

The arrays were selected by the number of parameters (variables) and the number of levels (states). However, the effect of many different parameters on the performance characteristic in a condensed set of experiments can be examined using the orthogonal array experimental design proposed by Taguchi. The selection of the orthogonal array is based on the number of parameters and the levels of variation for each parameter.

Table (5.2) The factors that may have an effect on the SLS process

Controlled factors	Uncontrolled factors
- Part bed Temperature , T	- Chamber temperature variation
- Laser Power, LP	- Composite homogeneity
- Powder base thickness, BT	- Moisture in the material
- Cooling time , CT	- Optical properties
- Filler ratio FR	- Machine condition
- Layer thickness $L_t$	- Building position
- Scan speed ... etc.	- Size of building part ... etc.

Table (5.3) List of SLS experimental parameters and their factor levels

Parameters	Number of levels	Description	
		1	2
Part bed temperature , T [°C]	2	170	172
Laser power, LP [W]	2	8	10
Powder base thickness, BT [mm]	2	20	40
Layer cooling time , CT [s]	2	One part	Group of parts
Filler ratio, FR [w%]	2	10	40

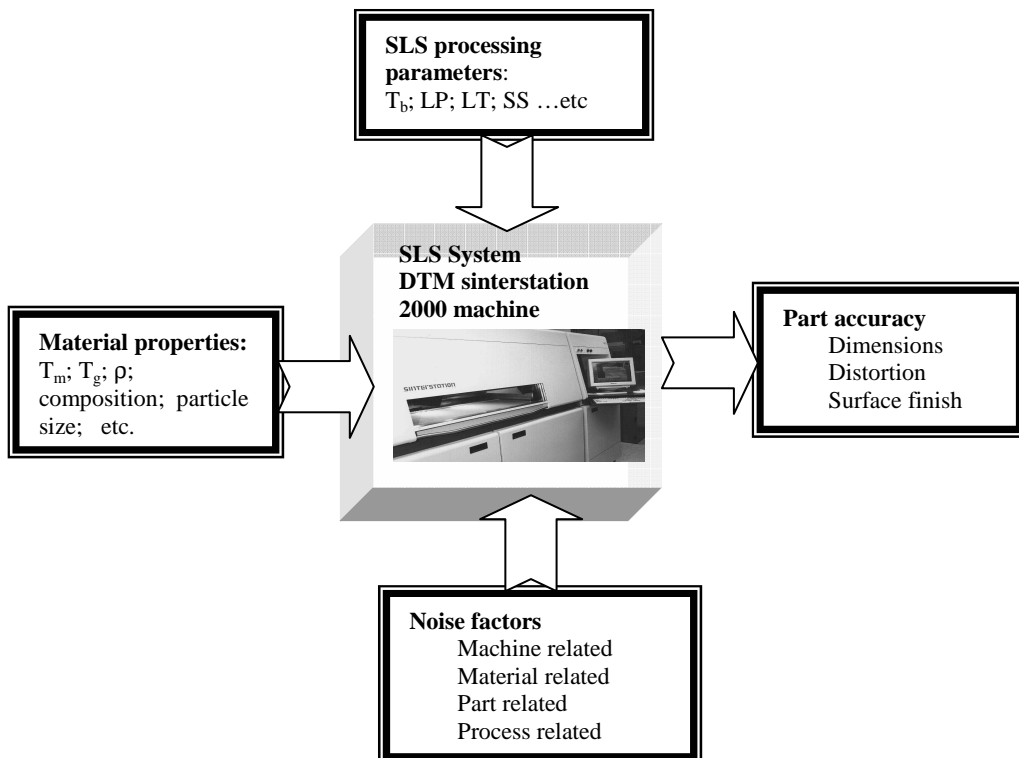


Fig (5.7) The model of the SLS process in the Taguchi method

Determining what levels of a variable to test requires an in-depth understanding of the process, including the minimum, maximum and current value of the parameter. Therefore, knowing the number of parameters and the number of levels, the proper orthogonal array can be selected [118].

As mentioned above, there are many SLS parameters that have some effect on the geometric accuracy of sintered parts. In this way, since five control factors were studied in this investigation, two levels of each factor were considered, the lowest array that can represent this design is a modified  $L_8$  array, as shown in Table (5.4). The number of levels for all parameters in the experimental design was chosen to be the same to aid in the selection of a proper orthogonal array.

An orthogonal array of the  $L_8 (2^5)$  type was selected to be used for these experiments. This design required eight experiments with five parameters at two levels of each. In the notation  $L_8 (2^5)$ , L indicates that the information is based on the Latin square arrangement of factors. A Latin square arrangement is a square matrix arrangement of factors with separable factor effects. The number 8 of the notation states the number of experiments required when using the orthogonal array while the number 5 of the notation is the maximum number of factors that can be studied using the array. The number 2 of the notation indicates the number of factor levels. The interactions were neglected. Table (5.5) shows the filled-in  $L_8$  for experimental runs and level combinations. This setup allows the testing of all five variables without having to run  $32 [= 2^5 = (2 \text{ temperatures})(2 \text{ laser powers})(2 \text{ powder base thicknesses})(2 \text{ layer cooling times})(2 \text{ filler ratios}]$  separate trials. With the actual variables and states (levels), the  $L_8$  array should look like the one represented in Table (5.5) which shows

Table (5.4) Layout of the L8 orthogonal array

Exp. No	A	B	C	D	E
1	1	1	1	1	1
2	1	1	1	2	2
3	1	2	2	1	1
4	1	2	2	2	2
5	2	1	2	1	2
6	2	1	2	2	1
7	2	2	1	1	2
8	2	2	1	2	1

Table (5.5) The filled in  $L_8$  for experimental runs and level combinations

Exp. No	Part bed temperature (A) [°C]	Laser power (B) [W]	Powder base thickness (C) [mm]	Layer cooling Time (D) [s]	Filler Ratio (E) [wt%]
1	170	8	20	O	10
2	170	8	20	G	40
3	170	10	40	O	10
4	170	10	40	G	40
5	172	8	40	O	40
6	172	8	40	G	10
7	172	10	20	O	40
8	172	10	20	G	10

the five control factors and their level setting values. The values of the parameters were chosen to comply with the manufacturer's recommendations.

#### **5.4. Curling measurement procedure**

According to the experimental plan shown in Table (5.4) several samples were fabricated in pure PA12, PA12/CP00 and PA12/CP03 on the Sinterstation 2000 sintering machine. Figure (5.5) shows the test bar used in curling study. In this particular case, the problem to be solved is to determine the optimal processing parameters that lead, as much as possible, to a minimal amount of curling on sintered parts. Curling is generally defined as a departure from a desired flat shape of a produced part. A method to measure curling on sintered parts has been proposed. The method is based on measurement of the out-of-plane edges of a curled specimen.

In order to determine the amount of curling, measurements of the thickness of the cleaned and sandblasted test bars were required. These were carried out by using a digital micrometer. The test bar for which curling was to be measured was first placed with its top surface facing upwards onto a flat measuring table, as shown in Fig (5.8). The measuring table was taken as the reference for measurements. Curling was examined by measuring the upward edges of the produced bars. The measurements were performed using a Mitutoyo HDS digital height gauge (Fig 5.8). The procedures of curling measurement were as follows: (a) the testing bar was placed on the flat surface of the measuring table; (b) the height gauge was moved down until its stylus touched the edge of the testing bar to measure the maximum vertical distance of the point on the edge of the bar from a flat reference plane; (C) the curling amount was then calculated by the formula:  $C = h_{\max} - t_a$ , as a difference in height between the

average thickness at the centre and maximum height at the outer edges of the specimen. The measuring principle is shown in Fig (5.9). Each run would have two data values collected. Therefore, a total of  $8 \times 2 = 16$  data values were collected per trial. The measured values obtained from test bars showed that curling amount on the samples sintered in PA12/CP03 system was notably small compared to that observed on samples produced from pure PA12 or PA12/CP00 system. So based on this fact the measured data of PA12/CP03 system were adopted for analysis in this investigation. The results of measurements of curling are shown in Table (5.6). These data were used in the statistical analysis by employing main effects, signal-to-noise ratio (S/N) and ANOVA analyses as explained in the section below.

### **5.5. Statistical analysis of experimental data**

To this point, the experimental design has been determined and the trials have been carried out. The measured performance characteristic from each trial can be used to analyse the relative effect of the different parameters on curling.

#### *Selection of the quality characteristic*

Basically, there are three types of quality characteristics in the Taguchi methodology such as the-smaller-the-better, the-larger-the-better and the-nominal-is-best. Smaller curling values represent a better or improved quality characteristic. The formula for the three types are given as follows [115]:

$$\text{Nominal the best: } S/N = 10x \log \left( \frac{\bar{y}^2}{S^2} \right)$$

$$\text{Larger the better: } S/N = -10x \log \left( \frac{1}{n} \sum_{i=1}^n \frac{1}{y_i^2} \right)$$

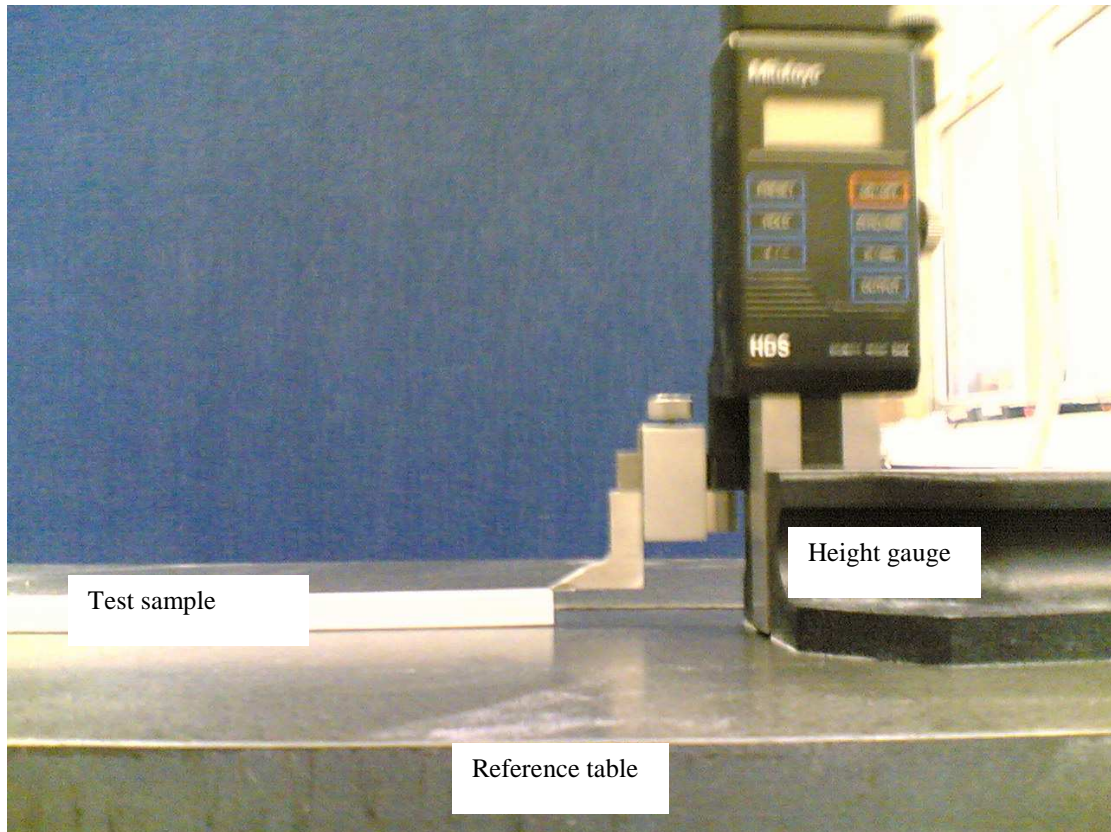


Fig (5.8) Measurement arrangement of curling

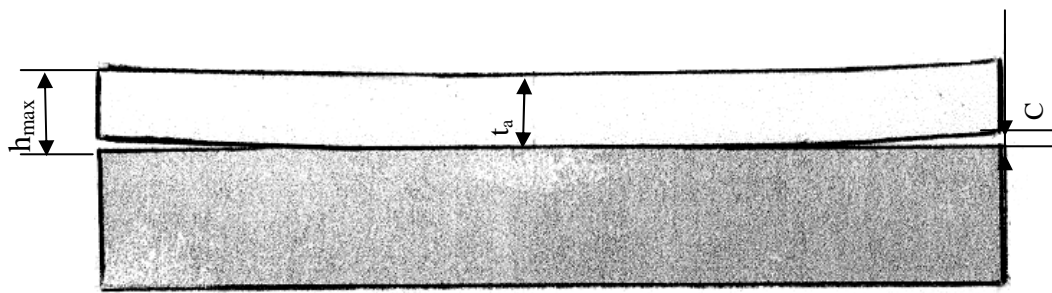


Fig (5.9) Definition for symbols:  $C$ ;  $t_a$ ;  $h_{\max}$

Table (5.6) Values of thickness and curling for L8 orthogonal array from three sets of experiments

Run No.	Trial 1							
	Sample Thickness [mm]				Height [mm]			Curling [mm]
	Left	Centre	Right	$t_{avg,T1}$	$h_{Left}$	$h_{Right}$	$h_{avg}$	$C_{T1}$
1	10.049	10.029	10.011	10.03	11.84	11.63	11.735	1.705
2	10.139	10.137	10.052	10.11	11.84	12.07	11.955	1.845
3	10.167	10.338	10.352	10.28	10.48	10.39	10.435	0.155
4	10.166	10.450	10.168	10.26	11.29	11.29	11.290	1.030
5	10.186	10.396	10.300	10.29	10.36	10.67	10.515	0.225
6	10.218	10.319	10.331	10.29	11.01	11.17	11.090	0.800
7	10.180	10.118	10.140	10.15	11.79	12.27	12.030	1.880
8	10.200	10.329	10.232	10.25	11.36	11.59	11.475	1.225
Run No.	Trial 2							
	Part Thickness [mm]				Height [mm]			Curling [mm]
	Left	Centre	Right	$t_{avg,T2}$	$h_{Left}$	$h_{Right}$	$h_{avg}$	$C_{T2}$
1	10.054	10.059	9.900	10.00	11.71	11.34	11.525	1.525
2	9.640	10.068	9.500	9.77	11.65	11.78	11.715	1.715
3	10.069	10.170	10.141	10.13	10.85	10.92	10.885	0.755
4	10.137	10.136	10.094	10.12	10.84	10.64	10.740	0.620
5	10.193	10.285	10.221	10.23	11.36	11.68	11.520	1.290
6	9.983	10.283	10.021	10.09	10.97	11.44	11.205	0.235
7	10.268	10.569	10.009	10.28	11.56	11.89	11.725	1.445
8	10.090	10.116	10.064	10.09	11.57	11.71	11.640	1.550
Run No.	Trial 3							
	Part Thickness [mm]				Height [mm]			Curling [mm]
	Left	Centre	Right	$t_{avg,T3}$	$h_{Left}$	$h_{Right}$	$h_{avg}$	$C_{T3}$
1	10.040	10.027	9.939	10.00	12.17	11.99	12.080	2.080
2	9.754	10.118	9.731	9.87	12.45	12.06	12.255	2.255
3	10.015	10.137	10.166	10.11	11.46	11.46	11.460	1.350
4	10.206	10.400	10.342	10.32	11.21	11.39	11.300	0.980
5	10.112	10.236	10.148	10.16	10.73	11.41	11.070	0.910
6	10.177	10.313	10.198	10.23	10.72	11.19	10.955	0.725
7	10.179	10.109	10.125	10.14	12.43	11.88	12.155	2.015
8	10.252	10.214	10.228	10.23	11.88	11.52	11.700	1.470

Smaller the better:  $S/N = -10x \log \left( \frac{1}{n} \sum_{i=1}^n y_i^2 \right)$

The nominal-is-best characteristics include the loss of functions that the system output should reach; larger-the-better characteristics mean that when the output becomes larger, it should be better; smaller-the-better characteristics are such that the smaller the output of the system, the better the characteristics are [116].

The study of distortion of a flat part is very important because the distortion will affect part stability, especially when the part is to be used for tooling. Therefore, in order to have accurate parts, the amount of curling must be as small as possible. Curling is an undesirable phenomenon in the SLS process and it has to be minimised. The most desired value is zero. In terms of geometrical accuracy, less curling is the indication of better performance of the process. Therefore, a smaller-the-better quality characteristic was selected in this investigation for obtaining optimum processing parameters for minimum curling.

### **5.5.1. Main effects**

These are separate effects of each factor and are commonly called main effects. The primary goal in conducting this type of experiment is to optimise the parameter level for each factor, so that the output performance measure gives a low amount of curling. The average value of curling for each factor (A, B, C, D and E) at each level (level 1 and level 2) was obtained and the results are summarised in Table (5.8). Fig (5.10) presents the main effect graph for the average amount of curling. This graph is based on the average curling presented in Table (5.7). The quality characteristics investigated in this study was “the-smaller-the-better” owing to the fact that smaller

Table (5.7) Experimental results for curling measurements (PA12/CP03 system)

Exp No	Part bed temperature [°C]	Laser power [W]	Powder base thickness [mm]	Layer cooling Time [s]	Filler Ratio [wt%]	C <sub>T1</sub>	C <sub>T2</sub>	C <sub>T3</sub>	C <sub>avg</sub> (Mean)
1	170	8	20	O	10	1.705	1.525	2.080	1.895
2	170	8	20	G	40	1.845	1.715	2.255	1.938
3	170	10	40	O	10	0.155	0.755	1.350	0.753
4	170	10	40	G	40	1.030	0.620	0.980	0.877
5	172	8	40	O	40	0.225	1.290	0.910	0.808
6	172	8	40	G	10	0.800	0.235	0.725	0.587
7	172	10	20	O	40	1.880	1.445	2.015	1.780
8	172	10	20	G	10	1.225	1.550	1.470	1.415

Table (5.8) Level averages for main effects

Symbol	Parameters/Factors	Average curling [mm]	
		Level 1	Level 2
A	Part bed temperature, T [°C]	1.366	1.147
B	Laser power, LP [W]	1.307	1.206
C	Powder base thickness, PBT [mm]	1.757	0.756
D	Layer cooling time, LCT [s]	1.309	1.204
E	Filler ratio, FR [w%]	1.162	1.351

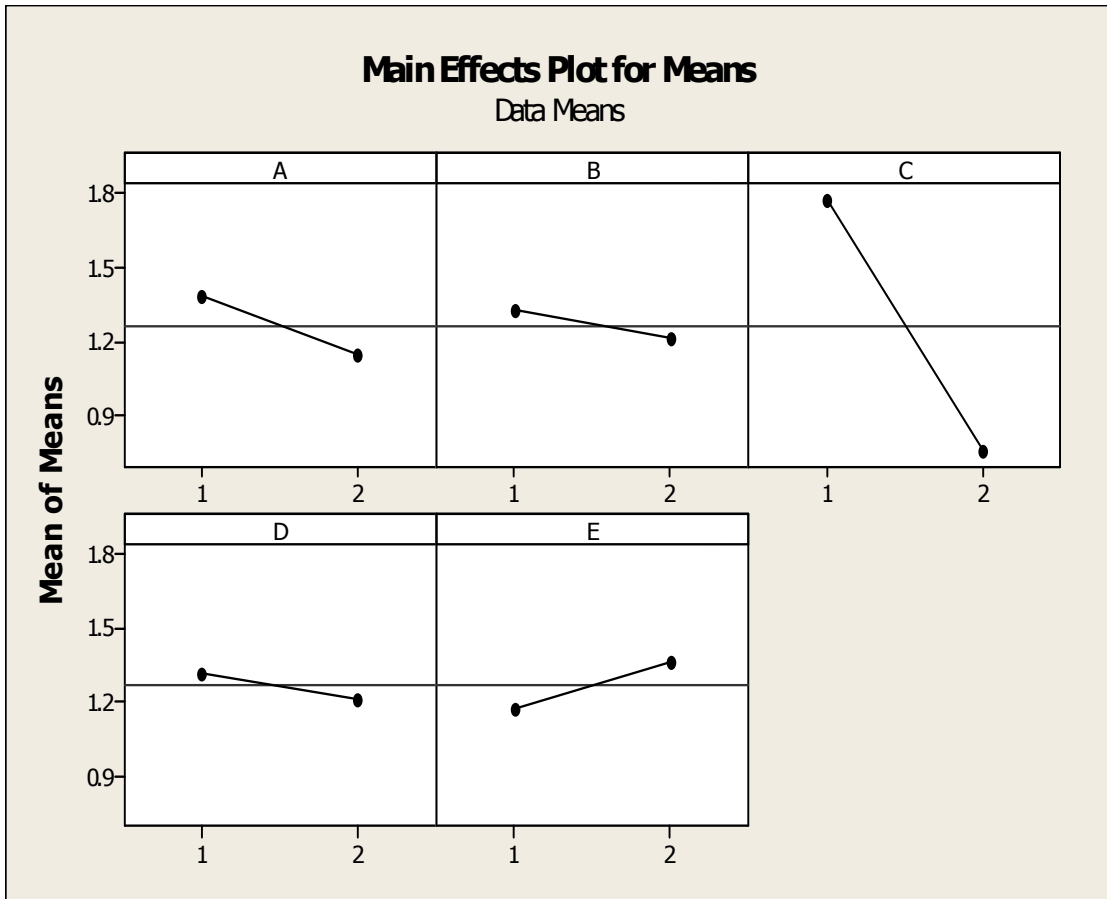


Fig.(5.10) Main effects graphs for average curling

- A Part bed temperature
- B Laser power
- C Powder base thickness
- D Layer cooling time
- E Filler ratio

curling represents higher quality of parts in terms of geometrical accuracy. Thus, for the smallest curling, the best parameter levels were: part bed temperature at level 2 (A2), laser power at level 2 (B2), powder base thickness at level 2 (C2), layer cooling time at level 2 (D2) and filler ratio at level 1 (E1).

### 5.5.2. Analysis using signal to noise (S/N) ratio

To determine the effect each variable has on the output, the signal-to-noise ratio (or the SN number) needs to be calculated for each experiment conducted. In the Taguchi method, the S/N ratio is a measure of quality characteristic deviation from the desired value. The term signal represents the desirable value (mean) and the noise represents the undesirable value (standard deviation from the mean) for the output characteristic [118].

The signal-to-noise ratio is used in evaluating the quality of the product and is an objective measure of quality that takes both the mean and variance into account. The signal-to-noise ratio measures the level of performance and the effect of noise factors on performance and is an evaluation of the stability of the performance of output characteristics. As mentioned above, for determining the signal-to-noise ratio for the curling response, a smaller-the-better type S/N ratio was implemented and introduced. In the case of minimising the quality characteristic, the SN ratio is calculated using equation (5.1):

$$S/N = -10x \log \left( \frac{1}{n} \sum_{i=1}^n y_i^2 \right) \quad \text{where} \quad \left( \frac{1}{n} \sum_{i=1}^n y_i^2 \right) = MSD \quad \dots (5.1)$$

In the equations above, n is the number of trials for experiment i,  $y_i$  is the value for  $i$ th trial in that experiment, i is the experiment number and MSD is the mean square deviation.

In this study, three trials for each experiment were conducted. The S/N ratios for eight experiments were calculated for the target value using equation (5.1). The data obtained are presented in Table (5.9). Shown below is an example for the calculation of the SN ratio:

$$SN1 = -10 \log \left( \frac{1}{3} \sum_{i=1}^3 1.705^2 + 1.525^2 + 2.080^2 \right) = -5.033 \quad \dots (5.1-a)$$

After calculating the S/N ratio for each experiment, the average S/N value was calculated for each factor and level (equations 5.2). This was done as shown below:

$$SN_{j,i} = \frac{\sum_i^4 SN_i}{N_{j,i}} \quad \text{where } j = A; B; C; D; E \quad \text{and } i = 1; 2 \quad \dots(5.2)$$

$$SN_{A,1} = \frac{SN1 + SN2 + SN3 + SN4}{4} = \frac{-5.03 - 5.81 + 0.94 + 0.96}{4} = -2.236 \quad \dots(5.2-a)$$

$$SN_{A,2} = \frac{SN5 + SN6 + SN7 + SN8}{4} = -0.881 \quad \dots (5.2-b)$$

### *Significance of each source*

From Table (5.9), it can be seen that experiment number 6 yielded the highest S/N ratio and the smallest MSD. For this experiment, the combination of parameters and their levels was A2, B1, C2, D2 and E1 as indicated in Table (5.5). This result was different from that obtained from the main effect analysis and did not represent the optimum combination of parameters and their levels. However, this shows that in the present investigation, the combination of parameters and their levels A2, B1, C2, D2

Table (5.9) The S/N ratio results for curling

Exp. No	A	B	C	D	E	T1	T2	T3	MSD	SN [db]
1	170	8	20	O	10	1.705	1.525	2.080	3.186	-5.033
2	170	8	20	G	40	1.845	1.715	2.252	3.805	-5.809
3	170	10	40	O	10	0.155	0.755	1.350	0.805	+0.939
4	170	10	40	G	40	1.030	0.620	0.980	0.802	+0.959
5	172	8	40	O	40	0.225	1.290	0.910	0.848	+0.718
6	172	8	40	G	10	0.800	0.235	0.725	0.407	+3.904
7	172	10	20	O	40	1.880	1.445	2.015	3.227	-5.089
8	172	10	20	G	10	1.225	1.550	1.470	2.021	-3.056

Table (5.10) The range of each parameter

Level	A	B	C	D	E
1	-2.236	-1.555	-4.747	-2.116	-0.811
2	-0.881	-1.562	+1.630	-1.000	-2.305
$\Delta$	1.355	0.007	6.376	1.116	1.494
Rank	3	5	1	4	2

and E1 yielded the optimum quality characteristic with minimum variance around the target value, and it could serve as a possible initial optimal process parameter setting.

The range (delta,  $\Delta$ ) of the SN for each parameter was calculated from equation (5.3) and then entered into Table (5.10). The larger the  $\Delta$  value for a parameter, the larger the effect the variable has on the amount of curling. This is because the same change in signal causes a larger effect on the output variable being measured. The effect of the factor was then calculated by determining the range [118]:

$$\text{Difference } (\Delta_i) = \text{highest value} - \text{lowest value} \quad \dots (5.3)$$

It can be seen that powder base thickness had the largest effect on the amount of curling and that laser power had the smallest effect on curling.

### **5.5.3. Data analysis by the ANOVA technique**

The data coming from the experimental trials needed to be evaluated by the analysis of variance (ANOVA). The main objective of the analysis was to determine the influence of every parameter on the variance of the result, regarding the total variance of all the parameters.

Analysis of variance is a method of partitioning variability into identifiable sources of variation. In this work, ANOVA was conducted to find the significance factors that affected the amount of curling on a selective laser sintered specimen. This analysis was performed on the S/N ratios to obtain the percentage contribution of each of the factors.

The relative percentage contribution among the factors was determined by comparing their relative variance.

Basically, ANOVA helped with computing quantities such as degrees of freedom, sums of squares, variance, *F*-ratio, pure sum of square and percentage contribution. The example calculations of these quantities, based on the ANOVA analysis of the data in Table (5.9), are shown below and the results are summarised in Table (5.11). The following were the ANOVA terms used for analysing the experimental results [116]:

- **Sum of squares (SS)**: It is the sum of squares of all the trial run results.

$$SS = \sum_1^N y_{1,1}^2 + y_{2,1}^2 + \dots + y_{i,j}^2 \quad \text{i is experiment number ; j is trial number}$$

- **Total sum of squares ( $SS_T$ )**: It is the difference between the sums of squares of all the trial run results and the Correction Factor (*CF*).

$$SS_T = \sum_{i=1}^N y_i^2 - CF \quad y_i \text{ is the value of each result}$$

- **Correction factor (CF)**: the term that reduces the variation of the process.

$$CF = \frac{T^2}{N} \quad T \text{ is the sum of all results; } N \text{ is the total number of results}$$

- **Degrees of freedom (*f*)**: the number of degrees of freedom for a factor is equal to one less than the number of levels of that factor.

- **Variance (V)**: the variance of each factor is determined by the sum of the squares of each trial sum of results involving the factor divided by the degrees of freedom of the factor.

$$V_i = \frac{SS_f}{f} \quad SS_f \text{ is the sum of squares of the factor; } f \text{ is the degrees of freedom}$$

- **Variance ratio (*F*)**: it is the ratio of variance of each factor to the error variance.

$$F_i = \frac{V_f}{V_e}$$

- **Percentage of contribution (P):** the percentage of the contribution of each factor is the ratio of the factor sum of squares to the total sum of squares.

$$P_i = \frac{SS_f}{SS_T}$$

- **Degree of freedom (f)**

Total degrees of freedom:

$$f_T = N - 1 = 8 - 1 = 7$$

where N is the total number of results.

For factor A,

$$f_A = l_A - 1 = 2 - 1 = 1$$

where  $l_A$  is the number of levels for factor A.

For error:

$$f_e = f_T - f_A - f_B - f_C - f_D - f_E = 7 - 1 - 1 - 1 - 1 - 1 = 2$$

- **Sum of squares (SS)**

Total sum of squares:

$$SS_T = \sum_{i=1}^N y_i^2 - CF = (1.895^2 + \dots + 1.415^2) - \frac{(1.895 + \dots + 1.415)^2}{8} = 2.218$$

$$SS_A = \frac{(\sum A_1)^2}{N_{A1}} + \frac{(\sum A_2)^2}{N_{A2}} - \frac{T^2}{8}$$

$$= \frac{(1.895 + 1.938 + 0.753 + 0.877)^2}{4} + \frac{(0.808 + 0.587 + 1.780 + 1.415)^2}{4}$$

$$- \frac{(1.895 + \dots + 1.415)^2}{8} = 0.095$$

For error:

$$\begin{aligned}SS_e &= SS_T - SS_A - SS_B - SS_C - SS_D - SS_E \\ &= 2.218 - 0.095 - 0.020 - 2.003 - 0.022 - 0.071 = 0.007\end{aligned}$$

**- Variance (V):**

$$V_i = \frac{SS_i}{f_i}$$

For factor A:

$$V_A = \frac{SS_A}{f_A} = \frac{0.095}{1} = 0.095$$

For error:

$$V_e = \frac{SS_e}{f_e} = \frac{0.007}{2} = 0.003$$

**- F-ratio (F):**

For factor A:

$$F_A = \frac{V_A}{V_e} = \frac{0.095}{0.003} = 31.667$$

**- Percentage contribution (P)**

For factor A:

$$P_A = \frac{SS_A}{SS_T} \times 100 = \frac{0.095}{2.218} \times 100 = 4.28\%$$

Table (5.11) shows the results of the ANOVA for the curling investigation. Based on the main effect, the optimal combination of parameters and their levels for achieving the minimum amount of curling was determined to be A2, B2, C2, D2 and E1, i.e. part bed temperature at level 2 (172°C), laser power at level 2 (10 W), powder base

Table (5.11) ANOVA table

Source	<i>f</i>	SS	V	F	P [%]
Part bed temperature (A)	1	0.095	0.095	31.667	4.28
Laser power (B)	1	0.020	0.020	6.667	0.90
Powder base thickness (C)	1	2.003	2.003	667.667	90.31
Layer cooling time (D)	1	0.022	0.022	7.333	0.99
Filler ratio (E)	1	0.071	0.071	23.667	3.20
Error	2	0.007	0.003	1	0.32
Total	7	2.218			100%

thickness at level 2 (40 mm), layer cooling time at level 2 (G) and filler ratio at level 1 (10 wt%).

The results reveal that the powder base thickness had the maximum contribution, which was 90.31%, to the quality characteristic. The factors: part bed temperature with 4.28% followed by filler ratio with 3.20%, layer cooling time with 0.99% contribution then laser power which was 0.90% were not significant affecting factors for minimum curling. Fig (5.11) reveals the percent contribution of the factors.

In the three previous subsections, several tools, techniques and equations were discussed. Each of these tools is well-known and extensively used in the scientific and engineering professions. Just as with any tool, the intent and the results need to be compared and grounded with process knowledge. However, statistical methods cannot prove that a factor (or factors) has a particular effect. They only provide guidelines as to the reliability and validity of results. Properly applied statistical methods do not allow anything to be proven experimentally, but they do allow the likely error in a conclusion to be measured or to the attached level of confidence to a statement. The primary advantage of statistical methods is that they add objectivity to the decision-making process. Statistical techniques coupled with good engineering or process knowledge and common sense will usually lead to sound conclusions [124].

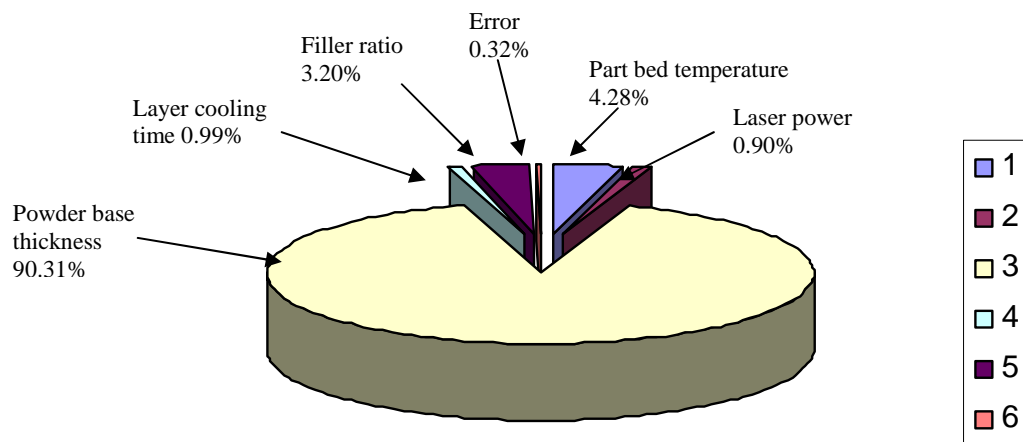


Fig (5.11) Percentage contributions of process parameters on the amount of curling on sintered parts

## 5.6. Summary

This study applied the Taguchi method to establish the optimal set of control parameters for minimising curling on selective laser sintered parts from polyamide composites. On the basis of the results obtained from the present investigation, the following can be concluded:

- The combination of parameters and their levels for the optimum amount of curling is A2B2C2D2E1, i.e. part bed temperature (172°C), laser power (10 W), powder base thickness (40 mm), layer cooling time (G), and filler ratio (10 wt%).
- The contributions of part bed temperature, laser power, powder base thickness, layer cooling time and filler ratio are 4.28%, 0.90%, 90.31%, 0.99% and 3.20%, respectively, where it was found that the powder base thickness is the most effective factor in the occurrence of the curling phenomenon.

## **Chapter 6 - Conclusions and Suggestions for Future Work**

This research has examined the effect of filler content and its surface treatment as well as two of processing parameters with the aim of showing their influence on the mechanical properties and geometric accuracy of selective laser sintered parts from GB/PA12 composites. In this chapter, the results obtained are summarised and then possible future directions are discussed.

### **6.1. Conclusions**

This work has demonstrated the effect of different parameters, such as weight ratio and surface treatment of filler particles, part bed temperature and energy density on the mechanical properties and geometric accuracy of glass bead-filled PA12 composites.

The addition of coated glass beads to polyamide 12 improves the tensile strength, elastic modulus, flexural strength and flexural modulus, but generally reduces the impact strength and the ductility of polyamide 12 with increasing weight ratio of the glass beads under the experimental conditions applied.

Beside laser power, part bed temperature and other operating parameters covering the SLS process, the improvements achieved in the mechanical properties and geometric accuracy of glass bead-filled polyamide 12 composites could be attributed to the good interfacial bonding between the polyamide matrix and the glass beads. Furthermore, this study clearly demonstrated, from SEM micrographs taken of the surfaces of the tensile fracture cross-sections, that the incorporation of the coupling agent to glass beads improves the mechanical properties of the PA12/GB composites.

A higher energy density of the CO<sub>2</sub> laser beam results in better fusion of the polymer particles, enabling a more compact structure with a smoother surface to the build. When the energy density becomes excessively high, however, degradation of the polymer will occur, leading to a slight drop in the density of sintered test parts and blistering of the polymeric material at the surface.

Furthermore, the work presented in this thesis has demonstrated that rigid fillers can generally be used to increase the mechanical properties and improve the geometric accuracy of sintered components in PA12/GB composites. In chapters 4 and 5, experimental evidence for these improvements is presented for PA12/GB composite systems. Chapter 4 provides evidence for the hypothesis made in chapter 1 on the importance of interfacial adhesion. In particular, this was investigated using silane surface-modified glass beads.

There is very little information from previously published work on the influence of coupling agents on curling. The results of statistical analysis and analysis of variance presented in chapter 5 provide evidence for the effectiveness of filler content and its surface treatment on reducing the amount of curling. On the basis of the results obtained, a combination of parameters A2B2C2D2E1 and their levels have been shown to yield an optimum amount of curling (with minimum variance about the target) on selective laser sintered parts in PA12/CP03 composites. The effect of the processing parameters applied on curling differed from one parameter to another, however, the contribution of powder base thickness seemed to be the highest, whereas other considered parameters had a negligible effect on curling.

In general, the addition of glass particles to polyamide 12 improved the behaviour of curling of PA12/GB composites. The comparison between samples fabricated in pure PA12, PA12/CP00 and PA12/CP03 revealed that the samples from PA12/CP03 were significantly flat and more accurate.

As mentioned in chapter 1, this research was driven by an effort to answer the main research questions that surrounded the improvement of the mechanical properties and geometric accuracy of selective laser sintered components. The research questions of this thesis were answered by mapping the research activities to the research questions, where the testing of the hypotheses was accomplished mainly by physical experimentation. Those questions and hypotheses and the methods described for testing these hypotheses are explained as follows:

**Testing of hypothesis 1:** The background information for this was presented in section 2.3 of chapter 3. This task was executed by mixing PA 12 and glass bead powders in different weight percentages. This combination was chosen as a model composite since it showed a number of experimental advantages.

**Testing of hypothesis 1.1:** Interfacial adhesion is a decisive factor in determining the properties of composites. Appropriate adjustment of interphase properties and adhesion strength is a very important condition for achieving acceptable properties. This issue was experimentally examined in chapters 4 by mechanical testing of sintered parts in PA12/CP00 system (uncoated) and PA12/CP03 system (coated).

**Testing of hypothesis 2:** In chapter 5, the experiments performed to test the geometric accuracy of the selective laser sintered parts were established with DOE using the process parameters and material properties that expected to have some influence on

curling. Curling was measured by building a number of test bars. Data were collected and statistically analysed for factors influence using S/N ratio, main effects and ANOVA technique.

**Testing of hypothesis 2.1:** chapter 5 has documented this issue. The investigation shows that, beside the processing parameters, it is possible to reduce the shrinkage and hence, the amount of curling by adding glass beads to polyamide 12.

## **6.2. Suggestions for Future Work**

Some of the new directions that future research can take are as follows:

### **Materials**

This work investigated the effect of composite material properties and processing parameters on mechanical properties and geometric accuracy. The preliminary investigation of the composite system has shown promising results. The present investigation could be expanded to explore:

- other fillers such as wollastonite, talc, mica and kaolin
- different particle sizes and shapes
- interface adhesion using other modifiers such as stearic and titanate coupling agents

### **Experiments**

There are several interesting aspects of this research that can be pursued further, among the following:

- conducting experiments on the current material composite with other SLS machines in order to compare the results and determine whether or not the achieved improvements are common

- conducting experiments with other geometries, various sizes, different positions and locations to widen the knowledge base of SLS geometric accuracy, particularly warping and curling phenomena

### **Machines and equipment**

Automation in rapid manufacturing techniques is still an open area to researchers. A selective laser sintering machine working in production may need an automated process for mixing, cleaning and re-feeding unused material. Integration and combination of SLS machines with conventional machine tools (industrial robots, manipulators, fixtures from a flexible system for handling of parts, removal of waste material, removal of the part from the machine and parts finishing) is one of challenges facing researchers, engineers and designers alike.

Additionally, the development of a versatile laboratory-scale SLS machine which can be employed to produce standard testing samples before using powdered material in main production could be beneficial for accurately and quickly predicting the mechanical properties and accuracy of SLS processes.

Continuation of this experimental work by other researchers will be beneficial for materials development and accuracy characterisation in rapid manufacturing techniques. The experimental techniques are readily transferable to virtually any material system used in rapid manufacturing.

## 7. Appendix

### 1- Polyamide 12 (PA 12, PA 2200)<sup>(\*)</sup>

#### PrimePart

PA12 EOS GmbH - Electro Optical Systems

#### Product Texts

PrimePart, a whitish polyamide 12 powder, is due to its reduced material usage an economical alternative for PA 2200.

Apart from that PrimePart and PA 2200 have identical material properties.

Laser-sintered parts made from PrimePart possess excellent material properties:

- high strength and stiffness
- good chemical resistance
- excellent long-term constant behaviour
- high selectivity and detail resolution
- various finishing possibilities (e.g. metallisation, stove enamelling, vibratory grinding, tub colouring, bonding, powder coating, flocking)
- bio compatible according to USP/level VI/121 °C
- suitable for food contact in compliance with the EU Plastics Directive 2002/72/EC (exception: high alcoholic foodstuff) Typical applications of the material are fully functional, economic plastic parts of highest quality.

Due to the excellent mechanical properties the material is often used to substitute typical injection moulding plastics. The biocompatibility allows its use e.g. for prostheses, the high abrasion resistance allows e.g. the realisation of movable part connections.

#### Mechanical properties Value Unit Test Standard

Mechanical properties	Value	Unit	Test Standard
Flexural Modulus, 23°C	1500	MPa	ISO 178
Flexural Strength	58	MPa	ISO 178
Izod Impact notched, 23°C	4.4	kJ/m <sup>2</sup>	ISO 180/1A
Shore D hardness (15s)	75	-	ISO 868 ISO 868
Ball indentation hardness	78	MPa	ISO 2039-1

#### 3D Data Value Unit Test Standard

3D Data	Value	Unit	Test Standard
The properties of parts manufactured using additive manufacturing technology (e.g. laser sintering, stereolithography, Fused Deposition Modelling, 3D printing) are, due to their layer-by-layer production, to some extent direction dependent. This has to be considered when designing the part and defining the build orientation.			
Tensile Modulus (X Direction)	1700	MPa	ISO 527-1/-2
Tensile Modulus (Y Direction)	1700	MPa	ISO 527-1/-2
Tensile Strength (X Direction)	50	MPa	ISO 527-1/-2
Tensile Strength (Y Direction)	50	MPa	ISO 527-1/-2
Strain at Break (X Direction)	24	%	ISO 527-1/-2
Charpy impact strength (+23°C, X Direction)	53	kJ/m <sup>2</sup>	ISO 179/1eU
Charpy notched impact strength (+23°C, X Direction)	4.8	kJ/m <sup>2</sup>	ISO 179/1eA

#### Thermal properties Value Unit Test Standard

Thermal properties	Value	Unit	Test Standard
Melting temperature (10°C/min)	176	°C	ISO 11357-1/-3
Vicat softening temperature (50°C/h 50N)	163	°C	ISO 306

#### Other properties Value Unit Test Standard

Other properties	Value	Unit	Test Standard
Density (lasersintered)	930	kg/m <sup>3</sup>	EOS Method

#### Characteristics

Processing	Delivery form	Chemical Resistance	Ecological valuation
Laser Sintering	White	General Chemical Resistance	US Pharmacopeia Class VI Approved

<sup>(\*)</sup> Last change: 2010-10-15 Source: www.materialdatacenter.com Page: 1/1

The data correspond to our knowledge and experience at the time of publication. They do not on their own represent a sufficient basis for any part design, neither do they provide any agreement about or guarantee the specific properties of a product or part or the suitability of a product or part for a specific application. It is the responsibility of the producer or customer of a part to check its properties as well as its suitability for a particular purpose. This also applies regarding the consideration of possible intellectual property rights as well as laws and regulations. The data are subject to change without notice as part of EOS' continuous development and improvement processes.

## PA 2200 Balance 1.0<sup>(\*)</sup>

PA12 EOS GmbH - Electro Optical Systems

### Product Information

This whitish fine powder PA 2200 on the basis of polyamide 12 serves with its very well-balanced property profile a wide variety of applications.

Laser-sintered parts made from PA 2200 possess excellent material properties:

- high strength and stiffness
- good chemical resistance
- excellent long-term constant behaviour
- high selectivity and detail resolution
- various finishing possibilities (e.g. metallisation, stove enamelling, vibratory grinding, tub colouring, bonding, powder coating, flocking)
- bio compatible according to EN ISO 10993-1 and USP/level VI/121 °C
- approved for food contact in compliance with the EU Plastics Directive 2002/72/EC (exception: high alcoholic foodstuff)

Typical applications of the material are fully functional plastic parts of highest quality. Due to the excellent mechanical properties the material is often used to substitute typical injection moulding plastics. The biocompatibility allows its use e.g. for prostheses, the high abrasion resistance allows e.g. the realisation of movable part connections.

120µm layer thickness

The advantage of the Balance parameter set is equilibrium. The layer thickness of 120µm offers a perfect balance between production costs, mechanical properties, surface quality and accuracy. It is therefore suitable for parts with varying geometries, dimensions and requirements.

<b>Mechanical properties</b>	<b>Value</b>	<b>Unit</b>	<b>Test Standard</b>
Flexural Modulus, 23°C	1500	MPa	ISO 178
Izod Impact notched, 23°C	4.4	kJ/m <sup>2</sup>	ISO 180/1A
Shore D hardness (15s)	75	-	ISO 868 ISO 868

<b>3D Data</b>	<b>Value</b>	<b>Unit</b>	<b>Test Standard</b>
The properties of parts manufactured using additive manufacturing technology (e.g. laser sintering, stereolithography, Fused Deposition Modelling, 3D printing) are, due to their layer-by-layer production, to some extent direction dependent. This has to be considered when designing the part and defining the build orientation.			

Tensile Modulus (X Direction)	1750	MPa	ISO 527-1/-2
Tensile Modulus (Y Direction)	1750	MPa	ISO 527-1/-2
Tensile Modulus (Z Direction)	1750	MPa	ISO 527-1/-2
Tensile Strength (X Direction)	48	MPa	ISO 527-1/-2
Tensile Strength (Y Direction)	48	MPa	ISO 527-1/-2
Tensile Strength (Z Direction)	42	MPa	ISO 527-1/-2
Strain at Break (X Direction)	18	%	ISO 527-1/-2
Strain at Break (Y Direction)	18	%	ISO 527-1/-2
Strain at Break (Z Direction)	4	%	ISO 527-1/-2
Charpy impact strength (+23°C, X Direction)	53	kJ/m <sup>2</sup>	ISO 179/1eU
Charpy notched impact strength (+23°C, X Direction)	4.8	kJ/m <sup>2</sup>	ISO 179/1eA

<b>Thermal properties</b>	<b>Value</b>	<b>Unit</b>	<b>Test Standard</b>
Melting temperature (10°C/min)	176	°C	ISO 11357-1/-3
Vicat softening temperature (50°C/h 50N)	163	°C	ISO 306

<b>Other properties</b>	<b>Value</b>	<b>Unit</b>	<b>Test Standard</b>
Density (lasersintered)	930	kg/m <sup>3</sup>	EOS Method

<b>Characteristics</b>			
<b>Processing</b>	<b>Delivery form</b>	<b>Chemical Resistance</b>	<b>Ecological valuation</b>
Laser Sintering	White	General Chemical Resistance	US Pharmacopeia Class VI Approved

<sup>(\*)</sup> Last change: 2010-03-21 Source: www.materialdatacenter.com

The data correspond to our knowledge and experience at the time of publication. They do not on their own represent a sufficient basis for any part design, neither do they provide any agreement about or guarantee the specific properties of a product or part or the suitability of a product or part for a specific application. It is the responsibility of the producer or customer of a part to check its properties as well as its suitability for a particular purpose. This also applies regarding the consideration of possible intellectual property rights as well as laws and regulations. The data are subject to change without notice as part of EOS' continuous development and improvement processes.

## PA 2200 Performance 1.0<sup>(\*)</sup>

PA12 EOS GmbH - Electro Optical Systems

### Product Information

This whitish fine powder PA 2200 on the basis of polyamide 12 serves with its very well-balanced property profile a wide variety of applications.

Laser-sintered parts made from PA 2200 possess excellent material properties:

- high strength and stiffness
- good chemical resistance
- excellent long-term constant behaviour
- high selectivity and detail resolution
- various finishing possibilities (e.g. metallisation, stove enamelling, vibratory grinding, tub colouring, bonding, powder coating, flocking)
- bio compatible according to EN ISO 10993-1 and USP/level VI/121 °C
- approved for food contact in compliance with the EU Plastics Directive 2002/72/EC (exception: high alcoholic foodstuff)

Typical applications of the material are fully functional plastic parts of highest quality. Due to the excellent mechanical properties the material is often used to substitute typical injection moulding plastics. The biocompatibility allows its use e.g. for prostheses, the high abrasion resistance allows e.g. the realisation of movable part connections.

100µm layer thickness

Performance is the parameter set of choice for parts with high demands on mechanical properties and fracture behaviour, especially when the part is going to be subjected to multiaxial loading in all three directions. Performance parts are characterized by the highest degree of isotropic strength and rigidity. The choice of 100µm layer thickness results in fine resolution and also very high surface quality and detail resolution.

<b>Mechanical properties</b>	<b>Value</b>	<b>Unit</b>	<b>Test Standard</b>
Flexural Modulus, 23°C	1500	MPa	ISO 178
Izod Impact notched, 23°C	4.4	kJ/m <sup>2</sup>	ISO 180/1A
Shore D hardness (15s)	75	-	ISO 868 ISO 868

<b>3D Data</b>	<b>Value</b>	<b>Unit</b>	<b>Test Standard</b>
The properties of parts manufactured using additive manufacturing technology (e.g. laser sintering, stereolithography, Fused Deposition Modelling, 3D printing) are, due to their layer-by-layer production, to some extent direction dependent. This has to be considered when designing the part and defining the build orientation.			

Tensile Modulus (X Direction)	1800	MPa	ISO 527-1/-2
Tensile Modulus (Y Direction)	1800	MPa	ISO 527-1/-2
Tensile Modulus (Z Direction)	1800	MPa	ISO 527-1/-2
Tensile Strength (X Direction)	50	MPa	ISO 527-1/-2
Tensile Strength (Y Direction)	50	MPa	ISO 527-1/-2
Tensile Strength (Z Direction)	50	MPa	ISO 527-1/-2
Strain at Break (X Direction)	20	%	ISO 527-1/-2
Strain at Break (Y Direction)	20	%	ISO 527-1/-2
Strain at Break (Z Direction)	10	%	ISO 527-1/-2
Charpy impact strength (+23°C, X Direction)	53	kJ/m <sup>2</sup>	ISO 179/1eU
Charpy notched impact strength (+23°C, X Direction)	4.8	kJ/m <sup>2</sup>	ISO 179/1eA

<b>Thermal properties</b>	<b>Value</b>	<b>Unit</b>	<b>Test Standard</b>
Melting temperature (10°C/min)	176	°C	ISO 11357-1/-3
Vicat softening temperature (50°C/h 50N)	163	°C	ISO 306

<b>Other properties</b>	<b>Value</b>	<b>Unit</b>	<b>Test Standard</b>
Density (lasersintered)	930	kg/m <sup>3</sup>	EOS Method

<b>Characteristics</b>			
<b>Processing</b>	<b>Delivery form</b>	<b>Chemical Resistance</b>	<b>Ecological valuation</b>
Laser Sintering	White	General Chemical Resistance	US Pharmacopeia Class VI Approved

<sup>(\*)</sup> Created: 2011-02-23 Source: [www.materialdatacenter.com](http://www.materialdatacenter.com)

The data correspond to our knowledge and experience at the time of publication. They do not on their own represent a sufficient basis for any part design, neither do they provide any agreement about or guarantee the specific properties of a product or part or the suitability of a product or part for a specific application. It is the responsibility of the producer or customer of a part to check its properties as well as its suitability for a particular purpose. This also applies regarding the consideration of possible intellectual property rights as well as laws and regulations. The data are subject to change without notice as part of EOS' continuous development and improvement processes.

## PA 2200 Speed 1.0<sup>(\*)</sup>

PA12 EOS GmbH - Electro Optical Systems

### Product Information

This whitish fine powder PA 2200 on the basis of polyamide 12 serves with its very well-balanced property profile a wide variety of applications.

Laser-sintered parts made from PA 2200 possess excellent material properties:

- high strength and stiffness
- good chemical resistance
- excellent long-term constant behaviour
- high selectivity and detail resolution
- various finishing possibilities (e.g. metallisation, stove enamelling, vibratory grinding, tub colouring, bonding, powder coating, flocking)
- bio compatible according to EN ISO 10993-1 and USP/level VI/121 °C
- approved for food contact in compliance with the EU Plastics Directive 2002/72/EC (exception: high alcoholic foodstuff)

Typical applications of the material are fully functional plastic parts of highest quality. Due to the excellent mechanical properties the material is often used to substitute typical injection moulding plastics. The biocompatibility allows its use e.g. for prostheses, the high abrasion resistance allows e.g. the realisation of movable part connections.

150µm layer thickness

The Speed parameter set applies the classic 150µm layer thickness which is popular and widespread on the market due to its allround qualities. This parameter set offers slightly higher surface quality than Top Speed.

Mechanical properties	Value	Unit	Test Standard
Flexural Modulus, 23°C	1500	MPa	ISO 178
Izod Impact notched, 23°C	4,4	kJ/m <sup>2</sup>	ISO 180/1A
Shore D hardness (15s)	75	-	ISO 868 ISO 868

3D Data	Value	Unit	Test Standard
The properties of parts manufactured using additive manufacturing technology (e.g. laser sintering, stereolithography, Fused Deposition Modelling, 3D printing) are, due to their layer-by-layer production, to some extent direction dependent. This has to be considered when designing the part and defining the build orientation.			

Tensile Modulus (X Direction)	1700	MPa	ISO 527-1/-2
Tensile Modulus (Y Direction)	1700	MPa	ISO 527-1/-2
Tensile Modulus (Z Direction)	1650	MPa	ISO 527-1/-2
Tensile Strength (X Direction)	48	MPa	ISO 527-1/-2
Tensile Strength (Y Direction)	48	MPa	ISO 527-1/-2
Tensile Strength (Z Direction)	42	MPa	ISO 527-1/-2
Strain at Break (X Direction)	18	%	ISO 527-1/-2
Strain at Break (Y Direction)	18	%	ISO 527-1/-2
Strain at Break (Z Direction)	4	%	ISO 527-1/-2
Charpy impact strength (+23°C, X Direction)	53	kJ/m <sup>2</sup>	ISO 179/1eU
Charpy notched impact strength (+23°C, X Direction)	4,8	kJ/m <sup>2</sup>	ISO 179/1eA

Thermal properties	Value	Unit	Test Standard
Melting temperature (10°C/min)	176	°C	ISO 11357-1/-3
Vicat softening temperature (50°C/h 50N)	163	°C	ISO 306

Other properties	Value	Unit	Test Standard
Density (lasersintered)	930	kg/m <sup>3</sup>	EOS Method

Characteristics			
Processing	Delivery form	Chemical Resistance	Ecological valuation
Laser Sintering	White	General Chemical Resistance	US Pharmacopeia Class VI Approved

(\*) Created: 2011-02-23 Source: [www.materialdatacenter.com](http://www.materialdatacenter.com)

The data correspond to our knowledge and experience at the time of publication. They do not on their own represent a sufficient basis for any part design, neither do they provide any agreement about or guarantee the specific properties of a product or part or the suitability of a product or part for a specific application. It is the responsibility of the producer or customer of a part to check its properties as well as its suitability for a particular purpose. This also applies regarding the consideration of possible intellectual property rights as well as laws and regulations. The data are subject to change without notice as part of EOS' continuous development and improvement processes.

## PA 2200 Top Quality 1.0<sup>(\*)</sup>

PA12 EOS GmbH - Electro Optical Systems

### Product Information

This whitish fine powder PA 2200 on the basis of polyamide 12 serves with its very well-balanced property profile a wide variety of applications.

Laser-sintered parts made from PA 2200 possess excellent material properties:

- high strength and stiffness
- good chemical resistance
- excellent long-term constant behaviour
- high selectivity and detail resolution
- various finishing possibilities (e.g. metallisation, stove enamelling, vibratory grinding, tub colouring, bonding, powder coating, flocking)
- bio compatible according to EN ISO 10993-1 and USP/level VI/121 °C
- approved for food contact in compliance with the EU Plastics Directive 2002/72/EC (exception: high alcoholic foodstuff)

Typical applications of the material are fully functional plastic parts of highest quality. Due to the excellent mechanical properties the material is often used to substitute typical injection moulding plastics. The biocompatibility allows its use e.g. for prostheses, the high abrasion resistance allows e.g. the realisation of movable part connections.

60µm layer thickness

The parameter set TopQuality is used for very small to medium-sized parts with extremely fine, fragile geometries and geometric elements and the strictest requirements in surface quality are best served by this parameter set. It applies a layer thickness of 60µm, which is approximately the thickness of a grain of the plastic powder normally used today. The typical stair-step effect on upward and downward-pointing geometry elements can practically no longer be seen on TopQuality parts. The mechanical attributes of TopQuality parts are satisfyingly close to the levels of Performance parts.

Mechanical properties	Value	Unit	Test Standard
Flexural Modulus, 23°C	1500	MPa	ISO 178
Izod Impact notched, 23°C	4.4	kJ/m <sup>2</sup>	ISO 180/1A
Shore D hardness (15s)	75	-	ISO 868 ISO 868

3D Data	Value	Unit	Test Standard
The properties of parts manufactured using additive manufacturing technology (e.g. laser sintering, stereolithography, Fused Deposition Modelling, 3D printing) are, due to their layer-by-layer production, to some extent direction dependent. This has to be considered when designing the part and defining the build orientation.			

Tensile Modulus (X Direction)	1900	MPa	ISO 527-1/-2
Tensile Modulus (Y Direction)	1900	MPa	ISO 527-1/-2
Tensile Modulus (Z Direction)	1850	MPa	ISO 527-1/-2
Tensile Strength (X Direction)	52	MPa	ISO 527-1/-2
Tensile Strength (Y Direction)	52	MPa	ISO 527-1/-2
Tensile Strength (Z Direction)	52	MPa	ISO 527-1/-2
Strain at Break (X Direction)	20	%	ISO 527-1/-2
Strain at Break (Y Direction)	20	%	ISO 527-1/-2
Strain at Break (Z Direction)	7	%	ISO 527-1/-2
Charpy impact strength (+23°C, X Direction)	53	kJ/m <sup>2</sup>	ISO 179/1eU
Charpy notched impact strength (+23°C, X Direction)	4.8	kJ/m <sup>2</sup>	ISO 179/1eA

Thermal properties	Value	Unit	Test Standard
Melting temperature (10°C/min)	176	°C	ISO 11357-1/-3
Vicat softening temperature (50°C/h 50N)	163	°C	ISO 306

Other properties	Value	Unit	Test Standard
Density (lasersintered)	930	kg/m <sup>3</sup>	EOS Method

Characteristics			
Processing	Delivery form	Chemical Resistance	Ecological valuation
Laser Sintering	White	General Chemical Resistance	US Pharmacopeia Class VI Approved

(\*) Created: 2011-02-23 Source: [www.materialdatacenter.com](http://www.materialdatacenter.com)

The data correspond to our knowledge and experience at the time of publication. They do not on their own represent a sufficient basis for any part design, neither do they provide any agreement about or guarantee the specific properties of a product or part or the suitability of a product or part for a specific application. It is the responsibility of the producer or customer of a part to check its properties as well as its suitability for a particular purpose. This also applies regarding the consideration of possible intellectual property rights as well as laws and regulations. The data are subject to change without notice as part of EOS' continuous development and improvement processes.

## PA 2200 Top Speed 1.0<sup>(\*)</sup>

PA12 EOS GmbH - Electro Optical Systems

### Product Information

This whitish fine powder PA 2200 on the basis of polyamide 12 serves with its very well-balanced property profile a wide variety of applications.

Laser-sintered parts made from PA 2200 possess excellent material properties:

- high strength and stiffness
- good chemical resistance
- excellent long-term constant behaviour
- high selectivity and detail resolution
- various finishing possibilities (e.g. metallisation, stove enamelling, vibratory grinding, tub colouring, bonding, powder coating, flocking)
- bio compatible according to EN ISO 10993-1 and USP/level VI/121 °C
- approved for food contact in compliance with the EU Plastics Directive 2002/72/EC (exception: high alcoholic foodstuff)

Typical applications of the material are fully functional plastic parts of highest quality. Due to the excellent mechanical properties the material is often used to substitute typical injection moulding plastics. The biocompatibility allows its use e.g. for prostheses, the high abrasion resistance allows e.g. the realisation of movable part connections.

180µm layer thickness

TopSpeed is a very economical parameter set for parts with medium to high requirements of quality and mechanical load and high cost pressure. Particularly large and relatively thick-walled parts can usually profit from this layer thickness, mostly without any noticeable impairment from the fast build-up rates.

Mechanical properties	Value	Unit	Test Standard
Flexural Modulus, 23°C	1500	MPa	ISO 178
Izod Impact notched, 23°C	4.4	kJ/m <sup>2</sup>	ISO 180/1A
Shore D hardness (15s)	75	-	ISO 868 ISO 868

3D Data	Value	Unit	Test Standard
---------	-------	------	---------------

The properties of parts manufactured using additive manufacturing technology (e.g. laser sintering, stereolithography, Fused Deposition Modelling, 3D printing) are, due to their layer-by-layer production, to some extent direction dependent. This has to be considered when designing the part and defining the build orientation.

Tensile Modulus (X Direction)	1600	MPa	ISO 527-1/-2
Tensile Modulus (Y Direction)	1600	MPa	ISO 527-1/-2
Tensile Modulus (Z Direction)	1600	MPa	ISO 527-1/-2
Tensile Strength (X Direction)	45	MPa	ISO 527-1/-2
Tensile Strength (Y Direction)	45	MPa	ISO 527-1/-2
Tensile Strength (Z Direction)	38	MPa	ISO 527-1/-2
Strain at Break (X Direction)	18	%	ISO 527-1/-2
Strain at Break (Y Direction)	18	%	ISO 527-1/-2
Strain at Break (Z Direction)	3	%	ISO 527-1/-2
Charpy impact strength (+23°C, X Direction)	53	kJ/m <sup>2</sup>	ISO 179/1eU
Charpy notched impact strength (+23°C, X Direction)	4.8	kJ/m <sup>2</sup>	ISO 179/1eA

Thermal properties	Value	Unit	Test Standard
Melting temperature (10°C/min)	176	°C	ISO 11357-1/-3
Vicat softening temperature (50°C/h 50N)	163	°C	ISO 306

Other properties	Value	Unit	Test Standard
Density (laser-sintered)	930	kg/m <sup>3</sup>	EOS Method

Characteristics			
Processing	Delivery form	Chemical Resistance	Ecological valuation
Laser Sintering	White	General Chemical Resistance	US Pharmacopeia Class VI Approved

(\*) Created: 2011-02-23 Source: [www.materialdatacenter.com](http://www.materialdatacenter.com)

The data correspond to our knowledge and experience at the time of publication. They do not on their own represent a sufficient basis for any part design, neither do they provide any agreement about or guarantee the specific properties of a product or part or the suitability of a product or part for a specific application. It is the responsibility of the producer or customer of a part to check its properties as well as its suitability for a particular purpose. This also applies regarding the consideration of possible intellectual property rights as well as laws and regulations. The data are subject to change without notice as part of EOS' continuous development and improvement processes.

## PA 3200 GF<sup>(\*)</sup>

PA12-GB EOS GmbH - Electro Optical Systems

### Product Information

PA 3200 GF is a whitish, glass-filled polyamide 12 powder, which is characterised by an excellent stiffness in combination with good elongation at break.

Laser-sintered parts made from PA 3200 GF possess excellent material properties:

- high stiffness
- high mechanical wear-resistance
- good thermal loadability
- excellent surface quality
- high dimensional accuracy and detail resolution
- good processability
- excellent long-term constant behaviour

A typical application for PA 3200 GF is the usage e.g. for final parts within the engine area of cars, for deep-drawing dies or any other application which requires particular stiffness, high heat distortion temperature and low abrasive wear.

Mechanical properties	Value	Unit	Test Standard
Flexural Modulus, 23°C	2900	MPa	ISO 178
Flexural Strength	73	MPa	ISO 178
Izod Impact notched, 23°C	4.2	kJ/m <sup>2</sup>	ISO 180/1A
Shore D hardness (15s)	80	-	ISO 868 ISO 868
Ball indentation hardness	98	MPa	ISO 2039-1

3D Data	Value	Unit	Test Standard
The properties of parts manufactured using additive manufacturing technology (e.g. laser sintering, stereolithography, Fused Deposition Modelling, 3D printing) are, due to their layer-by-layer production, to some extent direction dependent. This has to be considered when designing the part and defining the build orientation.			

Tensile Modulus (X Direction)	3200	MPa	ISO 527-1/-2
Tensile Modulus (Y Direction)	3200	MPa	ISO 527-1/-2
Tensile Modulus (Z Direction)	2500	MPa	ISO 527-1/-2
Tensile Strength (X Direction)	51	MPa	ISO 527-1/-2
Tensile Strength (Y Direction)	51	MPa	ISO 527-1/-2
Tensile Strength (Z Direction)	47	MPa	ISO 527-1/-2
Strain at Break (X Direction)	9	%	ISO 527-1/-2
Charpy impact strength (+23°C, X Direction)	35	kJ/m <sup>2</sup>	ISO 179/1eU
Charpy notched impact strength (+23°C, X Direction)	5.4	kJ/m <sup>2</sup>	ISO 179/1eA

Thermal properties	Value	Unit	Test Standard
Melting temperature (10°C/min)	176	°C	ISO 11357-1/-3
Vicat softening temperature (50°C/h 50N)	166	°C	ISO 306

Other properties	Value	Unit	Test Standard
Density (lasersintered)	1220	kg/m <sup>3</sup>	EOS Method

Characteristics		
Processing	Delivery form	Features
Laser Sintering	White	Low Coefficient of Friction

(\*) Created: 2011-02-21 Source: [www.materialdatacenter.com](http://www.materialdatacenter.com)

The data correspond to our knowledge and experience at the time of publication. They do not on their own represent a sufficient basis for any part design, neither do they provide any agreement about or guarantee the specific properties of a product or part or the suitability of a product or part for a specific application. It is the responsibility of the producer or customer of a part to check its properties as well as its suitability for a particular purpose. This also applies regarding the consideration of possible intellectual property rights as well as laws and regulations. The data are subject to change without notice as part of EOS' continuous development and improvement processes.

## 2. Glass beads

### SPHERIGLASS® Solid Glass Spheres: A Glass

Potters A glass spheres are manufactured from a soda lime glass composition, like window glass. The refractive index of A-glass is 1.51 - 1.52.

SPHERIGLASS® solid A glass spheres are available in mean particle sizes from 7 to 200 microns. The 3000 and 4000 grade products, with a typical mean particle size of 35-25 microns, are the product most commonly used for resin extension in polymer applications. The 5000 and 6000 grade products are most commonly used in paints and coatings.

In general, smaller spheres improve impact strength. Larger spheres tend to improve flow properties.

Typical Particle Size	
Product Grade	Mean Value
1922	203
2024	156
2227	119
2429	85
2530	71
2900	42
3000	35
4000	25
5000	11
6000	7

### 3. Coupling Agents Coatings

#### High performance Glass Microspheres coatings for increased adherences in Thermoplastic and Thermoset applications.

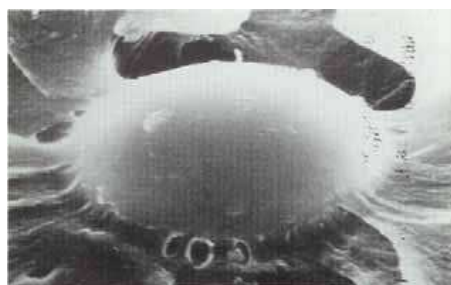
Spheriglass® solid glass microspheres are extensively used in most thermoplastic and thermosetting resin systems as an inorganic functional filler and reinforcement. When the microspheres are used, processability and resin composite performances are enhanced, while overall manufacturing costs are reduced.

#### Coatings

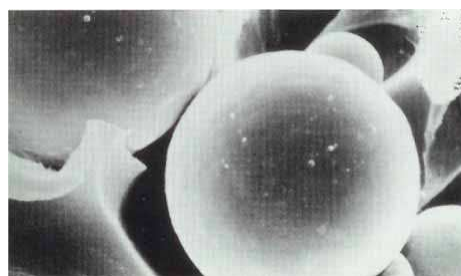
Interfacial Bonding, between the glass beads and the polymer can be enhanced by the use of a coupling agent (coating). These agents are being applied to the microspheres during manufacture, in molecular layers to obtain maximum adhesion. This improved bonding manifests itself in improved properties of the moulded section. Accordingly, elastic modulus and strength are significantly improved. Surface treatment has also been shown to improve melt viscosity, most likely due to improved wetting.

#### Benefits of using Spheriglass® with coupling agents

- o Lowers viscosity of filled resins
- o Increase overall reinforcement loading capacity
- o Reduces processing equipment wear and energy usage
- o Provides excellent flow-out in intricate and thin wall designed moulds
- o Provides final product with improved hardness, dimensional stability, surface finish and machinability
- o Improve composite properties by improving dispersion of other fillers and additives



Coated



Uncoated

The effect of the coupling agent on the interfacial bond can be seen by the contrasting figures above. In the figure on the right, one can see the pulling away of a polymer from an uncoated microsphere as the test specimen is stretched. In the figure on the left, resin is strongly adhered to the microsphere and no separation between the resin and the microsphere is discernible.

#### Coupling Agents Improve properties of resins filled with Spheriglass® glass microspheres

Polyamide 6				
Properties	Unit	Unfilled	Spheriglass® 3000 (30% by wt.)	
No Coupling Agent		CP03		
Tensile Strength	MPa	47.3	32.0	50.8
Tensile Elongation	%	66.7	23.6	30.3
Izod Notched	KJ/m <sup>2</sup>	7.0	3.2	4.9
Izod Un-Notched	KJ/m <sup>2</sup>	61.2	36.6	25.4
Flexural Modulus	KJ/m	1712	2152	2686
Flexural Strength	MPa	69.8	70.1	89.2
HDT	Mpa	51.4	67.6	60.0
Mould Shrinkage	°C	□1.5	1.3	1.2
	%			

Spherglass microspheres are available with coatings of three different coupling agents – CP01, CP02 and CP03; all are formulated for optimum performance within specific resin systems. In certain resin systems, such as fluorocarbons and silicones, coupling agent are less effective. Consult the charts below for recommended usage.

#### Recommended Coupling Agents For Use With Spherglass®

FOR USE IN THERMOPLASTIC RESIN SYSTEMS			
Resin Type	Coating	Resin Type	Coating
Acrylics	CP01	Polyethylene	CP01
Acetal	CP02 - CP03	Polyimide	CP03
ABS	CP01	Polymethyl Methacrylate	CP01
Cellulostics	CP02 – CP03	Polyphenylene Oxide	CP03
Fluoroplastics	None Recommended	Polypropylene	CP03
Ionomer	CP02 – CP03	Polystyrene	CP01
PBT / PET	CP02 – CP03	Polysulfone	CP03
Polyamide	CP03	Polyvinyl Chloride (PVC)	CP03
Polycarbonate	CP02 - CP03	Styrene Acrylonitrile (SAN)	CP01

FOR USE IN THERMOSETTING RESIN SYSTEMS			
Resin Type	Coating	Resin Type	Coating
Alkyd	CP01	Polyester	CP01
Epoxy	CP02 - CP03	Silicones	CP01
Melamine	CP02 - CP03	Urea-Formaldehyde	CP03
Phenol-Formaldehyde	CP03	Urethanes	CP03
Phenolic	CP03	Vinyl Ester	CP01

#### Spherglass® microspheres benefits

Spherglass® solid glass microspheres are available in sizes ranging from 5 to 250 microns in diameter. In addition to the benefits outlined earlier, Spherglass® offers:

- Solid smooth transparent shape Non flammability
- Lowest surface-to-volume ratio Uniform dispersion
- High Abrasion resistance Low uniform shrinkage
- High compressive strength High Flexure modulus

#### Other products

- Luxsil® Cosmetic Microspheres
- SpheriWhite® Colour-Enhancing Solid Glass Microspheres
- Q-Cel® Ultra-Light Hollow Glass Microspheres
- SpheriCel® Ultra-Fine Weight Reducing Hollow Glass Microspheres
- GlassFill® Ultra-Fine Powdered Glass

#### Safety Information

Glass composition and coatings used with Potters Europe microspheres are non-toxic and present no hazard with regard to ingestion, inhalation or contact. Material Safety Data Sheets are available upon request.

Information contained in this publication (and otherwise supplied to users) is based on our general experience and is given in good faith, but we are unable to accept the responsibility in respect of factors which are outside our knowledge or control. Spherglass, SpheriWhite, Luxsil, Q-Cel, SpheriCel, GlassFill are registered trademarks of Potters Industries Inc. and affiliated companies. Ref: 3-03-007-1-09.doc

## 8. References

- [1] E. C. Santos, M. Shiomi, K. Osakada and T. Laoui (2006): *Rapid manufacturing of metal components by laser forming*. Int. J. of Machine Tools and Manufacture 46. 1459–1468
- [2] C. E. Majewski; B. S. Hobbs; N. Hopkinson (2007): *Effect of bed temperature and infra-red lamp power on the mechanical properties of parts produced using high-speed sintering*. Virtual and Physical Prototyping, Vol. 2, Iss. 2, pp 103 – 110. Loughborough University, UK
- [3] A. Rosochowski, A. Matuszak (2000): *Rapid tooling: The state of the art*. Journal of materials processing technology 106, 191- 198
- [4] I. Abd Aziz (2010): *Microstructure and mechanical properties of Ti-6Al-4V produced by selective laser sintering of pre- alloyed powder*. M.Eng. Thesis University of Waikato Hamilton, New Zealand
- [5] D. C. Thomson (1995): *The optimization of part orientation for solid freeform manufacture*. M.Sc. thesis in engineering, faculty of the graduate school of the University of Texas at Austin
- [6] B. E Davis (2001): *Characterization and calibration of stereolithography products and processes*. M.Sc. Thesis, Georgia Institute of Technology

- [7] Ö. İlkün (2005): *Effects of production parameters on porosity and hole properties in laser sintering rapid prototyping process*. M.Sc. thesis in mechanical engineering. Middle East Technical University. Turkey
- [8] S. K. Singhal, P. K. Jain, P. M. Pandey (2008): *Adaptive Slicing for SLS Prototyping*. Computer-Aided Design & Applications, 5(1-4), 412-423. India
- [9] Y. Yan , S. Li, R. Zhang, F. Lin, R. Wu, Q. Lu, Z. Xiong, X. Wang (2009): *Rapid Prototyping and Manufacturing Technology: Principle, Representative Technics, Applications, and Development Trends*. Tsinghua Science & Technology, Volume 14, Pages 1-12, China
- [10] J. P. Schultz (2003) : *Modeling heat transfer and densification during laser sintering of viscoelastic polymers*. PhD dissertation in Materials Science and Engineering. The faculty of the Virginia Polytechnic. Institute and State University. USA
- [11] C. M. Tekin (2009): *Mechanical characterization and modeling of porous polymeric materials manufactured by selective laser sintering*. M.Sc. Thesis in mechanical engineering. Middle East Technical University. Turkey
- [12] D.T Pham, R.S Gault (1998): *A comparison of rapid prototyping technologies*. International Journal of Machine Tools and Manufacture, Vol. 38, Issues 10-11, pp 1257-1287. UK

- [13] B. Wendel, D. Rietzel, F. Kühnlein, R. Feulner, G. Hülner, and E. Schmachtenberg (2008): *Additive Processing of Polymers*. Macromolecular Materials and Engineering. Macromolecular Materials and Engineering, 293:799–809. Germany.
- [14] [http://www.efunda.com/processing/rapid\\_prototyping/](http://www.efunda.com/processing/rapid_prototyping/). [Accessed 3 Feb.2011].
- [15] A. Dolenc (1994): *An overview of rapid prototyping technologies in manufacturing*. Institute of Industrial Automation, Helsinki University of technology
- [16] US 5121329 (1992), inv.: S. Crump.: *Apparatus and method for creating three-dimensional objects*.
- [17] <http://www.mne.psu.edu/lamancusa/rapidpro/primer/chapter2.htm>. [Accessed 3 Feb.2011].
- [18] J. Park, M. J. Tari, H. T. Hahn, (2000): *Characterization of the laminated object manufacturing (LOM) process*. Rapid Prototyping Journal, Vol. 6 Iss: 1, pp.36 – 50. Mechanical and Aerospace Engineering Department, University of California, Los Angeles, USA
- [19] S. Kumar (2010): *Selective laser sintering: Recent advances*. CSIR National Laser Centre, South Africa
- [20] <http://www.lasersintering.com/sls-information.php#sls>. [Accessed 3.Feb .2011]

- [21] P. K. Jain, P. M. Pandeyand, P.V.M. Rao (2008): *Experimental investigations for improving part strength in selective laser sintering*. Virtual and Physical Prototyping. Taylor & Francis. Delhi, India.
- [22] N. Hopkinson, P. Dickens, (2001): *Rapid prototyping for direct manufacture*. Rapid Prototyping Journal, Vol. 7 Iss: 4, pp.197 – 202
- [23] C.E. Majewski, H. Zarringhalam, D. Toon, U. Ajoku, N. Hopkinson, M.P. Caine (2009): *The use of off-line part production to predict the tensile properties of parts produced by Selective Laser Sintering*. Journal of Materials Processing Technology. Vol. 209, Issue 6, Pages 2855-2863. UK
- [24] R.D. Goodridge, M.L. Shofner, R.J.M. Hague, M. McClelland, M.R. Schlea, R.B. Johnson, C.J. Tuck (2010): *Processing of a Polyamide-12/carbon nanofibre composite by laser sintering*. Polymer Testing. Vol. 30, Issue 1, Pages 94-100
- [25] F. Klocke, C. Wagner, C. Ader (2005): *Development of an Integrated Model for Selective Metal Laser Sintering*. Fraunhofer-Institute of Production Technology IPT, Aachen, Germany
- [26] J. D. Williams, C. R. Deckard, (1998): *Advances in modeling the effects of selected parameters on the SLS process*. Rapid Prototyping Journal, Vol. 4 Iss: 2, pp.90 – 100. Clemson University, Clemson, South Carolina , USA

- [27] X.C. Wang & J.P. Kruth (2000): *Energy absorption and penetration in selective laser sintering: A ray tracing model*. Proceedings of the International Conference on Mathematical Modelling and Simulation of Metal Technologies pages:673-682. K. U. Leuven - Department of Mechanical Engineering - Division PMA
- [28] S. Kolossov, E. Boillat, R. Glardon, P. Fischer, M. Locher (2004): *3D FE simulation for temperature evolution in the selective laser sintering process*. Int. J. of Machine and Manufacture. Vol. 44, Issues 2-3, Pages 117-123. University of Bern, Switzerland
- [29] B. Pei-kang, C. Jun, L. Bin and W. Wen-feng (2006): *Numerical simulation of temperature field during selective laser sintering of polymer-coated molybdenum powder*. Transactions of Nonferrous Metals Society of China. Vol. 16, Supplement 2, Pages s603-s607. China
- [30] R. B. Patil, V. Yadava (2007): *Finite element analysis of temperature distribution in single metallic powder layer during metal laser sintering*. Int. J. of Machine Tools and Manufacture. Vol. 47, Issues 7-8, Pages 1069-1080. India
- [31] K.M. Fan, K.W. Wong, W.L. Cheung (2007): *Reflectance and transmittance of TrueForm<sup>TM</sup> powder and its composites to CO<sub>2</sub> laser*. Rapid Prototyping Journal, Vol. 13, Iss: 3, pp.175 – 181

[32] W. N. dos Santos, J. A. M. Agnelli, P. Mummery, A. Wallwork (2007): *Effect of recycling on the thermal properties of polymers*. Polymer Testing. Vol. 26, Issue 2, Pages 216-221

[33] G. B. M.l Cervera, G. Lombera, (1999): *Numerical prediction of temperature and density distributions in selective laser sintering processes*. Rapid Prototyping Journal, Vol. 5 Iss: 1, pp.21 – 26. National University of Mar del Plata, Argentina

[34] S. L. Israel, T. D. Hawkins, and S. C. Hyman (1966): *Thermal properties of solid and porous tungsten at temperature to 5000 F*. National Aeronautics and space administration. Washington, D. C. USA

[35] J. K. Carson, S. J. Lovatt, D. J. Tanner, A. C. Cleland (2005): *Thermal conductivity bounds for isotropic, porous materials*. International Journal of Heat and Mass Transfer. Volume 48, Issue 11, Pages 2150-2158

[36] Y. Zhang, A. Faghri (1999): *Melting of a subcooled mixed powder bed with constant heat flux heating*. International Journal of Heat and Mass Transfer, Volume 42, Number 5, pp. 775-788. USA

[37] D. Tolksdorf, E. Westkämper (2006): *Developments in precision product manufacturing for laser-sintering*. 3ed international Conference Multiscale Materials Modeling, Freiburg , Germany

[38] N. P. Juster, (1994): *Rapid prototyping using the selective sintering process*. Assembly Automation, Vol. 14 Iss: 2, pp.14 – 17. Department of Mechanical Engineering, University of Leeds

[39] D T Pham, S Dimov, F Lacan (1999): *Selective laser sintering: applications and technological capabilities*. Proc IMechE, Part B: Journal of Engineering Manufacture. Volume 213, Number 5, Pages 435-449 / 1999, University of Wales, Cardiff UK

[40] A. Franco (2007): *An apparatus for the routine measurement of thermal conductivity of materials for building application based on a transient hot-wire method*. Applied Thermal Engineering. Vol. 27, Issues 14-15, Pages 2495-2504. Italy

[41] H. Czichos, D. Klaffke, E. Santner, M. Woydt (1995): *Advances in tribology: the materials point of view*. Wear. Vol. 190, Issue 2, Pages 155-161. Berlin, Germany

[42] J.-P. Kruth, M.C. Leu and T. Nakagawa (1998): *Progress in Additive Manufacturing and Rapid Prototyping*. CIRP Annals - Manufacturing Technology. Vol. 47, Issue 2, Pages 525-540

[43] A. V. Gusarov, T. Laoui, L. Froyen, V. I. Titov (2003): *Contact thermal conductivity of a powder bed in selective laser sintering*. International Journal of Heat and Mass Transfer. Vol. 46, Issue 6, Pages 1103-1109

[44] <http://www.3trpd.co.uk/sls.htm>. [Accessed 3. Feb. 2011].

[45] <http://www.eos.info/en/products/materials-for-plastic-system>. [Accessed in 3. Feb. 2011]

[46] <http://www.nwuav.com/materialPDFs/alumide.pdf>. [Accessed in 3.Feb.2011]

[47] <http://www.windform.it/sito/>. [Accessed in 3.Feb.2011]

[48] T. S. Gates (2003): *On the Use of Accelerated Test Methods for Characterization of Advanced Composite Materials*. National Aeronautics and Space Administration. Langley Research Centre, Hampton, Virginia. USA

[49] M. Xanthos (1<sup>st</sup> edition) (2005): *Front Matter, in Functional Fillers for Plastics*, Wiley-VCH Verlag GmbH & Co. KGaA, Weinheim, FRG. USA

[50] W. Shen, C. Y. Tang, C. P. Tsui and L. H. Peng (2002): *Effects of two damage mechanisms on effective elastic properties of particulate composites*. Composites Science and Technology. Volume 62, Issues 10-11, Pages 1397-1406

[51] Alberola, N. D. and Mele, P. (1996): *Viscoelasticity of polymers filled by rigid or soft particles: Theory and experiment*. Polymer Composites, Polymer Composites. Vol. 17, Issue 5, Pages 751–759

[52] Shirin Shokoohi, Ahmad Arefazar (2009): *Silane Coupling Agents in Polymer-based Reinforced Composites*: Journal of Reinforced Plastics and Composites. vol. 28 no. 17 2131-2142. Tehran, Iran

- [53] D. Metin, F. Tihminlioğlu, D. Balköse, S. Ülkü (2004): *The effect of interfacial interactions on the mechanical properties of polypropylene/natural zeolite composites*. Composites Part A: Applied Science and Manufacturing. Volume 35, Issue 1, Pages 23-32. Turkey
- [54] R. K. Y. Li, J. Z. Liang, S. C. Tjong (1998): *Morphology and dynamic mechanical properties of glass beads filled low density polyethylene composites*. Journal of Materials Processing Technology. Volume 79, Issues 1-3, Pages 59-65
- [55] Liang, J.-Z. (2007): *Tensile properties of hollow glass bead- filled polypropylene composites*. Journal of Applied Polymer Science. Vol. 104, Issue 3, Pages 1697-1701, China
- [56] A. Meddad, B. Fisa (1997): *Filler– matrix debonding in glass bead-filled polystyrene*. Journal of Materials Science. Volume 32, Number 5, 1177-1185. Canada
- [57] Shao-Yun Fu, Xi-Qiao Feng, Bernd Lauke, Yiu-Wing Mai (2008): *Effects of particle size, particle/matrix interface adhesion and particle loading on mechanical properties of particulate– polymer composites*. Composites Part B: Engineering. Volume 39, Issue 6, Pages 933-961
- [58] N. D. Alberola, P. Mele (1997): *Interface and mechanical coupling effects in model particulate composites*. Polymer Engineering & Science. Vol. 37, Issue 10, Pages 1712- 1721, France

- [59] B. Caulfield, P.E. McHugh, S. Lohfeld (2007): *Dependence of mechanical properties of polyamide components on build parameters in the SLS process*. Journal of Materials Processing Technology. Vol. 182, Issues 1-3, Pages 477-48, Ireland
- [60] W.A.Y Yusoff, A.J Thomas (2008): *The effect of employing an effective laser sintering scanning strategy and energy density value on eliminating “Orange peel” on a selective laser sintered part*. International Association for Management of Technology IAMOT
- [61] P. K. Jain, P. M. Pandey, P. V. M. Rao (2008): *Effect of delay time on part strength in selective laser sintering*. The International Journal of Advanced Manufacturing Technology. Vol. 43, Issu.1-2, 117-126
- [62] I. Gibson, D. Shi, (1997): *Material properties and fabrication parameters in selective laser sintering process*. Rapid Prototyping Journal, Vol. 3 Iss: 4, pp.129 – 136. The University of Hong Kong
- [63] Y Wang, Y Shi, S Huang (2005): *Selective laser sintering of polyamide-rectorite composite*. Proc. IMechE Vol. 219 Part L: J. Materials: Design and Applications. People's Republic of China
- [64] T J Gill, K K B Hon (2004): *Experimental investigation into the selective laser sintering of silicon carbide polyamide composites*. Proc IMechE, Part B: Journal of Engineering Manufacture, Vol. 218, Issue 10, Pages 1249-1256

[65] K.K.B. Hon, T.J. Gill (2007): *Selective Laser Sintering of SiC/Polyamide Composites*. CIRP Annals - Manufacturing Technology, Vol. 52, Issue 1, P 173-176.

The University of Liverpool

[66] A. Mazzoli, G. Moriconi, M. G. Pauri (2007): *Characterization of an aluminum-filled polyamide powder for applications in selective laser sintering*. Materials & Design. Vol. 28, Issue 3, Pages 993-1000. Italy

[67] U Ajoku, N Saleh, N Hopkinson, R Hague, P Erasenthiran (2006): *Investigating mechanical anisotropy and end-of-vector effect in laser-sintered nylon parts*. Proc. IMechE Vol. 220 Part B: J. Engineering Manufacture. JEM537 © IMechE, UK

[68] G.V. Salmoria, J.L. Leite, R.A. Paggi, A. Lago, A.T.N. Pires (2008): *Selective laser sintering of PA12/HDPE blends: Effect of components on elastic/plastic behaviour*. Polymer Testing. Vol 27, Issue 6, Pages 654-659. Brazil

[69] C Majewski, H Zarringhalam, N Hopkinson (2008): *Effect of the degree of particle melt on mechanical properties in selective laser-sintered Nylon-12 parts*. Proc. IMechE Vol. 222, Issue 9, Part B: J. Engineering Manufacture, Pages 1055-1064

[70] P. K. Jain, P. M. Pandey, P. V. M. Rao (2008): *Effect of delay time on part strength in selective laser sintering*. The International Journal of Advanced Manufacturing Technology. Volume 43, Numbers 1-2, 117-126. India

[71] P. K. Jain, P. M. Pandey, P. Rao (2010): *Selective laser sintering of clay-reinforced polyamide*. Polymer Composites, Vol. 31, Issue 4, pp 732–743. India

[72] J. Yang, Y. Shi, C. Yan (2010): *Selective Laser Sintering of Polyamide 12/Potassium Titanium Whisker Composites*. Journal of Applied Polymer Science, Vol. 117, Issue 4, pp. 2196–2204. China.

[73] N. Raghunath, Pulak M. Pandey (2007): Improving accuracy through shrinkage modelling by using Taguchi method in selective laser sintering. International journal of machine tools & manufacture. ISSN 0890-6955, vol. 47, n6, pp. 985-995. India

[74] K. Senthilkumaran, Pulak M. Pandey, P.V.M. Rao (2009): *Influence of building strategies on the accuracy of parts in selective laser sintering*. Materials & Design. Volume 30, Issue 8, Pages 2946-2954. India

[75] K.W. Dalgarno, T.R.C. Childs, I. Rowntree, L. Rothwell (1996): *Finite Element Analysis of Curl Development in the Selective Laser Sintering Process*. Department of Mechanical Engineering, University of Leeds, Leeds, LS2 9JT, UK

[76] N. M. Jamal, KW Dalgarno: *Analysis of the influence of the viscoelasticity in curl development in SLS*. School of Mechanical Engineering, University of Leeds, Leeds, LS2 9JT, UK

- [77] M. Berzins, T.H.C. Childs, K.W. Dalgarno, G. Ryder and G. Stein (1995): *Densification and distortion in selective laser sintering of polycarbonate parts*. In Solid Freeform Fabrication Symposium 1995, proceedings of the conference held in Austin, Texas, ISSN 1053-2153, pp. 196-203. USA
- [78] H. Chung, S. Das (2006): *Processing and properties of glass bead particulate-filled functionally graded Nylon-11 composites produced by selective laser sintering*. Materials Science and Engineering: A, Volume 437, Issue 2, Pages 226-234
- [79] I. M. Ward, P R Pinnock (1966): *The mechanical properties of solid polymers*. Br. J. Appl. Phys. 17 3
- [80] [www.tciamerica.com/](http://www.tciamerica.com/) [Accessed 5. Feb .2011]
- [81] [www.specialchem4polymers.com/](http://www.specialchem4polymers.com/) [Accessed 5. Feb .2011]
- [82] S. Shokoohi, A. Arefazar (2009): *Effect of Processing Conditions and Coupling Agents on ABS/SGF Composites Properties*. Journal of Reinforced Plastics and Composites, vol. 28 no. 9 1059-1073. Iran
- [83] A. C. Miller and J. C. Berg (2003): *Effect of silane coupling agent adsorbate structure on adhesion performance with a polymeric matrix*. Composites Part A: Applied Science and Manufacturing. Volume 34, Issue 4, Pages 327-332

[84] L. W. Vick, R. G.Kander (1997): *Ambient temperature compaction of polycarbonate powder*. Polymer Engineering & Science, Vol. 37, Issue 1, Pages120–127, USA

[85] B. Weidenfeller, M. Höfer, F. R. Schilling (2004): *Thermal conductivity, thermal diffusivity, and specific heat capacity of particle filled polypropylene*. Composites Part A: Applied Science and Manufacturing. Vol. 35, Issue 4, Pages 423-429

[86] A. E. Tontowi, T.H.C. Childs, (2001): *Density prediction of crystalline polymer sintered parts at various powder bed temperatures*. Rapid Prototyping Journal, Vol. 7 Iss: 3, pp.180 - 184

[87] J.-P. Kruth, G. Levy, R. Schindel, T. Craeghs, E. Yasa: *Consolidation of Polymer Powders by Selective Laser Sintering*. Proceedings of the 3rd International Conference on Polymers and Moulds Innovations pages:15-30

[89] W. A. Yusoff, (2007): *An investigation of the orange peel phenomenon*. PhD. thesis, Cardiff University, Manufacturing Engineering Centre, Cardiff, UK

[90] C. Nelson, K. McAlea, D. Gray (1996): *Improvements in SLS part accuracy*. DTM Corporation. Austin, Texas 78754

[91] R. D. Goodridge, R. J.M. Hague, C. J. Tuck (2010): *An empirical study into laser sintering of ultra-high molecular weight polyethylene (UHMWPE)*. Journal of Materials Processing Technology. Volume 210, Issue 1, Pages 72-80

[92] L. Hao, M.M. Savalani, Y. Zhang, K.E. Tanner and R.A. Harris (2006): *Effects of material morphology and processing conditions on the characteristics of hydroxyapatite and high-density polyethylene biocomposites by selective laser sintering*. Proceedings of the Institution of Mechanical Engineers, Part L: Journal of Materials: Design and Applications, 220 (3), pp. 125-137 E. UK

[93] J. Cheng, S. Lao, K. Nguyen, W. Ho, A. Cummings, and J. Koo (2005): *SLS Processing Studies of Nylon 11 Nanocomposites*. The University of Texas at Austin, Mechanical Engineering Department, University Station 2200, Austin, TX 78712

[94]. Li, X., Shi, Y., Huang, S. Jixie Gongcheng Xuebao (2002): *Investigation on preheating of powder in SLS machine*. Chinese Journal of Mechanical Engineering, China. Vol. 38, no. 3, pp. 94-98

[95] T.J. Gornet, K.R. Davis, Dr. T.L. Starr, K.M. Mulloy (2002): *Characterization of selective laser sintering*. Materials to determine process stability. Rapid Prototyping Center, J.B. Speed Engineering School, University of Louisville. USA

[96] I. Švab, V. Musil, M. Leskovic: *The Adhesion Phenomena in Polypropylene/Wollastonite Composites*. Acta Chim. Slov. 2005, 52, 264–271

[97] K. M.S Gautham (April 2000): *A Design Tool to Control Roughness in Rapid Prototyping*. AutoDes, INC., Novi, MI, Henderson, Mark, Ph.D., Industrial Engineering, Arizona State University, Tempe, AZ

[98] X. Wang, (1999): *Calibration of shrinkage and beam offset in SLS process*. Rapid Prototyping Journal, Vol. 5, Iss. 3, pp.129 – 133. Artificial Intelligence Laboratory, University of Wales, Cardiff, UK

[99] S.S. Dimov, D.T. Pham, K.D. Dotchev, A.I. Ivanov (1999): *Dimensional accuracy of CastForm Polystyrene patterns produced by Selective Laser Sintering*.

Manufacturing Engineering Centre, Cardiff University, Cardiff, United Kingdom

[100] B. Van Hooreweder, F. De Coninck, D. Moens, R. Boonen, P. Sas (2010): *Microstructural characterization of SLS-PA12 specimens under dynamic tension/compression excitation*. Polymer Testing. Volume 29, Issue 3, Pages 319-326

[101] X. Shen, J. Yao, Y. Wang, J. Yang (2004): *Density Prediction of Selective Laser Sintering Parts Based on Artificial Neural Network*. Advances in Neural Networks- ISNN 2004. Lecture Notes in Computer Science, Volume 3174/2004, Pages153-165

[102] A. R. Lockwood (2006): *Toughening mechanisms in composites of miscible polymer blends with rigid filler particles*. PhD. Thesis, Massachusetts Institute of Technology, Dept. of Chemical Engineering, USA

[103] J. G. Lyons, J. E. Kennedy, S. Lordan, L. M. Geever, C. L. Higginbotham: *Characterisation of the effects of a titanium micro particle filler on a polyether-block-amide host matrix*. Journal of Materials Science. Volume 45, Number 12, 18 March 2010, Pages 3204-3214

[104] J. Liang, R. Li, (2000): *Effect of filler content and surface treatment on the tensile properties of glass-bead-filled polypropylene composites*. Polymer International. Vol. 49, Issue 2, Pages 170–174. People's Republic of China

[105] Y. Zhou, V. Rangari, H. Mahfuz, S. Jeelani, P.K. Mallick (2005): *Experimental study on thermal and mechanical behavior of polypropylene, talc/polypropylene and polypropylene/clay nanocomposites*. Materials Science and Engineering: A. Volume 402, Issues 1-2, Pages 109-117

[106] B. S. Yoon, J. Y. Joang, M. H. Suh, Y. M. Lee, S. H. Lee (1997): *Mechanical properties of polypropylene/polyamide 6 blends: Effect of manufacturing processes and compatibilization*. Polymer Composites. Vol. 18, Issue 6, Pages 757–764

[107] I. L. Dubnikova, S. M. Berezina, A. V. Antonov (2004): *Effect of rigid particle size on the toughness of filled polypropylene*. Journal of Applied Polymer Science, Vol. 94, Issue 5, Pages 1917–1926

[108] [http://www.thetestlab.com/pdf/ASTM-D5045\\_Fracture\\_Toughness\\_Testing.pdf](http://www.thetestlab.com/pdf/ASTM-D5045_Fracture_Toughness_Testing.pdf)  
[Accessed 8. Feb. 2011].

[109] B.B. Johnsen, A.J. Kinloch, R.D. Mohammed, A.C. Taylorand, S. Sprenger (2007): *Toughening mechanisms of nanoparticle- modified epoxy polymers*. Polymer: Volume 48, Issue 2, Pages 530-541

[110] J. Wu, Y. -W Mai (1996): *The essential fracture work concept for toughness measurement of ductile polymers*. Polymer Engineering & Science, Vol. 36, Issue 18, Pages 2275–2288

[111] S. M. Zebarjad, S. A. Sajjadi, M. Tahani (2004): *Influence of filler particles on deformation and fracture mechanism of isotactic polypropylene*. Journal of Materials Processing Technology, Volume 155, Issue 127, Pages 1459-1464

[112] R. J. Damani, Ch. Schuster, R. Danzer (1997): *Polished notch modification of SENB-S fracture toughness testing*. Journal of the European Ceramic Society. Volume 17, Issue 14, Pages 1685-1689

[113] J. Lee and A. F. Yee (2000): *Fracture of glass bead/ epoxy composites: on micro-mechanical deformations*. Polymer. Volume 41, Issue 23, Pages 8363-8373

[114] R. Hague; S. Mansour; N. Saleh (2004): *Material and design considerations for rapid manufacturing*. International Journal of Production Research, 1366-588X, Volume 42, Issue 22, Pages 4691 – 4708

[115] W. J. Deng, C. T. Chen, C. H. Sun, W. C. Chen, C. P. Chen (2008): *An Effective Approach for Process Parameter Optimization in Injection Molding of Plastic Housing Components*. Polymer-Plastics Technology and Engineering, Volume 47, Number 9, pp. 910-919(10). Taiwan

[116] J.-P. Kruth, S. Kumar (2005): *Statistical Analysis of Experimental Parameters in Selective Laser Sintering*. *Advanced Engineering Materials*. Vol. 7, Issue 8, Pages 750–755

[117] H.-Te Liao, J.-Ren Shie, (2007): *Optimization on selective laser sintering of metallic powder via design of experiments method*. *Rapid Prototyping Journal*, Vol. 13 Iss: 3, pp.156 – 162.

[118] [http://controls.engin.umich.edu/wiki/index.php/Design\\_of\\_experiments\\_via\\_taguchi\\_methods:\\_orthogonal\\_arrays](http://controls.engin.umich.edu/wiki/index.php/Design_of_experiments_via_taguchi_methods:_orthogonal_arrays). [Accessed 11 Feb.2011].

[119] Y. H. Chen<sup>1</sup>, S. C. Tam, W. L. Chen, H. Y. Zheng (1996): *Application of Taguchi Method in Optimization of Laser Micro- Engraving of Photomasks*. *International Journal of Materials and Product Technology*. Vol. 11, No.3/4, pp. 333 - 344

[120] L.A. Dobrzański, J. Domaga, J.F. Silva (2007): *Application of Taguchi method in the optimisation of filament winding of thermoplastic composites*. *Archives of Materials Science and Engineering*. Vol. 28, Issue 3, March 2007, Pages 133-140

[121] B. Ozcelik, T. Erzurumlu (2006): *Comparison of the warpage optimization in the plastic injection molding using ANOVA, neural network model and genetic algorithm*. *Journal of Materials Processing Technology*. Volume 171, Issue 3, Pages 437-445

[122] R. Konda, K.P. Rajurkar, R.R. Bishu, A. Guha, M. Parson (1999): *Design of experiments to study and optimize process performance*. International Journal of Quality & Reliability Management, Vol. 16 Iss: 1, pp.56 – 71. USA

[123] B. Berginc, Z. Kampuš, B. Šuštaršič (2006): *The use of the Taguchi approach to determine the influence of injection-moulding parameters on the properties of green parts*. Journal of Achievements in Materials and Manufacturing Engineering. Volume 15, Issue 1-2. Ljubljana, Slovenia

[124] D. C. Montgomery, 5<sup>th</sup> Edition, 2001: *Design and Analysis of Experiments*. John Wiley & Sons, INC; USA